Robust control design strategies applied to a DVD-Video player

Giampaolo Filardi

▶ **To cite this version:**

Giampaolo Filardi. Robust control design strategies applied to a DVD-Video player. Automatic. Université Joseph-Fourier - Grenoble I, 2003. English. NNT : . tel-00197521

HAL Id: tel-00197521

https://theses.hal.science/tel-00197521v1

Submitted on 14 Dec 2007

HAL is a multi-disciplinary open access archive for the deposit and dissemination of scientific research documents, whether they are published or not. The documents may come from teaching and research institutions in France or abroad, or from public or private research centers.

L'archive ouverte pluridisciplinaire **HAL**, est destinée au dépôt et à la diffusion de documents scientifiques de niveau recherche, publiés ou non, émanant des établissements d'enseignement et de recherche français ou étrangers, des laboratoires publics ou privés.

UNIVERSITÉ JOSEPH FOURIER - GRENOBLE

given by the library

PHD THESIS

For obtaining the degree of

DOCTEUR DE L'UJF

Special field : Automatique – Productique

prepared at the

Laboratoire d'Automatique de Grenoble - INPG

in the context of the École Doctorale

Électronique, Électrotechnique, Automatique, Télécommunications, Signal

presented and sat by

Giampaolo FILARDI

the 1^{st} of December 2003

Title:

ROBUST CONTROL DESIGN STRATEGIES APPLIED TO A DVD-VIDEO PLAYER

PHD supervisors : Alina VODA-BESANCON
Olivier SENAME

JURY

M.	M. de MATHELIN	Examiner	Professor at the ENSP Strasbourg
M.	J. STOUSTRUP	Examiner	Professor at the Aalborg University, DK
M.	P. NONIER	Examiner	Project leader at ST Microelectronics
M.	H. J. SCHROEDER	Examiner	Project leader at ST Microelectronics
Mme	A. VODA-BESANÇON	PHD supervisor	Maître de conférences à l'UJF-LAG
M.	O. SENAME	PHD supervisor	Maître de conférences à l'INPG-LAG
M.	L. DUGARD	President	Research Director at the CNRS - LAG

UNIVERSITÉ JOSEPH FOURIER - GRENOBLE

attribué par la bibliothèque

THÈSE

pour obtenir le grade de

DOCTEUR DE L'UJF

Spécialité : Automatique – Productique

préparée au

Laboratoire d'Automatique de Grenoble - INPG

dans le cadre de l'École Doctorale

Électronique, Électrotechnique, Automatique, Télécommunications, Signal

présentée et soutenue par

Giampaolo FILARDI

le 1^{er} Décembre 2003

Titre:

STRATÉGIES DE CONTRÔLE ROBUSTE DE LECTEURS DE DISQUES DVD

Directeurs de thèse: Alina VODA-BESANCON
Olivier SENAME

JURY

M.	M. de MATHELIN	Rapporteur	Professeur à l'ENSP Strasbourg
M.	J. STOUSTRUP	Rapporteur	Professeur à l'Université d'Aalborg, DK
M.	P. NONIER	Examinateur	Chef de projet chez ST Microelectronics
M.	H. J. SCHROEDER	Examinateur	Chef de projet chez ST Microelectronics
Mme	A. VODA-BESANÇON	Directeur de thèse	Maître de conférences à l'UJF-LAG
M.	O. SENAME	Directeur de thèse	Maître de conférences à l'INPG-LAG
M.	L. DUGARD	Président	Directeur de Recherches CNRS - LAG

Contents

List of Figures

List of Tables

Résumé

Introduction

Cette thèse est le résultat de mes trois dernières années de travail de recherche concernant la synthèse de systèmes de contrôle et commande appliquée aux procédés industriels, et elle représente pour moi non seulement l'aboutissement de mon doctorat, mais aussi la somme de quatre ans de travail et de vie passés en France.

Ce travail a pour cadre la commande sous contraintes industrielles du sytème d'asservissement de position du faisceau laser, utilisé dans les lecteurs de disques optiques CD (Compact Disc) et DVD (Digital Versatile Disc). La collaboration entre le *Laboratoire d'Automatique de Grenoble* et la société *STMicroelectronics* Grenoble, signataire d'un contrat C.I.F.R.E (Convention Industrielle pour la Formation et la Recherche d'Emploi) avec l'*A.N.R.T* (Association Nationale de Recherche Technique) a permis la réalisation de développements théoriques sans perdre de vue un objectif important qui est l'application d'algoritmes de commande robuste au système de positionnement du faisceau laser d'un lecteur DVD industriel.
Dans ce contexte, j'ai été chargé d'analyser et d'améliorer les performances du système de contrôle d'un lecteur de disques CD et DVD, mis au point dans le laboratoire d'application de *STMicroelectronics* Grenoble, comme banc d'essai, et ensuite introduit sur le marché des produits multi-media grand public.

Les dispositifs optiques sont largement utilisés aujourd'hui pour mémoriser en format numérique une grande quantité de données informatiques, de la musique ou de la vidéo. Les applications de ce type de systèmes dans des produits technologiques grand public comme les lecteurs DVD demandent l'amélioration du comportement de suivi de piste du faisceau laser, pour répondre aux spécifications de performance imposées par une densité ac-

crue de l'information enregistrée sur les supports optiques, et un temps d'accès à l'information beaucoup plus rapide que dans les lecteurs optiques de première génération.

Remerciements

Le travail présenté dans cette thése a été élaboré au sein du laboratoire d'application *Front-end* de la division DVD de *STMicroelectronics* Grenoble. Les développements théoriques et les données expérimentales ont été suggérés et analysés par l'équipe de recherche du *Laboratoire d'Automatique de Grenoble*. Je voudrais particulièrement remercier mes directeurs de thèse M.me *Alina Voda Besançon* et M. *Olivier Sename*, qui ont continuellement cordonné mon travail et su stimuler mon intérêt envers la recherche.
Je souhaite aussi remercier tous ceux qui m'ont aidé pendant la période de temps passée au laboratoire d'application DVD *Front-end* de *STMicroelectronics* Grenoble. Je pense à M. *Pascal Nonier*, responsable de l'équipe d'application DVD *Front-end*, et à M.*Heinz-Jöerg Schroeder* responsable du projet DVD enregistrable, leur avis m'a toujours été utile lors de la résolution des problèmes techniques liés aux contraintes industrielles et d'implémentation.
Je n'oublie pas non plus l'aide que j'ai reçue de la part de tous mes collègues de l'équipe d'application DVD *Front-end* : M.elle *Claire Verilhac*, M.me *Roselyne Haller*, M. *Jean-Michel Goiran*, M. *Yann Morlec*, M. *Laurent Lavernhe*, M. *Thierry Avons-Bariot*, M. *Mickael Guene*, M. *Patrick Simeoni* et M. *Christophe Viroulaud*.
Un remerciement particulier à M. *Stefano Groppetti*, responsable du service DVD *Front-end*, pour avoir integré mon travail de recherche au sein des activitées de l'équipe d'application, et pour m'avoir considéré comme un membre effectif de la division DVD depuis mon arrivée.

Pour terminer, je ne peux pas manquer de remercier mes parents, qui m'ont toujours aidé dans les moments difficiles et encouragé à accepter les défis les plus intéressants et stimulants pour mon avenir. Ma présence leur a sûrement manqué, tout comme la leur m'a manqué pendant ces quatre derničres années passées loin de chez moi...merci infiniment.

Le problème de commande pour les lecteurs de disques optiques

Comme tous les équipements qui utilisent l'encodage MPEG (Moving Picture Experts Group), technologie qui est universellement employée pour comprimer les données audio et vidéo avant émission ou enregistrement, les lecteurs de disques DVD se composent de deux sous-systèmes, notamment la partie *Front-End* et la partie *Back-End*.
Le sous-système *Front-End* gère toutes les fonctions nécessaires pour extraire les données encodées en format MPEG sur le disque, tandis que la partie *Back-End* décode ces données pour récréer l'information originellement enregistrée.

Mon travail de recherche fait partie d'un projet destiné à analyser et valider un circuit intégré *Front-End* produit par STMicroelectronics, permettant de reproduire en lecture l'information contenue sur des supports optiques de type CD audio (CD-DA), CD photo et vidéo, CD et DVD re-enregistrables (CD-R, CD-RW, DVD-R et DVD-RW) à simple ou double couche.

L'objectif de ce travail de recherche est l'étude du système d'asservissement de position de la tête optique de lecture des disques, et la réalisation, sur plateforme d'essai STMicroelectronics, de nouveaux types de régulateurs plus performants et plus robustes face aux variations paramétriques et aux incertitudes de modélisation du système.

La partie servo d'un lecteur de disques optiques CD et DVD est composée de plusieurs sous-blocs, qui rendent le système complexe à concevoir et analyser. De plus, les boucles de commande qui sont en charge de positionner correctement le laser le long des directions verticale et radiale, représentent un sujet intéressant du point de vue de la synthèse des systèmes de contrôle, car ils sont les plus difficiles à réaliser et analyser, comme l'ont déjà mis en évidence Dettori [9], Dotsch et al. [17], Pohlmann [44], Stan [53] et Steinbuch et al. [57].
Pour ces raisons le thème central de ce travail sera sera l'étude et la réalisation, sur solution cible STMicroelectronics, de nouvelles boucles de commande utilisées pour contrôler les déplacements fins de la tête optique des lecteurs de disques CD et DVD.

Le marché des produits multimedia grand public

L'évolution rapide de la technologie des semi-conducteurs a permis d'appliquer des algorithmes complexes de calcul à un ensemble croissant d'applications qui constituent aujourd'hui une nouvelle classe de produits multimedia grand public, nommée "Digital Consumer Products".
Ce marché est en rapide évolution parce qu'il offre aux consommateurs des produits performants, fonctionnels à des prix abordables. Les segments du marché traditionnel des ordinateurs et des télécommunications est en expansion car eux aussi utilisent la même technologie. En même temps, la complexité des circuits intégrés qui peuvent être construits à l'intérieur d'un seul chip de silicium a atteint un stade où un système complet peut être effectivement intégré dans un seul chip. Donc, la filière traditionnelle des produits électroniques est en train de céder la place à un nouveau type d'affaires où le fournisseur de systèmes intégrés dans un seul chip prend une place d'une importance prépondérante. Cette tendance est en train de changer la façon d'opérer de l'industrie des semi-conducteurs, car pour réussir dans le marché des systèmes intégrés, les producteurs doivent savoir maîtriser différentes techniques et avoir plusieurs compétences.

STMicroelectronics est une société multinationale de semi-conducteurs et leader dans le développement de solutions intégrées dans le domaine des applications en micro-électronique. La compagnie offre à ses partenaires un approche système qui inclut une propriété hardware et software, des connaissances dans le domaine des applications et des technologies avancées qui lui permettent d'optimiser et proposer des solutions globales.

Pour cela la société a développé un réseau mondial d'alliances stratégiques, comprenant le développement des produits avec des partenaires de premier rôle, développement technologique avec les clients et d'autres fournisseurs de semi-conducteurs. Elle investit, en outre, une partie significative de son chiffre d'affaire dans la recherche et le développement, afin de combiner ses forces avec celles des meilleures écoles d'ingénieurs. Le partenariat entre l'I.N.P.G (*Institut National Polytechnique de Grenoble*) et le L.A.G (*Laboratoire d'Automatique de Grenoble*), ainsi que la recherche et le développement appliqué à la sysnthèse d'un système intégré de commande des lecteurs DVD qui se trouve à la base de ce travail, s'inscrivent dans ce contexte.

Différences entre les technologies DVD et CD

Comme les CD, les disques DVD contiennent des données gravées sous forme de trous (*pits*) microscopiques sur des sillons (*tracks*) qui évoluent en forme de spirale sur la surface du disque. Tous les lecteurs de disques CD et DVD utilisent un faisceau laser pour lire les informations gravées en format numérique le long de ces sillons. Toutefois, les DVD utilisent des méthodes différentes de modulation de l'information et de correction d'erreur et les sillons sont plus étroits que pour les CD.
La distance, mesurée en direction radiale, entre deux pistes physiquement adjacentes (appelée *track pitch*) a été réduite de 1.6 μm pour les CD à 0.74 μm pour les disques DVD, afin d'augmenter la densité des données enregistrées sur la surface du disque [59], et passer d'une capacité maximale de 650 Mb sur un CD, à 4.70 Gb sur un DVD à couche simple. De plus, les disques DVD peuvent contenir jusqu'à quatre fois plus de trous qu'un disque CD sur la même surface. Le fait que les pistes soient plus proches demande qu'un type particulier de laser, qui ne peut pas lire les CD-audio, les CD-ROM et les CD-R/RW, soit utilisé pour lire les disques DVD. Par conséquent, le système de contrôle utilisé dans les lecteurs DVD doit garantir un niveau de précision et d'atténuation des perturbations plus élevé que dans les lecteurs de disques CD.

Pourquoi un lecteur de DVD ?

Le problème de commande pour un lecteur de disques DVD est similaire à celui défini pour un lecteur CD, et il consiste à garantir que le faisceau laser, utilisé pour lire les données, suive les pistes gravées sur le disque. Contrairement aux anciens lecteurs de disques en vinyle, où un capteur piezo-électrique était guidé par contact avec les sillons le long du rayon du disque, dans les lecteurs de disques optiques, seul le faisceau laser touche la surface du disque. Le suivi de piste doit être donc garanti par une boucle d'asservissement à rétroaction, qui dans les applications industrielles est couramment réalisée en utilisant des simples régulateurs de type PID.

Jusqu'à aujourd'hui, dans les lecteurs DVD produits par STMicroelectronics, les niveaux désirés de performance du système de contrôle ont été atteints en utilisant des méthodologies heuristiques de synthèse et de "tuning" des paramètres, ou grâce à des améliorations coûteuses des procédés de fabrication du système.

L'objectif de cette thèse est d'analyser une solution intégrée "bas coût", utilisée pour asservir la position de la tête optique de lecture de disques DVD, et voir si de meilleures performances et une meilleure robustesse peuvent être atteintes avec des méthodologies avancées de synthèse du système de contrôle, afin de minimiser les coûts présents pendant la phase de production du dispositif. En même temps, notre but est aussi de présenter une méthodologie utile pour la synthèse des systèmes de contrôle de suivi de pistes, qui pourrait être utilisée pour des produits futurs.

La nécessité d'améliorer les performances du système de contrôle de position de la tête de lecture pour compenser les tolérances présentes pendant la phase de fabrication, et d'atténuer les effets des perturbations externes, fait du lecteur DVD un bon candidat pour tester des nouvelles techniques de synthèse robuste et utiliser des outils d'analyse récemment développés dans les domaines de la synthèse et de la modélisation des systèmes de contrôle en boucle fermée.

Motivations de la thèse

Comme indiqué dans l'introduction, les spécifications de performance strictes, imposées par une densité accrue de l'information enregistrée sur les supports optiques, demandent une amélioration du comportement du suivi de piste des disques. De plus, en raison de l'augmentation des capacités de stockage et vitesse de rotation des disques, le système de contrôle doit garantir un positionnement du faisceau laser plus précis, pour faire face aux tolérances des paramètres du système, et accroître son insensibilité aux perturbations externes, comme précisé par Vidal et al. [65].

En général, les méthodes de synthèse des systèmes de contrôle, qui sont basées sur une description mathématique du comportement du système, constituent des outils indispensables pour satisfaire aux contraintes industrielles. En effet, par expérience on sait que pour synthétiser un système de contrôle robuste et fiable il vaut mieux prendre en compte la dynamique exacte du système, qu'appliquer de façon répétitive des méthodologies de synthèse basées sur un réglage fin des paramètres.

En accord avec les objectifs industriels fixés par STMicroelectronics, en accord avec les exigences de recherche qui nous ont poussée à trouver des solu-

tions innovantes, une amélioration des performances du système de contrôle a été obtenue en utilisant des modèles mathématiques du système. La restriction d'ordre de nouveaux types de contrôleurs à implémenter sur la plateforme experimentale impose une contrainte industrielle importante pour la synthèse.
Les spécifications de performance, utilisées pour la synthèse des correcteurs, demandent que l'amplitude des signaux d'erreur de position ne dépassent pas certaines limites maximales définies dans [59], malgré la présence de perturbations externes et incertitudes paramétriques lieées aux tolérances de fabrication. Comme présenté dans Gu [25] et Xie et al. [68], l'automaticen doit donc faire face aux limitations physiques et aux contraintes d'implémentation afin d'obtenir le comportement désiré du système. La synthèse d'un système de contrôle peut être donc formulée comme un problème d'optimisation, qui prend en compte les spécifications de performance et les incertitudes paramétriques associées.

Différentes techniques de synthèse de systèmes de contrôle et commande appliquées aux lecteurs de disques CD ont déjà été présentées dans des publications et thèses, comme notamment dans Dettori [10], [11], [12], [15] et [14]. Dans ces travaux la synthèse de contrôleurs est obtenue par un compromis entre les performances et la robustesse vis à vis des variations des paramètres du système. En revanche, ces résultats ne sont pas utilisables dans notre cas à cause des contraintes d'implémentation sur l'ordre du contrôleur. D'autres travaux traitent le même problème en utilisant des techniques plus complexes, comme dans Callafon et al. [7], Dotsch et al. [17], Katayama et al. [36], Stan [53], Steinbuch et al. [55] Steinbuch et al. [57] et Vidal et al. [66]. Néanmoins, rien n'a encore été publié concernant le problème de contrôle de position du faisceau laser pour les lecteurs de disques DVD.

Dans ce contexte, notre objectif est de présenter des méthodologies de synthèse des systèmes de contrôle à appliquer à des prototypes industriels de lecteurs DVD, en utilisant une description mathématique du modèle des actionneurs de position. Ces procédures sont proposées pour obtenir des contrôleurs de complexité réduite, capables de satisfaire les spécifications de performance des disques DVD.
Une amélioration du comportement du système en termes de suivi de piste et d'atténuation des perturbations externes est obtenue grâce à des algorithmes de commande qui utilisent la connaissance du modèle physique du système. De plus, les principes de base de la μ-theorie sont utilisés pour

évaluer l'influence des variations paramétriques sur le dispositif de lecture. L'identification fréquentielle du modèle du procédé, accompagnée par la synthèse du système de contrôle et l'évaluation de ses performances, constituent les points essentiels traités dans ce travail.
A cause des contraintes d'implémentation liées à la nature du système, l'ordre des contrôleurs calculés doit être limité, ces limitations étant analysées en simulation avant la phase de réalisation pratique. Les résultats expérimentaux, obtenus sur la plate-forme prototype de STMicroelectronics, sont présentés à la fin pour comparer la solution de commande actuellement utilisée et fournie aux clients avec celles synthétisées le long de cette thèse.

Organisation de la thèse

Le travail de recherche, dont cette thèse représente une synthèse, a été organisé et accompli de la façon suivante :

Le chapitre 2 se compose de deux parties. Dans la première partie, un court exposé concernant l'histoirique des dispositifs optiques est présenté, ainsi qu'une description des formats de disques CD et DVD existants. Dans la deuxième partie le système servo-mécanique d'un lecteur de disques CD et DVD est détaillé en étant composé de deux sous parties : les dispositifs optiques, qui récupèrent les données et génèrent les signaux d'erreur de position, et la partie servo proprement dite, qui a en charge le contrôle de position de la tête de lecture par rapport à la surface du disque.
Comme une modélisation exacte des phénomènes physiques responsables de la génération des signaux d'erreurs peut se révéler très utile pour la mise en place d'outils de simulation, les principes optiques à la base de ces phénomènes sont içi présentés. Enfin, les objectifs de commande sont definis.

Dans le chapitre 3 on donne une description du lecteur CD/DVD proposé par STMicroelectronics afin de pouvoir définir exactement le problème de commande et de considérer les contraintes industrielles liées à la structure hardware du système d'essai. Les propriétés physiques des actionneurs électro-magnetiques de position du faisceau laser sont aussi étudiées, et un modèle mathématique de ces dispositifs est présenté à la fin de ce chapitre.

L'identification fréquentielle du procédé constitue le sujet central du chapitre 4. Cette procédure utilise des données expérimentales, mesurées à l'aide d'un analyseur dynamique de signaux, unies à un algorithme itératif d'ajustement

des paramètres, pour calculer un modèle mathématique simplifié du procédé. L' analyse de performances obtenues avec le contrôleur actuellement utilisé pour les applications industrielles, et l'étude des phénomènes de couplage entre les deux boucles de positionnement vertical (*focus*) et radial (*tracking*) terminent ce chapitre.

Le chapitre 5, qui traite des méthodologies de synthèse de contrôleurs robustes pour un lecteur DVD, (s'organise en trois parties.
Dans la première partie, des notions théoriques générales sur les méthodes de commande robuste sont présentées. Ensuite, une synthèse H_∞, basée sur la connaissance des spécifications de performances et sur un modèle simplifié du procédé, est effectuée afin d'obtenir un contrôleur robuste pour la boucle d'asservissement de position de tête de lecture en direction radiale. Ce régulateur a été calculé en utilisant des fonctions de pondération qui traduisent, sur les fonctions de sensibilité du système en boucle fermée, les spécifications de performances des disques DVD. Après réduction de son ordre, le contrôleur ainsi calculé est implémenté et validé sur la plate-forme d'essai. Les résultats d'analyse et de robustesse sont présentés et comparés avec ceux obtenus avec la solution industrielle actuellement utilisée, à la fin de cette partie. Dans la deuxième partie on présente d'abord des notions théoriques qui concernent la synthèse de régulateurs robustes capables de garantir la stabilité même en présence de variation paramétrique du système. Ces incertitudes sont ensuite prise en considération afin d'obtenir un ensemble de modèles mathématiques du procédé, et le theorème du petit gain est utilisé pour analyser les performances et la robustesse en stabilité de la solution obtenue. Comme cette approche ne mène à des résultats valables que dans le pire des cas des incertitudes du système, ne permettant pas d'identifier quels paramètres peuvent affecter l'efficacité de la commande, dans la troisième partie de ce chapitre, des concepts dérivés de la μ-analyse sont appliqués. Les résultats démontrent qu'une représentation structurée des incertitudes paramétriques du système permet de déterminer de quel paramétre physique il faut tenir compte pour améliorer ou ne pas dégrader les performances et la robustesse de la commande.

Pour terminer, les conclusions et les perspectives de cette thèse sont présentées dans le chapitre 6.

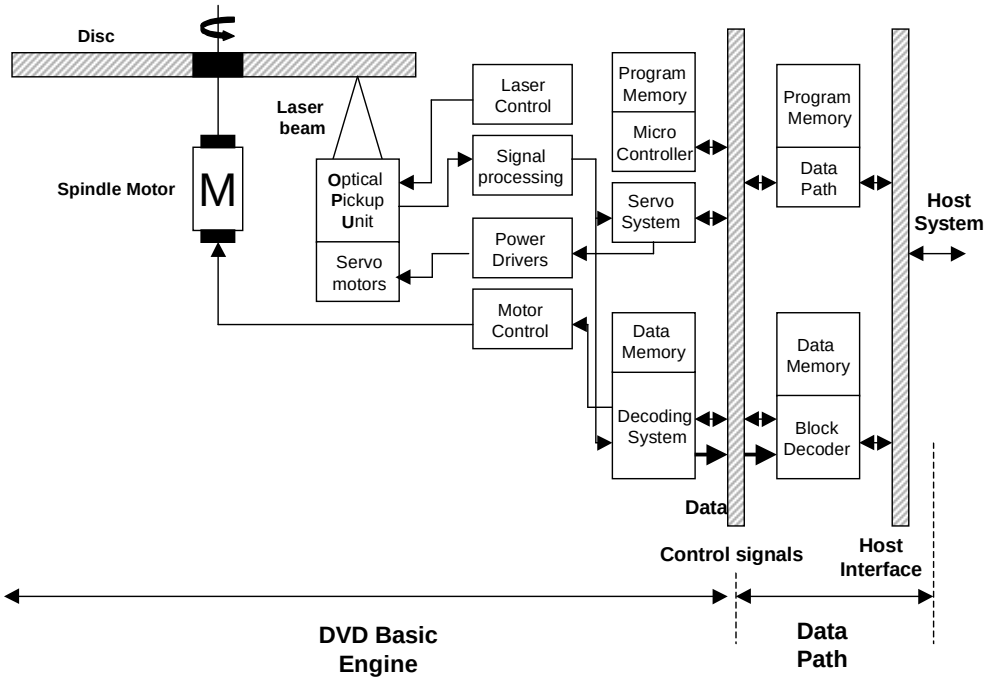

Figure 1: Schéma-bloc de l'architecture d'un lecteur DVD.

Chapitre 2 : Description du système

Dans ce chapitre on donne une description générale du fonctionnement du lecteur de disques DVD, et on définit le problème de contrôle de positionnement de la tête de lecture.

Notre contribution à ce chapitre peut être inscrite dans le contexte de la pure description du système sous étude. La figure 1 montre l'architecture de base d'un lecteur DVD, où on peut distinguer un moteur de base, utilisé pour récupérer les informations encodées sur le disque, et une partie dédiée à l'acheminement des données vers un système ôte qui traite l'image et le son.

Dans une première partie on a présenté les différents formats de disques CD et DVD actuellement disponibles, ainsi que leur structure physique.
Ensuite, on a détaillé les dispositifs optiques utilisés pour la génération des signaux d'erreur de position et pour reproduire l'information gravée sur la surface du disque.
Ils existent très peu de publication concernant les principes physiques et la modèlisation des dispositifs optiques utilisés dans les lecteurs CD et DVD, comme cité dans Born and Wolf [3], Bouwhuis et al. [4], et [5]. De plus, il est très difficile de pouvoir obtenir des informations suffisamment complètes et détaillées, à partir des spécifications techniques des systèmes optiques disponibles aujourd'hui sur le marché.

Dans le but de calculer des modèles linéaires à complexité réduite de tels dispositifs et de pouvoir ensuite les utiliser dans des schémas de simulation, on a appliqué l'optique géométrique et les principes d'analyse harmonique de la lumière, comme présenté par Hnilička et al. [26], [27], [28], [29], et [30]. Une synthèse de ces travaux, auxquels j'ai participé de manière significative, est présentée en annexe et répresentent à notre avis une contribution non négligeable à cette recherche.

Dans la deuxième partie de ce chapitre, on a inclus la partie de modèlisation des actionneurs eléctromechaniques de position du laser, ainsi que la définition du problème de commande imposé par les spécifications industrielles de performance du système.

La table 1 contient les valeurs de la déviation maximale de la position nominale x_{max}, de l'accélération du spot lumineux $\ddot{x}_{max}$ et du maximum de l'erreur de position h_{max} pour un disque DVD, spécifiées pour une vitesse linéaire de lecture égale à $v_a = 3.49m/s$

Table 1: *Valeurs de la déviation maximale de la position nominale x_{max}, de l'accélération du spot lumineux $\ddot{x}_{max}$ et du maximum de l'erreur de position h_{max} pour un disque DVD, spécifiées pour une vitesse linéaire de lecture égale à $v_a = 3.49m/s$*

Paramètres et conditions	Radial	Focus
x_{max} pour $f \leq f_{rot}$	$\pm 50\mu m$	$\pm 0,3mm$
$\ddot{x}_{max}$ pour $f_{rot} \leq f \leq 1.1KHz$	$1.1m/s^2$	$8m/s^2$
h_{max} pour $f_{rot} \leq f \leq 1.1KHz$	$\pm 0.022\mu m$	$\pm 0.23\mu m$

L'objectif du contrôle est de limiter l'amplitude maximale des signaux d'erreur de position le long des directions verticale et radiale, même en présence de perturbations périodiques causées par les imperfections du disque (excentricité ou déviations verticales).

Les spécifications de performance [59], qui établissent les valeurs maximales pour les amplitudes des signaux d'erreur, ainsi que pour les déviations de la position nominale et l'accélération du laser, peuvent être traduites en termes de gabarits fréquentiels sur le spectre des signaux d'erreur, comme montré dans Dettori [10].

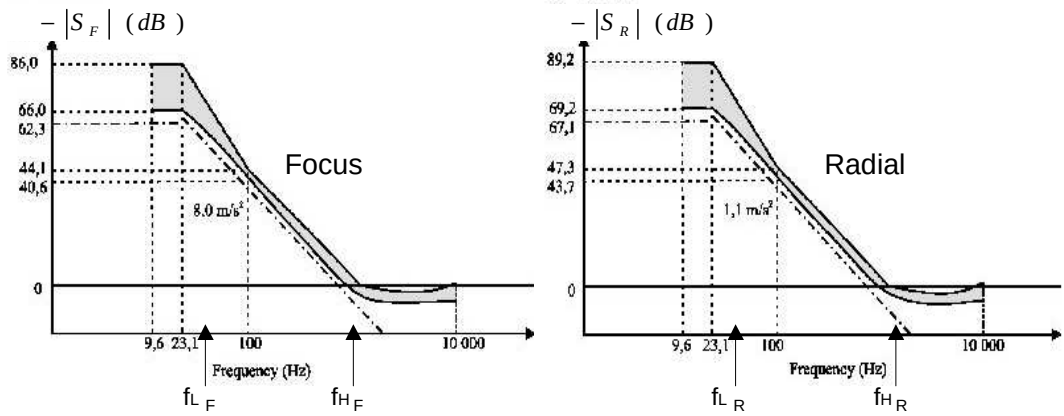

Figure 2: Spécifications de performance des boucles focus et tracking en terme de gabarits fréquentiels sur $S(s)^{-1}$, $N = 1$.

Chapitre 3 : Description du problème de commande

Dans ce chapitre on décrit le système industriel considéré. Cette partie de présentation de tous les sous blocs hardware et modules software composant le système, a été a été considérée comme indispensable pour mieux comprendre son fonctionnement global, et prendre en compte les contraintes industrielles lors de la phase d'implémentation.

Notre contribution à ce chapitre est double. Premièrment, dans le contexte d'un pur travail d'application, j'ai développé le code assembleur nécessaire pour qu'un DSP embarqué dans la solution industrielle puisse réaliser les filtres numériques de commande. Bien que moins spéculative, cette première partie du travail de recherche a permis de réaliser les boucles d'asservissement de position du laser d'un lecteur DVD aujourd'hui présent sur le marché.

Après cette phase d'implémentation et de compréhension des contraintes industrielles, une analyse des performances d'un régulateur déjà existant a été fournie, en imposant, comme montré dans la figure 2, les gabarits fréquentiels sur les fonctions de sensibilité du système bouclé (voir au paragraphe 3.6.1).

Deuxièmement, les modèles physiques des actionneurs de position du faisceau laser ont été calculés à partir des spécifications techniques contenues dans [43] ou [45]. Ceci a permis d'obtenir des modèles nominaux linéaires des actionneurs, et d'évaluer les incertitudes dues aux tolérances des paramètres physiques.
La figure 3 montre un schéma-bloc du système de position de la lentille optique utilisé pour le calcul du modèle physique des actionneurs. Comme expliqué dans le paragraphe 3.7 la fonction de transfert entre la tension d'entrée aux actionneurs $V(s)$ et la position en μm du faisceau laser $X(s)$ a

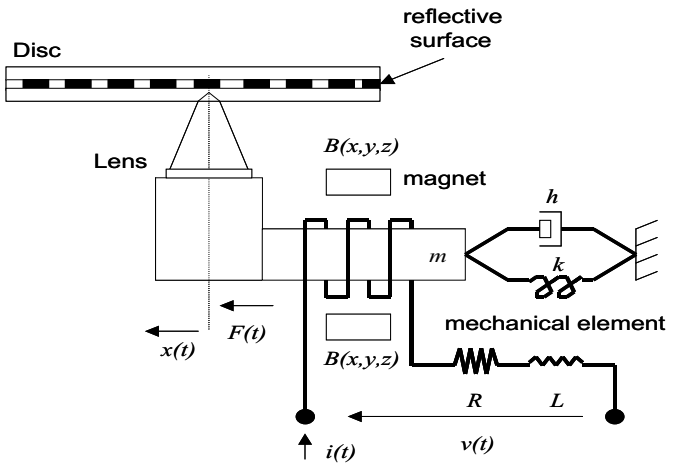

Figure 3: Modèle physique des actionneurs de position de la lentille optique.

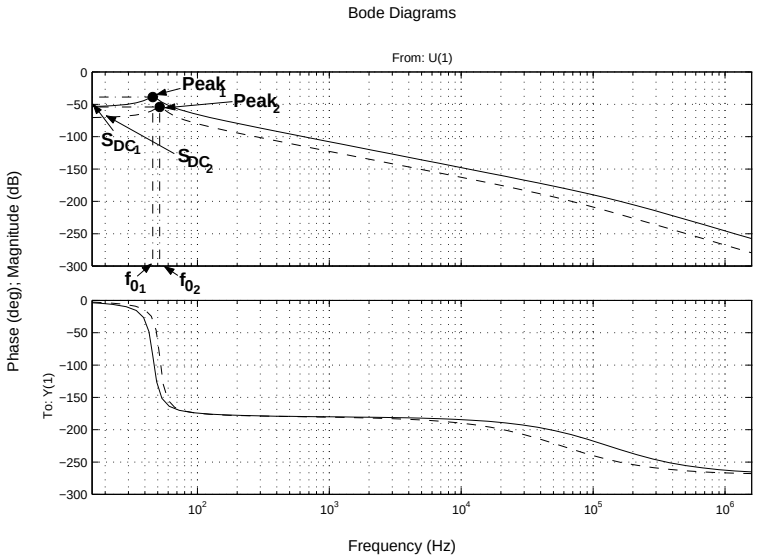

Figure 4: Diagrammes de Bode de deux types d'actionneurs de position présents actuellement dans le commerce.

la forme suivante :

$$H(s) = \frac{X(s)}{V(s)} = \frac{\frac{K_e}{ML}}{s^3 + \left(\frac{R}{L} + \frac{D}{M}\right)s^2 + \left(\frac{DR}{ML} + \frac{k}{M} + \frac{K_e^2}{ML}\right)s + \frac{kR}{ML}} \qquad (1)$$

Dans la figure 4 on montre à titre d'exemple les diagrammes de Bode de deux types d'actionneurs de position présents actuellement dans le commerce Afin de valider ces modèles mathématiques, indispensables pour la synthèse de nouveaux types de régulateurs, une procédure d'identification du procédé sera effectuée dans le chapitre suivant en utilisant la mesure des réponses en fréquence des fonctions de sensibilités du système en boucle fermée.

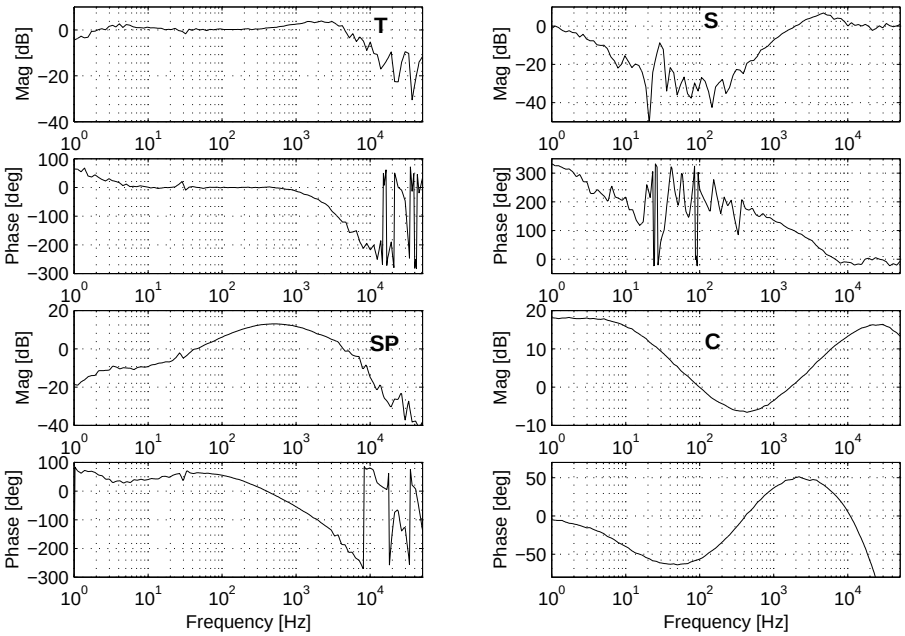

Figure 5: Réponses fréquentielles mesurées des quatres fonctions de sensibilité du système en boucle fermée $\widehat{T}(j\omega)$, $\widehat{S}(j\omega)$, $\widehat{SP}(j\omega)$ et $\widehat{C}(j\omega)$.

Chapitre 4 : Identification du procédé

Comme présenté dans le chapitre 2, le système de contrôle d'un lecteur DVD est formé de trois parties principales : les étages de conversion courant-tension (*drivers*) qui alimentent les actionneurs de position, les dispositifs optiques et les actionneurs de la lentille. Les deux premiers composants peuvent être considérés respectivement comme deux gains constants g_d et g_{opt}, et les actionneurs peuvent être modélisés en utilisant les équations physiques présentées dans le chapitre précédent.
Néanmoins, une description exacte des dynamiques du procédé n'est pas évidente à obtenir car, dans les lecteurs de disques optiques, la position instantanée de la piste ou de la surface du disque n'est pas directement mesurable. De plus, les signaux d'erreur de position, obtenus à partir de la différence entre les positions de la piste sur laquelle on veut se positionner et le laser, sont générés par des dispositifs optiques, dont le fonctionnement peut être considéré comme linéaire seulement dans un intervalle limité de valeurs de déplacements de la lentille autour d'une position d'équilibre.
En tenant compte du travail déjà développé pour un lecteur de disques CD et présenté par Dettori [10], on présente dans ce chapitre la procédure suivie pour identifier le procédé à partir des réponses fréquentielles mesurées des fonctions de sensibilité du système bouclé, comme présenté en figure 5.

Notre objectif est de valider, à travers des résultats expérimentaux, les modèle physique des actionneurs calculés dans le chapitre précédent et d'envisager

si des dynamiques non modélisées et des incertitudes paramétriques doivent être aussi prises en compte pendant la synthèse de nouveaux types de contrôleurs. En outre, cette approche permet d'estimer plus précisément le comportement des dispositifs optiques, afin d'obtenir un schéma simple et utilisable en simulation pour la boucle de contrôle globale.

Les essais ont été obtenus en mesurant, en fréquence, les fonctions de tranfert du système en boucle fermée avec un analyseur dynamique de signaux. Les résultats expérimentaux montrent que le modèle physique des actionneurs de position reste valide autour d'une certaine distance de la piste à suivre. Une évaluation des performances et de la robustesse du système de contrôle actuellement utilisé est effectuée après la validation du modèle.
Les résultats expérimentaux et de simulation montrent encore que le contrôleur actuel est robuste vis à vis des variations paramétriques du modèle du procédé, bien qu'il ne le soit pas par rapport à des disques qui présentent une excentricité supérieure à une valeur nominale.
Dans la dernière partie de ce chapitre, on a étudié les phénomènes de couplage existants éventuellement entre les deux boucles d'asservissement de position la tête optique. Cette analyse a été effectuée à travers la mesure des réponses en fréquence des transferts de boucle fermée.
On remarque que, dans l'intervalle de fréquences dans lequel le système de contrôle doit agir, l'interaction dynamique entre les deux boucles est relativement faible. On peut donc considérer que le système de contrôle d'un lecteur de disques optiques est découplé en deux sous-systèmes indépendants (systèmes de type SISO=*Single Input Single Output*) avec, respectivement une seule entrée (l'erreur de position) et une seule sortie (le signal qui guide les actionneurs), comme montré en figure 6.
Les résultats obtenus dans ce chapitre seront utilisés par la suite pour synthétiser un nouveau type de contrôleur de position du laser à ordre réduit, basé sur une approche de type H_∞.

Chapitre 5 : Synthèse H_∞ des systèmes robustes de contrôle et commande

Dans ce chapitre on présente une procédure de synthèse de contrôleurs qui est basée sur la connaissance des modèles physiques des actionneurs de position du laser. Ceci afin de calculer des nouveaux régulateurs robustes capables d'obtenir des meilleures performances en terme de suivi de piste (*track following*).

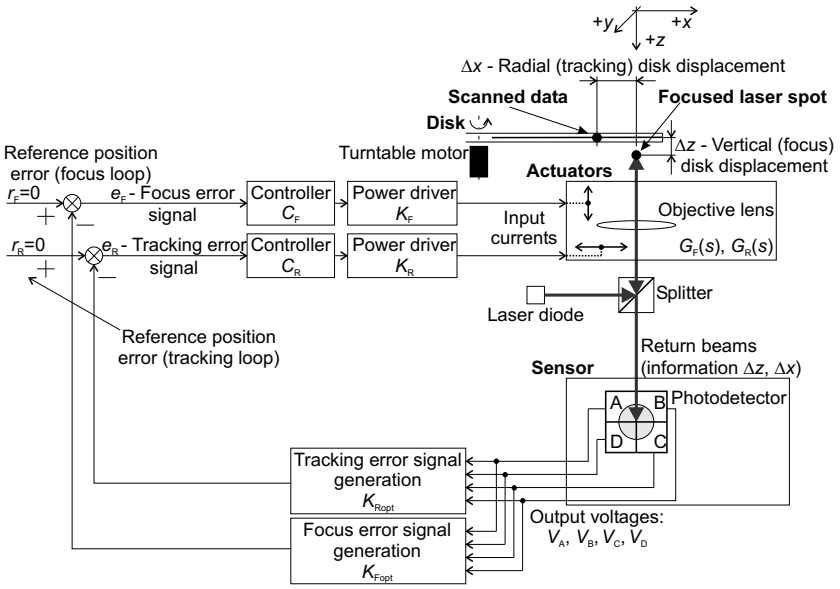

Figure 6: Scéma-bloc des boucles d'asservissement de position en focus et tracking de la lentille optique.

Ainsi qu'il a été mentionné dans le chapitre 3, les contraintes sur l'ordre des contrôleurs sont motivées par le besoin de limiter les coûts de la synthèse, et pour rendre l'implémentation de ces filtres numériques possible sur des applications industrielles, telles que le lecteur DVD mis à disposition par les laboratoires de STMicroelectronics.

Dans l'approche standard de type H_∞, les contrôleurs issus de la synthèse sont solutions de problèmes d'optimisation, basés sur la connaissance des modèles physiques du procédé et des fonctions de pondération qui représentent en fréquence des spécifications de performances.

Comme présenté dans le paragraphe 5.4.1, dans le cas des lecteurs de disques optiques, les critères de robustesse et performance ainsi que la forme des fonctions de transfert en boucle fermée sont prise en compte afin de spécifier un critère de type H_∞ à minimiser.
La figure 7 représente le schéma-bloc du système de contôle utilisé pour ce type de synthèse. L'ordre des régulateurs correspondants sera égal à celui du modèle plus ceux des fonctions de pondération utilisées pendant la synthèse. Dans ce travail on ne considère que des solutions du problème de commande d'ordre réduit, afin de respecter les contraintes de complexité maximale des algorithmes à implémenter sur le DSP (*Digital Signal Processing*) actuellement utilisé dans la solution industrielle.

Généralement, on considère que le modèle utilisé pour la synthèse d'un régulateur est équivalent au système pour lequel le contrôleur est conçu.

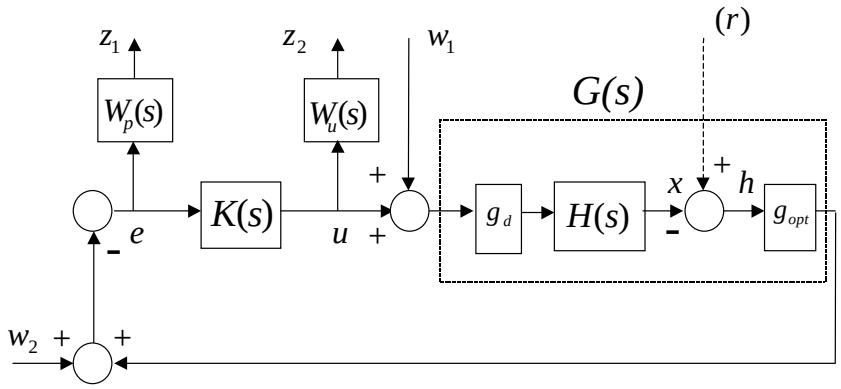

Figure 7: Schéma-bloc utilisé pour la synthèse d'un controleur de type H_∞.

Néanmoins, un modèle ne donne, de façon générale, qu'une description approximative du procédé. Donc, le régulateur synthétisé sur la base de ce modèle donnera des performances différentes pour le système nominal et pour le procédé réel. Ce type de comportement dépend principalement des variations paramétriques du système, causées par les tolérances présentes pendant la fabrication et par l'ancienneté du dispositif de lecture.
Dans le cas des lecteurs CD et DVD, bien que des améliorations sont observées en termes de temps d'accès, de capacité de stockage et densité de l'information enregistrée sur le disque, très peu a été fait pour adapter les systèmes de contrôle aux différents types de lecteurs et améliorer leurs performances vis à vis des tolérances paramétriques. Ceci explique pourquoi il est nécessaire que la robustesse des solutions calculées soit garantie.

Une approche de type H_∞ est utilisée dans ce chapitre pour calculer un contrôleur robuste capable d'asservir la position du faisceau laser en direction radiale. Les résultats sont montrés dans la figure 8. La synthèse montre que, après réduction d'ordre, ce régulateur implémenté attenue les effets perturbateurs dus aux imperfections du disque (excentricité et déviations verticales), comme representé dans les figures 9 - 12.
Enfin, en considérant les variations paramétriques des modèles des actionneurs, on construit un ensemble des modèles incertains. L'influence de chacun de ces paramètres est évaluée sur les performances du système nominal, selon deux approches.

Premièrement, en considérant l'ensemble des variations paramétriques plausibles, un gabarit majorant les incertitudes du modèle nominal a été calculé, et le thèoreme du petit gain est appliqué afin de vérifier si la robustesse en stabilité et en performance du système bouclé sont satisfaites pour la variation considerée des paramètres (approche non structurée).

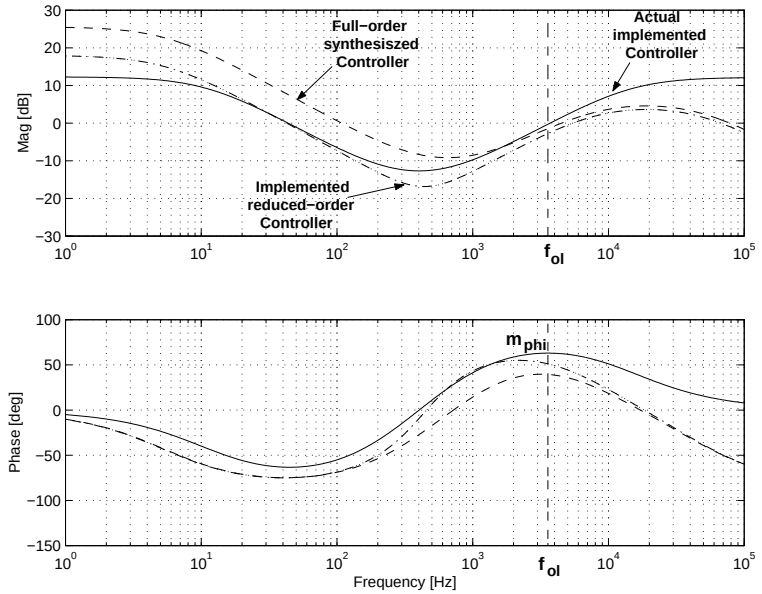

Figure 8: Amplitude et phase des contrôleurs de la boucle de tracking. Contôleur actuellement utilisé (ligne continue), contrôleur H_∞ d'ordre complet (ligne tirets), contrôleur H_∞ d'ordre réduit (ligne pointillée-tirets) implémenté sur le système industriel.

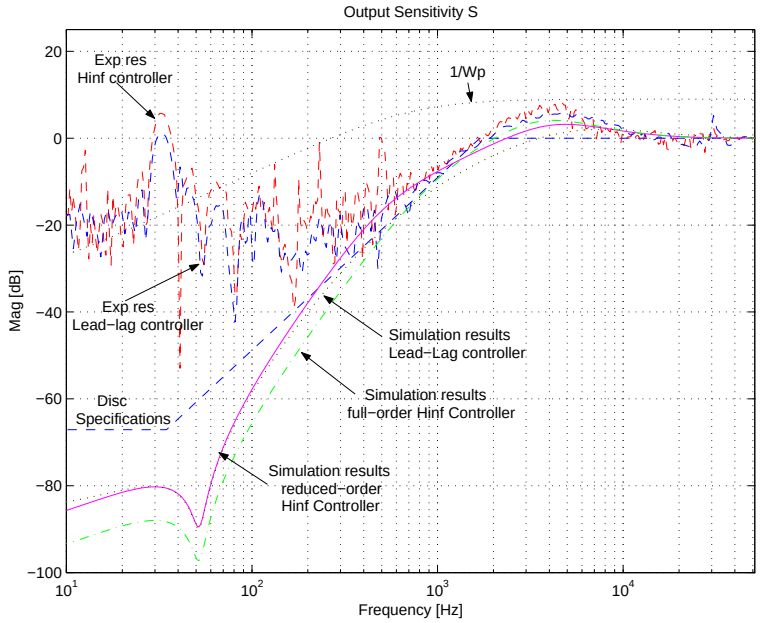

Figure 9: Amplitude de la fonction de sensibilité en sortie du système S.

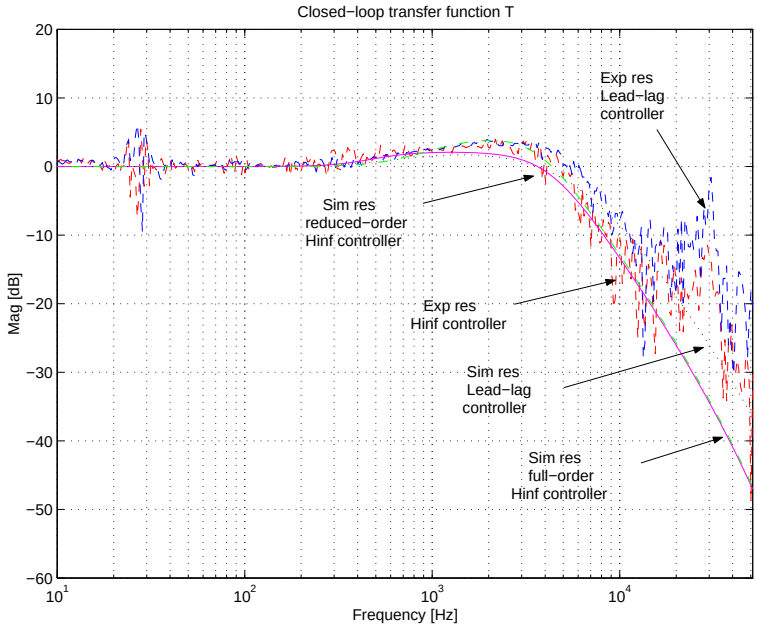

Figure 10: Amplitude de la fonction de transfer du système en boucle fermée T.

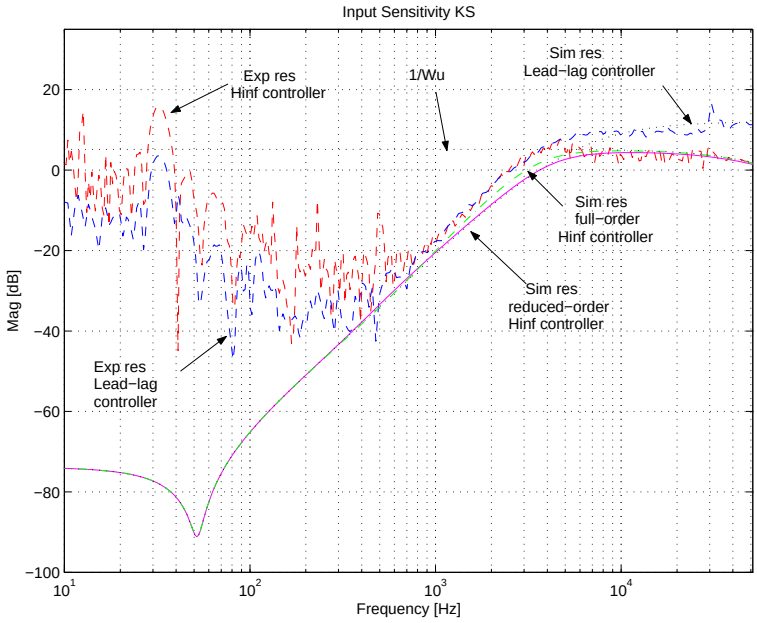

Figure 11: Amplitude de la fonction de sensibilité en entrée du système KS.

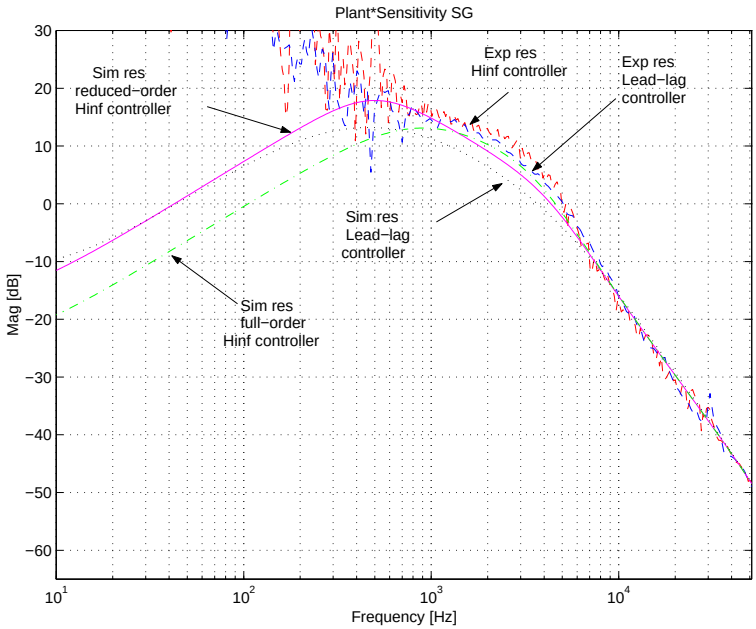

Figure 12: Amplitude de la fonction SG du système.

Cette approche donne des résultats conservatifs, d'une part parce qu'elle considère le pire des cas des incertitudes paramétriques, d'autre part parce qu'elle ne donne aucune indication sur le ou les paramètres qui peuvent se révéler "critiques" pour la stabilité et les performances du système.

Pour ces raisons, on a considéré des incertitudes de type "structuré" supposées réelles et normalisées en amplitude. De cette façon, l'analyse de robustesse en stabilité et en performance est évaluée en utilisant les outils récemment développés pour la μ-analyse. Les résultats expérimentaux et de simulation confirment que le contrôleur, issu de la synthèse H_∞, garantit la stabilité en boucle fermée et permet de respecter les spécifications de performances lorsqu'une grande incertitude sur les paramètres du système existe.

Notre contribution à ce chapitre est d'avoir donné, pour des lecteurs de disques optiques, une méthodologie de synthèse de commande simple et générale, qui est conseillée lors de l'existence de variations inconnues des paramètres physiques du procédé. Cette approche permet de calculer des régulateurs qui sont plus précis, puissants et simples à implémenter.
De plus, on a mis en évidence l'importance des interactions entre la phase de projet du dispositif de lecture, et la synthèse du système de contrôle. Pendant la conception de l'unité de lecture (OPU=*Optical Pick-up Unit*), on devrait prendre en compte les spécifications de robustesse et performances imposées par le contrôleur utilisé, pour réduire la durée de la phase de projet et garantir des meilleures performances robustes. Bien évidemment, cette méthodologie peut être appliquée à d'autres familles de lecteurs optiques.

Conclusions

La motivation principale qui nous a poussé à entreprendre ce travail de recherche est d'appliquer des méthodologies avancées de contrôle et commande, afin de développer et réaliser de nouveaux régulateurs robustes pour des lecteurs industriels de disques optiques.

Ce travail a été effectué suivant deux axes: d'un coté, comme une des limitations techniques de synthèse des systèmes de commande est causée par une inexacte description du modèle, une identification en boucle fermée est effectuée pour évaluer un modèle plus précis du procédé, comme décrit dans le chapitre 4.
D'un autre coté, les strictes spécifications de performance données pour les lecteurs de disques optiques nécessitent que les systèmes d'asservissement de position du laser soient robustes, vis à vis des variations paramétriques du procédé, et qu'ils garantissent de bonnes performances.
Comme mesure de performance on a choisi l'habilité du contrôleur à suivre correctement les pistes, malgré la présence de perturbations périodiques causées par les asymétries des disques. Après implémentation, la robustesse de la solution conçue est évaluée en regardant si le système bouclé reste stable et performant même en présence d'incertitudes paramétriques du système.

Notre objectif consiste donc à montrer comment en considérant une procédure d'identification du modèle suivie par une methode avancée de synthèse, on peut améliorer les performances et la robustesse d'un système industriel de contrôle, qui fut généralement réglé heuristiquement.

Cette approche est justifiée par les deux observations suivantes :

- Les systèmes de contrôle implémentés actuellement pour les lecteurs de disques optiques, sont limités par la carence de précision des modèles utilisés pour la synthèse.
  Ceci est en particulier vrai pour les lecteurs de disques DVD, pour lesquels le cahier des charges établit des spécifications plus strictes à respecter que pour les lecteurs CD.

- Les techniques existantes d'identification des procédés donnent des modèles très précis mais complexes des actionneurs de position des lecteurs optiques. Cependant, il en résulte que les régulateurs cal-

culés ont un ordre trop élevé pour être implémentés sur des systèmes industriels.

Un modèle nominal d'ordre réduit du procédé est donc considéré pour pouvoir synthètiser des contrôleurs de position du faisceau laser à complexité réduite . La robustesse vis à vis des incertitudes paramétriques du système est analysée en considérant un ensemble de modèles plausibles du procédé. Les performances sont évaluées en terme d'amplitudes des fonctions de transfert en boucle fermée, qui donnent des indications sur l'atténuation des perturbations, sur la vitesse de réponse du système de contrôle et sur la consommation d'énergie des actionneurs, comme discuté dans le chapitre 5.

Contributions personnelles

Dans le contexte de la stratégie décrite ci-dessus, pour la synthèse de contrôleurs à complexité réduite et pour une analyse successive de robustesse, les points suivants ont été abordés dans ce travail :

- Comme établi par le contrat de recherche *C.I.F.R.E.* (*Contrat Industriel de Formation et Recherche*), une activité de développement a été accomplie au démarrage des travaux de recherche. Afin de permettre à l'auteur d'acquérir de l'expérience, les filtres numériques, utilisés pour réaliser les boucles d'asservissement de position du faisceau laser, ont été implémentés dans un DSP. Cette partie du travail a aussi permis d'évaluer les performances et la robustesse de la solution de contrôle actuellement utilisé sur la plateforme industrielle, ainsi que pour comprendre les problèmes liés à la phase d'implémentation. On a donc réalisé les systèmes d'asservissement de position du laser de deux lecteurs présents sur le marché (*PIONEER DV350-DV351* et series).

- La procédure de modélisation physique des actionneurs de position est considérée comme non suffisamment precise afin d'obtenir des modèles fiables pour la synthèse des nouveaux régulateurs. Le procédé réel a donc été identifié pour vérifier si les modèles calculés représentent avec exactitude la dynamique du procédé réel.

- Le modèle du procédé a été identifié en mesurant les réponses en fréquence des fonctions de transferts du système en boucle fermée avec un analyseur dynamique de signaux. Deux types de *pick-ups* optiques, présents dans le commerce, ont été utilisé à ce fin : le *PIONEER M1* et le *SANYO DV33*. Les résultats expérimentaux montrent que

la dynamique du procédé est décrite de manière satisfaisante par un transfert de troisième ordre. Le gain optique est estimé en imposant que l'amplitude du transfert du système en boucle ouverte a un gain unitaire à la bande passante désirée.

- L'analyse de performances de la solution industrielle qui est actuellement utilisée montre que ce type de contrôleur permet d'obtenir la bande passante désirée et de respecter le temps de réponse spécifié dans [59]. Celui-ci garantit aussi que les perturbations périodiques sont rejetées, bien que bien que les mesures laissent apparaître que le niveau désiré d'atténuation aux basses fréquences n'est pas atteint et que les bruits de mesure en haute fréquence peuvent perturber les acquisitions.

- Les indicateurs de robustesse confirment que le régulateur actuel est robuste vis à vis des variations paramétriques du système. Toutefois, les essais réels révèlent qu'il ne garantit pas un comportement robuste vis à vis de disques ayant une excentricité supérieure à une valeur nominale. Ce comportement est du au fait que les variations des déviations des disques n'ont pas été prises en compte pendant la phase de modélisation du procédé.
  L'analyse des phenomènes de couplage révèle que, dans l'intervalle de fréquences où le contrôleur doit agir, les interactions dynamiques entre les deux boucles d'asservissement de position restent relativement faibles.

- Une synthèse de type H_∞ basée sur la connaissance du modèle du procédé est proposée pour calculer un régulateur d'ordre réduit, capable d'obtenir des meilleures performances et un rejet plus important des perturbations.
  Les applications au système industriel ont montré que :

  - Le modèle identifié du procédé permet d'évaluer de façon fiable la stabilité en robustesse et les performances en termes de gabarits fixés sur les transferts de boucle fermée, à condition que l'ordre du contrôleur soit réduit et qu'il ne diffère pas trop de la solution actuellement utilisée.
  - Un problème d'importance majeure pendant la phase de synthèse réside dans le choix des fonctions de pondération utilisées pour résoudre le problème sub-optimale de type H_∞. On choisit des

pondérations d'ordre réduit, afin de respecter les contraintes industrielles et éviter ainsi que le régulateur résultant soit d'ordre trop élevé.

- L'avantage de résoudre un problème de sensibilité mixte de type H_∞ est représenté par le fait de considérer deux seules fonctions de pondération, à travers lesquelles il est possible d'imposer que tous les transferts de boucle fermée se trouvent au dessous de certaines limites pour respecter les objectifs de performance et robustesse.
- Le contrôleur synthétisé garantit que la stabilité nominale du système et les spécifications de performances sont satisfaites. A différence du régulateur actuellement utilisé, la nouvelle solution permet de réduire l'amplitude des signaux de commande aux actionneurs, dans des zones où les bruits de mesure deviennent significatifs.

- La stabilité en robustesse et la stabilité en performance du nouveau contrôleur sont analysées, quand les incertitudes paramétriques réelles et des perturbations bornées sont considérées comme agissantes sur le système. Deux méthodologies ont été appliquées afin d'évaluer l'influence de ces dernièeres sur le système industriel, comme expliqué dans ce qui suit :

  - Un ensemble de modèles est obtenu en faisant varier les paramètres d'un modèle "moyen" à l'intérieur d'un certain intervalle de valeurs. Ensuite, on analyse le pire cas de comportement du système et le calcul d'une fonction de pondération donne un majorant fréquentiel des incertitudes qui inclut tous les modèles possibles du procédé. Les résultats démontrent que le système en boucle fermée est stable et qu'il satisfait les spécifications de performances, pour tous les modèles perturbés calculés autour du modèle nominal, jusqu'au pire cas des incertitudes.
  - Pour calculer les intervalles de confiance des paramètres physiques, pour lesquels la stabilité et les performances en robustesse sont garanties, on utilise la définition de la valeur singulière structurée et les outils offerts par la μ-analyse. L'avantage d'appliquer une telle méthode est qu'elle prend en compte la structure de la matrice du système bouclé, donnant de plus précises indications sur les intervalles de confiance des paramètres physiques. Les résultats expérimentaux montrent que le contrôleur synthétisé reste stable pour une grande incertitude sur le modèle, et que

les spécifications de performance sont satisfaites pour une large variation de ces paramètres.

Ces méthodologies mettent en évidence l'importance des interactions entre le projet des dispositifs de lecture et la synthèse du système de contrôle.

Perspectives

Les résultats issus de ce travail de recherche ont démontré qu'une méthodologie de synthèse robuste des systèmes de contrôle, appliqués à un procédé industriel, demande la prise en compte des incertitudes. Ceci afin d'évaluer, de façon systematique, la robustesse des performances du système bouclé.

Dans ce travail on a considéré l'influence des incertitudes causées par les variations paramétriques des modèles utilisés pendant la synthèse.
Néanmoins, les performances du système dépendent aussi d'une connaissance exacte des régulateurs qui opèrent en boucle fermée. L'utilisation des données expérimentales et des modèles physiques, pendant la synthèse, devrait donc être appliquée à la phase de modélisation du système et des régulateurs.

Un autre point, qui n'a pas été traité dans ce travail, mais qui reste toutefois important pour l'évaluation de la robustesse du système vis à vis des disques ayant différente excentricité, est l'influence que les déviations des disques peuvent avoir pendant la phase de modélisation des actionneurs.
Pour la suite, il serait convenable de vérifier si les incertitudes des modèles, liées à ces déviations, donnent des informations intéressantes sur la nature et l'influence de ce type de perturbations. De plus, la disponibilité de modèles plus précis, qui prennent en compte ces imperfections, peut contribuer de manière déterminante à la synthèse de contrôleurs plus performants en terme de suivi de piste et de comportement robuste. Ce point peut être d'importance capitale pour la synthèse de contrôleurs robustes adaptés à des vitesses de rotation plus élevées. En fait, pour ces derniers, une bande passante désirée plus large peut vouloir dire amplification des perturbations périodiques sur les signaux d'erreur de position du laser.

Pour terminer, un problème fréquent sur les dispositifs optiques du marché grand public est la variation des comportements des lecteurs causés par les conditions climatiques et par l'age. Il est évident qu'il existe un besoin

de modèles qui tiennent en compte aussi de ce type de variations du comportement pour un grand nombre de dispositifs en vue de la synthèse de régulateurs robustes et performants.

Dans ce travail on a présenté une approche simple et efficace pour le calcul d'un modèle fiable des incertitudes paramétriques du procédé réel, à partir des spécifications techniques des deux actionneurs de position du faisceau laser. En vue de la synthèse de régulateurs pour un grand nombre de dispositifs optiques de lecture, cette méthodologie demande néanmoins une investigation plus approfondie du comportement global du système, et la possibilité d'évaluer des modèles de commande en appliquant différents algorithmes d'identification.

Foreword

This thesis is the result of my last three years of research on Control System design applied to industrial systems, and it represents for me not only the final act of my Ph.D. research, but also the sum of four years of work and life experience in France.

This work is the result of a financial and research agreement between the company *STMicroelectronics* and the *A.N.R.T* (Association Nationale de Recherche Technique) in the context of a Ph.D. thesis, called C.I.F.R.E (Convention Industrielle pour la Formation et la Recherche d'Emploi).
The author has been in charge of analyzing the features of a DVD-video player servo system, realized and already introduced in the digital consumer market by the semiconductors supplier company *STMicroelectronics*.

The study has been completely carried out in the DVD division application laboratory of *STMicroelectronics* of Grenoble. Theoretical approaches and experimental data have been suggested and analyzed by the research team of the *Laboratoire d'Automatique de Grenoble*.

Particularly, I want to acknowledge my two Ph.D. supervisors, Mme *Alina Voda Besançon* and M. *Olivier Sename*, whose advice has always encouraged me and stimulated my interest to the topic of my work.
I would like also to thank all the people that helped me during the time spent in the *STMicroelectronics* application laboratory. I think to M. *Pascal Nonier*, the DVD Front-End application team manager, and to M. *Heinz-Jöerg Schroeder* the DVD recorder technical advisor, whose assistance and advice have always been helpful to me, when I had to face practical problems related to the industrial system implementation. I cannot indeed forget the support and the precious help given by all the colleagues that work in the application laboratory : Melle *Claire Verilhac*, Mme *Roselyne Haller*, M. *Jean-Michel Goiran*, M. *Yann Morlec*, M. *Laurent Lavernhe*, M. *Thierry*

Avons-Bariot, M. *Mickael Guene*, M. *Patrick Simeoni* and M. *Christophe Viroulaud*.
A special thank to M. *Stefano Groppetti*, the DVD Front-End division director, for having integrated my research in the application team activities, and considered me as an effective member of the division, from my arrival.

Finally, I cannot miss the occasion to express my love to my parents, who have always supported me through-out all my life and who have been certainly missing my presence, as I have been missing them, during these last four years.

Giampaolo Filardi.

"Grenoble, chaque rue une montagne" (Henry Beyle Stendhal)

Ai miei genitori,

per avermi sempre sostenuto ed incoraggiato.

Glossary

Acronyms for DVD player

AC	Alternate Current
AC-3	Dolby's surround sound digital audio system
ADC	Analog to Digital Converter
AGC	Automatic Gain Control
ALU	Arithmetic Logic Unit
CAV	Constant Angular Velocity
CD	Compact Disc
CD-DA	Compact Disc Digital Audio
CD-i	Compact Disc interactive
CD-R	Compact Disc Recordable (write once)
CD-ROM	Compact Disc Read-Only Memory
CD-RW	Compact Disc Recordable-Writable (re-writable)
CIRC	Cross-Interleaved Reed-Solomon Code
CLV	Constant Linear Velocity
CPU	Central Process Unit
DAC	Digital to Analog Converter
DC	Direct Current
DMA	Direct Memory Access
DSA	Dynamic Signal Analyzer
DSP	Digital Signal Processor
DVD	Digital Versatile Disc
DVD-R	Digital Versatile Disc Recordable (write once)
DVD-RAM	Digital Versatile Disc Rewritable
DVD-ROM	Digital Versatile Disc Read-Only Memory
DVD-RW	Digital Versatile Disc Recordable-Writable (re-writable)
ECC	Error Correction Code
EDC	Error Detection Code
EFM	Eight-to-Fourteen Modulation
FE	Focus Error
FFT	Fast Fourier Transform
Gb	Giga byte
GMB	Gain of the Main spot Beam
HF	High Frequency

HPF	High-Pass Filter
IC	Integrated Circuit
Kb	Kilo byte
Laser	Light amplification by stimulated emission of radiation
LFT	Linear Fractional Transformation
LTI	Linear Time Invariant
LPF	Low-Pass Filter
LSB	Least Significant Bit
Mb	Mega byte
MIMO	Multiple Input Multiple Output
MMCD	Multi Media Compact Disc
MLP	Median Lossless Packing
M-PEG	ISO/CCITT Moving Pictures Expert Group
MSB	Most Significant Bit
MTF	Modulation Transfer Function
NA	Numerical Aperture
NCU	Non Linear Control Unit
OPU	Optical Pick-up Unit
PCM	Pulse Code Modulation
PLL	Phase Locked Loop
PRML	Partial Response Maximum Likelihood
RAM	Random Access Memory
RLL	Run-Length Limited
RMS	Root Mean-Squared
ROM	Read Only Memory
RSPC	Reed-Salomon Product Code
SD	Super Disc
SISO	Single Input Single Output
SMAC	Smart Multiplier and Adder
SNR	Signal-to-Noise Ratio
TE	Tracking error

Symbols

A	Maximum amplitude of the radial deviation from the track
A/D	Analog to Digital
A_0	Optical amplitude of the zeroth diffracted order
A_1	Optical amplitude of the first diffracted order
A_D	Detection level for the HF signal
A_s	Amplitude of the sinus wave, used in the AGC procedure

$\underline{A_{sw}}$	Swept sine DC offset level, in V
$\overline{A_{sw}}$	Swept sine peak amplitude, in V_{pk}
$\vec{B}$	Magnetic field, in T
B_{C}	DSP coefficients binary wordlength
B_{D}	DSP data binary wordlength
$c_{i_{Dec}}$	Value of a DSP 8-bit coefficient, in decimal
$c_{i_{Hex}}$	Value of a DSP 8-bit coefficient, in hexadecimal
$d_{i_{Dec}}$	Value of a DSP 16-bit data register, in decimal
$d_{i_{Hex}}$	Value of a DSP 16-bit data register, in hexadecimal
$r_{i_{Hex}}$	Value of a DSP 25-bit limiter output, in hexadecimal
d	Pit depth, in μm
d_{R}	Radial distance of the spot with respect to the disc center hole, in mm
D/A	Digital to Analog
D	Damping constant (viscous friction), in Ns/m for linear displacement
f	Frequency, in Hz
f_c	Cross-over frequency of the open loop transfer function, in Hz
f_S	Bandwidth of the output sensitivity function, in Hz
f_t	Bandwidth of the closed-loop transfer function, in Hz
$f_{c_{\mathrm{F}}}$	Cross-over frequency of the focus open loop transfer function, in Hz
$f_{c_{\mathrm{R}}}$	Cross-over frequency of the radial open loop transfer function, in Hz
f_{ch}	Channel bit rate, in Mb/s
$f_{H_{\mathrm{F}}}$	Focus open loop transfer function highest corner frequency, in Hz
$f_{H_{\mathrm{R}}}$	Radial open loop transfer function highest corner frequency, in Hz
f_{kT}	Frequency of a kT 8:16 modulation pattern, in Hz
$f_{L_{\mathrm{F}}}$	Focus open loop transfer function lowest corner frequency, in Hz
$f_{L_{\mathrm{R}}}$	Radial open loop transfer function lowest corner frequency, in Hz
f_0	Actuator resonance frequency, in Hz
f_{pit}	Temporal frequency generated by the spiral track scanning
f_{rot}	Disc rotational frequency, in Hz
f_s	Sampling frequency used for digital computation in the servo DSP
f_{Dec}	Sampling frequency used in the servo Decimation block
$f_{s_{DSA}}$	Sampling frequency used by the Dynamic Signal Analyzer
f_{SysClk}	Front-End system clock frequency
F	Force moving the actuator, in N
G_{if}	Constant gains of the focus loop controller implementation scheme
G_{it}	Constant gains of the radial loop controller implementation scheme
g_{opt}	Constant defining the optical gain per unit of length, in cm^{-1}
g_d	Actuator drivers gain, in V/A
h	Spot position error signal as controlled by a focus/radial servo loop
h_{max}	Maximum allowable amplitude of the spot position error signal, in m

I_3	Modulation peak value, generated by the shortest pit/lands pattern
I_{3H}	HF highest reflectivity amplitude, for the shortest pit/lands pattern
I_{3L}	HF lowest reflectivity amplitude, for the shortest pit/lands pattern
I_{14}	Modulation peak value, for the largest pit/lands pattern
I_{14H}	HF highest reflectivity amplitude, for by the largest pit/lands pattern
I_{14L}	HF lowest reflectivity amplitude, for the largest pit/lands pattern
K_{if}	Coefficients value of the focus loop controller implementation scheme
K_{it}	Coefficients value of the radial loop controller implementation scheme
K_e	Back-emf constant, in Wb/m
k	Elastic constant of a spring, in N/m
$\overrightarrow{l}$	Spool geometric length, in m
L	Inductance of the actuator coils, in H
L_{kT}	Physical length of a pit/land, measured along the disc spiral
L_{3T}	Physical length of the shortest pit/land, measured along the disc spiral
L_{14T}	Physical length of the longest pit/land, measured along the disc spiral
M	Moving mass of the actuator, in Kg
N	Over-speed (X-factor) of the disc scanning velocity
NA	Numerical aperture
N_{av}	Number of averages used by the DSA in swept sine mode
N_f	Number of frequency points used by the DSA in swept sine mode
N_{sw}	Number of resolution lines used by the DSA in swept sine mode
n_{C}	Number of coefficients contained in the DSP coefficient RAM
n_{D}	Number of data memory locations contained in the DSP data RAM
p	Spatial period of the disc pit/land structure, in μm^{-1}
q	Track pitch, in μm
Q	Amplitude of the actuator peak at f_0, in dB
r	Disc radius at the current read-out point, in mm
R	Electrical resistance of the actuator, in Ω
R_{Airy}	Radius of the Airy disc, in μm
R_{sw}	Swept sine resolution R_{sw}
s	Laplace complex variable
$s(t)$	Sinus wave, used in the AGC procedure, as function of time
S_{DC}	Actuator DC sensitivity, in mm/V
S_{ini}	Initial position of data clusters along the disc spiral
S_{fin}	Final position of data clusters along the disc spiral
t	Time, in s
t_r	Rise time of the system closed-loop response, in s
$t_{r_{\mathrm{F}}}$	Rise time of the focus system closed-loop response, in s
$t_{r_{\mathrm{R}}}$	Rise time of the radial system closed-loop response, in s
T_{in}	Swept sine integration time, in s

v_a	Linear velocity of recorded data, in m/s
V_{pk}	Peak amplitude, in V
x	Actuator linear displacement along the radial direction, in m
x_{max}	Maximum deviations from nominal position, in m
x_{in}	Position of the *lead-in* area with respect to the disc center hole, in m
x_{out}	Position of the *lead-out* area with respect to the disc center hole, in m
$\ddot{x}_{max}$	Maximum acceleration of the scanning point, in m/s^2
z	Actuator linear displacement along the vertical direction, in m
ΔN_{tr}	Number of tracks crossed during a seek action
ΔS	Closed-loop minimum required DC sensitivity, in dB
Δx	Spatial frequency of the periodic pits grating, in μm^{-1}
Δz	Focal depth, in μm
α	Multiplicative coefficient
α_1	Temporary variable
α_2	Temporary variable
α_3	Factor of the photo-detector quadrants phase contribution
β	Pit length
γ	Pit width
ϵ	Disc nominal eccentricity, in μ m
ζ	Multiplicative factor used for the swept sine time-depending frequency
θ	Vector of the optical device unknown parameters
κ	Value of an arbitrary DSP data memory location
κ_m	Arbitrary scale factor used to represent DSP data
λ	Laser wavelength, in nm
μ	Magnetic permeability
ϱ	Vector of the optical device known parameters
τ	Time constant, in s
φ_m	Phase margin, in deg
Φ_{max}	Laser spot opening angle, in rad
χ	Value of an arbitrary DSP coefficient memory location
χ_m	Arbitrary scale factor used to represent DSP coefficients
ψ_{10}	Phase shift between zeroth and first diffracted orders, in rad
ω	Angular frequency, in rad

Notation

$3T$	Smallest modulation pattern
$14T$	Largest modulation pattern
$C(s)$	Controller transfer function
$C_{\mathrm{F}}(s)$	Focus loop Controller transfer function

$C_{\mathrm{R}}(s)$	Radial Controller transfer function
$e(t)$	Spot position error signal, as function of time
$e_{\mathrm{F}}(t)$	Spot position focus error signal, as function of time
$e_{\mathrm{F}}(\Delta z)$	Spot position focus error signal, as function of Δz
$\hat{e}_{\mathrm{F}}(\Delta z, \theta)$	Model of the spot position focus error signal, as function of (Δz, θ)
$e_{\mathrm{R}}(t)$	Spot position radial error signal, as function of time
$e_{\mathrm{R}}(\Delta x)$	Spot position radial error signal, as function of Δx
$\hat{e}_{\mathrm{R}}(\Delta x, \theta)$	Model of the spot position radial error signal, as function of (Δx, θ)
$E(s)$	Spot position error signal, in Laplace domain
$f(t)$	Force, as function of time, as function of time
$F(s)$	Force, in Laplace domain
FE	Measured focus error signal, at the output of a DSP register
F_{out}	Measured focus actuator signal, at the output of a DSP register
$H(s)$	Actuator plus power drivers transfer function
$H_{ACT}(s)$	Actuator transfer function
$i(t)$	Electrical current, as function of time
$I_{det}(t)$	Intensity of the reflected light received by the photo-detector
$I(s)$	Electrical current, in Laplace domain
$J(\theta)$	Weighted least-square criterium used for curve fitting
kT	Modulation pattern of $k-1$ zeros between two ones
K_{F}	Gain of the focus loop actuator driver
K_{R}	Gain of the focus loop actuator driver
$L(s)$	Open-loop transfer function
$MTF(\Delta x)$	Modulation transfer function, as function of the spatial frequency Δx
$P(s)$	Plant transfer function
$P_{est}(j\omega)$	Estimated plant transfer functions
$Puu(j\omega)$	Power spectrum of the signal u
$r(t)$	Disturbances affecting the control loop (tracking disturbance)
$\widehat{R}$	Radial error signal power spectrum, in Hz/V^2
$S_{\mathrm{i}}(t)$	Photo-detector high-frequency content
$S(s)$	Perturbation-output transfer function
$SP(s)$	Perturbation-input transfer function
TE	Measured radial error signal, at the output of a DSP register
T_{out}	Measured radial actuator signal, at the output of a DSP register
$T(s)$	Closed-loop transfer function
$u(t)$	Actuators control signal, as function of time
$U(s)$	Actuators control signal, in Laplace domain
$v(t)$	External excitation signal, as function of time

$V(s)$	External excitation signal, in Laplace domain
$x(t)$	Linear displacement, as function of time
$X_a(t)$	Actuator position with respect to the sledge, in m
$X(s)$	Linear displacement, in Laplace domain
$\Xi(j\omega)$	Coherence function, used during curve fit procedure

Chapter 1

Introduction

Optical disc drives are widely used today to hold music, store data or record digital movies. Applications of optical disc drive systems in consumer electronic products demand an enhancement of tracking control behavior to respect strict performance specifications imposed by an increasing information density recorded on the optical disc and a faster data access-time.

This work has been carried out at the DVD (Digital Versatile Disc) division application laboratories of STMicroelectronics Grenoble, and it deals with controllers design methodologies applied to a large consumer-mass product such as the DVD-video player.
Like all equipment that uses MPEG (Moving Picture Experts Group), the technology that is almost universally employed to compress audio-video content before it is broadcasted or recorded, DVD players contain two basic subsystems known as the *Front-End* and the *Back-End*.
The Front-End handles all of the functions required to extract the compressed MPEG data stream from the DVD disc, while the Back-End decodes the MPEG data to recreate the original content.
This research has been included in a project intended to analyze and validate a low cost and highly integrated STMicroelectronics Front-End chip, that supports dual laser for audio CD (CD-DA), for Photo and Video CD, for CD Recordable (CD-R) and Rewritable (CD-RW) and for both DVD-RW and DVD+RW, single and dual layer.
The objective of this work is the study of all the aspects linked to the optical disc reading-head servo control system, and the implementation of the servo system control algorithms on a prototype hardware platform.
The DVD-video player control part is usually composed by several blocks,

which renders the system wide and complex to analyze. Furthermore, the control loops that are in charge of positioning the laser spot along the vertical and the radial directions, represent an interesting challenge for control design, since they are the most critical and interesting to analyze, as already pointed out in Dettori [9], Dotsch et al. [17], Pohlmann [44], Stan [53] and Steinbuch et al. [57].
These are the reasons why this work will mostly focus on the study and implementation of control loops used in industrial systems to position the laser spot along the vertical and the radial directions.

1.1 Digital Consumer Market

The accelerating evolution of semiconductor technology has allowed sophisticated digital computing to be applied to an ever-increasing range of applications, creating a whole new class of "Digital Consumer Products".
The market for these products is exploding because consumers are being offered increasing performance and functionality at affordable prices. The traditional Computer, Communications and Consumer market segments are merging as they increasingly employ the same digital technology. At the same time, the complexity of the circuits that can be built on a silicon chip has reached the point where a complete system can be effectively integrated on a single chip. So, the traditional electronics value chain is giving way to a new business model where the System-on-Chip supplier takes a central role. This, in turn, is changing the way the semiconductor industry operates, since to succeed in the System-on-Chip market, semiconductor manufacturers will have to be masters of many different skills.

STMicroelectronics is a global independent semiconductor company and is a leader in developing and delivering semiconductor solutions across the spectrum of microelectronics applications. It offers its partners a total system approach that includes hardware and software intellectual property, application knowhow and a broad range of advanced technologies, that allow the company to optimize the overall solution, not just one chip.

Whether the end product is a mobile phone, an automotive engine controller, an industrial robot or a DVD player, the design team is likely to be working with digital data and software algorithms and using microprocessors or Digital Signal Processors. These products are aimed at cost-sensitive mass markets, but employ advanced digital computing techniques to provide

levels of performance and functionality, that could not have been achieved using traditional analog technologies.

For these reasons the Company has developed a worldwide network of strategic alliances, including product development with key customers, technology development with customers and other semiconductor manufacturers, and is investing a significant proportion of its sales in R&D to combine forces with top engineering schools. The partnership with the I.N.P.G (*Institut National Polytechnique de Grenoble*) and with the L.A.G (*Laboratoire d'Automatique de Grenoble*) is inscribed in this context, and the character of research and development of System-on-Chip products for DVD consumer market is at the basis of this work.

1.2 How does DVD technology differ from CD ?

Like CDs, DVD discs store data in microscopic grooves running in a spiral around the disc. All the DVD drive types use laser beams to scan these grooves, which contains the pre-recorded digital information. But DVDs use a new modulation and error correction methods, and smaller tracks.
The distance, measured in the radial direction, between adjacent physical track centerline (called *track pitch*) has been reduced from 1.6 μm for CDs to 0.74 μm for DVD discs, in order to increase the data density stored on the disc surface [59], and pass from a maximum storage capacity of 650 Mb on a CD, to 4.70 Gb on a DVD disc single layer. Moreover, DVD discs can contain about four times as many pits as a CD disc in the same area. The narrow tracks require in addition a special laser having shorter wavelength, which can't read CD-Audio, CD-ROM, CD-R and CD-RW.
As consequence, the DVD player control system has to guarantee a much higher level of accuracy and disturbance rejection than the one required for standard CD player.

1.3 Why a DVD Player ?

The control problem for a DVD player is similar to the one defined for the CD player mechanism, and it consists of guaranteeing that the laser beam used to read the data follows the track on the disc. Contrary to the old vinyl discs players, where the piezo-electric or magnetic transducer was guided by the tracks along the disc radius, in optical disc drives only the light touches the disc. Track following should be thus guaranteed by means of feedback

control, that in the current industrial applications is achieved with simple PID controllers. In the last years, however, the optical storage device mechanisms have been used for an increasing number of new applications, like the CD-ROM, Photo and Video CD, DVD-ROM and Video DVD. These new applications require higher performance levels than the original audio system conceived for CD, since higher data density on the disc and shorter data access time are demanded.

Up to now, in the DVD-video player devices produced by STMicroelectronics, the desired levels of performance have been achieved by heuristic control design and tuning, and trough expensive improvements in the system manufacturing.

The aim of this Ph.D. thesis, is to analyze a low-cost and highly integrated circuits (IC) for DVD-video players, and investigate if higher performances and robustness properties can be achieved with a more advanced control design, to allow complexity and cost reduction in manufacturing the device. Our goal is meanwhile to provide a methodology useful for designing track following control loops, that may be used for a large quantity of future products.

The demand of improving the control system performance to compensate drives manufacturing tolerances and improve disc playbility, makes the DVD-video player a good candidate for testing robust control design techniques, and use analysis tools recently developed in the field of feedback system synthesis and modelling.

1.4 Motivations of this Work

As stated in section 1, strict performance specifications imposed on optical disc drive systems demand an enhancement of tracking control behavior. In addition, due to the higher storage capacity and disc rotational speed, the spot position control system must be more accurate to cope with parameter tolerances due to mechanism mass production, as outlined in Vidal et al. [65], and guarantee an insensitivity to external disturbances, like shocks and vibrations.
Feedback control design, usually based on a mathematical description of system behavior, is a useful tool to satisfy these requirements. From experience in fact, it is well known that a robust and reliable control design is achieved

if an accurate knowledge of the plant dynamics is taken into account during the synthesis, rather than repeatedly applying fine-tuning methodologies.
Accordingly to the industrial objectives, fixed by the financial supporter of this work, and to research requirements of finding innovative solutions, an enhanced tracking control system performance and disturbance attenuation is pursued by designing controllers on the basis of a mathematical parametric model of the system. An important specification for implementation purposes is that a controller design procedure should deliver controllers of reduced complexity.
Main specifications, given in [59], for DVD players control design, define hard bounds on the amplitude that the position error signal has to respect, despite the presence of external disturbances and system parametric uncertainty caused by industrial manufacturing tolerances. As stated in Gu [25] and Xie et al. [68], the designer has to face up to physical limitations and constraints in imposing the desired system behavior. Hence, the control synthesis can be formulated as an optimization control problem, where performance specifications are taken into account and plant norm-bounded parametric uncertainties are assumed.
Control system design techniques applied to CD mechanisms have already been exposed in several papers and Ph.D thesis as in Dettori [10], [11], [12], [15] and [14]. In these works the control design is achieved by considering a trade-off between system performance specifications and robustness with respect to system parameters variations. Other studies treat the laser spot position control problem of a CD player by using more complex design technics as in Callafon et al. [7], Dotsch et al. [17], Katayama et al. [36], Stan [53], Steinbuch et al. [55] Steinbuch et al. [57], and Vidal et al. [66], but none has been published about control design techniques applied to a DVD player.
In this context, our aim is to present controllers design methodology to apply to an industrial DVD-video player spot positioning control system, by using a mathematical description of the plant. This synthesis is proposed to compute restricted complexity controllers able to comply with tough DVD disc specifications, and to experiment the achieved solutions on an industrial benchmark. An enhanced tracking performance and disturbance attenuation is obtained via norm-based control design, and the influence of drive parametric uncertainties on the system performance and robustness is analyzed by means of μ-theory.
Frequency-domain plant identification, model-based controllers design, and evaluation of performance and robustness via plant uncertainty description, are the main points treated in this work. Due to implementation constraints,

controllers complexity is kept limited, and design limitations are evaluated in simulation, before the implementation step. Experimental results, obtained on the STMicroelectronics industrial benchmark, are finally presented to compare the current industrial solution and the computed controllers.

1.5 Outline of the Work

A brief outline of this work is presented in the sequel :

Chapter 2 is substantially divided in two parts. In the first part we briefly redraw optical storage devices history and present a short overview of available CD and DVD discs formats. In the second part a general DVD player servo mechanism is presented as composed by two main parts : the optics, that retrieves the data and generates the error signals, and the servo system, that has to control the laser beam position with respect to the disc surface. Since an accurate model of position error signals generation can be useful to build a more precise servo system simulator, optical system principles and simplified analytical and numerical models of optics are firstly presented. Then, the control objectives are described.

In chapter 3 the servo system description of the DVD-video player proposed by STMicroelectronics, together with the control problem definition are given. An overview of the actual servo system solution together with implementation constraints are given. Physical properties of an electromechanic actuator of a DVD, and plant physical modelling are also presented.

In chapter 4 a frequency-domain identification of the plant is proposed. This procedure employs experimental data and curve fitting in order to obtain a simplified mathematical model of the plant. Performance analysis of the current radial controller and the study of coupling phenomena between focus and radial loop end this chapter.

Chapter 5, which treats the robust control design of the DVD-video player, can be divided in three parts.
In the first part, theoretical background on robust control is given. Then, based on performance specifications and simplified plant model knowledge, an H_∞ norm-based controller design is performed by imposing frequency templates on the system closed-loop sensitivity functions. After controller

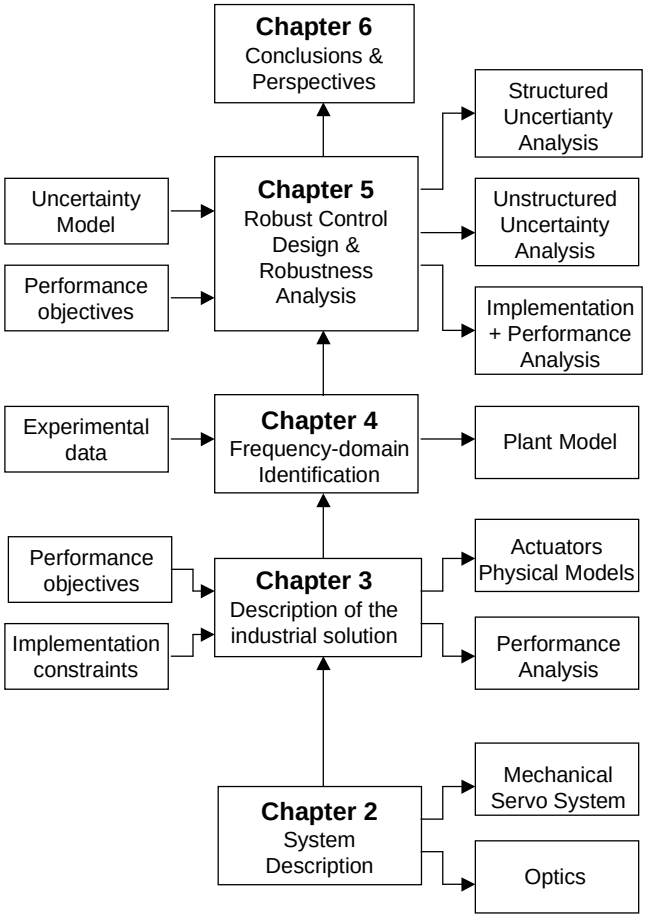

Figure 1.1: Thesis outline

order reduction, the achieved solution is implemented and tested on the industrial system, and performance and robustness analysis are presented. These results are finally compared to those obtained with the actual industrial controller.
In the second part, theoretical background on robust control design of a general system presenting parametric uncertainty is given. Parametric uncertainty are then considered to build an uncertainty model set and robust stability and performance analysis is performed by using the small gain theorem. Since this approach leads to conservative results which do not allow to identify the whole set of physical parameters to whom the control is sensitive to, in the third part of this chapter, μ-analysis is applied. Results show that to enhance controller robustness and performance, structured parametric uncertainty modelling represents a key step.
Conclusions and perspectives of the work are presented in chapter 6.

The thesis structure is schematically represented in fig. 1.1.

Chapter 2

The DVD Video Player System

2.1 Introduction

This Chapter is devoted to the description of the DVD player, and to the definition of the control problem.
Before going further in treating the control problem, we have considered necessary to describe the general principles which make the system work. This would render the subject of this work more accessible and easier to understand to the reader.
The contribution of our investigation to this chapter thus can be inscribed in the context of a pure description of the system under study, although the presentation of optics and the description of principles used to generate the servo and the read-out signals, represent in our opinion a non negligible part of our research work.
Models of the position error signal generation, important from control point of view, are often briefly explained in the literature, or treated by the mean of very complex and non linear optical theories, as in Born and Wolf [3], Bouwhuis et al. [4], and Braat [5]. In addition, little information on optical pick-up unit is usually available, from technical specifications.
Therefore, opto-geometrical and harmonic analysis have been applied to obtain approximated models of the error signal generation, as presented in Hnilička et al. [26], [27], [28], [29], and [30].
A summary of these works, as well as the obtained results, for the achievement of which the author has given a significant contribution, will be further discussed and presented in appendix A.

In section 2.2 a brief history of high-capacity devices is drawn, and in section 2.3 an overview of available DVD discs formats is presented. In section 2.4 and 2.5 the physical descriptions of the disc layout and of the system architecture are given. In section 2.6 the DVD optical system is sketched, and we give a detailed description of the optical procedure used in industrial systems for generating the position errors and the data read-out signals. In Section 2.7 the servo mechanical systems is presented.
Finally, in sections 2.8 and 2.9 the industrial control objectives together with the track disturbance description are presented, and conclusions are drawn in section 2.10.

2.2 High-capacity storage devices : a brief history

In this work we will refer to the DVD-Video format, originally conceived for pre-recorded movie playback.
The DVD and the CD represent today the most successful consumer products ever introduced on the consumer electronic market. Although the original CD format was intended for digital audio playback, its features have opened the way towards different multi-media applications, as the Compact Disc Read-Only Memory (CD-ROM), the Compact Disc interactive (CD-i), the Photo and Video CD, the CD Recordable (CD-R) and the CD Rewritable (CD-RW) [54].
Optical media as CDs and DVDs present several specific advantages in data storing. As first advantage, the plastic disc offers a support for storing a large amount of information in a small, light and easily-to-handle medium. Under this point of view, one of the main strengths of optical discs is their accepted standardization, that can be translated into a world-wide compatibility. As a second aspect, the recorded data are not affected by dust and fingerprints, making the optical discs extremely suitable for software distribution, data exchange and video and audio playback. Thirdly, since only the laser beam touches the disc surface, there is no disc degradation taking place during playback, no matter how often the disc is being used ! Finally the quality of the recorded information remains unchanged in time, even under large climatic variations.
In the late 60s, Philips developed the laser video disc, the first application of the laser for a consumer electronics product. The 30 cm disc was capable of storing up to 60 minutes of analog video per side. A low power laser was used to read the video information stored in pits in the disc surface. The

video and audio signals were represented in analog form by these pits which were arranged in a spiral pattern, like vinyl records.
The Compact Disc was launched in 1982 for high quality digital audio and has become one of the most successful examples of consumer electronics technology. The main difference between CDs and laser discs, apart from the size of disc, is that the CD uses a digital technique where the pits indicate whether a data bit is '0' or '1'. In 1984 the CD Audio specification was extended to CD-ROM for computer applications and was subsequently extended to other formats all based on the audio compact disc format.
DVD appeared in 1994 as two competing formats, Super Disc (SD) and Multimedia CD (MMCD). DVD now is the result of an agreement by both camps on a single standard to meet the requirements of all the various industries involved. DVD-Video and DVD-ROM players have been available since 1997. DVD-Audio was launched in 2000. The first versions of DVD-R and DVD-RAM have been available since 1998, with consumer models becoming available during 2001.

Before considering the DVD technology, it is interesting to briefly explore the large variety of optical storage media present nowadays on the market. In what follows, a short description of DVD disc standards and performance indicators is given. For what concerns CD discs, it can be said that they supports a range of pre-recorded formats for music, computer data, video, games and other applications. These formats are shown in fig. 2.1.
The Compact Disc, as a CD-ROM can also store computer data for PC applications. The CD interactive (CD-i), the Photo CD and the Video CD are format developed for multimedia entertainment, for storing photo files with suitable resolution for display and printing, and for containing up to 74 minutes of video using MPEG-1 plus menus and play-lists respectively. The data on a CD-ROM disc are divided into sectors containing user data and additional error correction codes. CD-i, Video CD and Photo CD are all based on the CD-ROM XA (CD-ROM for Extended Applications), which has been designed to allow audio and other data to be interleaved and read simultaneously. This avoids the need to load images first and then play CD audio tracks.

2.3 DVD Formats

DVD is a multi-application family of optical disc formats for read-only, recordable and re-writable purposes that offers high capacity data storage

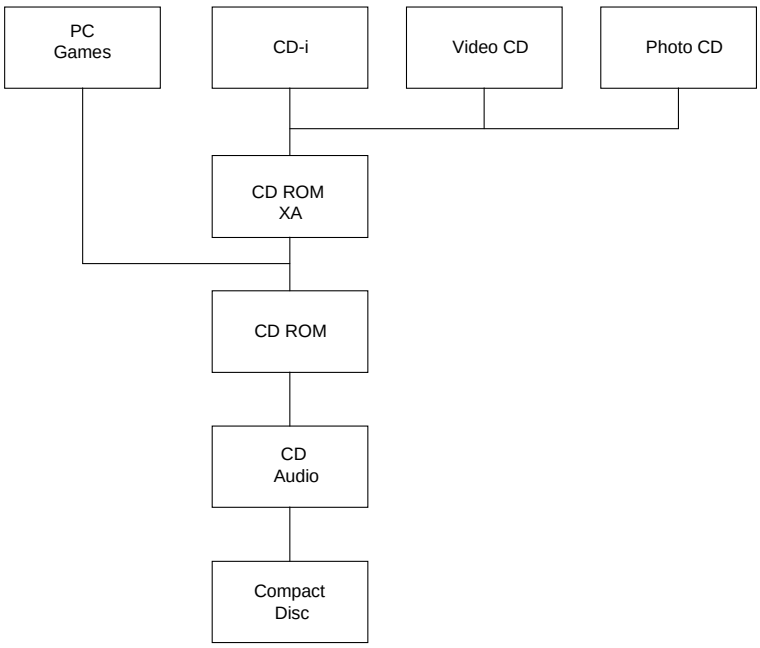

Figure 2.1: An overview of the Compact Disc standards.

medium. This technology offers an optical disc with a much larger capacity than the compact disc, since it allows to accommodate a complete movie on a single disc with very high quality multi-channel audio. The main features of the DVD formats are :

- Backwards compatibility with current CD media
- Designed from the outset for video, audio and multimedia
- 3 to 5 languages and 4 to 6 subtitles per title on one disc
- 135 minutes of movie recorded on one side of a single disc
- Digital copy protection for DVD video and DVD-Audio
- Chapter division and access, multi-angle
- Manufactory cost similar to current CD costs

DVD formats have the advantage of being compatible with current CD media, due to a specific optical design. All DVD hardware will play audio CDs and CD-ROMs and even though its physical dimensions are identical to compact disc, with the single-layer/dual-layer and single/double sided options, this format offers up to 4.7 GB read-only capacity per layer or 8.5 GB per side maximum.

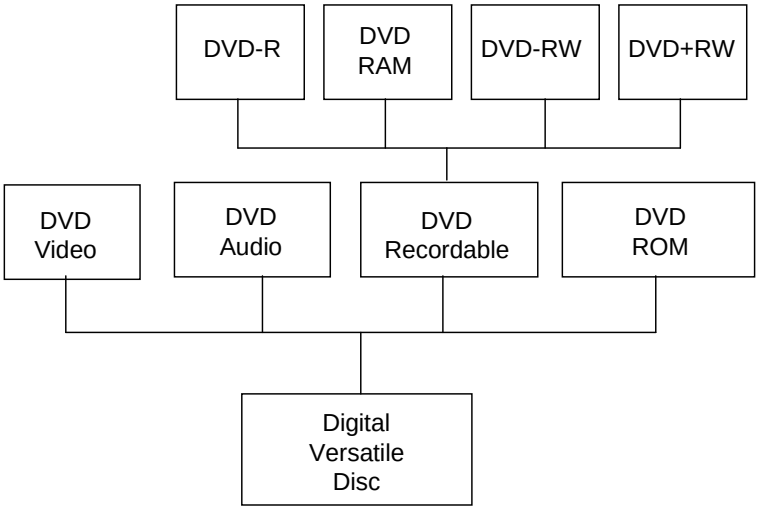

Figure 2.2: An overview of the Digital Versatile Disc standards.

The DVD formats, designed from the outset for video, audio and multimedia, offer a wide range of applications, as represented in fig. 2.2 :

- DVD-Video for full length movies with high quality video on one disc
- DVD-ROM for enhanced multimedia and game applications
- DVD-Audio for higher quality music, surround sound and optional video, graphics and other features
- Recordable and re-writable versions (DVD +/−R and DVD +/−RW)

2.3.1 DVD Video

DVD-Video has become the chosen format for high quality movies, TV series and music videos, since it offers a wide range of features including surround sounds, subtitling, choice of display formats and user interactions for non-linear video applications. This format is a global standard for pre-recorded video and was originally designed to meet the requirements of the movie industry, in particular for a complete movie on a single 'compact' optical disc. DVD-Video players were launched in Japan on November 1996 and in Europe in 1998, and since this product has grown faster than any other consumer electronics format in these regions. With the introduction of recordable and rewritable versions the DVD-Video is now set to replace VHS for home video recording and playback of pre-recorded video. The DVD-Video specifications was written by the DVD Forum working group, which includes

a number of tasks groups concerned by both read-only and recordable disc formats [59]. A more detailed description of the DVD Forum working group is presented in appendix B.

2.3.2 DVD Audio

DVD audio is the last member of the DVD family introduced on the market, designed to be the next generation high-quality audio format and able to offer very high quality, surround sound, longer playing times and additional features that are non available on CDs. DVD audio discs can also carry video and limited interactivity guaranteeing a capacity of at least 74 minutes of high quality full surround and Dolby Digital sound audio. This format could grow into a mass-market suitable for all music genres and for coupling together DVD audio and DVD-based navigation systems useful in the automotive field.

2.3.3 DVD Recordable

The DVD family would be incomplete without recordable versions. CD recordable discs were introduced in 1988 and CD-RW (the re-writable version) was introduced about 15 years after the first read-only CD was launched. Both write-once and re-writable DVD discs have been developed and are now available. There exist five different formats, all with a capacity of 4.7 GB per side : the DVD-R (write-once), the DVD-RAM (re-writable), the DVD-RW and the (re-writable), the DVD+R and the DVD+RW (re-writable). The DVD-RAM and DVD-RW are the two official re-writable DVD formats. Both formats use phase change recording where the active layer is made to change between amorphous and crystalline state by means of a laser at different power. DVD+RW is a re-writable format introduced in October 2001 by the DVD+RW Alliance (HP, Philips, Ricoh, Sony, Yamaha, Verbatim/Mitsubishi Chemical, Dell and Thomson), but it is not supported by the DVD Forum. DVD-RW discs can be used for videotape replacement, PC backup as well as home video recording. For PC applications like multisession writing, where users need to add data at a later date, DVD+RW's better defect management ensures that data is accurately written to and read from the disc.
Compatibility of DVD recordable format is an issue nowadays as not all these formats will play on existing DVD players and DVD-ROM drives.
In February 2002 a DVD consumer player producers forum has taken place in Japan to define guidelines for a new digital movie recording format called

Blu-ray Disc, that will use a 405 nm blue-violet laser to achieve over two-hour digital high definition video recording. The Blu-ray Disc will enable to record, re-write and playback of up to 27 GB of data on a single sided single layer 12 cm diameter DVD/CD size phase-changing optical disc.

2.3.4 DVD-ROM

DVD-ROM can be compared with CD-ROM, but it provides at least 7 times the capacity of a CD-ROM, so that it can store much more data. The term DVD-ROM can be used to define both the physical and logical format of pre-recorded DVD discs and also refers to computer multimedia applications of DVD. DVD-ROM disc are being used for games, multimedia or other computer based applications, where a big amount of pre-recorded data is needed, and its requirements have been established by the Technical Working Group, representing the computer industry.

2.4 Data reading and disc physical layout

The DVD player is a device that optically decodes and reproduces digital data stored on a reflective plastic disc. The DVD technical specifications are contained in five books published by Toshiba [59], and listed in table 2.1.

Table 2.1: *DVD Book Specifications*

Book	Name	Part1 Physical	Part2 Application
A	DVD-ROM	Read-only	Not defined
B	DVD-Video	Read-only	MPEG-2 video
C	DVD-Audio	Read-only	MLP[1]/PCM[2]
D	DVD-R	Write once	Not defined
E	DVD-RAM/RW	Re-writable	Not defined

Remark 1 *MLP : Meridian Lossless Packing, compression decoding needed to accommodate the highest quality in surround sound.*

Remark 2 *PCM : Pulse Code Modulation for multi-channel and stereo encoding format.*

Table 2.2 summarizes the physical parameters of DVD and compares them with those of CD. Although identical in appearance, DVDs and CDs differ in a number of key physical parameters. To meet the requirements for 133 minutes of high quality video on one side of a single disc, it is required to

Table 2.2: *Physical parameters of CD and DVD*

Parameters	CD	DVD
Layers	single	single/dual
Substrate thickness	1.2 mm	0.6 mm
Sides	1	2
Capacity	0.68 GB	4.7/17 GB
Track pitch	1.6 μm	0.74 μm
Minimum pit length	0.83 μm	0.4 μm
Scan velocity v_a	1.3 m/s	3.49/3.84 m/s
Wavelength	780 nm	635/650 nm
Numerical aperture	0.45	0.6
Modulation	EFM [3]	8 to 16
ECC[4]	CIRC[5]	RSPC[6]
Subcode/Tracks	Yes	No

Remark 3 *EFM : Eight to Fourteen Modulation used on every CD for modulation and error correction.*

Remark 4 *ECC : Error Correction Code. CDs use CIRC[5], DVD discs use RSPC[6].*

Remark 5 *CIRC : Cross Interleaved Red-Solomon Code, which adds two dimensional parity information, to correct errors in CDs, and also interleaves the data on the disc to protect from burst errors.*

Remark 6 *RSPC : Reed-Solomon Product Code to correct errors in DVDs.*

use a thinner substrate (0.6mm in DVDs instead of 1.2mm for CDs) two of which are bonded together, as presented in fig 2.3, to form a disc that has the same thickness than a CD. The use of a sandwich of two substrates allows a range of formats from one layer to four and one or two sides, giving capacities from 4.7 GB to as much as 17.1 GB, as presented in fig 2.4.
On a DVD disc, data are stored in files, that are accessible using a file system common to all DVD discs. The digital information is organized as sectors of 2048 bytes plus 12 bytes of header data as shown in fig. 2.5. Blocks of 16 sectors are error protected using RSPC (Reed Solomon Product Code). The PI and PO data are parity bytes calculated horizontally and vertically over the data bytes. In addition DVD uses an 8 to 16 modulation scheme, giving pit lengths of 3 to 14 (minimum to maximum length) compared with CD's 3 to 11 obtained with EFM (Eight to Fourteen) modulation. This makes the jitter specification slightly tighter for DVD discs.

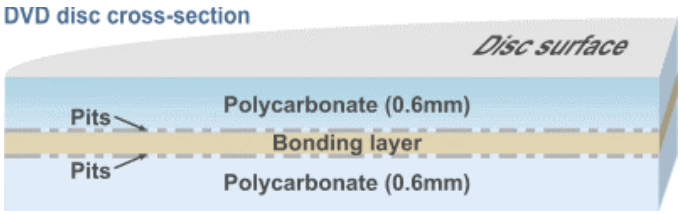

Figure 2.3: Schematic view of the DVD cross section.

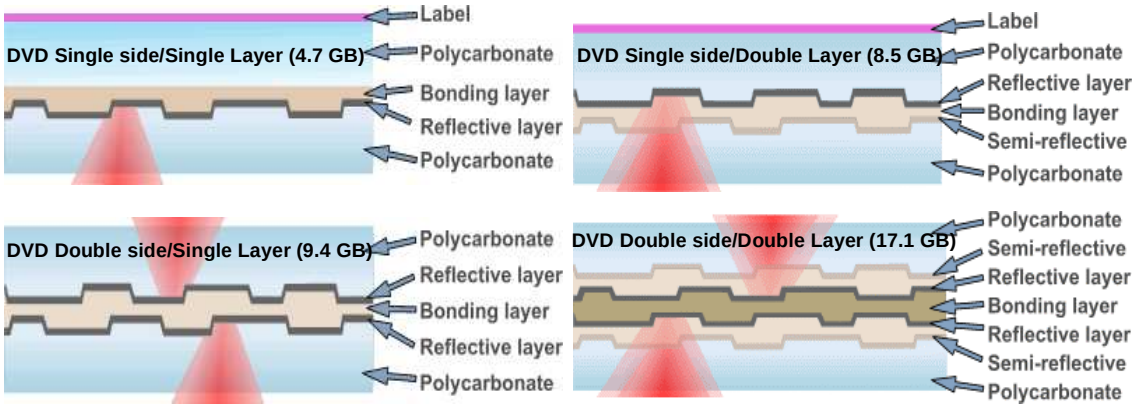

Figure 2.4: Schematic view of DVD formats.

Data are physically contained on a spiral-shaped track that evolves from the innermost to the outermost position of the disc. The track is constituted by a sequence of *pits* of varying length located at varying distance from each other, as shown in fig. 2.6. The shape of the pits is prefixed and their length can be distinguished because of the discrete distribution along the track, as shown in fig. 2.7. Pits length β is always multiple of the minimum pit length, fixed equal to 0.4 μm for a DVD disc, and the the distance of two subsequent track locations along the disc radius q (*track pitch*) is equal to 0.74 μm. The width of the pit is indicated with γ. Another important parameter of the pit geometry is its depth d, fixed equal to 80 nm for a DVD disc. Its value determines the reflected laser beam phase, generating then constructive or destructive beam interferences. The binary signal is given by the relief of the track that is detected via light intensity measurements.

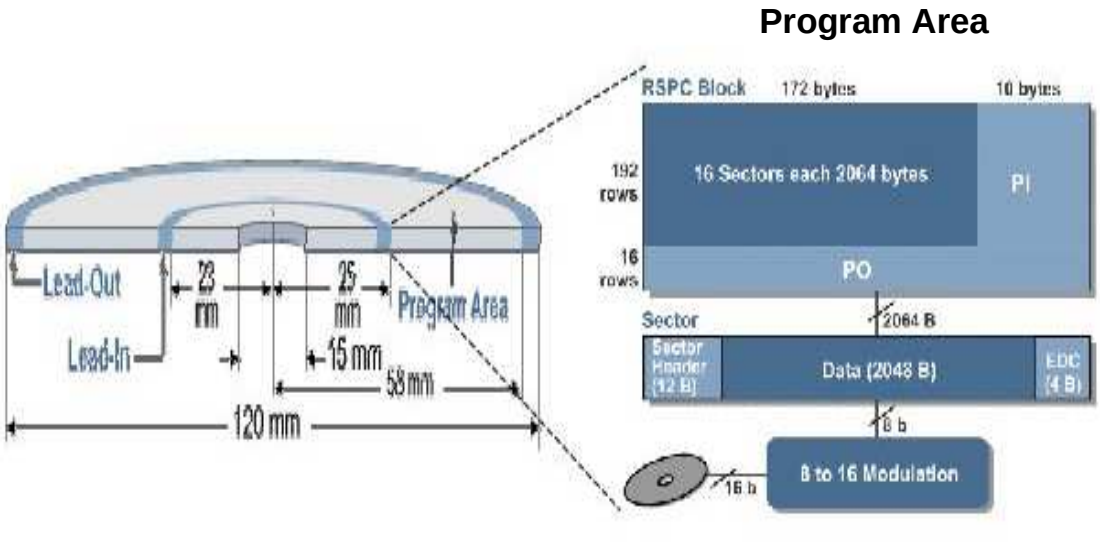

Figure 2.5: Schematic view of data organization on a DVD disc.

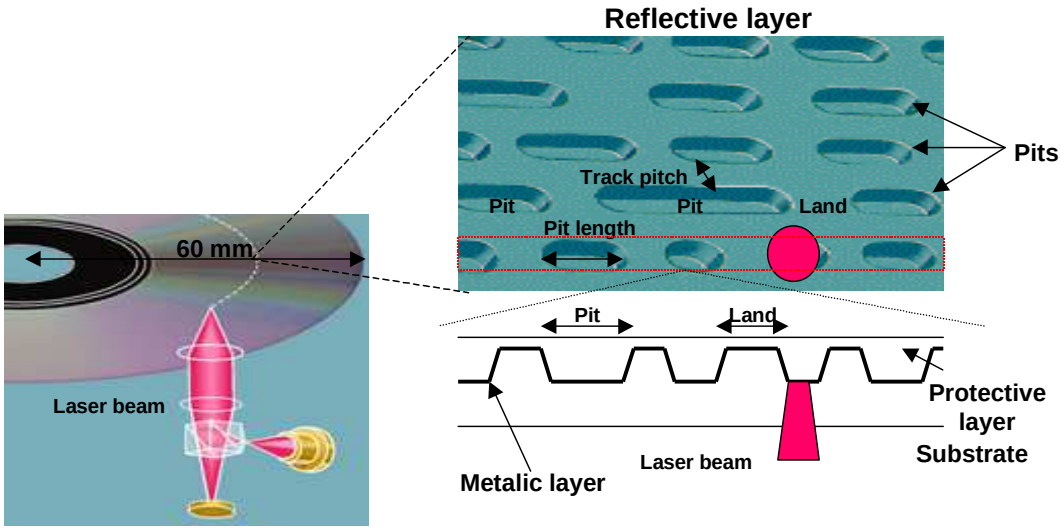

Figure 2.6: Schematic view of the DVD disc impressed structure.

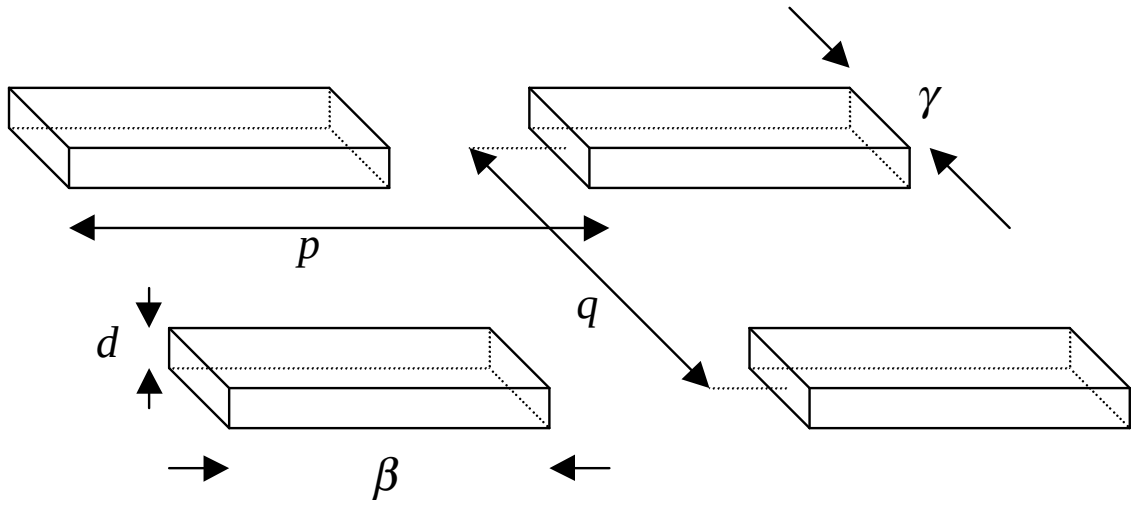

Figure 2.7: Simplified view of the disc impressed structure.

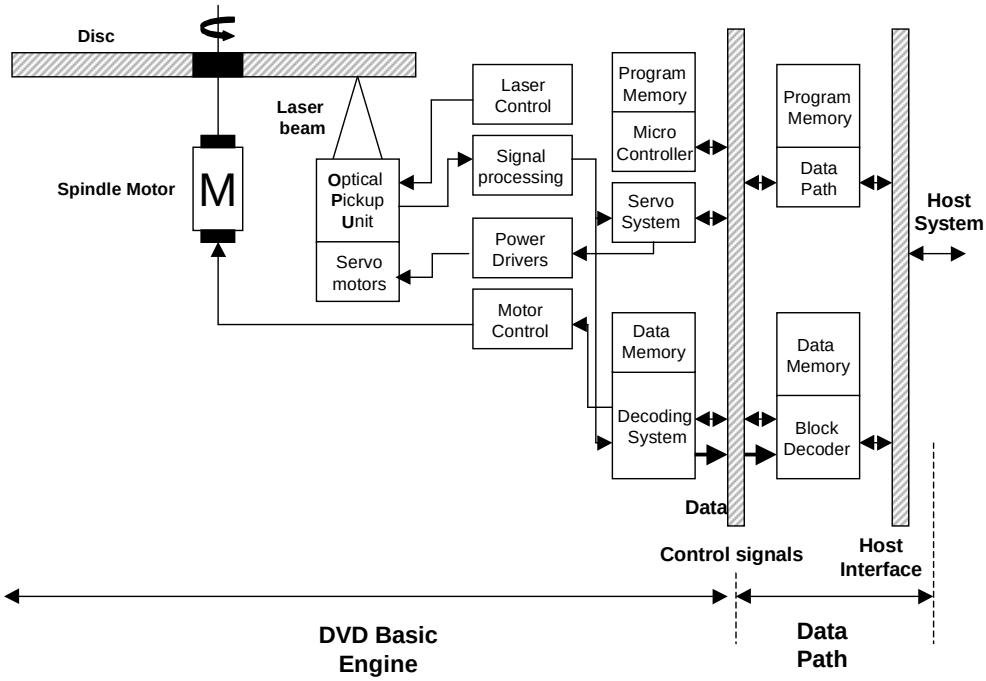

Figure 2.8: Schematic view of the DVD architecture.

2.5 DVD drive architecture

Almost all DVD drives, rely on the same system architecture. In general, the drive can be divided into a basic engine and a data path, separated by a control signals bus, as presented in fig. 2.8. Apart from other specific DVD functions, the data path provides also the interface between the basic engine and the host system.

The rotating disk is read out without any mechanical contact with its surface, and an optical pick-up unit (OPU) generates a laser beam to the disk and receives back the reflected light, optically modulated by the disk geometrical structure. The OPU contains, among other components, a semiconductor laser, optical elements to guide the laser beam, and a photo detector used to transform the optical power into current.

By properly processing this current, two servo signals are derived for positioning the laser beam along the disk radius and spiral, respectively. At the same time, a high-frequency signal, carrying the information recorded on the disk, is also extracted and forwarded to the decoding electronics.

The laser beam displacement along the vertical and radial directions, with respect to the disk, is accomplished by two voice-coil motors. These actuators keep the laser beam on track and in focus by executing fine displacements. An additional servo motor is also used to perform large displacements of the laser spot along the disk radial direction. This electromechanical construction is usually called as "two-stage" or "sledge-actuator" servo [54]. Functionalities of all electromechanical components are governed by a

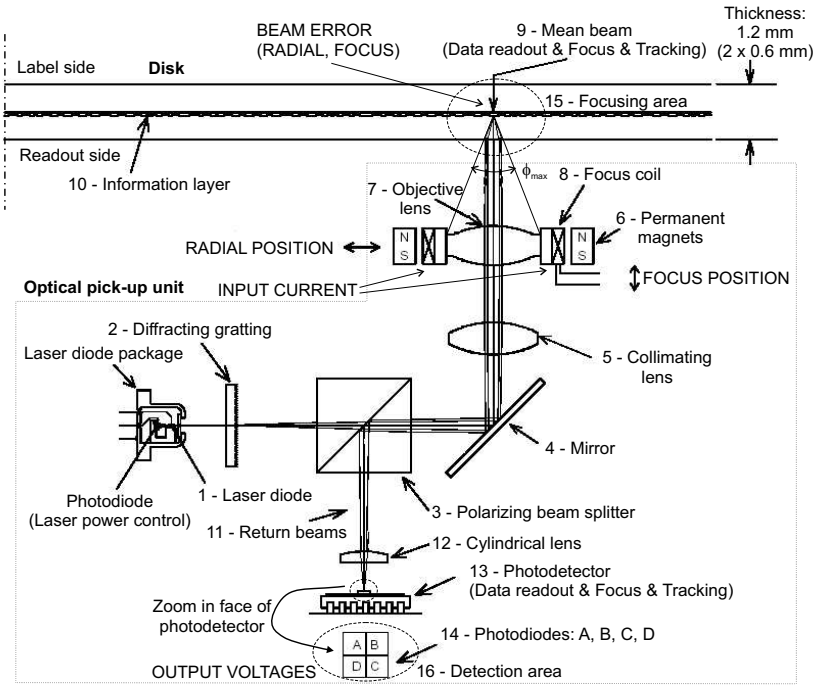

Figure 2.9: Block scheme of the optical pick-up unit (OPU).

firmware running on a micro controller. The decoding electronics process the incoming high-frequency signal and regenerates the digital data, stored on the disc, that are then processed by the data path and send to the host system. In the following sections a more detailed description of the DVD optics and servo mechanical subsystem is presented.

2.6 The Optics

For applications such as reading digital information from an optical medium as a DVD, the need for a real-time control of the objective lens position is imperative. The laser beam, which is used to read the recorded data from the disk, must be focused on its surface and follow the track very accurately. This task is accomplished by the position control loops, which use the position error signals, generated by the optical device, to deliver inputs to the vertical and radial actuators. Thus, it becomes of paramount importance to physically describe optics behavior, and model their influence on the control loops.

Many methods have been developed to generate focus or tracking error signals, starting from the reflected laser beam, as exposed in Born and Wolf [3], Bouwhuis et al. [4], Braat et al. [6], Isaloilović [34], Pohlmann [44], and Stan [54], and implemented in industrial products, like CD and DVD-video players. Nevertheless, most of them have dealt with optical disc drives readout signal generation, or jitter and cross-talk measurements, which require to apply complex algorithms, and give only an indication about compati-

bility between CD and DVD drives. Modelling of position error signal of optical disc drives is often shortly explained in the literature, and rough approximations are assumed to skip non-linear effects due to disc imperfections, optical misalignment, and cross-coupling phenomena. In addition, there exist simulation programs having numerical models of optical signal generation, but they are only available for company research use.
So, despite its practical importance from control point of view, no complete analytical or numerical model of the error signals generation is available in the literature, to our knowledge.

It is not our intention in this section to discuss about error signals generation modelling, because this is not the main goal of this work. This subject will be treated in appendix A, where the works presented in Hnilička et al. [26], [27], [28], [29], and [30] are exposed. Here, only a general description of the optical system, used to generate the servo signals in DVD players, is presented.

A DVD disc is composed of transparent substrates of polycarbonate, which contain a continuous spiral of impressed pits, and are covered with a thin metallic layer. The laser beam reads this profile trough the transparent substrate, by detecting the reflected amount of light, as shown in fig. 2.9.
The system is composed of an optical pick-up unit (OPU) that retrieves data from the disc. A laser diode (1) emits a light beam, having a wavelength $\lambda = 650\ nm$ for DVD discs, which is guided trough the optical elements (2, 3, 4, 5, 7) to the disc information layer (10). The objective lens (7) can be moved along the vertical direction, to correctly focus the spot on the disc, and in the radial direction, to perform track following. This lens is suspended by two leaf spring and its position is controlled by electromagnets, disposed along the vertical and the radial directions. To focus the incident beam on the disc, and to allow fine displacements of the objective lens along the disc radius, a focus and a radial coil (8) are placed in the electromagnetic field generated by a permanent magnet (6). The main beam of the incident light (9) hits the disc at a focusing area (15), and it is reflected by the information layer (10). The reflected beam (11) passes trough optical elements (3, 4, 5) to be focused, by mean of a cylindrical lens (7), on a four-quadrant photo-detectors (13).

The light reflected by pits can be described as an electromagnetic wave, characterized by the same amplitude but opposite phase to the incident beam. This produces destructive interferences that limits the amount of

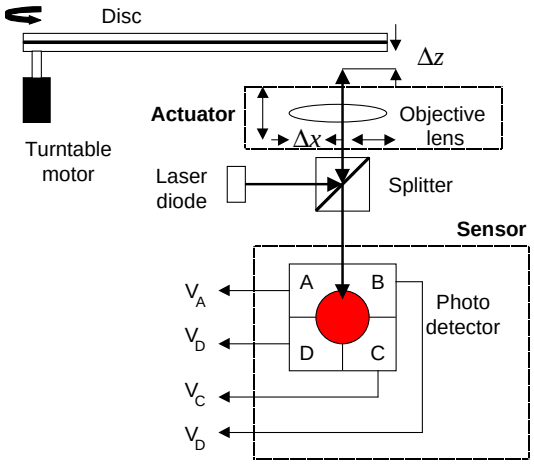

Figure 2.10: Block-scheme of the DVD optical system.

light coming back from the pits. Besides between the pits, lands behaves like a mirror with 100 % of reflectivity. Therefore, the light reflected by lands results to be brighter.
In fig.2.10 the block-scheme of the DVD optical system is presented. The four photo-detectors (A, B, C, D), receive the light reflected from the disc surface, and generate the output voltages V_A, V_B, V_C and V_D that are used to retrieve both data recorded on the disc, and position error signals (*focus* and *tracking* errors), used to measure the displacement of the laser spot, with respect to the track position and the disc surface.

2.6.1 Optical Error Signals

From physical optics it is well known that the light beam passing trough an aperture of dimension smaller than the light wavelength λ gives rise to far-field diffraction. It can be shown that a similar phenomenon is also produced if the aperture is situated before a converging lens. This principle is used in CD and DVD drives, since the pits pre-impressed structure acts as a circular aperture, through which the laser beam is reflected and send to the objective collimating lens.
The resulting light intensity can be described by a squared first-order Bessel function, having maximum intensity in correspondence of a bright circular region, called *airy disc*, that is surrounded by alternate dark and bright discs as it is shown in fig. 2.11. In practice, the *airy disc* is the smallest area identified by the laser spot on the disc surface.
The airy disc radius is given by :

$$R_{airy} = \frac{0.6}{NA}\lambda = 0.65\mu m \tag{2.1}$$

where $NA = 0.6$ is the objective lens numerical aperture, and $\lambda = 650\ nm$. The numerical aperture is generally defined as $NA = \sin(\Phi_{max})$, where

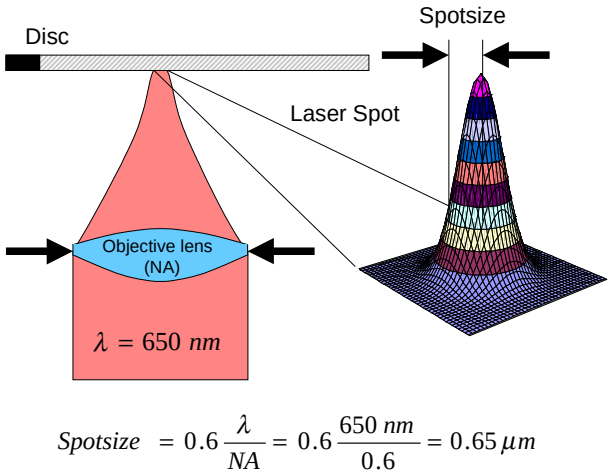

Figure 2.11: The laser spot and its light intensity.

Φ_{max} is the so-called *opening* angle, as shown in fig.2.9.
The method used in a DVD system for data read-out is that of the scanning microscope [4]. Further information can be found in [6], [28], [26].
The principle is based on the fact that sequence of pits and lands forms along the disc a two-dimensional diffraction grating, as shown in fig. 2.6 and fig. 2.7. This grating splits the incident light into multiple diffraction orders. Data read-out is accomplished by capturing, with photo-detectors, the amount of light which is inside the *overlapping* regions, formed by the light zeroth and first diffracted orders. In fig. 2.7 p denotes the smallest spatial period always equal to twice the shortest pit length. For simplicity we assume, in this figure, that p is constant along the tangential direction. The main grating is formed by a sequence of pits having variable length and disposed, in the the tangential direction, along a spiral-shaped trajectory. The other grating is disposed along the disc radius and has fixed period q equal to the track pitch. The information data is coded on the first type of grating, which is tangential to the disc spiral and moves with a given linear velocity Nv_a.
The incident laser spot decodes the information by detecting the light in the overlapping regions, where destruction diffraction phenomena take place, as shown in fig. 2.12. Here, the far field pattern generated by a disc with a regular information pattern is presented. The centers of the diffracted orders are off-set by a distance $\pm X_0 = \pm\lambda/(pNA)$ and $\pm Y_0 = \pm\lambda/(qNA)$ in the X and Y directions. NA is the numerical aperture of the scanning laser beam with a wavelength λ. The detection region is the inner part of the

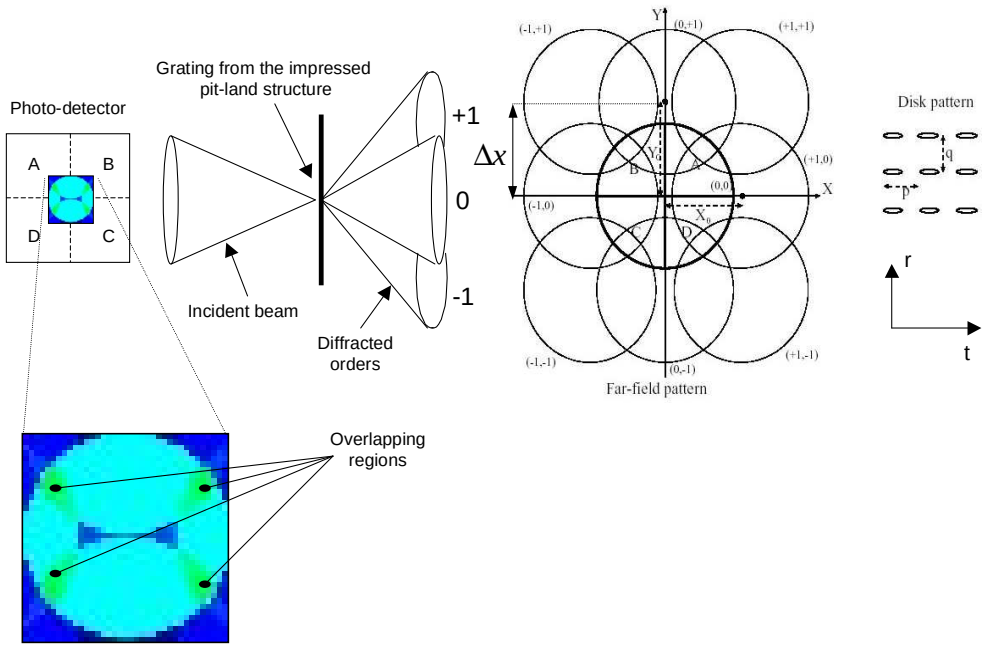

Figure 2.12: Diffracted light zero and first orders, due to the impressed pits and land grating structure. $\Delta x = \lambda \setminus (pNA)$

zeroth order (heavy circle). X and Y denote the track and the radial directions, respectively. Since the pits and lands structures have variable length, these overlapping regions are affected by a spatial modulation of frequency $\Delta x = \lambda \setminus (pNA)$ (spatial frequency of periodic pits in the grating).

For control design purposes it is interesting to know how the voltages delivered by the four quadrant photo-detectors are generated. These signal are proportional to the intensity of the light received by the photo-detector, which is given by [6], [4] :

$$I_{det}(t) = 2A_0^2\left[1 + \left(\frac{A_1}{A_0}\right)^2 + 2\left(\frac{A_1}{A_0}\right) MTF(\Delta x)\cos\psi_{10}\cos\left(\frac{2\pi N v_a}{p}t\right)\right] \tag{2.2}$$

where A_0 and A_1 are the amplitudes of the zeroth and first diffracted order respectively, ψ_{10} is the phase shift existing between them, and MTF is the modulation transfer function, which describes the behavior of the optical system in the optical frequency domain.
The MTF gives basically a measure of the accumulated overlapping areas depicted in fig. 2.12, which depend on the spatial frequency Δx, as follows

[35] and [54] :

$$MTF(\Delta x) = \frac{2}{\pi} \arccos\left(\frac{\Delta x}{2}\right) - \frac{\Delta x}{\pi}\sqrt{1 - \left(\frac{\Delta x}{2}\right)^2} \tag{2.3}$$

2.6.2 Focus error signal

Numerous optical properties have been used to generate focus error signal from small disc displacement in CD players, as presented in Bouwhuis et al. [4] and Stan [54], but for DVD systems, the astigmatic method is the most widely used. The principle of the astigmatic method is based upon an optical aberration, called *astigmatism*. This distortion is usually introduced by cylindrical lens (12), see fig.2.9. Fig. 2.13 represents the simplified model of the reflected beam optical path, presented in fig.2.9 from the focusing area (15) to the detection area (16). An astigmatic image is rotated with respect to its optical axis z and a focus error signal e_{F} can be extracted if a special arrangement of the four photodiodes A, B, C, D is used. The focus error signal is given by :

$$e_{\mathrm{F}}(\Delta z) = (V_{\mathrm{A}} + V_{\mathrm{C}}) - (V_{\mathrm{B}} + V_{\mathrm{D}}) \tag{2.4}$$

where V_{A}, V_{B}, V_{C}, V_{D} are voltages from the quadrants A, B, C, D of the photo-detector and Δz is the distance between the disc information layer and the objective lens (see fig.2.10). The signal e_{F} is feed back to the servo system to control the actuator fine displacement along the vertical direction. Usually, an optical system containing a cylindrical lens can be considered formed by two different sub-systems along the *sagital* (xz) and the *meridial* (yz) planes, respectively. The separation of the whole optical system in the two orthogonal planes allows to use the theory of a system formed by two centered thin lenses which are easier to describe, as stated in Born and Wolf [3].

The photo-detector (13) provides a non-linear bipolar focus error characteristic $e_{\mathrm{F}}(\Delta z)$, usually called *S-curve*, which is used to determine if the laser spot is correctly focused on the disc information layer.
In fig. 2.14 an example of the *S-curve* measured in the time-domain $e_{\mathrm{F}}(t)$ is presented. This characteristic has been obtained from the industrial DVD-video player available in the STMicroelectronics laboratories. As discussed in subsection 2.6.1, the light reflected from the impressed pit/land grating is focused on a four quadrant photo-detector, by means of optical elements.

This spot can have variable size, depending on the de-focus Δz existing between the disc layer and the focus spot.
Looking at fig. 2.13 and fig. 2.14, the principle used to generate the focus error signal, in a DVD player, can be easily resumed as follows :

- In the *optimal* focus condition $\Delta z = 0$, the laser is correctly focused with respect to the disc layer, and all the light reflected by the disc is focused on the photo-detector as a circular spot, whose intensity is equally distributed on its four quadrants. In this situation, $(V_{\mathrm{A}} + V_{\mathrm{C}}) - (V_{\mathrm{B}} + V_{\mathrm{D}}) = 0$ and the so-called *focus point* is reached (see point C in fig.2.14), where the focus control loop can be locked.

- When $\Delta z > 0$ the laser is focused too far from the disc surface, and the reflected light forms on the photo-detectors an elliptical shaped spot. The amount of light reflected on the pair A and C is bigger than the one on the pair B and D, so $(V_{\mathrm{A}} + V_{\mathrm{C}}) - (V_{\mathrm{B}} + V_{\mathrm{D}}) > 0$ and the point A is reached on the focus S-Curve.

- When $\Delta z < 0$ the laser is focused too close from the disc surface, and the reflected light forms on the photo-detectors an elliptical shaped spot. The amount of light reflected on the pair B and D is bigger than the one on the pair A and C, so $(V_{\mathrm{A}} + V_{\mathrm{C}}) - (V_{\mathrm{B}} + V_{\mathrm{D}}) < 0$ and the point B is reached on the focus S-Curve.

- When the de-focusing Δz becomes bigger (or smaller) than a pre-fixed value (see [28]), then the laser spot is reflected on the photo-detectors as a slanting straight line. In these cases, points D and E of fig.2.14 delimit the so called *linear zone* of the focus error S-curve. Inside this region the photo-detector behavior can be assumed linear, and a gain proportional to the slope of the S-curve, is used to characterize the relation between input and output signals. This is very useful for control design, as will be presented in section 2.8.

- When the laser spot is too far from the disc layer, the spot is said to be "out-of-focus", and the generated focus error signal would be zero, (from left to point F in fig.2.14). Similarly, the spot will be "out-of-focus" in the other direction, when the objective lens is too close to the disc layer, generating a reflected beam larger than the detector size (from right to point G in fig.2.14). In both cases the amount of light falling in the photo-detector is too weak to retrieve information about focusing. The *optimal* focus condition is recovered

by means of software servo algorithms, implemented on a dedicated micro controller.

Parameters characterizing the *S-curve* are specified in [43] and [45] : the area of the region delimited by its peaks is called *lock-on range*, and the physical distance corresponding to this area represents the voltage range in which the system is able to compensate the maximum actuator displacement to remain still locked. The *acquisition range* is defined as the maximum distance from the focus point C, in which e_{F} is large enough to still allow the system to perform focusing. Finally, the *S-curve* symmetry gives an indication on the quality of the error detection procedure. A very asymmetric *S-curve* would lead to measurement problems, since the system should be electronically adjusted to compensate the fact that the error signal e_{F} is not equal to zero at the system's best focus.

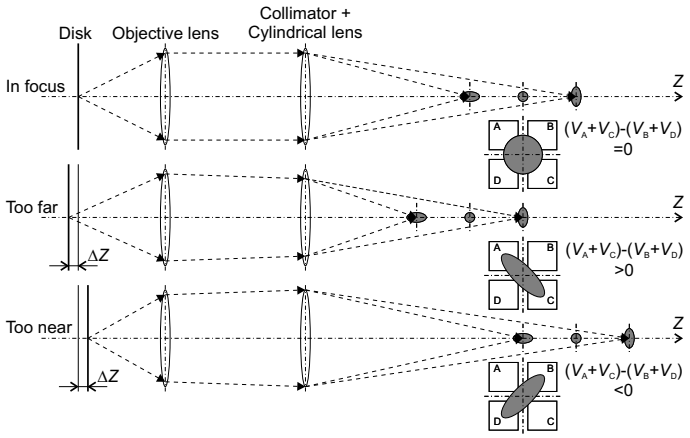

Figure 2.13: Astigmatic method for focus error signal generation.

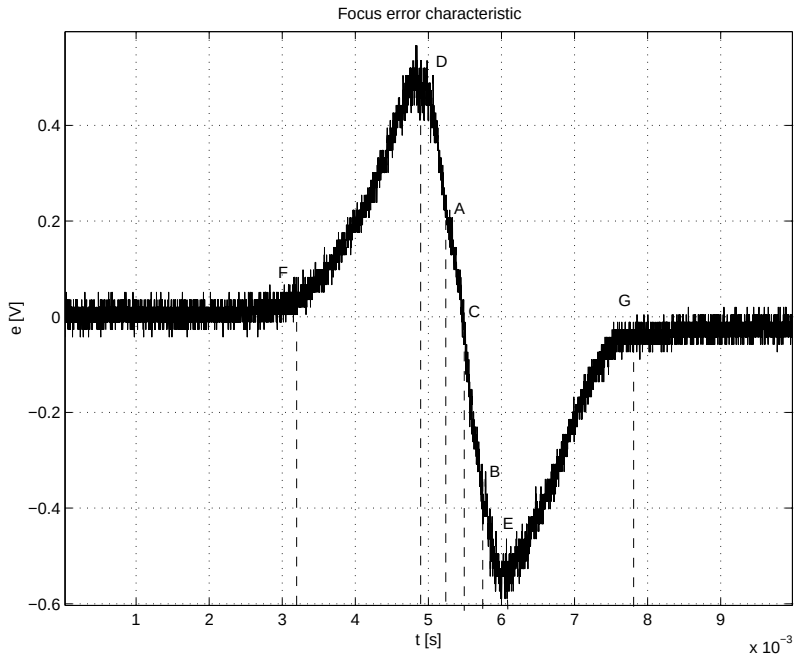

Figure 2.14: An example of S-curve measured, in the time-domain, from an industrial DVD-video player.

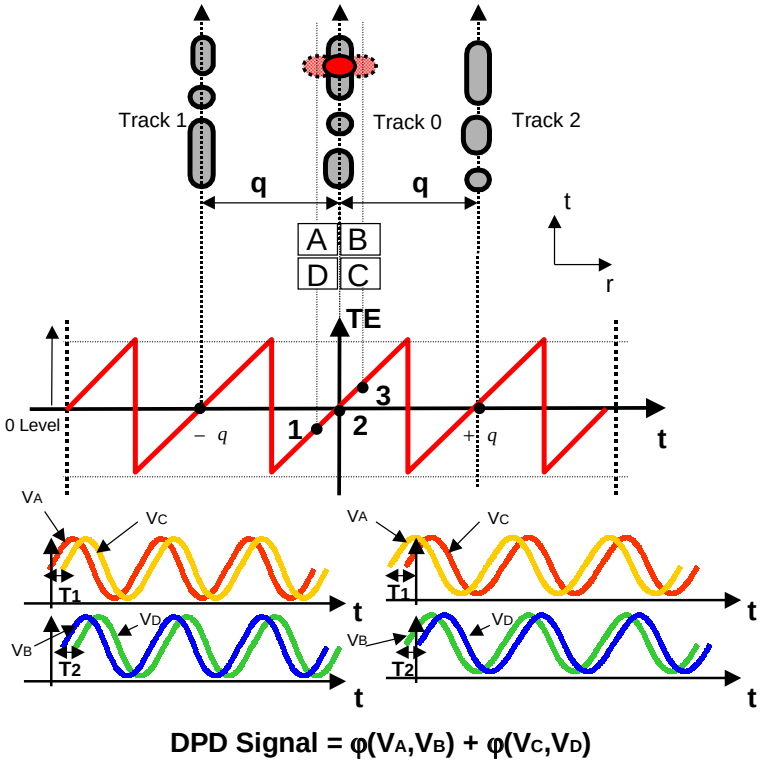

Figure 2.15: Example of DPD radial error signal generation.

2.6.3 Radial error signal

There exist many methods for generating the radial error signal e_{R} from the disc radial displacement Δx, for CD and DVD systems, as presented in Bouwhuis et al. [4], Pohlmann [44] and Stan [54]. The most common strategies are usually known as 3-beam method, radial push-pull detection, 3-beam push-pull, and radial wobble method.
For the DVD player a new method for radial error signal generation has been developed, since the smaller track pitch and the increased storage capacity have required to enhance the accuracy of the error detection strategy, while minimizing the alinement effort for the optics.

Nowadays the Differential Phase Detection (DPD) method is the one widely used in DVD systems, and there are two versions : a first method is based on the time-delay differences of the signals from photo-detectors A, B, C, D. One possibility to generate the track error signal e_{R}, is to calculate the sums of the signals from diagonal pairs of detector $(V_{\mathrm{A}}+V_{\mathrm{C}})$ and $(V_{\mathrm{B}}+V_{\mathrm{D}})$, and then measure the time difference between the rising and falling edges of this sum. This method is also called Differential Time Detection (DTD).

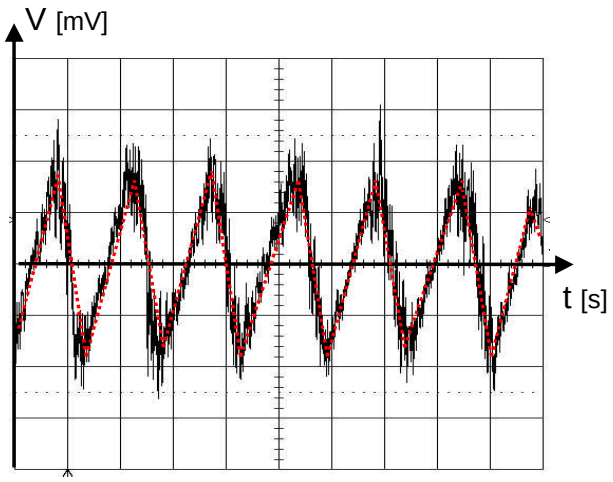

Figure 2.16: DPD radial error signal, generated by a DVD-video player optical pick-up.

A second possibility is to measure the phase differences between adjacent pairs of photodiode elements : $\varphi(V_{\mathrm{A}} + V_{\mathrm{B}}) + \varphi(V_{\mathrm{C}} + V_{\mathrm{D}})$, respectively. This signal is filtered, with a first-order low pass filter having a cut-off frequency of above 30 KHz, to give the final track error signal e_{R} [59]. This method is the one commonly called DPD, and an example of radial error signal generation, used for DVD players, is given fig. 2.15, where the point 2 corresponds to the "spot on-track" situation, besides points 1 and 3 indicate that the laser light is not perfectly centered on the scanned tack (Track 0 in fig. 2.15). q denotes the distance between two consecutive tracks, i.e. the *track pitch*.

In this work we consider this second method, since it is the one used on the industrial benchmark. One of its advantages is that the amplitude of the track error signal does not depend on the playback speed v_a, because if the rate of the edges on the detector is proportional to the playback speed, the value of time differences between edges is inversely proportional to the same parameter. Harmonic analysis and periodic data pattern are considered in Braat [5], to model the radial error signal generation in DVD players.

In fig.2.16 the measured (solid line) and the expected (dotted line) DPD radial error signal, generated by a DVD-video player, are plotted. It can be noticed that the measured signal is corrupted by noise when the laser spot is between two tracks, since the phase detection is disturbed by the *cross-talk* of the two adjacent tracks (see Bouwhuis et al. [4]).

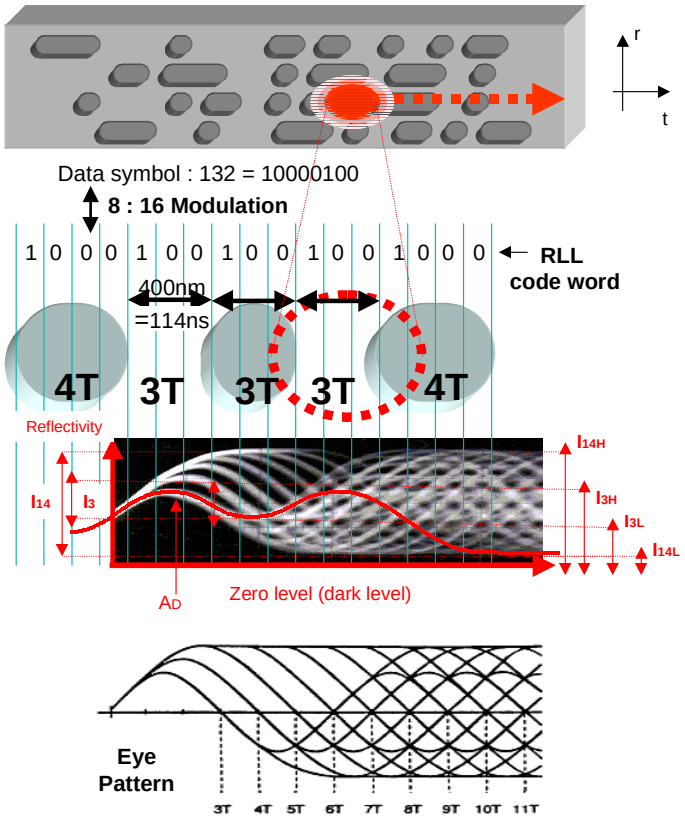

Figure 2.17: Example of HF generation for a pit/land impressed structure.

2.6.4 Generation of the HF signal

The binary data encoded on a DVD disc surface can be retrieved by summing-up the light intensity retrieved by the four photo-detector quadrants A, B, C and D. In such a way, a high-frequency signal (HF), modulated by the disc relief structure, is derived.

The so called *eye pattern* is presented in fig. 2.17, and it is obtained by superposing slices of the HF signal, synchronized with the PLL clock frequency, several times on an oscilloscope screen. Since the light reflected by pits is strongly affected by destructive interference, the HF signal reaches minimum and maximum values in correspondence of pit and land structures, respectively as can be seen in fig. 2.17.

The symbols impressed on the disc surface as sequence of pits and lands, are converted into retrievable data, by using the Eight-to-Sixteen modulation, which belongs to the class of run-length limited (RLL) codes, described in Immink [32] and Stan [54].

RLL codes are characterized by constraints in the symbol coding, where the minimum and the maximum number of identical symbols following each other is limited. In addition, from RLL codes it is also possible to retrieve the whole system clock frequency (self-clocking sequence). For the DVD

system, the minimum and maximum run-lengths are set equal to 3 and 14, respectively [59].

The minimum and the maximum fundamental frequencies of the modulation pattern can be computed by considering the channel bit rate, that is the frequency at which the binary sequence is coded, the run-length k, and the over-speed factor N, as indicated by :

$$f_{kT} = \frac{f_{ch}}{2k} N \tag{2.5}$$

where $f_{ch} = 26.16\ Mbit/s$ is the channel bit rate computed for $N = 1$, and $k = 3, \ldots, 14$. For $N = 1.5$, as on the industrial benchmark, we obtain $1.40Mhz \leq f_{kT} \leq 6.54Mhz$.

The physical length of the corresponding pit profile is given by [54] :

$$L_{kT} = k \frac{v_a}{f_{ch}} \tag{2.6}$$

where $v_a = 3.49\ m/s$ is the linear velocity of the recorded information. The length of the shortest and the longest pit/land are : $L_{3T} = 400\ nm$ and $L_{14T} = 1.866\ \mu m$, respectively.

From fig.2.17 some relevant parameter, characterizing the HF signal, can be distinguished :

- I_{14} and I_3 are the modulation peak to peak values, generated by the largest and the shortest lengths of pit or land, respectively when a 14 T or a 3T symbol is read on the disc.
- I_{14H} and I_{3H} are the highest reflectivity amplitudes of the HF signal, generated by the largest and the shortest lengths of pit or land respectively when a 14 T or a 3T symbol is read on the disc.
- I_{14L} and I_{3L} are the lowest reflectivity amplitudes of the HF signal, generated by the largest and the shortest lengths of pit or land respectively when a 14 T or a 3T symbol is read on the disc.
- The zero level is the no reflection level without disc, and it is also called *dark level*.

The above mentioned parameters shall satisfy the following relations [59] :

$$\frac{I_{14}}{I_{14H}} = 0.60 min \tag{2.7}$$

$$\frac{I_3}{I_{14}} = 0.15 \div 0.20 min \tag{2.8}$$

and

$$\frac{(I_{14Hmax} - I_{14Hmin})}{I_{14Hmax}} = 0.33 max \tag{2.9}$$

Finally, a detection level A_D is applied to the HF signal, to let the system correctly recover the digital information. This level should satisfy the so called *asymmetry condition*, defined in [59] and [54] :

$$-0.05 \leq \frac{(I_{14H} + I_{14L}) - (I_{3H} + I_{3L})}{2(I_{14H} - I_{14L})} \leq 0.15 \tag{2.10}$$

Equations (2.7), (2.8), (2.9), and (2.10) represent conditions that should be satisfied, to confirm that the disc is conform to the standards fixed in [59].

It is interesting to notice that the pit/land structure impressed on a DVD disc allows to retrieve, at the same time, the recorded data (used for audio and video reproduction), and the servo signals (needed to control the spot position during playback).

This is why an accurate description of data read-out, as well as error signal generation mechanisms, is fundamental for control design purposes.

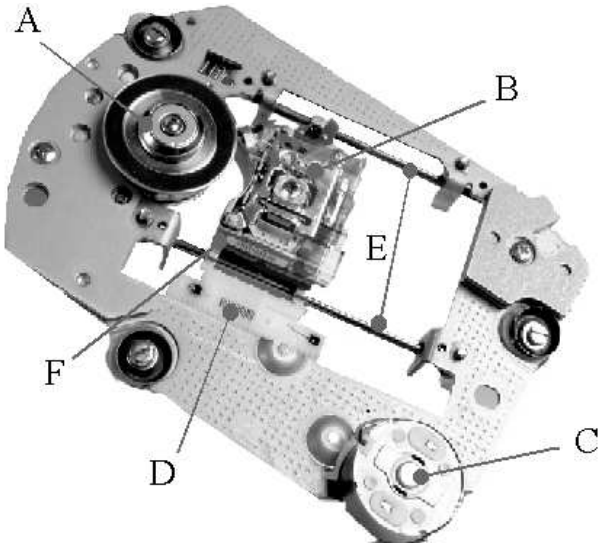

Figure 2.18: An industrial DVD mechanical servo system.

2.7 The Mechanical Servo System

The DVD-video player servo mechanics is mainly constituted by two control loops that keep the laser spot in focus on the disc information layer and, during playback, allow the beam to follow the disc spiral. The servo circuitry must also be able to allow high-speed tracks crossing in the radial direction without loosing focus, and to find the target location on the disc, where finally resume the playback state (long jump or jump-n-track modes). In addition, two other servo loops are used to regulate the speed of the turntable motor (spindle motor control) and to load/unload the disc (tray control), respectively.
In this work we focus on the control loops used to perform the actuators fine displacements along the vertical and radial directions, since they represent the most complex and critical feedback systems implemented in a DVD drive.
Two actuators are used to perform fine displacement of the laser objective lens along the vertical and the radial direction, in order to keep the laser spot in focus and on track. At the same time, the whole system, composed by actuators and optics, is positioned by a sledge at a raw radial location. The sledge, together with the turntable motor, the actuators and the optics, form a rigid body that presents the advantage to passively dump unwanted vibrations due to disc rotations.
A picture showing an industrial DVD mechanical servo system is presented in fig. 2.18, where letter A indicates the spindle motor, B the optical pick-up unit, C the tray motor, D a connection plug, E the chassis rails and F the sledge. A schematic representation of the construction of a DVD drive mechanical servo system is given in fig. 2.19, where it can be seen that the

sledge, the turntable motor and the turntable itself form a rigid body being further consolidate by what is commonly called the baseplate.
On a general DVD drive there are two rotary DC motor, placed inside the optical pick-up unit, for spinning the disc and load/unload the disc respectively. The other two motors are needed to achieve very fine laser spot positioning on the disc, and they rely on pairs of coils and permanent magnets which can move the objective lens in the vertical or in the radial direction. They are commonly designated as focus an radial actuators and they are presented in fig. 2.20.

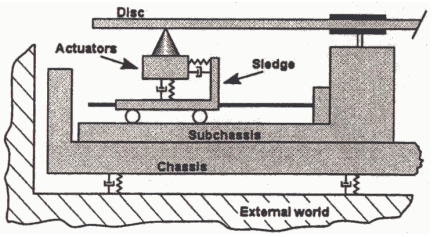

Figure 2.19: Representation of the DVD drive servo system mechanical construction.

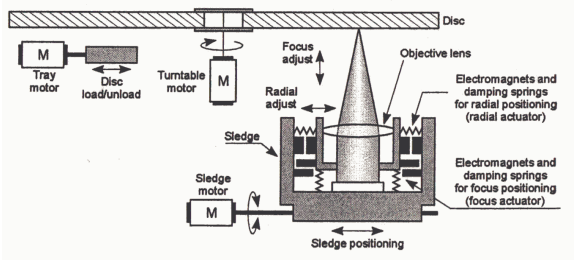

Figure 2.20: Schematic cross section of the DVD drive actuators.

In optical disc devices, to achieve the highest data capacity on the disc, a constant scan velocity is used for data read-out. This method allows to obtain a constant data density from the inside to the outside of the disc, and it consists in varying the disc rotational frequency accordingly to the position of the track that is being read, while the velocity v_a of the scanning spot is kept constant.

The disc rotational frequency f_{rot} is related to the scanning spot velocity v_a and to the actual spot position x along the disc radius, by the following relation :

$$v_a = 2\pi f_{rot} x \tag{2.11}$$

This behavior is known in DVD players as Constant Linear Velocity (CLV), and is achieved using a dedicated control loop. It is interesting to notice that the value of the scan velocity v_a is given in [59], where is said that $v_a = 3.49\ m/s$, and $v_a = 3.84\ m/s$ for a single layer (SL) and for a dual layer (DL) DVD disc respectively, as presented in table 2.2.
For data playback the disc rotational speed is set equal to Nv_a, where the constant N is a number usually referred as *over-speed factor* (or X-factor),

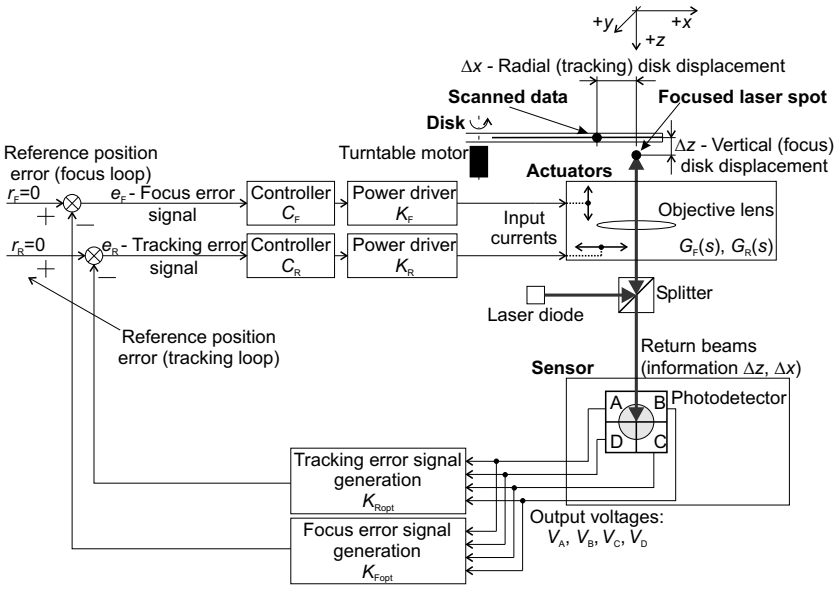

Figure 2.21: Block-scheme of the focus and radial loops control structure, used in an industrial DVD player.

that expresses the ratio between the read-out speed and the speed at which data have been originally impressed on the disc.

2.8 Focus and Radial Servo Loops : Control Problem Description

In order to correctly detect the relief of the track, the diameter of the laser spot on the disc surface and its distance from the track should be kept within a specified accuracy. Two separated controllers are used in order to complete these tasks : a focus controller guarantees that the spot is correctly focused on the information layer of the disc, and a radial controller keeps the displacement between the laser spot and the track position along the disc radius inside a fixed range. The goal of the control design is to minimize the magnitude of the position error between the laser spot and the real track position (in the radial direction) or the disc layer (in the vertical direction), despite the presence of disturbances. In fig.2.21 the equivalent block-diagram of both the spot positioning control loops is presented, where the the control system input and the output signals can be distinguished.
There exist different kinds of disturbance sources which affect the normal behavior of a DVD player. They can be summarized as follows :

- **Optical imperfections :** the laser diodes can produce a high frequency background noise, photo-detector optical misalignment and skew can cause asymmetry and cross coupling between the two control loops, disc warping and misalignment with respect to the spindle axis,

can finally generate harmonics having fundamental frequency equal to the spindle rotational frequency.

- **Internal disturbances :** these disturbances are mainly due to the spindle rotation and to the reaction force that the actuators develop on the drive baseplate and housing, during playback. Usually, also internal disturbances are synchronous with the spindle rotational frequency, introducing thus harmonics at this frequency. Disc eccentricity and vertical deviations belong to this class of disturbances.

- **External disturbances :** they are caused by environmental shocks and vibrations, and usually they are solved by buffering the data stream in a dedicated memory, and deliver them after error corrections.

- **Disc surface defects :** scratches, fingerprints and impressed pit and land imperfections can give spurious signals on the photo-detectors.

In fig.2.22 and fig.2.23 an overview of the disturbance and noise sources acting in both the control loops is shown. In these pictures, it is possible to distinguish additional sources of disturbance entering in the loops, as the noise introduced by the A/D and the D/A converters, the sensing noise, cross coupling phenomena and non linearities due to the error signals generation methods (see sections 2.6.2 and 2.6.3).

In this work we consider low-frequency disturbances mainly due to non perfect location of the hole at the center of the disc or non-perfectly orthogonal disc clamping. These imperfections may produce eccentricity in radial direction and vertical deviations. Shocks and vibrations are not taken into account since they are random events that don't often affect the behavior of a home DVD player. Since disc surface defects present high-frequency contents, we don't take them into account in the design of controllers, which are basically conceived to achieve limited bandwidth.

Under the control point of view, the influence of the different components as the power drivers, the A/D and D/A converters, the sensors and the error signal generation blocks, can be included in a high-level blocks, as shown in the schematic diagram of fig. 2.24. Here, we consider the controller, the objective lens actuator and the linear optical gain, to simplify the control loop scheme, and define the standard control problem.
This scheme can be applied to both the focus and the radial loops.

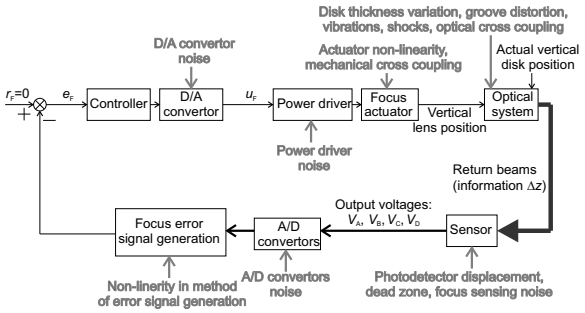

Figure 2.22: Disturbance sources acting in the focus control loop.

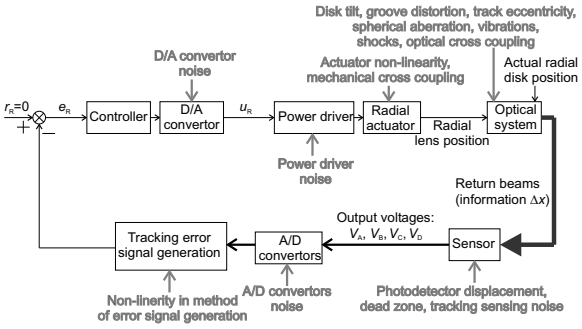

Figure 2.23: Disturbance sources acting in the radial control loop.

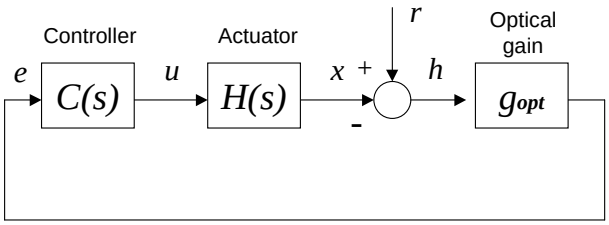

Figure 2.24: Schematic block diagram of the DVD mechanism control loop.

The laser spot position, denoted with x, is determined by the displacement of the objective lens and should coincides, at any moment, with the disc reflective layer (in case of the focus control loop) or with the center of the read-out track (in case of radial loop). The actual track position r, that is not available from measurements, can be considered as a disturbance signal acting at the output of $H(s)$, as stated in Dettori and Stribos [15], [17].
g_{opt} is the gain of the optical pick-up mechanism which converts the displacement h, between the track position r and the spot position x, into an electrical signal e. The laser spot must follow the disc deviations while disturbances will influence its controlled position. $C(s)$ is the controller transfer function, which processes the error signal e and generates the voltage u to drive the actuators.

The control problem consists in projecting the laser spot with high accuracy onto the track, in the vertical and in the radial direction, in a way that the error between the track and the spot positions should not exceed the

following bounds :

$$|e_{\mathrm{R}}(t)| \leq e_{\mathrm{R}}^{max} \quad and \quad |e_{\mathrm{F}}(t)| \leq e_{\mathrm{F}}^{max} \quad \forall \ \ t \tag{2.12}$$

where e_{R}^{max} and e_{F}^{max} are the maximum allowable tracking and focus error signals, specified in [59]. These specifications prescribe also values for the maximum deviations from nominal position x_{max}, for the maximum acceleration of the scanning point $\ddot{x}_{max}$, and for the maximum allowable value of the position error h_{max}. In table 2.3 and 2.4 these values are presented for DVD and CD discs when the scanning velocity $v_a = 3.49m/s$ for a DVD, and $v_a = 1.2m/s$ for a CD.

Table 2.3: *DVD discs standardized radial and vertical deviations from the track nominal position, specified at the disc scanning velocity* $v_a = 3.49\ m/s$

Parameters and conditions	Radial	Focus
x_{max} for $f \leq f_{rot}$	$\pm 50\mu m$	$\pm 0,3mm$
$\ddot{x}_{max}$ for $f_{rot} \leq f \leq 1.1KHz$	$1.1m/s^2$	$8m/s^2$
h_{max} for $f_{rot} \leq f \leq 1.1KHz$	$\pm 0.022\mu m$	$\pm 0.23\mu m$

Table 2.4: *CD discs standardized radial and vertical deviations from the track nominal position, specified at the disc scanning velocity* $v_a = 1.2\ m/s$

Parameters and conditions	Radial	Focus
x_{max} for $f \leq f_{rot}$	$\pm 70\mu m$	$\pm 0,5mm$
$\ddot{x}_{max}$ for $f_{rot} \leq f \leq 500Hz$	$0.4m/s^2$	$0.4m/s^2$
h_{max} for $f_{rot} \leq f \leq 500Hz$	$\pm 0.03\mu m$	$\pm 1\mu m$

2.9 The Track Disturbance

As it can be seen in fig. 2.24, the laser spot x should follow the track position signal r. For instance, in the radial direction, this signal is actually composed by the superposition of a known part $r_0(t)$, considered as the track reference position, and an unknown part $\overline{r}(t)$, which can be seen as a disturbance due to non perfectly spiral-shaped tracks or eccentric rotation of the disc.
Due to the geometry of the disc and to the rotational movement, the signal r can be modelled as follows :

$$r(t) = r_0(t) + \overline{r}(t) \tag{2.13}$$

This signal has a periodic nature, with fundamental frequency equal to the disc rotational frequency f_{rot}, and higher harmonics, due to the modulation

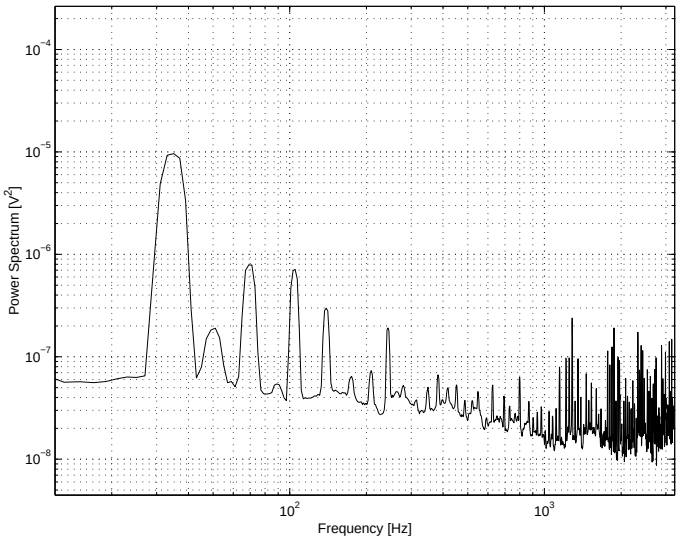

Figure 2.25: Measured power spectrum of the radial error, obtained for a disc rotating at about 33 Hz.

of the non-roundness of the track by the eccentric rotation of the disc. These harmonic components are visible in the measured radial error signal power spectrum, as shown in fig.2.25. This result has been obtained for a test disc having a nominal eccentricity of 0 μm.
The signal r is not directly measurable when it is considered as the absolute spot position, since the only measurable signal (by mean of photo-diodes) is the displacement between the track and the laser spot $h = r - x$. In addition, if in the radial direction r can be modelled as a superposition of a ramp and a disturbance (eq.2.13), the slope of the ramp is so small that it can be neglected, when the behavior of the servo system is analyzed around a track location. In fact, considering that the radius of the circular crown containing the data is 37 mm for a DVD disc, and the maximum playing time is about 4700 sec, the slope of the ramp is about 7.8710^{-6} m/sec, that can be neglected if the measurement last only few minutes.
The same assumptions are valid in the vertical direction, with the only difference that in this case $r_0(t)$ is a step and not a ramp signal.
These two facts lead us to consider the signal r as a disturbance, as also suggested by Dettori [10].

A model for the track signal spectrum can be derived by using specifications contained in [59]. Values presented in table 2.3 are used to determine

some bound on the track signal spectrum, accordingly to [10], as follows :

$$\begin{cases} \|\hat{R}\|_\infty \leq \|r\|_\infty = 50\mu m \\ \\ |\hat{R}| \leq (\frac{1.1m/s^2}{\omega^2}) \end{cases} \tag{2.14}$$

where $\|\hat{R}\|_\infty$ denotes the maximum value of the radial track spectrum and $\|r\|_\infty$ the maximum value of the track disturbance. It is clear that bounds (2.14) represent only a necessary condition on the maximum value that the error signal has to satisfy in the time domain, whether because the characteristics of the error signal vary from disc to disc, whether because harmonics of the track disturbance spectrum can sum in unknown way to the error.
Nevertheless, a more accurate characterization of the class of disturbance affecting the system can lead to a sensible improvement of control design. This is a difficult task for DVD players, since the track position is not directly measurable. The procedure we have followed to estimate the radial track spectrum $\hat{R}$ is summarized below (see also [9]) :

- a measure of the error signal power spectrum is performed, and the track spectrum $\hat{R}$ is estimated by multiplication with the inverse of the output sensitivity function, which is the transfer function from the disturbance to the error signal. These measurements are performed in closed-loop.

- the actuator displacement, measured in μm, is estimated by using test discs having known nominal eccentricity. For a reliable estimate we have chosen 4 test discs, having nominal eccentricity of 0, 50, 100 and 150 μm, respectively. Once the laser spot is correctly positioned with respect to a chosen track, the radial loop is opened, and the number of tracks jumped by the actuator along its maximum excursion, is counted by monitoring the radial error signal, as shown in fig.2.26. Then, by multiplying the number of jumped track by the track pitch $q = 0.74$ μm, it is possible to determine the actuator maximum displacement in μm (see fig.2.15).

The estimate of the track spectrum is shown in fig.2.27. It can be seen that the measured track spectrum (continuous line) is below the bounds (dash lines), fixed in eq.(2.14).
Even considering that the reconstruction method of the track disturbance spectrum can suffer from the fact that the control system strongly suppresses

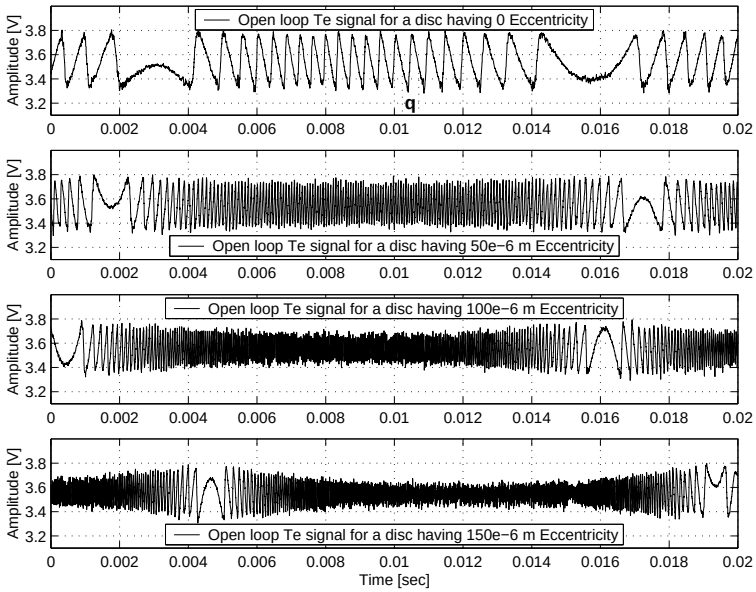

Figure 2.26: Open loop measurements of the radial error signal, used to estimate the actuator displacement in μm.

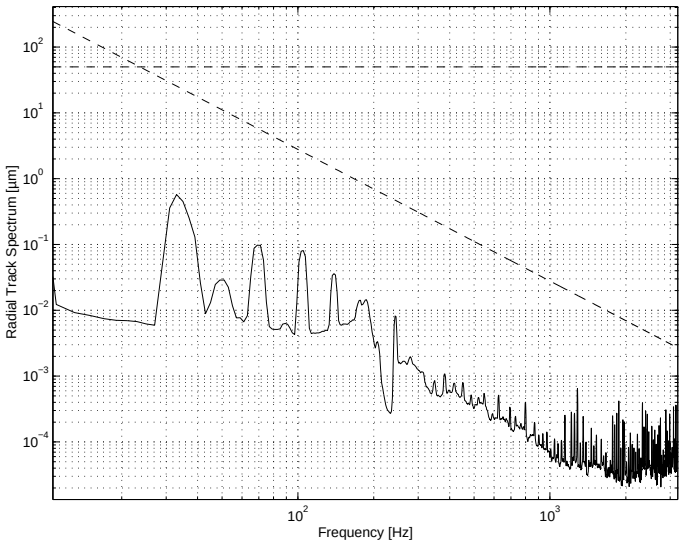

Figure 2.27: Radial track signal spectrum for a disc rotating at about 33 Hz. Dash lines: bounds given by the DVD specifications [59].

the disturbance signal, during closed-loop experiments, and that the measurements of the output sensitivity function are highly corrupted by noise at frequencies below 100 Hz, the figure shows that eq.(2.14) holds.

As known, the specifications given for the DVD control system demand a more accurate spot positioning, with respect to disc surface and track locations, than those given for a CD audio systems. The higher storage capacity demanded to DVDs makes the tracks closer, and consequently requires that harder bounds on the time-domain amplitude of the error signal are satisfied even under the presence of disturbance and plant uncertainty.
This makes DVD players control system more difficult to conceive and to design than usual CD controllers.
For these reasons the subject of this thesis represents an interesting challenge, in which the bound of error signals should be a trade-off with the level of robustness.

2.10 Conclusions

In this chapter we have described the DVD-video player.
In the first part of this chapter, we have presented the existing DVD formats together with their physical lay-out. After having sketched the DVD drive architecture, we have given a detailed description of optics, in order to clarify principles used to generate the servo and the read-out signals. Models of the position error signal generation will be presented in appendix A.
The second part of this chapter is devoted to the description of the electromechanical servo system and to the definition of the spot position control problem together with system's performance specifications. The main control objective is to impose a hard bound on the time-domain amplitude of the tracking errors, along the radial and the vertical directions, in the presence of periodic disturbances whose period varies with the rotational frequency of the disc. Finally, we have shown that these disturbance are due to the geometry of the disc and that, for the radial loop, time-domain specifications contained in [59] can be used to determine some bound on the track signal spectrum [10].
In the following chapters, the STMicroelectronics industrial solution will be described. Frequency domain performance specifications are given, as well as the description of the actual control solution.

Chapter 3

The ST DVD-video player : Control problem description

3.1 Introduction

This Chapter is devoted to present the industrial DVD-video player servo system. The basic idea is to give a more detailed description of the used hardware sub-blocks and software procedures.
Our contribution to this chapter is twofold. Firstly, under the practical implementation point of view, a pure work of code writing has been pursued, to let the dedicated DSP compute and implement the position control loops. Performance specifications and implementation constraints are also analyzed. This part of the work has carried out the realization of the control system of some relevant consumer-market product*.
Secondly, pure theory has been applied to compute the physical model of the spot positioning actuators, starting from technical specifications [43] and [45]. This allows to obtain a nominal linear model of the objective lens actuators, and to evaluate model uncertainty due to the variation of physical parameters.
The chapter is structured as follows : the industrial servo system is sketched in section 3.2, whereas in section 3.3 a more detailed description of its sub-blocks is given. In section 3.4 implementation constraints, due the actual industrial solution, are outlined. Section 3.5 is devoted to a general description of the positioning control loops contained in a DVD player, as well as to their practical implementation. In section 3.6 the actual control solution is described, together with the focus and the radial loops servo requirements. In section 3.7 a control-oriented model of the objective lens actuators is

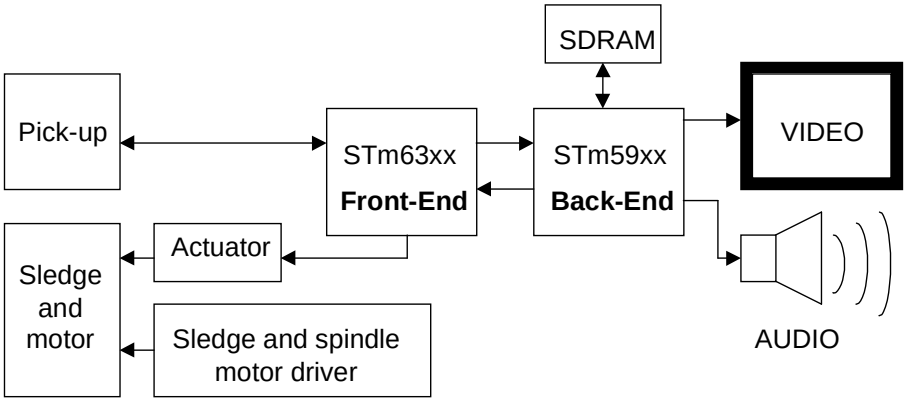

Figure 3.1: Connection between the DVD system FE and BE parts.

computed, by means of some simple electro-mechanic equations. Finally, in section 3.8 some concluding remarks end the chapter.

* *Pioneer DV 350 and DV 363 DVD-Video Players.*

3.2 STMicroelectronics System-on-Chip Solution for Optical Storage

One of the most important application areas for dedicated ICs is the rapidly expanding market for multimedia PCs, set top boxes, and digital video disc players. At the heart of most of these products is the digital image compression technology known as MPEG.
Like all equipment that uses this technology, a DVD player contain two basic subsystems known as the *front-end* and the *back-end*. The front-end handles all of the functions required to extract the compressed MPEG data stream from the received signal, while the back-end decodes the MPEG data to recreate the original content. DVD has already achieved the most successful consumer roll-out in history, and a key factor in this success has been the integration of highly complex electronics circuitry into a decreasing number of chips. Reducing the number of chips required for a complex system like a DVD player, means smaller and less expensive product, as well as increased system reliability and robustness. For these reasons STMicroelectronics has developed all the analog and digital electronic circuitry required for DVD playback in two chips : the *STm55xx* DVD Audio and Video Decoder (the *back-end*), and the *STm63xx* DVD Optical Disc Interface and Servo Control chip (the *front-end*). These two chips handle all of the DVD playback functions, from the analog interface to the optical unit, trough digital servo control, audio and video decoding, video encoding and digital to analog converter, to DVD system-level control functions, as shown in fig. 3.1.
The subject of this work is the study of the DVD-video player servo part. In what follows a general description of the digital servo control subsystem,

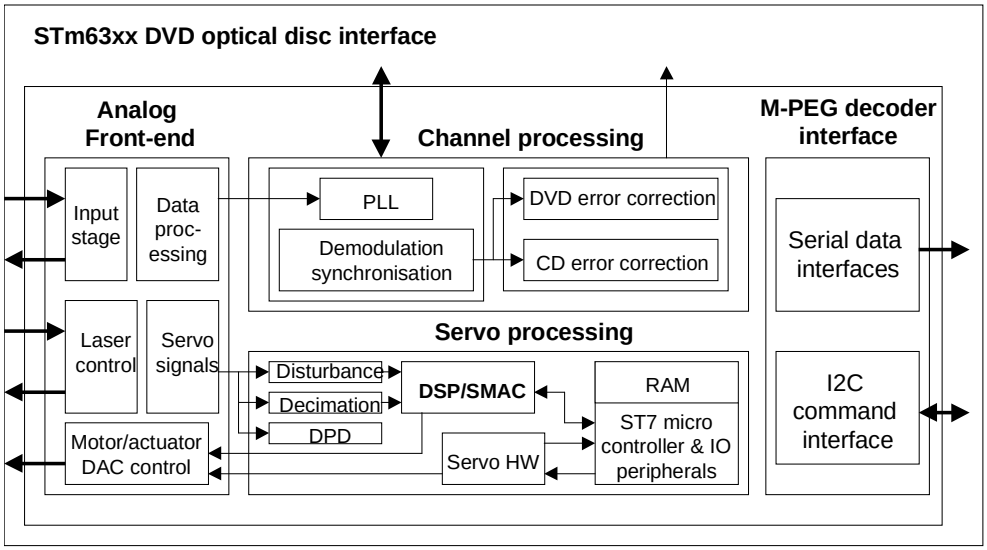

Figure 3.2: Interconnection scheme of the DVD player front-end chip.

included in the industrial *front-end* chip, is presented. Particularly we will focus on the spot position error signals processing, computed by a DSP, which is embedded in a dedicated micro-controller. The interconnection scheme of the STMicroelectronics front-end chip presented in fig. 3.2 is described below.
This device provides an optimum System-on-Chip solution for present DVD players, thanks to its programmable choice of functional modes. It handles DVD Video formats, DVD+R, DVD-R and DVD-RW playback up to $2X$ speed, as well as CD-Audio, CD-R, CD-RW playback, Video-CD and CD-ROM up to $6X$ speed. In conjunction with an internal memory that it shares with a standard back-end device, it allows to handle the error correction functions and servo tasks. This chip integrates all DVD front-end functions in four major blocks :

- **Analog Front-End** : this block provides the interface with the loader and supports connection to all of the leading pick-up devices on the market. It handles all functions required to process the signals from the photo-detector and transforms them into digital data, controls the laser loop, via focus and radial error signals, and generates the output for motor and actuator control. It includes gain-controlled amplifiers and offset stages for each photodiode signal, dual laser control with automatic detection and an array of A/D and D/A converters for servo signals, high-frequency data conversion and control of the pick-up's actuator and motor power drivers.

- **Channel Processing** : the Channel Processing block performs all of the required Data Acquisition and Error Correction functions, in-

cluding data and clock recovery via a PRML block (Partial Response Maximum Likelihood, that acts like a digital equalizer to shape the overall transfer function of the system), as well as sector ID (for DVDs) and sub-code (for CDs) decoding with error correction. The error correction module includes separate DVD and CD controllers that receive data from the acquisition module and perform RSPC (Red-Solomon Product Code, the error protection system used for DVD) or CIRC (Cross Interleaved Red-Solomon Code used on CD for error correction) decoding. The DVD decoder allows multi-pass corrections to improve performance, while the CD decoder supports both single and double-pass decoding and includes video-CD and CD-ROM support with data descrambling.

- **Servo Processing** : the servo processing module includes an *ST*7 8-bit micro-controller and a dedicated *SMAC* (Smart Adder and Multiplier), used to implement focus and radial loops spot positioning controllers. This block also realizes fast multiply and accumulate operations, required in digital filtering and similar computations, as well as dedicated hardware for decimation filters, defect management, focus search, wobble detection, Differential Phase Detection and other functions.

- **Back-End Interface** : this block transfers data from the *front-end* chip to an audio and video back-end decoder with a unified-memory mode, by using the Front End enhanced interface for the DVD format only.

3.3 The Servo System

As presented in fig. 3.2, the STm63xx is composed by several subsystems, each of whom has a specific functionality. Since the aim of this work is to show how to conceive, implement and analyze algorithms for laser position control of an industrial DVD player, we believe necessary to give a more detailed description of the *Servo Processing* subsystem.
Particularly, as the *SMAC* is the module used to implement the control digital filters, in what follows we will go further in presenting its architecture and functionalities, in order to present the actual industrial solution, and to better understand implementation constraints and performance limitations.

3.3.1 DSP/SMAC Module

The DSP/SMAC module is used for basic signal processing calculation. Thanks to its parallel architecture, it is able to perform, in one clock cycle, a sum, a multiplication, a shift and different buffer data transfers. This architecture is conceived to fast treat signals coming from the acquisition channel and sent to the pick-up actuator, to find and keep focus and tracking while reading a DVD disc. The SMAC is not a real Digital Signal Processor (DSP), but a dedicated multiplexer and accumulator, which is used for performing the calculation of the following filters :

- Focus and tracking error signals generation.
- Focusing and tracking digital servo control.
- Sledge control.
- Photo-detectors offset balance.
- Automatic Gain Control.
- Defect compensation.
- Track Zero Crossing (TZC) and Coarse track process.

In addition this module is also dedicated to observe some internal signals through serial interface for measurement such as focus and radial error, focus and radial signals to actuator, sinus wave or AGC signal.
The device has a RAM memory containing the code to be executed at each time a new signal sample is produced. The sampling frequency f_s of one whole computation can be set by the DSPIRQ signal (defined in 3.3.5), and it can assume values from 79.4 to 333 Khz. The frequency of one SMAC instruction cycle is called f_{SysClk} and, on the current industrial application, the chosen computational and the instruction cycle frequencies are $f_s = 123.45\ Khz$ and $f_{SysClk} = 80\ Mhz$, respectively.
The SMAC has a specific memory to contain coefficient values used to implement digital filters, and a data RAM to hold delayed and partial values. The ST7 micro-controller downloads coefficients and code into SMAC memories and data RAM, and it has also the possibility to read and write values into this memory during disc playback. On the other hand the SMAC can access to external registers or hardware blocks, which are normally used for specific functionalities. In term of data-flow exchange the ST7 behaves as a master and the DSP as a slave.

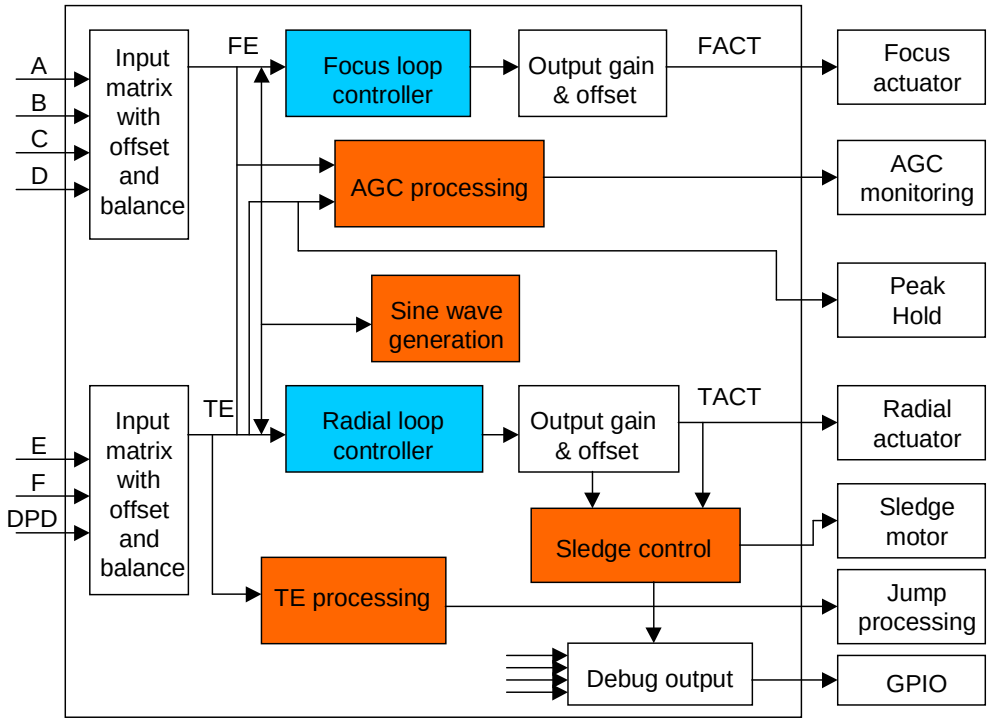

Figure 3.3: SMAC control path block diagram.

For its higher computational speed the SMAC is devoted to accomplish all those functions that require fast calculations, whereas the micro-controller handles all the "intelligent" functions, such as initialization of the SMAC coefficients and drive the actuators in the open-loop condition for track jumps and focus search. The SMAC control path block diagram is presented in fig.3.3.

3.3.2 ST7 Micro-Controller

The ST7 is the 8-bit micro controller unit used, in the current industrial solution, to execute the program stored in the embedded RAM memory of the STm63xx front-end device. Its core is built around a 8-bit arithmetic and logic unit (ALU), 6 internal registers that allow efficient data manipulation, and a controller clock, whose frequency is usually a sub multiple of the STm6316 master clock f_{SysClk}, and equals to $f_{Clk_{ST7}} = 10\ Mhz$. This device is interfaced with an on-chip oscillator, a reset block, address and data buses to access to memory and peripherals and an interrupt controller. Particularly the accumulator is an 8-bit register used to hold operands and results of arithmetic and logic operations. Its registers are two 8-bit registers used to create effective addresses and store temporary data. A 16-bit program counter register is then used to store the address of next instruction to be executed by the CPU. As result the ST7 can address up to 64 Kb of program memory.

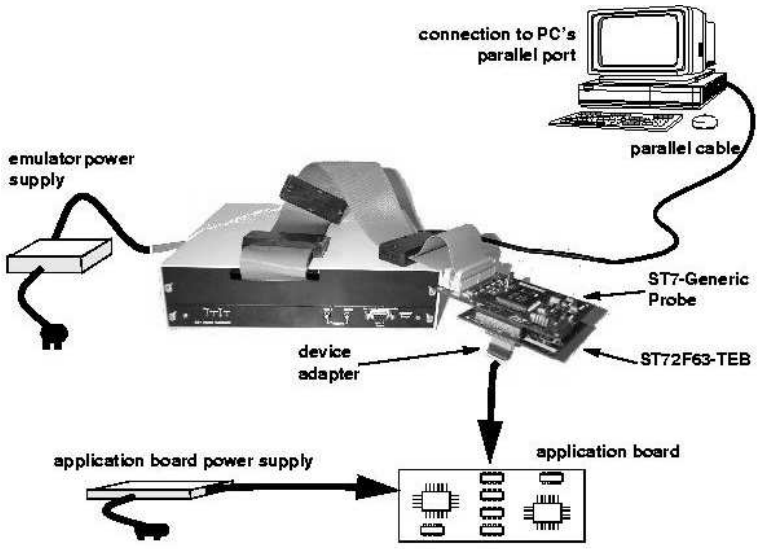

Figure 3.4: ST7 and emulator general configuration.

During the software development phase, the ST7 is programmed by using an emulator, that is connected to a PC. A dedicated debugger is provided to control and configure the emulator, which can interrupt the ST7 with high priority interrupts, to carry out specific debug operations. Once assembled and linked, the application software is directly downloaded into the ST7. As shown in fig.3.4, the development station performs a real-time emulation of the target device, thus allowing performance testing and debugging.

3.3.3 Disturbance block

This block consists of a mirror, a servo defect and acquisition defect detectors. It takes as inputs the signals coming from the servo and the acquisition A/D blocks, and processes them to give information on the quality of these signals. It generates several outputs, a MIRROR signal, and 3 defects signals that can then be used to react to defect, to a loss of focus and to count tracks. The inputs of this block come directly from A/D converters, at high sample rates. The outputs will be used by the ST7 μ-controller, by the track counting block, or by the actuators output switches.

3.3.4 Differential Phase Detection block

This module processes the inputs from the 4 photo-diodes to compute the radial error signals for control purposes. The Differential Phase Detection (DPD) method has been already discussed in section 2.6.3. The advantage of this method is that only an output offset correction is required for calibration.
The equalized analog inputs are processed by comparators, called slicers,

and 2 phase measurers to produce 4 phase values with respect the system clock signal. The input stage adapts the input of the 2 phase comparators, to different photodiodes layouts. Then the sum of the 2 phase comparators outputs represent the track error signal (see fig. 2.15). The DPD block provides DPD data to the decimation filter for track error generation in the *SMAC*, and digital slice levels for A, B, C and D to the analog front-end.

3.3.5 Decimation block

The purpose of the decimation block is to adapt the sampling frequency of the digitized servo signals coming from the analog front-end, and from the DPD block (differential phase detection) to the lower operating rate of the servo DSP. The decimation filter receives data from the servo A/D converters, as well as from the digital DPD block. The filters perform some low-pass filtering and reduce the sample rate (decimation) to match the needs of the servo DSP. The decimation ratio of all filters can be chosen in a wide range by the ST7 micro-controller. The digitized servo signals A, B, C, D, and the HF are acquired by the decimation module with a sampling rate of $f_{Dec_{(A,B,C,D)}} = f_{SysClk}/3$, E and F with a sampling rate of $f_{Dec_{(E,F)}} = f_{SysClk}/6$. The track error signal is provided by the DPD block, with a sampling rate of $f_{Dec_{(DPD)}} = f_{SysClk}$ ($f_{SysClk} = 80\ Mhz$ is the frequency at which one single instruction is computed inside the *SMAC*). These input signals are down-sampled by the decimation filter and are output to the *SMAC* module.

3.3.6 Digital to Analog converters

The servo D/A converters block accepts Digital data from the DSP, the CLV controller and ST7, and generates the analog electrical signals to drive the motors and pickup actuators via the external power stages. Additionally a reference signal for the external power driver is generated. The block contains four D/A converters, two for pickup actuators and two for motors.

3.4 Performance Limitations

As already exposed in sections 3.3.1, in the actual industrial solution the spot position control loops are implemented by using a dedicated DSP module, called SMAC.
Although this device is very cheap and simple to program, quantization effects due to the A/D converters, finite precision of digital computation and

rounding errors pose strong limitations on the complexity of the computational structure and on the choice of coefficients used to implement the digital filters. When implementing digital signal processing systems one must represent signals and coefficients in some digital number system that must always be of finite precision, since the output samples from the A/D converter are quantized and represented by binary numbers.

As stated in Oppenheim and Schafer [39], the operation of quantizing a number with a finite sequence of bits can be implemented by rounding or by truncation, but in both cases quantization is a non linear operation, which affects the implementation of linear time-invariant discrete-time systems in the following ways :

- When the parameters of the rational transfer function representing the system are quantized, the poles and the zeros move to new position in the discrete-time z-plane, so that the frequency response is perturbed from the original "un-quantized" transfer function. As consequence, the resulting system may no longer meet the original design specifications and even it might become unstable.

- Roundoff noise is due to the finite precision of the digital computation. It can be assumed that rounding and truncation operations can be represented as noise sources equal to the quantization error at the output of each quantizer, as stated in Oppenheim and Schafer [39].

- Overflow phenomena constitute also an another important point in discrete-time systems implementation, since if it is assumed that each fixed-point number represent a fraction, each node in the filter structure must be constrained to have a magnitude less than 1 to avoid overflow.

- When a stable discrete-time system is implemented with finite-register-length arithmetic, the output may continue to oscillate indefinitely while the input remains equal to zero. This effect is often referred to as *zero-input limit cycles behavior* and is a consequence either of the non linear quantizers or overflow of additions [39].

In the current industrial solution, inside the programmable DSP all data are represented in 2's complement. The maximum length of the DSP program is 640 instructions, each instruction has a length of 38-bits. A coefficient RAM can provide up to $n_C = 256$ fixed point coefficients, each of whom is

represented by a sequence of 8-bit. The first bit of a coefficient represents its algebraic sign, and the remaining 7 bits its magnitude. Thus, using a finite number of bits $(B_{\mathrm{C}}+1)$, an arbitrary coefficient χ is represented in 2's complement form as follows :

$$\chi = \chi_m \left(-b_{B_{\mathrm{C}}} + \sum_{i=B_{\mathrm{C}}-1}^{0} b_i 2^{-i} \right) \tag{3.1}$$

where $B_{\mathrm{C}} = 7$, χ_m is an arbitrary scale factor equal to 1 in our application, b_i's are either 0 or 1, and b_B is the sign-bit. If $b_{B_{\mathrm{C}}} = 0$, then $0 \leq \chi \leq \chi_m$ and if $b_{B_{\mathrm{C}}} = 1$ then $-\chi_m \leq \chi \leq 0$.
A data RAM is used with a direct read-write access mode for the DSP, and with an indirect read-write access mode for the ST7 micro-controller, by means of dedicated internal registers. The data RAM memory can contain up to $n_{\mathrm{D}} = 128$ memory locations of data, which are coded on 16 bits. Then, using a finite number of bits $(B_{\mathrm{D}}+1)$, data contained in an arbitrary memory location κ is represented in two's-complement form as follows :

$$\kappa = \kappa_m \left(-d_{B_{\mathrm{D}}} + \sum_{i=B_{\mathrm{D}}-1}^{0} d_i 2^{-i} \right) \tag{3.2}$$

where $B_{\mathrm{D}} = 15$, κ_m is an arbitrary scale factor equal to 1, d_i's are either 0 or 1, and $d_{B_{\mathrm{D}}}$ is the sign-bit. If $d_{B_{\mathrm{D}}} = 0$, then $0 \leq \kappa \leq \kappa_m$ and if $d_{B_{\mathrm{D}}} = 1$ then $-\kappa_m \leq \kappa \leq 0$. A multiplier performs a 8-bit $\times$ 16-bit signed multiplication and provides the results on 23 bits. At the output of the multiplier, saturation phenomena can occur if the coefficient and the data values are equal to the maximum allowable value, respectively. A shifter performs 7 bit logical shift with sign extension and LSB truncation, to execute double precision calculation. Then, an adder makes a signed addition with an A operand on 25 bits, a B operand on 23 bits to give the result on 23 bits. A programmable shifter is then used to perform multiplications or divisions, and a temporary register is also used to store intermediate results with the full length of 25 bits. Finally a limiter limits and truncates the results from 25 to 16 bits by using a magnitude truncation.
Hence, because of the finite precision of digital computation, the digital filters implementation structures must be carefully chosen and the controllers complexity should be limited to reduce the effects of rounding errors and quantization noise, as suggested in Whidborne and Yang [67].

A key point is represented by the choice of the coefficient values used for the digital implementation :

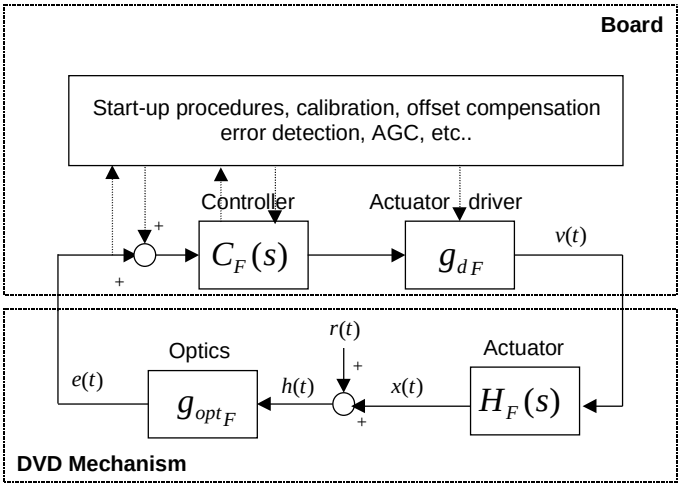

Figure 3.5: Block diagram of the focus control system.

- As stated above, they have to satisfy the fact that $-1 \leq \chi < 1$, to reduce rounding errors and avoid saturation phenomena.
- It is well known, from the Shannon theorem, that it is impossible to implement digital filters having cut-off frequencies higher than $f_s/2$. On the other side, if the value of f_s is high (as on the industrial benchmark), it becomes hard to implement digital filters having very low cut-off frequencies, since rounding and truncation phenomena do not allow to represent coefficients with necessary accuracy.

In the actual control solution adopted for a DVD-video player, the minimum required precision is of 8-bit for coefficients and of 16-bits for data. Controller order reduction and choice of the filter structures, are related to implementation constraints, such as the fixed number of bits used for represent coefficients and data, and to the chosen computational frequency f_s. All these factors have to be taken into account, during the controller implementation phase, when the DSP is programmed by using a dedicated assembler language. Each of them can be represented schematically as a functional block, as shown in fig.3.3 and discussed in what follows.

3.5 Servo Loops for Focus and Radial Adjustment

As already mentioned in section 2.8 both focus and radial servo loops use physical displacement as control variable. Each of them has to regulate the objective lens position $x(t)$ and employs an opto-electronic detector to generate the electrical error signal $e(t)$.
The simplified block diagram of the position control system, used for focus and radial tracking, are sketched in fig.3.5 and fig.3.6. The spot position error signal $h(t)$, relative to the disc surface or to the center of a track, is detected by optics, represented with a constant gain g_{opt}, which generate

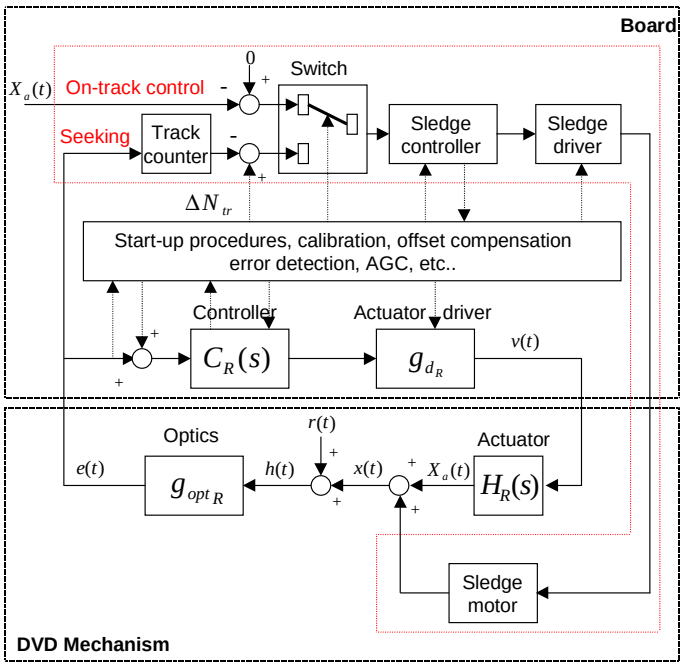

Figure 3.6: Block diagram of the radial control system.

the electrical error signal $e(t)$. The commonly used controller $C(s)$ and the actuator driver g_d feed the system with a voltage $v(t)$. $H(s)$ denotes the transfer function from $v(t)$ to the spot position $x(t)$. As stated in section 2.9, the actual track position $r(t)$ can be considered as a disturbance and is not directly available from measurements. It mainly includes vertical and radial track position deviations due to disc unbalance, eccentricity, unroundness, etc. and external disturbances from mechanical shocks and vibrations [70].

The laser beam is kept in focus by a circuit which includes a position loop and a dedicated control unit, as depicted in fig.3.5. The standard controller, which regulates the focus position, operates only in the linear region of the focus error S-curve, as discussed in section 2.6.2. This operation requires that the system is initialized, that the focus error is calibrated and that eventual offset are eliminated. In addition, the system has to be always monitored to detect possible loss of focus and initialize proper recovery algorithms. These crashes can overcome if the disc is unbalanced or if scratches and fingerprints are present on its surface.
The dedicated control unit is then devoted to assist the spot position controller during non linear operations, and take over the focus control if needed. Usually such operations are accomplished by dedicated hardware blocks and software procedures, whose decisions depend on information received from both focus and radial loops and spindle motor control.

Due to the large disc radial dimensions relative to track pitch, the spot position along the radial direction is controlled by a two-stage electro-mechanical system. A general block diagram of the radial control is depicted in fig.3.6, where three spot position radial control loops are represented. In the back-dashed lower part is contained the actuator fine displacement control loop. In the red-dotted upper part, are presented the radial seek and the radial on-track control loops, whose description is given in section 3.5.1 and 3.5.2. The actuator fine displacement is controlled by a standard lead-lag controller, whereas the sledge moves the laser spot outward and inward along the disc radius.
Also in the radial control system the non linear control unit takes care of initialization and start-up procedures, calibrations, crash detection and recovery, as well as automatic gain control (AGC) (see section 3.5.3).

3.5.1 On-Track Radial Control

The on-track radial control, also called track following control, is the state in which the radial servo system operates during disc playback. In this particular mode the laser spot must follow a given track, while the system delivers data to the host interface. What happens in practice is that the actuator accurate positioning is performed by the lower branch of fig.3.6, while the sledge is set to slowly follow the actuator movements, by means of a simple PID regulator. The signal to be tracked $X_a(t)$ is selected with a seek/read switch and represents the actuator position relative to the sledge, as given reference. During disc playback, the spot moves towards the outer disc radius, leaving the sledge behind. As the actuator displacement range is relatively small, the sledge has to advance but slowly, without following the fast laser spot movements. The actuator position with respect to the sledge can be measured by low-pass filtering the signal from the actuator lead-lag controller.

3.5.2 Radial Seek Control

The radial seek control is needed to be performed when the radial servo system has to place the laser spot on a track different from the present one. Usually the terms *data access* or *track jump* are also used to refer to a seek procedure (see fig.3.6).
When a seek command arrives from the host interface to the micro-controller, it has to firstly calculate the number of tracks ΔN_{tr} to be crossed. This value

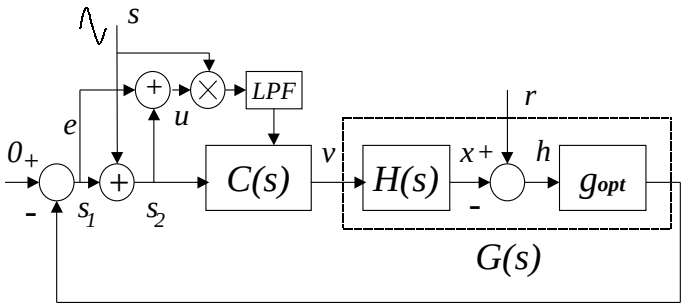

Figure 3.7: Automatic Gain Control block scheme.

can be computed as follows :

$$\Delta N_{tr} = \frac{1}{q}\sqrt{\frac{x_{in}^2}{4} + \frac{qv_aS_{fin}}{\pi}} - \frac{1}{q}\sqrt{\frac{x_{in}^2}{4} + \frac{qv_aS_{ini}}{\pi}} \tag{3.3}$$

where q is the track pitch, x_{in} is the inner diameter of the program area, v_a is the linear velocity of the recorded data, and S_{ini}, S_{fin} are the known initial and final position of data clusters along the disc spiral, respectively. The number of tracks crossed in the radial direction is usually counted with a counter, which uses the low-pass filtered radial error signal to increment its value at each track crossing. During this phase the sledge loop perform the seek action, and the actuator is set to follow the sledge displacement (the radial loop is open), while the track counter provides the feedback information. The sledge controller acts to increase the number of crossed tracks ΔN_{tr}, until a dedicated algorithm switches the radial control from sledge back to actuator loop in order to provide the track acquisition.

3.5.3 Automatic Gain Control

Several factors can usually determine the variation of the gain of the system : temperature, humidity and reflectivity of discs. An Automatic Gain Control (AGC) procedure is used to take into account gain variations of the system to control.

This process evaluates the system gain and, on-line, modifies the controller gain in order to keep the open-loop gain variations limited and avoid system instability and loss of performances. Indeed, if the static gain L_0 of the open-loop transfer function $L(s)$ varies, the open-loop cut-frequency f_c varies. This could give rise to instability of the loop, since the phase margin ϕ_m would vary depending on the open-loop gain variations. The AGC block scheme is presented in fig.3.7, where $C(s)$, $H(s)$, $G(s)$ and g_{opt} are given for both focus and radial loops.

Let us to define $\widehat{f_c}$ the target open-loop cutting frequency, and let assume that :

$$s(t) = A_s sin(2\pi \widehat{f_c} t) \tag{3.4}$$

is the sinus wave generated by an internal oscillator. In practice, the sine wave $s(t)$ is injected at the target frequency $\widehat{f_c}$ at the controller input, when the loop is closed. Two signals $s_1(t) = e(t)$ and $s_2(t) = s1(t) + s(t)$ are then summed, and the resulting signal is $u(t) = s_1(t) + s_2(t) = A_u sin(2\pi \widehat{f_c} t + \varphi)$. The AGC block target is to control the closed loop gain, so that at the target frequency $\widehat{f_c}$, specified in [59], $u(t)$ and $s(t)$ are in quadrature.

The transfer function from $u(t)$ to $s(t)$ is given by :

$$U(s) = S_1(s) + S_2(s) = -\frac{L(s)}{1+L(s)}S(s) + \frac{1}{1+L(s)}S(s) = \frac{1-L(s)}{1+L(s)}S(s) \tag{3.5}$$

where $L(s)$ denotes the system open-loop transfer function.

$U(s)$ has amplitude nearly constant, and phase shift of $\pi/2$ at the target open loop cut-frequency $\widehat{f_c}$. The product between $u(t)$ and $s(t)$ is computed as follows :

$$A_s sin(2\pi \widehat{f_c} t) A_u sin(2\pi \widehat{f_c} t + \varphi) = \frac{1}{2} A_s A_u [-cos(2\pi 2 \widehat{f_c} t + \varphi) + cos(-\varphi)] \tag{3.6}$$

and a first order low-pass filter (LPF), having a cut-off frequency of above 10 Hz, is then used to extract the continuous component :

$$\frac{1}{2} A_s A_u cos(\varphi)$$

If $cos(\varphi) = 0$, then $u(t)$ and $s(t)$ are in quadrature at $\widehat{f_c}$, and the loop gain is correct. Besides, if $cos(\varphi) > 0$ or $cos(\varphi) < 0$, then it is necessary to reduce or augment the controller gain in order to decrease or increase $|L(s)|$, respectively. The controller gain is automatically adapted by simply re-loading new coefficients values in its last stage coefficients.

3.6 The Actual Focus and Radial Control Solutions

In this section we describe the main servo control algorithms used in a DVD-video player, and implemented for STMicroelectronics on the commercial industrial solution. The ST7 micro-controller has been programmed to implement these algorithms, and the discrete-time computation is performed by the SMAC module, at a sampling frequency of $f_s = 123.45\ Khz$.

3.6.1 Focus and Radial Loops Servo Requirements

To specify the performance of the focus and tracking servo loops, the so-called normalized servo transfer functions are used in the DVD read-only disc specifications [59], to determine the nominal characteristics of the open loop transfer functions of both loops. These specifications are given when an over-speed factor $N = 1$ is considered, and they prescribe values for the maximum deviations of the spot from nominal position x_{max}, for the scanning point maximum acceleration $\ddot{x}_{max}$, and for the maximum allowable value of the position error h_{max} at given frequencies (see fig.2.24).
In table 2.3 of page 87 these values are presented for a disc scanning velocity $v_a = 3.49m/s$ and $f_{rot} = v_a/2\pi d_{\mathrm{R}}$, where d_{R} is the radial distance of the spot with respect to the disc center hole.

In what follows we describe how performance specifications can be translated as templates on the inverse of the closed-loop sensitivity function $S(s)$. System closed-loop performance criteria are also given. What is presented below is valid for both focus and tracking loops.

a) Templates on $S(s)^{-1}$:

For control design purposes it is convenient to describe performance specifications as weights on the closed-loop sensitivity functions. So, specifications contained in [59] are translated in the frequency-domain if the deviation of the spot from the nominal position $x(t)$ is modelled, in the acceleration zone, as an harmonic signal. The maximum acceleration $\ddot{x}_{max}(t)$ is obtained thus as follows :

$$x(t) = A\sin(\omega t) \Rightarrow |\ddot{x}_{max}(t)| = A\omega^2 \tag{3.7}$$

where A is the maximum amplitude of the radial deviation from the track. For $f \leq f_{rot}$ the lowest corner frequencies $f_{L_{\mathrm{F}}}$ and $f_{L_{\mathrm{R}}}$ on $S_{\mathrm{R}}(s)^{-1}$ and $S_{\mathrm{F}}(s)^{-1}$ are given by :

$$f_{L_{\mathrm{F}}} = \frac{1}{2\pi}\sqrt{\frac{\ddot{x}_{max_{\mathrm{F}}}}{x_{max_{\mathrm{F}}}}} = \frac{1}{2\pi}\sqrt{\frac{8}{0.3 * 10^{-3}}} \simeq 25.98Hz \tag{3.8}$$

$$f_{L_{\mathrm{R}}} = \frac{1}{2\pi}\sqrt{\frac{\ddot{x}_{max_{\mathrm{R}}}}{x_{max_{\mathrm{R}}}}} = \frac{1}{2\pi}\sqrt{\frac{1.1}{50 * 10^{-6}}} \simeq 23.6Hz \tag{3.9}$$

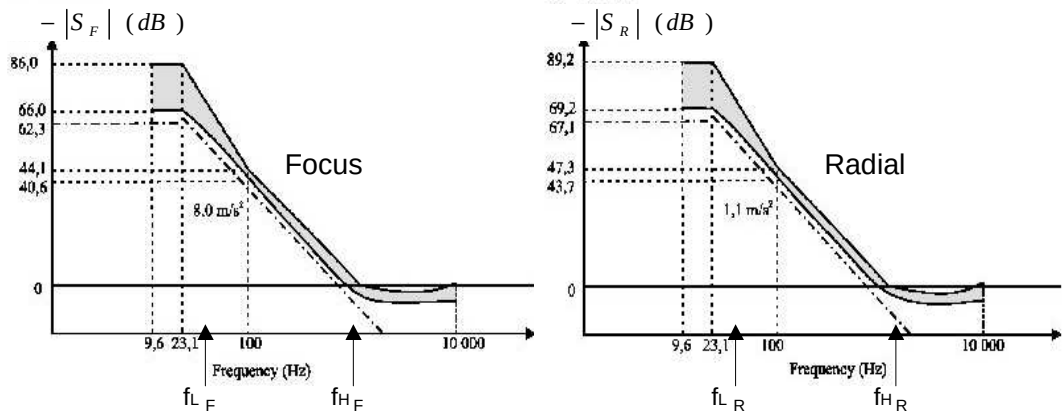

Figure 3.8: Representation of the focus and radial loops specifications in term of frequency-domain templates on $S(s)^{-1}$, $N = 1$.

Above f_L the amplitude is limited by the specified maximum acceleration up to the highest corner frequencies $f_{H_{\mathrm{R}}}$ and $f_{H_{\mathrm{F}}}$:

$$f_{H_{\mathrm{F}}} = \frac{1}{2\pi}\sqrt{\frac{\ddot{x}_{max_{\mathrm{F}}}}{h_{max_{\mathrm{F}}}}} = \frac{1}{2\pi}\sqrt{\frac{8}{0.23 * 10^{-6}}} \simeq 938.6Hz \tag{3.10}$$

$$f_{H_{\mathrm{R}}} = \frac{1}{2\pi}\sqrt{\frac{\ddot{x}_{max_{\mathrm{R}}}}{h_{max_{\mathrm{R}}}}} = \frac{1}{2\pi}\sqrt{\frac{1.1}{0.022 * 10^{-6}}} \simeq 1125.4Hz \tag{3.11}$$

The disc specifications are given for a disc rotating at a constant linear velocity. When the disc rotates at higher speeds, say Nv_a, the corner frequencies f_L and f_H must be linearly shifted by the over-speed factor N and the focus and radial accelerations have to be multiplied by the factor N^2. The restrictions on the radial and vertical deviations can be represented graphically in the frequency domain, as shown in fig.3.8, where the disc specifications are represented as requirements for the inverse of the output sensitivity function (see fig. 2.24) :

$$S(s)^{-1} = 1 + g_{opt}C(s)H(s) = 1 + L(s) \tag{3.12}$$

where $L(s) = g_{opt}C(s)H(s)$ is the open-loop transfer function. In order to fulfill [59], $S(s)^{-1}$ has to lie inside the grey area.
In practice what is used to define the system performance specifications is the minimum required sensitivity ΔS, expressed in dB and defined as follows [59] :

$$\Delta S = 20 \log\left(\frac{h_{max}}{x_{max}}\right) \tag{3.13}$$

The minimum required sensitivity levels ΔS_{F} and ΔS_{R}, for both focus and radial loops, can be derived from table 2.3.
For the focus loop, the amplitude of vertical deviations should be reduced, to avoid that the actuator vertical displacement is smaller than $\pm 0.23\ \mu m$.

These deviations are harmonics whose fundamental frequency is between 9 and 24 Hz, for $N = 1$. Then, it follows that :

$$\Delta S_{\mathrm{F}} = 20 \log \left(\frac{0.23 \mu m}{0.3 mm} \right) = -62.31 dB \tag{3.14}$$

or less is needed as minimum sensitivity level, at these low frequencies, to compensate the maximum amplitude of vertical deviations. For higher frequencies (above 1.1 Khz) we have :

$$\Delta S_{\mathrm{F}} = 20 \log \left(\frac{0.23 \mu m}{0.23 \mu m} \right) = 0 \, dB \tag{3.15}$$

For the tracking loop a similar approach can be considered. In this case the maximum allowed tracking error is ± 0.022 μm and, for low frequencies, the necessary sensitivity of the radial control loop becomes :

$$\Delta S_{\mathrm{R}} = 20 \log \left(\frac{0.022 \mu m}{50 \mu m} \right) = -67.13 dB \tag{3.16}$$

For high frequencies (above 1.1 Khz) we have :

$$\Delta S_{\mathrm{R}} = 20 \log \left(\frac{0.022 \mu m}{0.022 \mu m} \right) = 0 \, dB \tag{3.17}$$

Also in this case $S(s)$ must meet the requirement expressed by eq. (3.18). The sensitivity function $S(s)$ has to be equal or smaller than the minimum required sensitivity ΔS derived from the disc specifications [59] :

$$\Delta S \geq S(s) = \frac{1}{1 + L(s)} \Longrightarrow S(s)^{-1} = 1 + L(s) \geq \frac{1}{\Delta S} \tag{3.18}$$

Thus, $S(s)^{-1} = 1 + L(s)$ must lie above $1/\Delta S$, i.e. $-|S(s)|_{dB} \geq -\Delta S_{dB}$.

b) Closed-loop Bandwidth :

The control system performance is also characterized by the so-called *crossover* frequency f_c, defined as the frequency at which the the amplitude plot of the open-loop transfer function $L(s)$, obtained with the normalized servo system, crosses 0 dB. Its value is specified in [59] as follows :

$$f_c = \frac{N}{2\pi} \sqrt{\frac{3 \alpha \ddot{x}_{max}}{h_{max}}} \tag{3.19}$$

where α is a multiplicative coefficient that shall be 1.5 times bigger than the expected maximum spot acceleration $\ddot{x}_{max}$. According to table 2.3, $f_{c_{\mathrm{R}}} = 2.38$ KHz and $f_{c_{\mathrm{F}}} = 2$ KHz for the radial and the focus loop respectively, when $N = 1$.

c) Rise Time :

An additional information, concerning the system closed-loop performances, is given by the rise time t_r, i.e. the time it takes for the output to first reach 90 % of its final value. t_r usually verifies the following equation [51] :

$$t_r \simeq \frac{2.3}{2\pi f_c} \tag{3.20}$$

which leads to $t_{r_{\mathrm{R}}} = 0.153\ ms$, and $t_{r_{\mathrm{F}}} = 0.183\ ms$, for $N = 1$.

d) Steady-state Error :

For the focus loop, an important parameter, which defines the control system performance, is the *focal depth* Δz_{max} [4]. Δz_{max} establishes the maximum disc displacement between the actual position of the information layer and the position of the objective lens, and it is defined as follows :

$$\Delta z_{max} = \frac{\lambda}{2NA^2} \tag{3.21}$$

where $\lambda = 650\ nm$ s the laser wavelength, and $NA = 0.6$ is the objective lens numerical aperture, defined in section 2.6.1, which gives a typical value of $\Delta z_{max} = 0.903\ \mu m$ for a DVD-video player. The focus control loop should therefore control the objective lens within $\pm\Delta z_{max}$ at every moment, to avoid loosing focus (i.e. the read-out signal) during playback (see fig.2.14).

A similar parameter can be defined for radial loop. In fact, the track pitch p establishes the distance between the centerlines of a pair of adjacent physical tracks, along the radial direction. For optical disc drives it is a hard task to exactly quantify Δx_{max}, defined as the maximum radial displacement between the actual track and the objective lens positions, which still allows the system to correctly perform track following.
As rule of thumb usually a deviation of 10 % of the track pitch is considered as appropriate. This then leads to the following expression :

$$\Delta x_{max} \simeq 0.1p = 0.1 \cdot 0.74 \times 10^{-6} = 0.074 \mu m \tag{3.22}$$

The radial control loop should therefore control the objective lens radial displacement within $\pm\Delta x_{max}$ at every moment, to keep tracks following during playback.

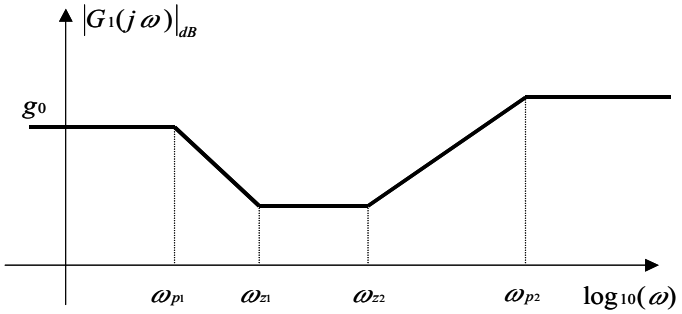

Figure 3.9: Bode plots of the standard focus and radial loops controller.

3.6.2 Current Spot Position Controllers

The current controller used in the focus and radial servo loops is a PID controller, whose transfer function $C(s)$ (see fig. 2.24) has the following form :

$$C(s) = g_0 \frac{(s+\omega_{z_1})(s+\omega_{z_2})}{(s+\omega_{p_1})(s+\omega_{p_2})} \tag{3.23}$$

Its simplified Bode amplitude plot is presented in fig.3.9.
A pole at very low frequency ω_{p1} provides an high level of the controller DC gain g_0, in order to guarantee the suppression of low frequency disturbances, as vertical deviation or eccentricity. These perturbations act on the system as harmonics, having a fundamental frequency proportional to the disc rotational frequency :

$$f_{rot} = \frac{v_a}{2\pi d_{\mathrm{R}}} \tag{3.24}$$

where $v_a = 3.49 m/s$ is the disc scanning velocity, specified in [59], and d_{R} is radial distance of the spot, with respect to the disc center hole. Usually in a DVD-video disc, data are recorded starting from an innermost to an outermost location. The first is called *lead-in* area, and correspond to $x_{in} = 23$ mm; the second one is called *lead-out* area and correspond to $x_{out} = 60$ mm. The periodic perturbations thus can affect the control system in a range of frequencies that goes from above 9 to 24 Hz, for an over-speed factor $N = 1$. This action stops at ω_{z1}. Then a second zero is added at ω_{z2} to perform a differential action needed to achieve the necessary phase margin ϕ_m, for robust stability of the loop. Finally a high frequency pole at ω_{p2} is used to reduce the effect of electro-mechanic resonance and measurement noise.

In section 4.8 the performances of this controller are analyzed by identifying the usual closed-loop sensitivity functions.

3.6.3 Industrial Implementation

As discussed in section 3.6.1 in the current application a DSP is used to process the error signals e and calculates the outputs v to the actuator's drivers. This task is accomplished by means of digital computation, with a

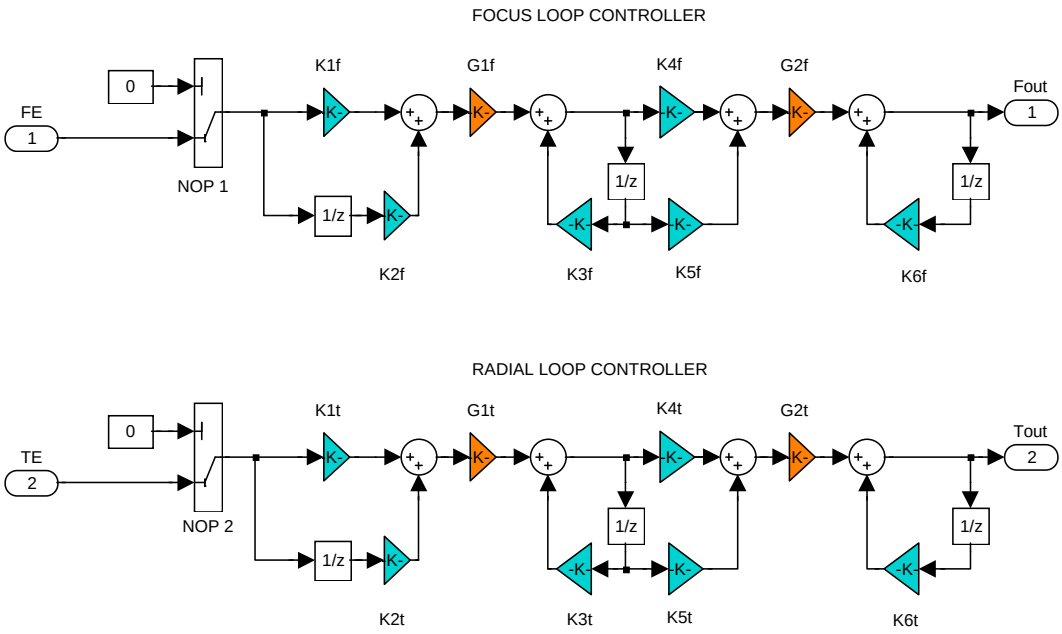

Figure 3.10: Block-scheme of the focus and radial loop controllers, implemented inside the DSP.

sampling frequency $f_s = 123.45\ Khz$. The discrete-time transfer function of the generic focus and radial loop controller has the following form :

$$C(z^{-1}) = g_0 \frac{(1 - b_1 z^{-1})(1 - b_2 z^{-1})}{(1 - a_1 z^{-1})(1 - a_2 z^{-1})} \tag{3.25}$$

where a_1, a_2, b_1 and b_2 are the controller discrete-time poles and zeros.

The block-scheme of the focus and of the radial loop controllers, implemented inside the dedicated DSP, are presented in fig.3.10, and the corresponding discrete-time transfer functions, from the controller output to the position error signal, are given by :

$$\frac{F_{out}}{FE} = G_{1f} G_{2f} \frac{(K_{1f} + K_{2f} z^{-1})}{(1 - K_{3f} z^{-1})} \frac{(K_{4f} + K_{5f} z^{-1})}{(1 - K_{6f} z^{-1})} \tag{3.26}$$

$$\frac{T_{out}}{TE} = G_{1t} G_{2t} \frac{(K_{1t} + K_{2t} z^{-1})}{(1 - K_{3t} z^{-1})} \frac{(K_{4t} + K_{5t} z^{-1})}{(1 - K_{6t} z^{-1})} \tag{3.27}$$

where G_{1f}, G_{2f}, G_{1t} and G_{2t} are constant gains, and K_{if}, K_{it}, $\forall i = 1 \ldots 6$ are coefficients, whose values define the location of the controllers poles and zeros in the discrete-time z-plane.

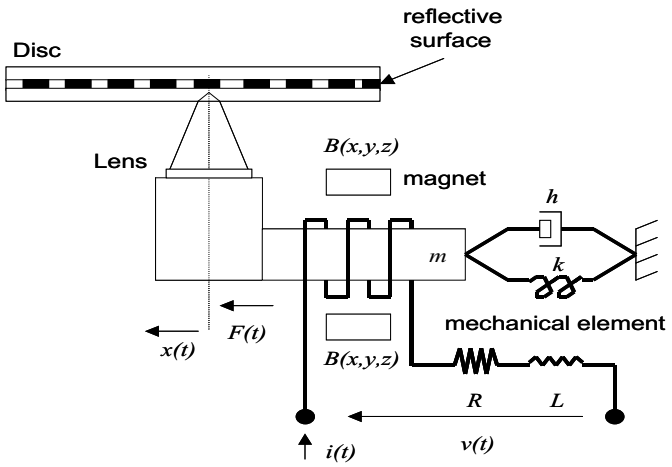

Figure 3.11: Actuators physical model.

3.7 Physical Models

A control-oriented mathematical model of the objective lens actuators can be developed by using physical principles. Focus and radial actuators are constituted by a lens attached to the pick-up body by two parallel leaf spring, and moved in vertical and radial direction by a voice coil and a magnet, as depicted in fig.3.11. The voltage $v(t)$, which controls the pick-up voice coil, and the laser spot position $x(t)$, are the actuator input and output signals. Due to the presence of the leaf springs, the mechanical part of the actuator can be modelled as a second order mass-spring system, having a resonance frequency of above $50Hz$.
The actuator mathematical model can be obtained by considering that the voltage $v(t)$ applied to the R-L circuit makes flow in it a current $i(t)$, which is solution of the following differential equation :

$$L\frac{\partial i(t)}{\partial t} + Ri(t) = v(t) - K_e\frac{\partial x(t)}{\partial t} \tag{3.28}$$

where $K_e\frac{\partial x(t)}{\partial t}$ is a term which takes into account the mutual interaction between the permanent magnets and the coil inductance.

By transforming eq.(3.28) into Laplace domain we obtain :

$$I(s) = \frac{1}{Ls+R}[V(s) - K_e sX(s)] \tag{3.29}$$

It is well known that in a magnetic field a current $i(t)$ produces a force $f(t)$, whose intensity is proportional to the current that flow in the spiral :

$$f(t) = K_e i(t) \Longrightarrow F(s) = K_e I(s) \tag{3.30}$$

where K_e is the back-emf constant, whose value depends on the spool geometric length $\overrightarrow{l}$, on the intensity of the magnetic field $\overrightarrow{B}$ in the circuit Γ,

and on the magnetic permeability constant μ, as follows :

$$K_e = \oint_{\Gamma} \frac{\overrightarrow{B} \times d\overrightarrow{l}}{\mu} \tag{3.31}$$

The force $f(t)$ $[N]$ acts on the objective lens mass M $[Kg]$, making the actuator moves. The model of the actuator mechanical part can be derived considering that the moving mass M is linked to an elastic spring and to a dumper, having elastic constant k and dumping factor D, respectively. The force $f(t)$, generated by the magnetic field $\overrightarrow{B}$ $[T]$, acts as *forcing* term in the following differential equation :

$$M\frac{\partial^2 x(t)}{\partial t^2} + D\frac{\partial x(t)}{\partial t} + kx(t) = f(t) \tag{3.32}$$

In practice it is useful to have a frequency-domain description of the system, thus a *Laplace* transform of eq.(3.32) is derived as follows :

$$\frac{X(s)}{F(s)} = \frac{1}{Ms^2 + Ds + k} \tag{3.33}$$

Combining together eq.(3.29), eq.(3.30) and eq.(3.33), the transfer function from $V(s)$ to $X(s)$, denoted by $H(s)$, is given by :

$$H(s) = \frac{X(s)}{V(s)} = \frac{\frac{K_e}{ML}}{s^3 + \left(\frac{R}{L} + \frac{D}{M}\right)s^2 + \left(\frac{DR}{ML} + \frac{k}{M} + \frac{K_e^2}{ML}\right)s + \frac{kR}{ML}} \tag{3.34}$$

For eq.(3.33) we have :

$$\frac{X(j\omega)}{F(j\omega)} = \frac{1}{k}\frac{1}{-\frac{M}{k}\omega^2 + j\frac{D}{k}\omega + 1} = \frac{1}{k}\frac{1}{-\frac{\omega^2}{\omega_0^2} + 2j\frac{\xi\omega}{\omega_0^2} + 1} \tag{3.35}$$

where :

$$\omega_0 = 2\pi f_0 = \sqrt{\frac{k}{M}} \tag{3.36}$$

is the resonance frequency, and :

$$Q = \frac{\omega_0^2}{\frac{D}{M}\sqrt{\omega_0^2 - \frac{1}{4}\left(\frac{D}{M}\right)^2}} \tag{3.37}$$

denotes the absolute value of the actuator amplitude peak, at the resonance frequency f_0. The elastic constant k ($[N/m]$), the dumping factor D

([Ns/m]), and the electro-magnetic constant K_e ([Wb/m]) can be derived from eq.(3.36), eq.(3.37) and from the value of the actuator DC sensitivity S_{DC} ([mm/V]), and resistor R ([Ω]), as follows :

$$k = M(2\pi f_0)^2 \tag{3.38}$$

$$D = (2\pi f_0)M\sqrt{2\left(1-\sqrt{1-\frac{1}{Q^2}}\right)} \tag{3.39}$$

$$K_e = kRS_{DC} \tag{3.40}$$

These quantities are computed from the values of two actuators physical parameters, as prescribed in technical specifications [43] and [45].

In table 3.1 and 3.2 the values of the physical parameters of two DVD-video actuators (Focus and Radial) are presented.

Table 3.1: *Values of the physical parameters of Pick-up 1 (for focus and tracking actuators), from Pioneer [43].*

Name	Description	Value Focus	Value Tracking
R	DC resistance of coil	$5.4 \pm 1.1\ \Omega$	$5.9 \pm 1.2\ \Omega$
L	Inductance of coil	$15 \pm 6\ \mu H$	$9 \pm 6\ \mu H$
M	Moving mass	$0.7\ g$	$0.7\ g$
S_{DC}	DC Sensitivity	$2.69\ mm/V$	$0.63\ mm/V$
f_0	Resonance frequency	$30 \pm 7\ Hz$	$47 \pm 7\ Hz$
Q_{dB}	Resonance peak	$\leq 15\ dB$	$\leq 15\ dB$

Table 3.2: *Values of the physical parameters of Pick-up 2 (for focus and tracking actuators), from Sanyo [45].*

Name	Description	Value Focus	Value Tracking
R	DC resistance of coil	$6.5 \pm 1\ \Omega$	$6.5 \pm 1\ \Omega$
L	Inductance of coil	$25 \pm 6\ \mu H$	$18 \pm 6\ \mu H$
M	Moving mass	$0.33\ g$	$0.33\ g$
S_{DC}	DC Sensitivity	$0.94\ mm/V$	$0.27\ mm/V$
f_0	Resonance frequency	$52 \pm 7\ Hz$	$52 \pm 7\ Hz$
Q_{dB}	Resonance peak	$\leq 20\ dB$	$\leq 20\ dB$

As illustration, the frequency responses of the tracking actuators (*Pick-up 1* and *Pick-up 2*) are shown in fig.3.12. Similar results can be obtained for the focus loop actuator.

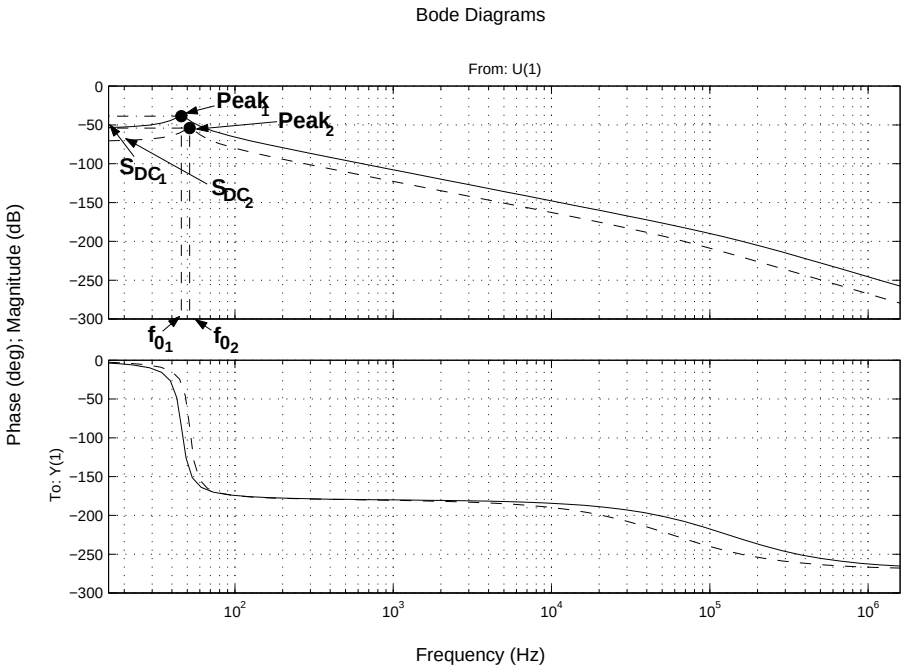

Figure 3.12: Bode diagram of two tracking actuators, used for an industrial DVD-video player. *Pick-up 1* (solid line) and *Pick-up 2* (dashed line).

3.8 Conclusions

In this chapter we have presented the industrial set-up used in our laboratories, to give a more detailed description of the used hardware sub-blocks and software procedures.
The control requirements have been computed in terms of frequency-domain bounds on the system sensitivity functions, and the actual control solution, used to implement the digital controllers, is then described to point out how the digital implementation is the main source of performance and controller order limitations.
In the last part of this chapter we have derived a control-oriented mathematical linear model of the objective lens actuators by using physical principles and values from technical specifications. To validate these models, further used to design new model-based controllers, a plant closed-loop identification procedure is performed, by measuring some system closed-loop frequency response. This will be the subject of the next chapter.

Chapter 4

System Identification

4.1 Introduction

As presented in section 2.8, the DVD drive servo system is composed by three main blocks : the power drivers, the optical devices and the objective lens actuator. The first two blocks can be respectively modelled with a constant gain g_d and g_{opt}, and the actuator can be modelled using physical equations, as presented in section 3.7.
Nevertheless, an accurate description of the plant dynamic is non trivial because, in CD and DVD players, the actual track position x is not directly available from measurements. In addition, the generation of the error signal e from the displacement $h = r - x$ between the track and the laser spot position (see fig.2.24) is provided by optical devices, whose behavior is far to be linear, as explained in sections 2.6.2 and 2.6.3.

This Chapter is devoted to frequency-domain plant identification of the DVD-video player servo system. The methodology already presented in Dettori [10], and based on measurement of closed-loop sensitivity functions, is used to identify the plant model and to validate the system closed-loop performance given in section 3.6.1.
Our aim is to validate, through experimental results, whether the plant physical model computed in section 3.7 gives a complete description of the system behavior, or if un-modelled dynamics and plant uncertainties have also to be taken into account in view of model-based control design.
Moreover, this approach will lead to estimate more accurately the behavior of optical devices, in order to derive a simple and not very time-consuming simulation scheme of the complete control chain, useful for control design

purposes. The identified plant model is validated through experimental results obtained on the industrial benchmark. Performance and robustness analysis of the current industrial solution is finally provided.

The chapter is organized as follows :

In section 4.2 a brief state of the art is presented, and in section 4.3 the sources of model uncertainty are discussed. In section 4.4 we present the set-up used to measure the system frequency responses. In section 4.5 a model of the system is derived through frequency domain measurements performed in open and closed-loop configurations. In open-loop, the frequency response of the implemented digital controller is measured. This result, together with the frequency responses of the closed-loop sensitivity functions, allows then to estimate the plant model. Section 4.6 is devoted to the computation of the plant model transfer function, by applying a curve fitting procedure on the measured data. Simulation and experimental results are then compared in section 4.7, to validate the actuator physical model presented in section 3.7. The system performance and robustness analysis are presented in section 4.8. In section 4.9 the coupling phenomena existing between the focus and the radial loops are studied and analyzed. Conclusions are presented in section 4.10.

4.2 State of the Art

In the literature, two different approaches used to deal with optical disc drives plant identification problems can be distinguished : a first class of works use parametric identification, by estimating unknown parameters in a predeterminate model structure, like presented in Callafon et al. [7], Van den Hof et al. [60], Van den Hof and Schrama [61], and Vidal et al. [65]. In the [7], [60], and [61] data, used for the identification procedure, is a frequency domain representation of a measured time sequence, by means of fast Fourier transform (FFT) in conjunction with periodic excitation. In [65] open-loop parametric system identification is provided by measuring the current through the coils of the actuators of a CD player, and the parameters of the plant transfer function are computed by minimizing the least-square loss function of the discrete-time ARX model. Since the only parameter which cannot be identified is the optical gain, this has been therefore estimated via closed-loop experiments.

In another class of works, linear continuous or discrete-time plant models are estimated using measured frequency response data. This methodology presents several advantages compared to the time-domain approach, as outlined in Ljung [38], Pintelon et al. [40], [41] and Pintelon and Schoukens [42], since frequency domain identification allows to easily validate the model, offering also the possibility to use frequency depending weights in order to modify its shape.

In Dötsch [18], [19], periodogram averaging in conjunction with periodic excitation signals are put forward as powerful means to estimate the CD servo mechanism plant frequency response, based on a large number of measurements data. In Callafon and Van den Hof [8], Dettori et al. [11], Donkelaar et al. [16], Van den Hof et al. [60], [61] a *Matlab* graphical user interface, called *FREQID*, is used to identify linear, time-invariant either continuous or discrete-time models on the basis of frequency domain data. The estimation of the model is obtained by applying a frequency weighted curve fit procedure on the available frequency response and by selecting a model order. Estimation routines based on the curve fitting with a least squares criterion have been implemented in the current distribution of *FREQID*. Between least-square methods, the one applied to CD mechanism is the so called *LSFITS* (Least Squares Curve Fitting with Schur weighting), which allows to parameterize the model with a left or right Matrix Fraction Description (MFD). This allows to represent the estimated models with a simple numerator/denominator continuous or discrete-time transfer function form [7].

On the other side, in Bittanti et al. [2], Dettori [10], Dettori and Scherer [12], [13], [14], Dettori and Stribos [15] and Steinbuch et al. [55], [56], [57] the continuous-time plant frequency response is identified trough closed-loop experiments and spectrum analysis techniques. The closed-loop transfer functions, defined in section 4.5.3 from eq.(4.15), (4.16) and (4.17), are computed by fitting the measured frequency responses. Model structures are carried-out by means of output error method associated to a least-square criterion [48].

In Steinbuch et al. [55], [56] and [57] frequency depending weighting functions are also used to improve the fit accuracy around the desired system bandwidth, where the measured data are more affected by a non proper behavior of the plant.

In our work, the main source of plant uncertainty we wish to take into account are due to parameters tolerances present during the plant manufacturing process. Such kind of uncertainties may produce differences, in term of frequency response, between the computed physical model and the one obtained from identification. This is particularly true at high-frequencies, where the most varying plant parameters (the voice coil resistance R and inductance L, as well as the objective lens moving mass M) may be responsible for *unexpected* dynamics (resonance peaks or different slopes in the plant magnitude frequency responses). Hence, our aim is to verify if such dynamics exist and if they are relevant in the frequency range of interest for model-based control design. To this end, the methodology presented in Dettori [10] and used to identify the plant frequency response of a CD servo mechanism, is applied to a DVD-video player servo system.

4.3 Model Uncertainty

In this chapter we will select a nominal and an uncertainty plant model of the DVD servo mechanism on the basis of frequency domain identification experiments conducted on two industrial mechanisms, denoted in what follows as *pick-up 1* and *pick-up 2*, respectively. It is clear, from the above discussion, that we cannot guarantee that these models represent a set of effective behavior, but there are no reasons to deny that the achieved nominal model can be close to the boundary of the set of possible behaviors.
In Section 3.7 we have presented a nominal model of the objective lens actuators (see eq.3.34), using electro-mechanical equations, the values of the physical parameters being obtained from technical specifications.
Nevertheless, manufacturing tolerances can generate variations in the dynamical behavior from player to player, causing different slopes of the actuator amplitude characteristic and possible location and damping of the system high-frequency resonance modes.
Due to the typical values of the voice coil resistance R and inductance L (see tables 3.1, 3.2 and eq.(3.29), these phenomena can usually occur for frequencies located above 30 KHz, and they can play an important role when is needed to achieve a high-bandwidth controller design, since they may cause loss of performance and even instability of the whole system. Also, from actuators technical specifications, it is difficult to determine whether high-frequency resonance modes exist, and where they are located, because no information is given about the actuators behavior at high frequencies.

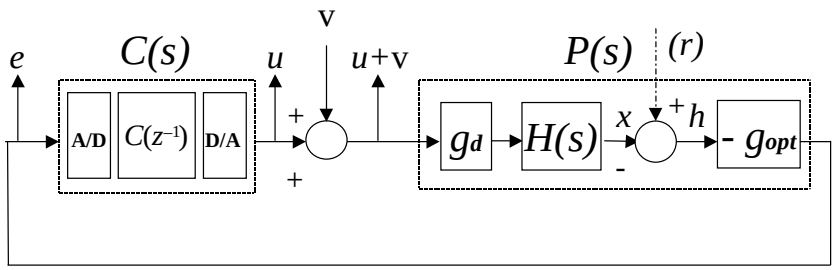

Figure 4.1: Block scheme of the experimental set-up used for identification.

The only way to estimate such kind of uncertainties is to repeat the measurements on a large number of players, in order to build a nominal model by considering the average of the observed behaviors. Then, all the observed behaviors can be included in a model uncertainty set, built around the nominal (average) model.
In chapter 5 the variations of the actuator physical parameters will be taken into account according to tables 3.1 and 3.2, to built a model uncertainty set, based on a parametric description of the DVD mechanism and norm-bounded real perturbations. This will allow to design an H_∞ controller, following industrial oriented control objectives and to perform an *a-posteriori* performance and robustness analysis.

4.4 The experimental set-up

For experimental purposes an STMicroelectronics test board, designed for video DVD player, has been available as industrial benchmark. Two different pick-ups have been used to implement servo algorithms and test the control system performance and robustness. This set-up allows to measure several signals and to inject external excitation in the control loops, in order to identify the plant frequency response. The block-scheme representing the experimental set-up used for identification is shown in fig.4.1, where two main blocks can be distinguished :

- The control block $C(s)$, composed by an A/D and a D/A converter, and a digital controller $C(z^{-1})$ as shown in fig.4.1. It processes the error signals e, provided from photo-detectors, to give the control signal u to the actuators drivers.

- The plant $P(s)$, composed by the objective lens actuator $H(s)$, the actuators drivers g_d, and the photo-detectors gain g_{opt}.

This scheme is valid for both focus and radial loops, so every signal can be interpreted as two-dimensional, with a focus and a radial component. The signals available from measurements are the error signal e provided by the optical devices, the controller output u, and the signal $(u + v)$, which is the

input to the actuator drivers. v is the external excitation injected in the loop for identifying the plant frequency response. r is the track reference position, interpreted as disturbance and which is added at the actuator output [9]. As already explained in sections 2.8 this is a fictitious signal, which represents the perturbation entering in the loop at the actuator's output. That is why in fig.4.1 r is put in brackets and it is summed to x.

Considering the focus loop as the first and the radial as the second loop, the nominal values of the driver gains used in *pick-up 1* and *pick-up 2*, respectively are the following :

$$g_{d1_{focus}} = g_{d1_{radial}} = 5.20 \ \ [V/A] \tag{4.1}$$

$$g_{d2_{focus}} = g_{d2_{radial}} = 12.55 \ \ [V/A] \tag{4.2}$$

The value of the gain of the optical devices g_{opt} is unknown and will be, therefore, considered as part of the model to be identified.

4.5 Frequency Domain Measurements

In a DVD-video player, data read-out is only possible when the laser spot is correctly positioned with respect to the disc layer and to the center of the target track, since the system cannot work if bounds (2.12) are not achieved for focus and radial error signals. In fact, correct spot positioning with respect to the disc layer or a fixed track is obtained only if the relative position error $h = r - x$ remains small enough to guarantee that bounds on e hold. Ideally, during playback it is required that $x(t) = r_0(t)$, $\forall t$ (if disc imperfections are neglected) and this is possible only when the spot position is fedback by a controller. This explains why signals used for identification purposes should be measured when the system is in closed-loop.

On the other side, open-loop experiments can only be performed to measure the frequency response of the internal controller $C(s)$, used on the industrial benchmark. Usually its parameters are known from design algorithms, and frequency response plots can be easily obtained from simulations.
However, during the qualification phase of the system-on-chip solution, it was required to verify if the implemented controller corresponded to the conceived one. This has allowed to evaluate a part of performance limitations. The fastest way to do that has consisted in tracing the frequency response of the synthesized controller, and in comparing it with the frequency response

Figure 4.2: The Agilent 35670A Dynamic Signal Analyzer.

of the implemented one. This task has been accomplished on a DVD-video player conceived for the consumer market, and successfully launched in mass production in May 2002.
From practical point of view, this procedure has allowed to validate the controller design, and it has been used to perform the plant closed-loop identification (see section 4.5.3), assuming the *a-priori* knowledge of the controller frequency response (see section 4.5.2).

4.5.1 Measuring using a Dynamic Signal Analyzer

For the measurements of the system frequency responses, an Agilent 35670A Dynamic Signal Analyzer (DSA) has been used [58] (see fig.4.2). This device includes different functionalities of several instruments at once, which make it ideal for R&D applications.
The DSA can generate an excitation signal as output, and measure two signals as input. The signals e, u, v and $u+v$ of fig.4.3 are used for estimation of frequency-response models. The channel "Source" is the device's output, which is directly connected to the system to be characterized (signal v in fig.4.3). Channel 1 is commonly the reference input channel, i.e. the input to the system. Channel 2 is the response channel of the system, which can be connected to signals e, u and $u+v$ of fig.4.3, depending on the system transfer function frequency response to measure.

Frequency responses are evaluated by dividing the channel 2 linear spectrum $P_{22}(j\omega)$, by the channel 1 linear spectrum $P_{11}(j\omega)$, as follows :

$$F(j\omega) = \frac{P_{22}(j\omega)}{P_{11}(j\omega)} \tag{4.3}$$

where $F(j\omega)$ is the frequency response of a generic transfer function $F(s)$, and :

$$P_{i,j}(j\omega) = \frac{1}{T_{in}} \int_{-T_{in}/2}^{T_{in}/2} p(t) e^{-j\omega t} dt, \quad \forall \ i = j = 1, 2 \tag{4.4}$$

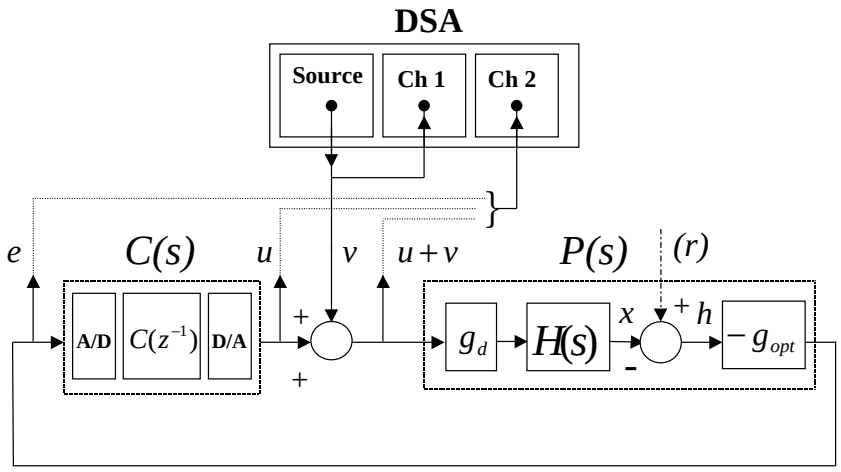

Figure 4.3: Connection scheme used for identification.

is the Fourier transform of a generic periodic signal $p(t)$, of period T_{in}.

Channel 1 is usually connected to the source channel in order to let the DSA compute the ratio between the linear spectra of the measured output to the system (taken on channel 2) and the injected excitation (taken on channel 1).

The acquired external signals (e, u and $u + v$) are sampled by the analyzer at a fixed frequency of $f_{s_{DSA}} = 128\ KHz$, which allows to provide sufficient data for a measurements span from 97.7 μHz to 51.2 KHz, and a minimum resolution of 61 μHz (800 lines display). Every sample is converted into 16-bit digital word, thanks to a 16-bits A/D converter, and the signal is then sampled at lower frequency, to adjust the frequency range specified by the user. In this way a single anti-aliasing filter is used for every frequency spans. After re-sampling, a time record of 1024 samples is created, multiplied for the selected window and Fourier transformed to 512 frequency domain samples.

A periodic excitation has been chosen to carry out system frequency response measurements. When such a signal is used, the measured system output has asymptotic zero variance and, the phase response can be accurately determined. This makes preferable to use a periodic excitation rather than white noise.
Particularly, we used a swept sine signal, which is a sine wave having a fixed amplitude and a frequency that is swept in the range of interest. With reference to fig.4.3, the external excitation signal v used for identification purposes, can be expressed as follows :

$$v(t) = \overline{A_{sw}} + A_{sw} \sin\left[w_i(t)t\right] \quad \forall i = 1, \ldots, N_f \tag{4.5}$$

where $w_i(t) = w_0 + \zeta t$ is the instantaneous frequency sweep, and $\zeta = (w_1 - w_0)/(t_0 - t_1)$ ensures that the desired frequency breakpoint w_1 at time t_1 is maintained. In our case, $w_0 = 0$, $w_1 = 2\pi \cdot (51.2)\ kHz$, $t_0 = 0$ and $t_1 = 136$ s.

The quantity $\overline{A_{sw}}$ denotes the DC offset level added to the swept sine, A_{sw} is its fixed peak amplitude, and w_i its frequency swept in the frequency range of interest.
When swept sine measurements are performed, the 35670A DSA "sweeps" its sinusoidal source through a series of discrete frequencies w_i, whose number is denoted with N_f. At each frequency the analyzer measure the magnitude and the phase of the system response. Such kind of measurement provides extremely good signal-to-noise ratios (SNR), which helps to get exact measurements and to guarantee a dynamic range of 130 dB. The maximum allowed amplitude range of the source v is $\pm 5V_{pk}$ (AC), and the maximum value of the source DC offset $\overline{A_{sw}}$ is $\pm 10V$.
Before starting the measurements, important parameters have to be selected, as the swept resolution R_{sw}, the integration time T_{in}, the number of resolution lines N_{sw}, and the number of averages per frequency point N_{av}.

- The swept resolution R_{sw} gives the number of measurement frequencies in the selected range. Increasing the resolution will reduce the loss of data that fall between measurement points, but it will increase measurement time.

- The integration time T_{in} (see eq.4.4) is the period of time during which each point is measured, and defines, at each frequency, the number of cycles of the excitation signal that are integrated to compute the FFT transform. If this parameter is too small, transient effects could affect the output signal.

- The number of resolution lines N_{sw} defines the frequency resolution of the FFT. The bigger the frequency resolution is, the more accurate the calculation of the Fourier coefficients is, but this will increase the length of the time record, and will reduce the maximum measurable frequency range $[\omega_0, \omega_1]$.

- The number of average N_{av} defines the number of measurements done at each frequency. As the analyzer makes a series of averages, the result from the last completed measurements are combined, point by point, with the previous measurement. These combined results are

displayed as they are updated. Increasing the number of average helps to decrease the measurement variance.

The values of all these parameters have to satisfy a trade-off between measurement accuracy and duration.
Accuracy is required to avoid loss of data between two adjacent frequencies ω_i and ω_{i+1}, and to reduce measurements variance.
Short-time acquisitions would allow to acquire data in larger frequency intervals. Finally, averaging can be used to remove noise that affects the system during closed-loop acquisitions.
This is particularly important in optical disc drives, where the track position r (see fig.4.3) acts as a periodic disturbance added at the output of the plant and measurement noise is added by the optical devices.

The 35670A Dynamic Signal Analyzer technical characteristics are summarized in table 4.1.

Table 4.1: *Technical characteristics of the Agilent 35670A DSA.*

Frequency span	From 0 to 102.4 KHz at 1 channel From 0 to 51.2 KHz at 2 channels
Resolution lines N_{sw}	100, 200, 400 and 800
Amplitude Accuracy	[$\pm 2.92\%$ $\pm 0.025\%$]
Amplitude Range	[3.99 mV_{pk} 31.7 V_{pk}]
Dynamic range	[80 dB 130 dB]
Real-time bandwidth	25.6 KHz/1 channel
Input Impedance	1 $M\Omega$
Source Impedance	50 Ω
Source	Random, burst random, periodic chirp, burst chirp, colored noise, fixed sine, swept-sine, arbitrary source
Measurements	Linear, Cross and Power Spectrum, Coherence, Power, Spectral Density, Frequency Response, Time Waveform, Autocorrelation, Cross-Correlation, Histogram

Setting chosen for measurements :

For our experiments we have set a sweep resolution of $R_{sw} = 100$ points/sweep. The integration time has been fixed equal to $T_{in} = 5$ swept sine cycles, to

have longer integration times at low frequencies, where sweep sine cycles occurs slower.
At high frequencies the same number of cycles occurs in a shorter time. $N_{sw} = 400$ is the number of resolution lines considered during acquisitions, and a rms (root mean square) averaging mode has been selected with $N_{av} = 4$ averaging per frequency point, to reduce the measurement noise to its mean value. In order to let the actuator move inside its linear region and to avoid to lost the radial seek action, the maximum peak amplitude of the injected swept sine has been set equal to $A_{sw} = 30\ mV_{pk}$, and its DC offset of $\overline{A_{sw}} = 1$ V.

4.5.2 Open-loop measurements : Controller frequency response

The controllers frequency responses can be obtained by opening the loop, and measuring the control signal u, when an external periodic excitation is injected on the position error signal e. For this purpose, the dynamic signal analyzer has been connected to the system, as shown in fig.4.4.
In this picture GMB denotes the gain of the main spot beam, and its value can be measured by selecting appropriately the photo-detectors slice level. The coefficients C_{101} and $C_{30/34}$ are simple gains used inside the DSP to determine the amplitude of the input signals which enter to the digital filter $C(z^{-1})$. The block AGC denotes the value of a gain, tuned during the automatic gain control procedure, as explained in section 3.5.3.

R_1, R_2 and C are the resistors and the capacitor of the first stage of the actuators driver, whose value define the drivers gain as follows :

$$g_d \simeq \frac{R_2}{R_1} \tag{4.6}$$

The value of these parameters are presented in table 4.2, for *pick-up 1* and *pick-up 2*. As shown in fig.4.4, for open-loop measurements the pick-up is disconnected, and the control loop is open between the actuator drivers and the ADC. The source is directly connected to the A/D input, the reference channel (channel 1) is connected to the source, and the measured output (channel 2) to the actuator drivers output.
The ratio between measured data of channel 2 and channel 1 gives the global frequency response between points *output* and *input*.
In both cases, we used as input signal a swept sine having an amplitude of 30 mV_{pk}, a frequency variable between $\omega_0 = (2\pi)5\ Hz$ and $\omega_1 = (2\pi)51.2$

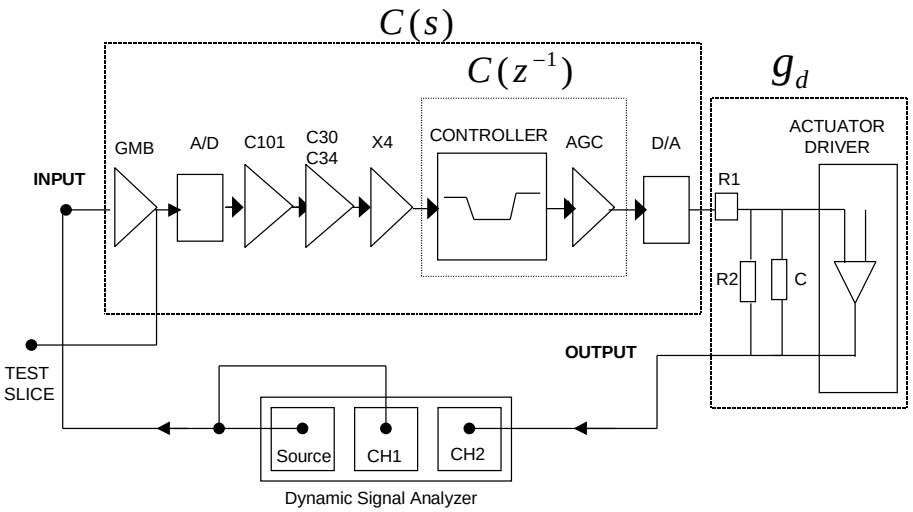

Figure 4.4: Experimental set-up used for controller identification.

Table 4.2: *Value of the setting used for pick-up 1 and pick-up 2*

	Pick-up 1	*Pick-up 2*
R_1	6.3 $k\Omega$	36 $k\Omega$
R_2	8.2 $k\Omega$	113 $k\Omega$
C	390 pF	39 pF
GMB	1.4 dB	1.4 dB
C_{101}	-6 dB	-6 dB
C_{30}	-12 dB	-18 dB
C_{34}	-12 dB	-12 dB
AGC_{focus}	12 dB	6.8 dB
AGC_{radial}	12 dB	8.6 dB

KHz, and a DC offset of $\overline{A_{sw}} = 2.8\ V$.

In fig.4.5 and 4.6 we present the Bode plots of the actual radial and focus loop controllers, used in the industrial solution for *pick-up 1* and *pick-up 2*, respectively.
It appears clearly that simulated and measured frequency responses match for both radial and focus loop controllers and for both pick-ups. It can be noticed that, for both loops and for both pick-ups, the measured characteristics reveal that during the controllers implementation phase, an extra high-frequency pole is added. It is well known, in fact, that in the digital implementation of a controller its frequency response is subjected to distortions due to the analog reconstruction of the controller output performed by the D/A converter, and the computational delay added inserted by the internal DSP registers.
In our case we can see that the amplitude distortion is negligible in the frequency range up to 20 kHz and that phase losses are of above 10 degrees

around 2 kHz, which is a typical value of the radial and focus loop closed-loop bandwidths.

In what follows we will denote with $C(j\omega)$ and with $\hat{C}(j\omega)$ the simulated and the measured controllers Bode plots, respectively.

The total DC gain expressed in dB and measured from *output* to *input*, is given by the DC gain of the digital filter $C(z^{-1})$ (which contains the AGC gain) plus the gains of the other blocks, included in the experimental set-up, as presented in fig.4.4 :

$$G_{DC_{TOT}} = G_{DC_{C(z^{-1})}} + GMB + C_{101} + C_{30/34} + 20\lg_{10}(4) + 20\lg_{10}(g_d) \quad (4.7)$$

a) Pick-up 1 :

We have, for both focus and radial loops (see table 4.2) :

$$GMB + C_{101} + C_{30/34} + 20\lg_{10}(4) + 20\lg_{10}(g_d) = -2.3dB \quad (4.8)$$

Thus, the static gain of the focus and radial loop controllers used for *pick-up 1* and defined as $G_{1F_{DC_{C(z^{-1})}}}$ and $G_{1R_{DC_{C(z^{-1})}}}$, respectively are given by :

$$G_{1F_{DC_{C(z^{-1})}}} = G_{1R_{DC_{C(z^{-1})}}} = G_{1_{DC_{TOT}}} + 2.3dB \quad (4.9)$$

a) Pick-up 2 :

The DC gains of these blocks are different for the focus and for the radial loop, as it can seen from table 4.2.

For the focus loop we have :

$$GMB + C_{101} + C_{30} + 20\lg_{10}(4) + 20\lg_{10}(g_d) = 0.665dB \quad (4.10)$$

which gives the static gain of the focus loop controller used for *pick-up 2* $G_{2F_{DC_{C(z^{-1})}}}$ as follows :

$$G_{2F_{DC_{C(z^{-1})}}} = G_{2F_{DC_{TOT}}} - 0.665dB \quad (4.11)$$

For for the radial loop we have :

$$GMB + C_{101} + C_{34} + 20\lg_{10}(4) + 20\lg_{10}(g_d) = 5.33dB \quad (4.12)$$

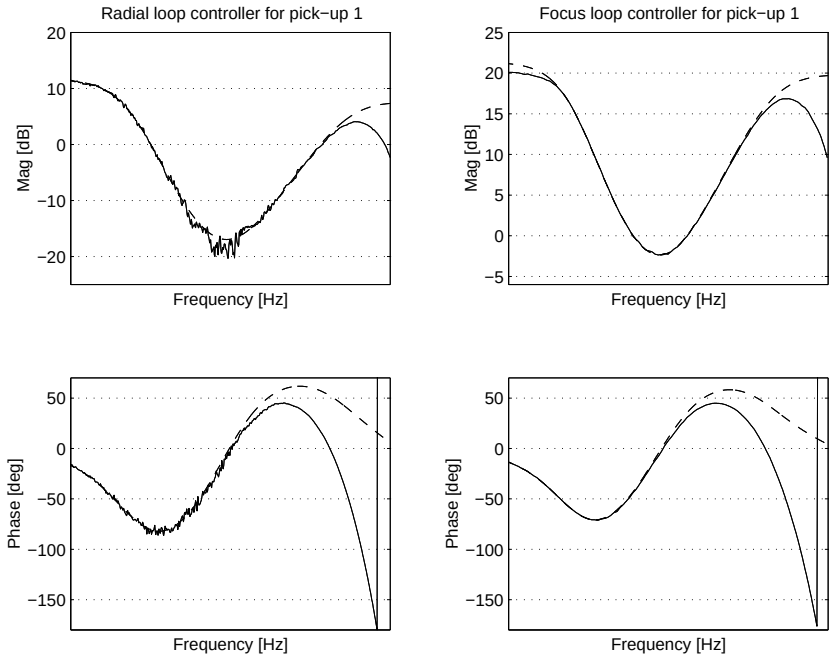

Figure 4.5: Simulated $C(j\omega)$ (dashed line) and measured $\hat{C}(j\omega)$ (solid line) frequency responses of the radial and focus loop controllers, implemented for *pick-up 1*.

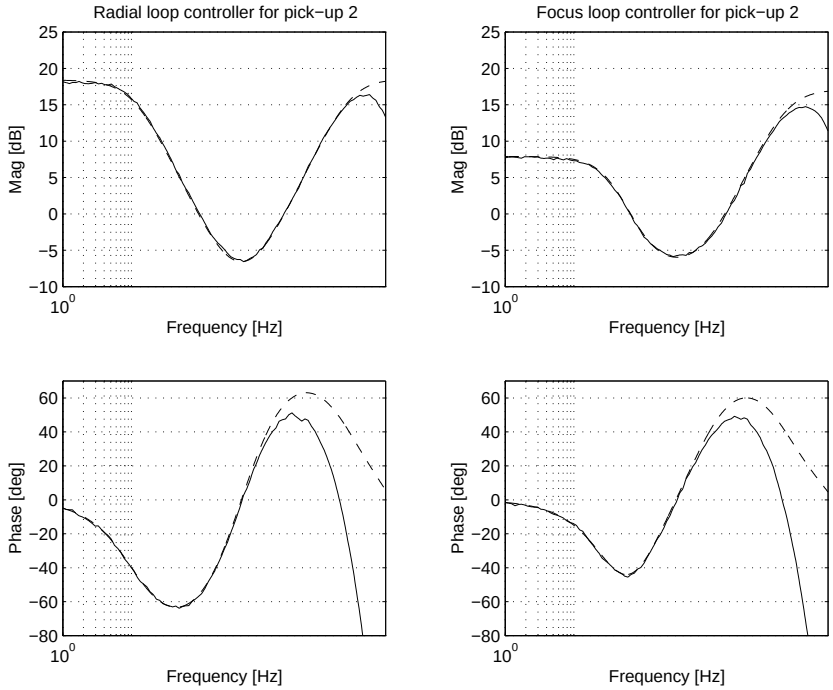

Figure 4.6: Simulated $C(j\omega)$ (dashed line) and measured $\hat{C}(j\omega)$ (solid line) frequency responses of the radial and focus loop controllers, implemented for *pick-up 2*.

which gives the static gain of the radial loop controller used for *pick-up 2* $G_{2R_{DC_{C(z^{-1})}}}$ as follows :

$$G_{2R_{DC_{C(z^{-1})}}} = G_{2R_{DC_{TOT}}} - 5.33dB \tag{4.13}$$

In order to correctly perform the system performance and robustness analysis, we have considered, for both pick-ups, the simulated controllers frequency responses shifted of the quantities $G_{1F_{DC_{C(z^{-1})}}}$, $G_{1R_{DC_{C(z^{-1})}}}$, $G_{2F_{DC_{C(z^{-1})}}}$ and $G_{2R_{DC_{C(z^{-1})}}}$, as shown in fig.4.5 and fig.4.6.

4.5.3 Closed-loop measurements : Plant frequency response

As explained in Section 4.5, closed-loop measurements are performed in order to derive the plant frequency responses $P(s)$, using an estimate of the closed-loop sensitivity functions.
In this section we will present experimental results obtained for the radial loop of two different pick-ups. Similar results can be obtained for the focus loop but they are not presented here, since we mainly focus in this work on track following control problem.

From the block diagram of fig.4.1, the plant transfer function is given by :

$$P(j\omega) = g_d g_{opt} H(j\omega) \tag{4.14}$$

This is the plant transfer function to be identified. By injecting the external signal v in the loop, the closed-loop frequency response from v to the control signal u is given by :

$$T(j\omega) = -\frac{g_d g_{opt} H(j\omega) C(j\omega)}{1 + g_d g_{opt} H(j\omega) C(j\omega)} = -\frac{P(j\omega) C(j\omega)}{1 + P(j\omega) C(j\omega)} \tag{4.15}$$

From v to $(u + v)$, the frequency response of the system output sensitivity function is obtained as follows :

$$S(j\omega) = -\frac{1}{1 + g_d g_{opt} H(j\omega) C(j\omega)} = -\frac{1}{1 + P(j\omega) C(j\omega)} \tag{4.16}$$

From v to e, the frequency response of the system input sensitivity function is finally obtained as follows :

$$SP(j\omega) = -\frac{g_d g_{opt} H(j\omega)}{1 + g_d g_{opt} H(j\omega) C(j\omega)} = -\frac{P(j\omega)}{1 + P(j\omega) C(j\omega)} = -S(j\omega) P(j\omega) \tag{4.17}$$

In what follows $\hat{T}(j\omega)$, $\hat{S}(j\omega)$, and $\widehat{SP}(j\omega)$ will denote the measured frequency responses of $T(j\omega)$, $S(j\omega)$, and $SP(j\omega)$, from experimental data, and their Bode plots, obtained for *pick-up 1* and *pick-up 2*, are shown in fig.4.7 and fig.4.8, respectively.
Unfortunately, as it can be seen from these figures, closed-loop measurements are very ill-conditioned : in order to let the DVD player operate, the control system should strongly suppress the disturbance signals v, making very difficult to retrieve good information about this disturbance from the position error signal e. Thus, even thought the best setting has been chosen for the dynamic signal analyzer parameters R_{sw}, T_{in}, N_{sw}, and N_{av} (see section 4.5.1), the measurements of the output sensitivity function $\hat{S}(j\omega)$ are highly corrupted by noise, at low-frequencies. This is due to the high DC attenuation level, required from disc specifications [59], and needed to suppress external disturbances (as eccentricity and vertical deviation) that reduces the output signal-to-noise ratio (SNR) and affect the control loop at these frequencies.

As stated in Dettori [10], the frequency response of the plant $P(s)$ can be obtained, from eq.(4.15), (4.16) and (4.17), in two different ways :

- If the controller frequency response is known, the estimate of the plant frequency response P_{est_1}, can be obtained from $S(j\omega)$ and $C(j\omega)$:

$$P_{est_1}(j\omega) = -\frac{1}{C(j\omega)}\left[1-\Big(1+P(j\omega)C(j\omega)\Big)\right] = -\frac{1}{C(j\omega)}\left[1+S(j\omega)^{-1}\right] \tag{4.18}$$

- If the controller frequency response is unknown, P_{est_2} can be computed by multiplying $SP(j\omega)$ by the inverse of $S(j\omega)$:

$$P_{est_2}(j\omega) = -\Big[1+P(j\omega)C(j\omega)\Big]\left[\frac{P(j\omega)}{1+P(j\omega)C(j\omega)}\right] = \frac{1}{S(j\omega)}\Big[SP(j\omega)\Big] \tag{4.19}$$

Measuring, with the dynamic signal analyzer, $\hat{S}(j\omega)$, $\hat{C}(j\omega)$ and $\widehat{SP}(j\omega)$ we obtain :

$$\hat{P}_{est_1}(j\omega) = -\frac{1}{\hat{C}(j\omega)}\left[1+\hat{S}(j\omega)^{-1}\right] \tag{4.20}$$

and :

$$\hat{P}_{est_2}(j\omega) = \frac{1}{\hat{S}(j\omega)}\left[\widehat{SP}(j\omega)\right] \tag{4.21}$$

These two methods are applied and compared, and in both cases we have obtained a model of the plant transfer function $P(s)$, given in eq.(4.14).

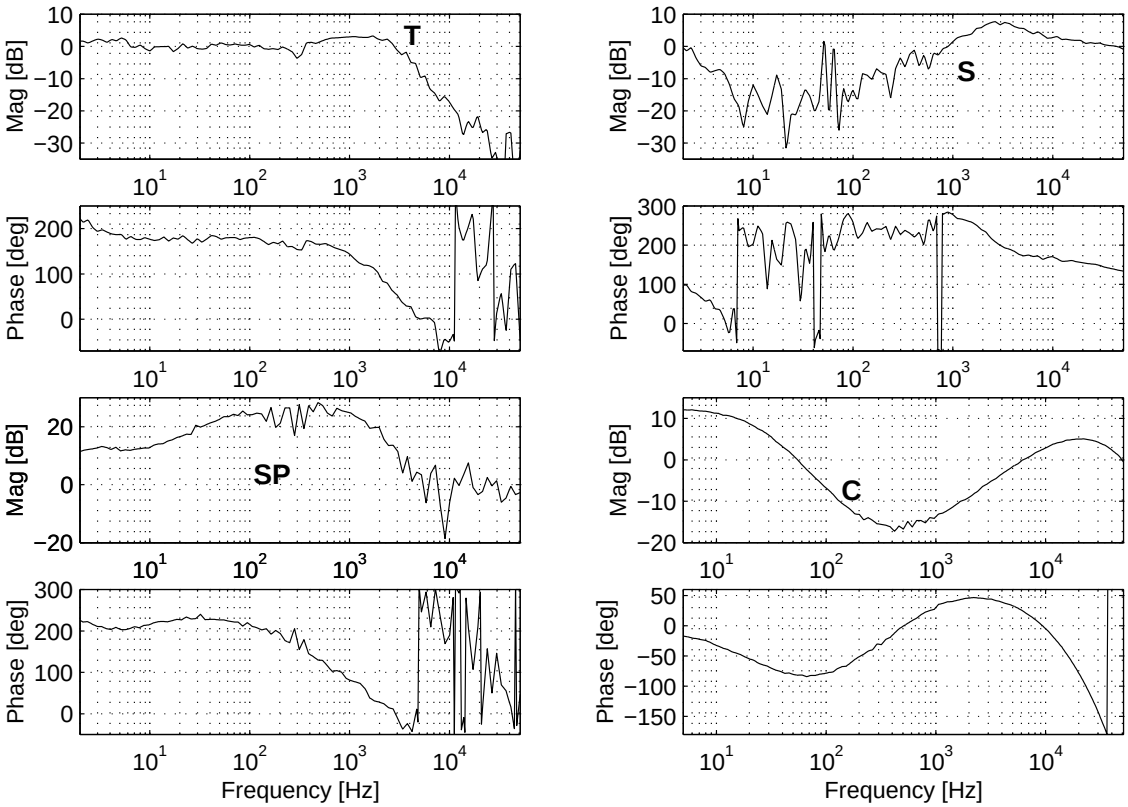

Figure 4.7: Measured frequency response of $\widehat{T}(j\omega)$, $\widehat{S}(j\omega)$, $\widehat{SP}(j\omega)$ and $\widehat{C}(j\omega)$, obtained for *pick-up 1 (radial loop).*

4.6 Curve Fitting Procedure

a) Choice of the method used to estimate $P(s)$:

In the previous section it has been shown that there exist two possibilities to compute the frequency response $P(s)$ of the spot position actuator, based on closed-loop measurements.
In this section, these procedures will be applied on the measured data acquired for *pick-up 1* and *pick-up 2*, and plotted in fig.4.7 and fig.4.8, respectively. In fig.4.9 and fig.4.10 are shown the frequency responses of $\hat{P}_{est_1}(j\omega)$ and $\hat{P}_{est_2}(j\omega)$, obtained for *pick-up 1* and *pick-up 2*, accordingly to eq.(4.20) and eq.(4.21). From these figures it can be noticed that :

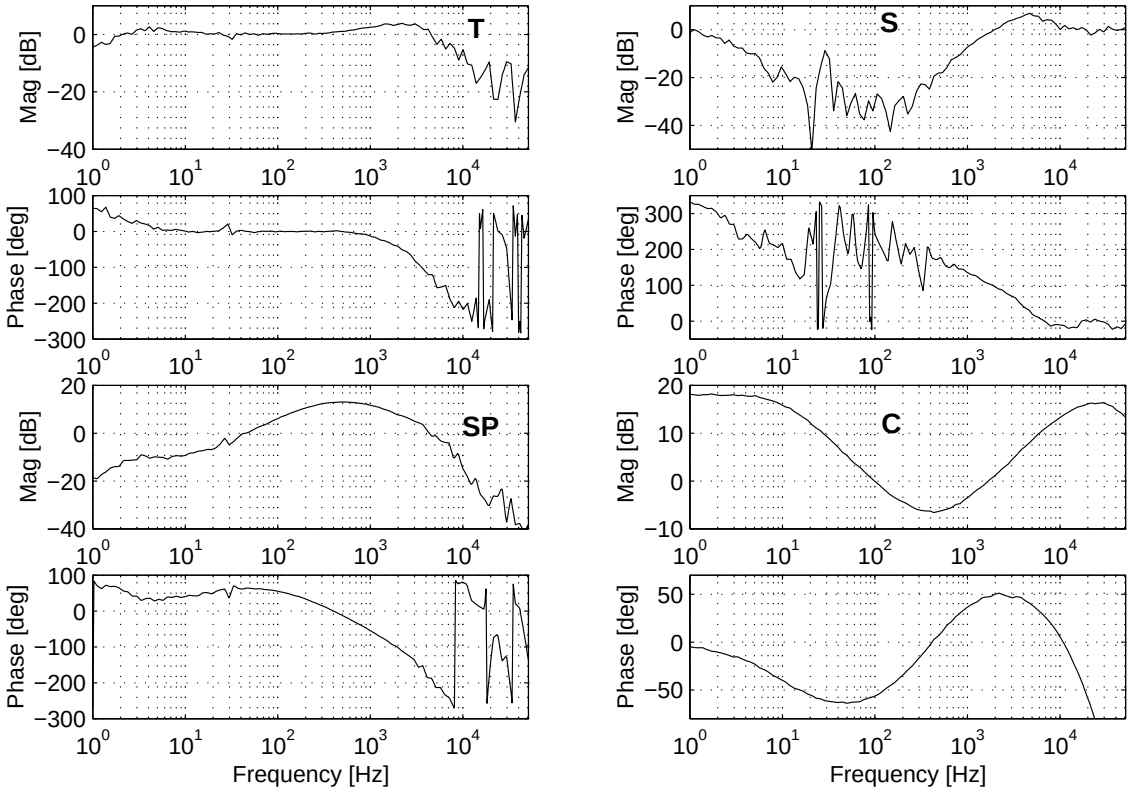

Figure 4.8: Measured frequency response of $\widehat{T}(j\omega)$, $\widehat{S}(j\omega)$, $\widehat{SP}(j\omega)$ and $\widehat{C}(j\omega)$, obtained for *pick-up 2 (radial loop).*

- For *pick-up 1*, the amplitude of $\hat{P}_{est_1}(j\omega)$ is unbounded for frequencies approaching 30 KHz, and this is due to the fact that the frequency response of $C(j\omega)$ goes to zero at this frequency, as shown in fig.4.7. Thus, in eq.(4.20), $\widehat{C}(j\omega)^{-1}$ grows unbounded and doesn't retrieve useful information about the plant dynamics at high frequencies. This behavior is also due to controller transfer function amplitude and phase distortions present at this frequency, as described in section 4.5.2 and shown in fig.4.5 and fig.4.6.
  Hence, we can only rely on $\hat{P}_{est_2}$ to estimate the plant behavior, at high frequencies. The same phenomenon is present for *pick-up 2*, though it is less pronounced than for *pick-up 1.*

- As expected, in both cases, the solid and the dashed curves have the same gains.

Consequently, it follows that it is preferable to derive the plant frequency response, for both pick-ups, by multiplying $\widehat{SP}(j\omega)$ by the inverse of $\hat{S}(j\omega)$, in order to obtain $\hat{P}_{est_2}(j\omega)$ (see eq.4.21).

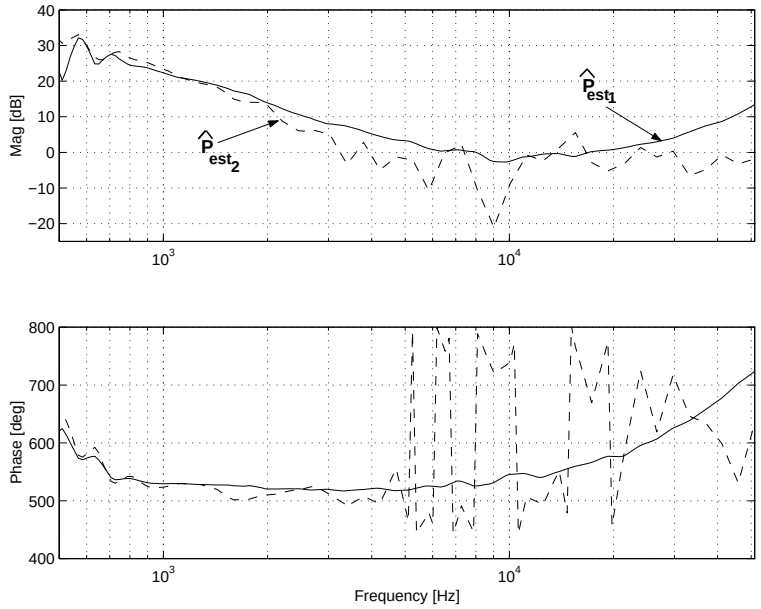

Figure 4.9: Frequency responses of $\hat{P}_{est_1}(j\omega)$ (solid line), and $\hat{P}_{est_2}(j\omega)$ (dashed line), obtained for *pick-up 1 (radial loop).*

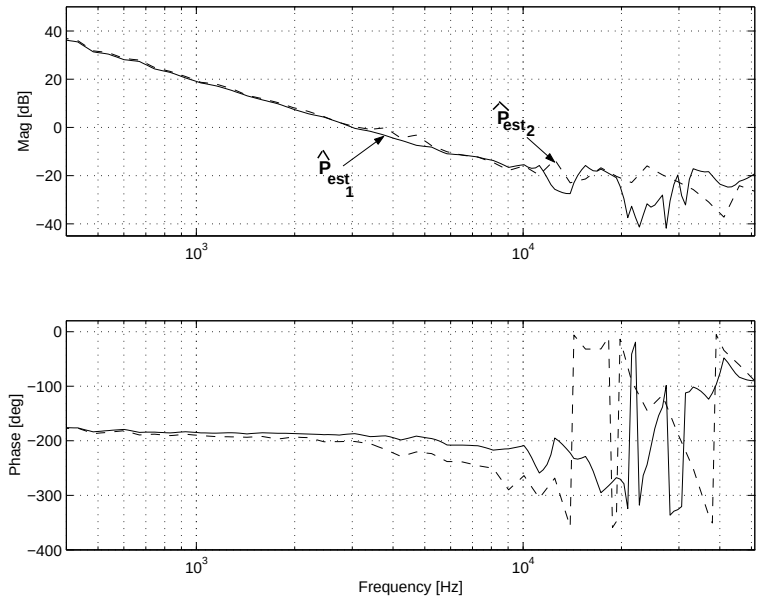

Figure 4.10: Frequency responses of $\hat{P}_{est_1}(j\omega)$ (solid line), and $\hat{P}_{est_2}(j\omega)$ (dashed line), obtained for *pick-up 2 (radial loop).*

b) Principles of Curve fitting procedure :

In the plant modelling procedure, the following step is to fit the estimated plant frequency response with a continuous-time transfer function. For this purpose we have used the curve-fit feature, offered by the Agilent 35607A Dynamic Signal Analyzer [58], which allows to find a linear mathematical model to closely approximate measured frequency responses.
The model is computed in continuous-time domain by calculating a weighted least-square fit of the frequency response data to a rational polynomial having the following form :

$$\Gamma(s) = K\frac{(a_1 s^0 + a_2 s^1 + a_3 s^2 + \ldots + a_n s^{n-1})}{(b_1 s^0 + b_2 s^1 + b_3 s^2 + \ldots + b_m s^{m-1})} \tag{4.22}$$

where $s = j\omega$, K is the system static gain, and $a_i,\ b_j\ \forall i = 1 \ldots n,\ j = 1 \ldots m$ are the coefficients of the fitted transfer function numerator and denominator, respectively.
Since $\Gamma(s)$ has real coefficients, its roots appear as real terms or complex and conjugate pairs.

The fundamental component of the curve fit routines is a non-iterative least-square complex data fitter. These routines, implemented inside the analyzer, use successively larger system orders until they find the best fit or until the maximum system order is reached. Typically the maximum allowable order is fixed equal to $O_{max} = 20$. The fitter starts with a numerator and denominator of orders n=1, m=1 and performs a fit using the curve-fit routine given this order. The algorithm then automatically performs a synthesis of the fit model and compares this frequency response to the measured one. If the fit is poor, the orders are incremented to n=2, m=2 and another fit is done. This search upwards in order continues until a good match is found or the upper bounds are reached, as described by the following criterion :

$$\Theta(\omega, n, m) = \sum_{n,m=1}^{O_{max}} \sum_{\omega=\omega_0}^{\omega_1} \left[\Gamma_{n,m}(j\omega) - \hat{\Gamma}_{n,m}(j\omega)\right]^2 \tag{4.23}$$

where $\hat{\Gamma}(j\omega)$ represents the frequency response measured $\forall\ \omega \in [\omega_0, \omega_1]$.
The routine holds the order at the first upper bound reached, and lets the other order climb to the higher order if the fits are poor.

If both upper bounds are reached before a good fit is found, the algorithm

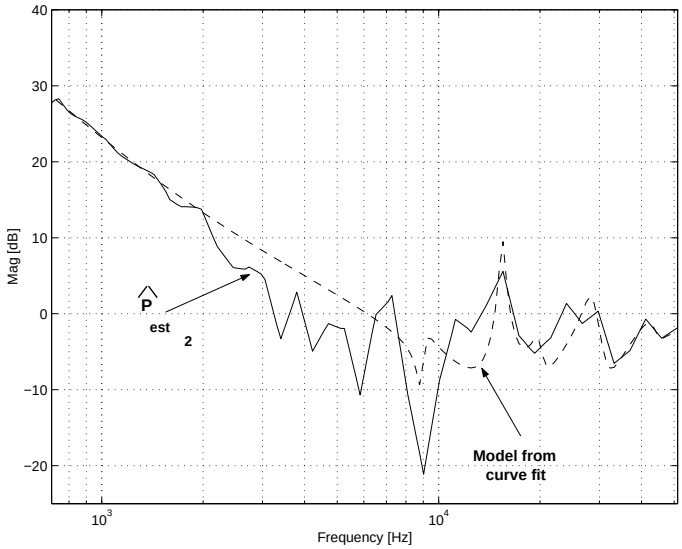

Figure 4.11: Amplitude plot of the plant frequency response ($\hat{P}_{est_2}$) together with the result of curve fitting , obtained for *pick-up 1.*

returns the fit which came closest to the measured frequency response.

During curve-fitting, the algorithm uses a coherence function which represents the portion of the output signal power spectrum $Pyy(j\omega)$ that is related to the input signal power spectrum $Puu(j\omega)$, according to the following relation :

$$\Xi(j\omega) = \frac{P_{uy}(j\omega)P^*uy(j\omega)}{Puu(j\omega)Pyy(j\omega)} \tag{4.24}$$

where $P_{uy}(j\omega)$ is the cross-spectrum between the input and the output signals, and $P^*uy(j\omega)$ its complex and conjugate.
$\Xi(j\omega)$ is a function of measurement variance, and it can vary from 0 (no coherence) to 1 (perfect coherence). A coherence value less than 1 indicates the presence of external noise, system non linearities, or unexpected input signals. Coherence is used to determine how large the difference can be between the synthesis of the fit model and the measured frequency response in defining a good fit.

c) Results obtained on the experimental set-up :

In fig.4.11 the fitted model and the measured plant $\hat{P}_{est_2}$ frequency responses are presented.
Since measurement are highly corrupted by noise at low frequency, we have used, from 1 to about 700 Hz, the third order physical model, given from eq.(3.34), to determine the plant low frequency modes. Besides, at high-frequencies (from 700 Hz to 51.2 KHz) the measurement input-output SNR is large enough to identify the plant dynamics, as shown in fig.4.11(*pick-up*

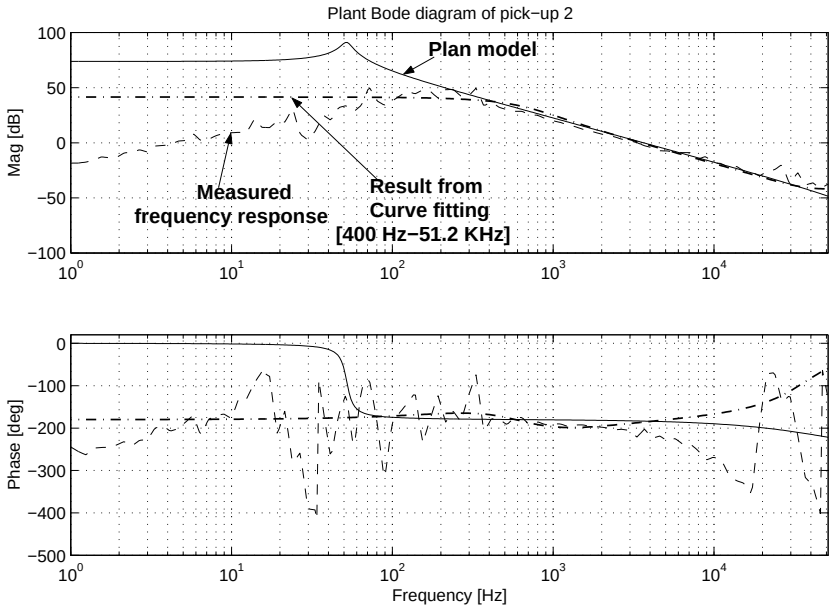

Figure 4.12: Bode plot of the plant model together with the result of measurements and curve fitting, obtained for *pick-up 2* in $[400 \div 5.210^3]$ Hz.

1) and fig.4.12 (*pick-up 2*), where it can be seen that the identified model of the plant $\hat{P}_{est_2}$ and the model obtained from curve fitting have the same slope of the actuator frequency response presented in fig.3.12.

For *pick-up 1*, this procedure has allowed to find a high-frequency resonance mode of the measured plant frequency response $\hat{P}_{est_2}$, which is taken into account in the fitted model (see fig.4.11). Since this mode is located quite far from the desired closed-loop bandwidth (at about 16 kHz), it can be neglected for model-based control design, and the complete plant model can be computed by taking into account the actuator transfer function (eq.3.34), and the gains of the power drivers g_d, given from eq.(4.6), of the optical device g_{opt}, estimated from technical specifications [59]. Hence, we have obtained a plant transfer function given by eq.(4.14) whose order is $n = 3$.

Nevertheless, for simulation purposes it would be interesting to include the identified high-frequency modes, in order to derive a more complex and accurate plant model, and check the closed loop behavior in this range of frequencies.

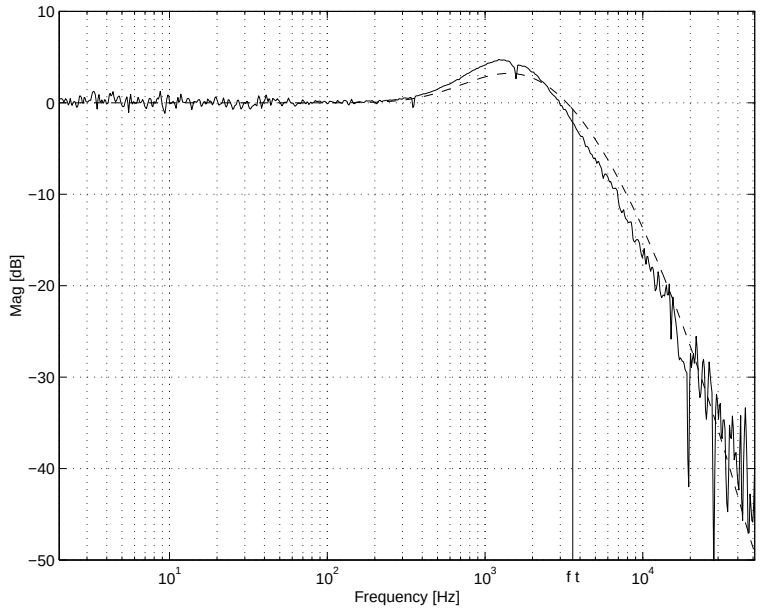

Figure 4.13: Measured frequency response of $\hat{T}$ (solid line) and simulation result (dashed line), obtained for *pick-up 1*.

4.7 Model Validation

In this section we wish to validate both the continuous-time model of the plant $P(s)$, obtained from curve fitting, and its frequency-domain response $\hat{P}_{est_2}$, computed in section 4.5.3, on which the model has been fitted.
The validation procedure is based on the following steps :

- Compute the frequency response of the system closed-loop transfer function $T(j\omega)$, on the basis of the frequency responses of the internal controller $C(j\omega)$, and of the plant model $P(j\omega)$, given from eq.(3.34) and eq.(4.14.
- Measure the effective closed-loop frequency response $\hat{T}(j\omega)$, using the implemented internal controller.
- Compare the measured and the computed closed-loop frequency response, in order to evaluate the quality of the plant frequency response reconstruction procedure, described in subsection 4.5.3.

In fig.4.13 and fig.4.14 are presented the simulated and the measured closed-loop transfer functions, computed for *pick-up 1* and *pick-up 2*.
From this figure it appears clearly that the model obtained for $P(s)$ is convenient.

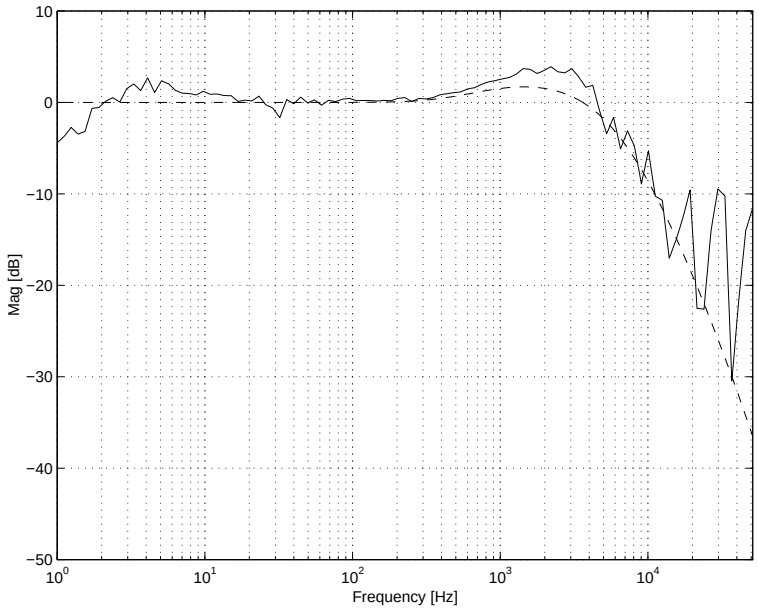

Figure 4.14: Measured frequency response of $\hat{T}$ (solid line) and simulation result (dashed line), obtained for *pick-up 2*.

4.8 Closed-loop identification for Performance Analysis and Robustness

The system performance analysis is performed in order to evaluate how the control scheme is able to follow the tracks, keeping the error signal within the specified bounds, and how disturbances and noise are rejected, during disc playback. The system performance criteria, defined in [51], have been computed by using gains and bandwidths of the system sensitivity functions (see eq.(4.15) - (4.17)).

4.8.1 Closed-loop performances

The closed-loop bandwidth f_t, defined as the frequency where $|T(j\omega)|$ crosses $-3dB$ from above, characterizes the performances of the control system. For frequencies upper f_t, the output noises affecting the control output are rejected.
From fig.4.7 it can be seen that the closed-loop bandwidth of the tracking loop is equal to $f_t = 3.5KHz$, when an over-speed factor is set equal to $N = 1.5$. This value corresponds to the specifications presented in [59], where is defined that $f_t \simeq f_c$, frequency at which the amplitude of the open loop transfer function crosses 0 dB (see eq.(3.19)).
An additional information, concerning the system closed-loop performances, is given from its rise time t_r, already defined in section 3.6.1.

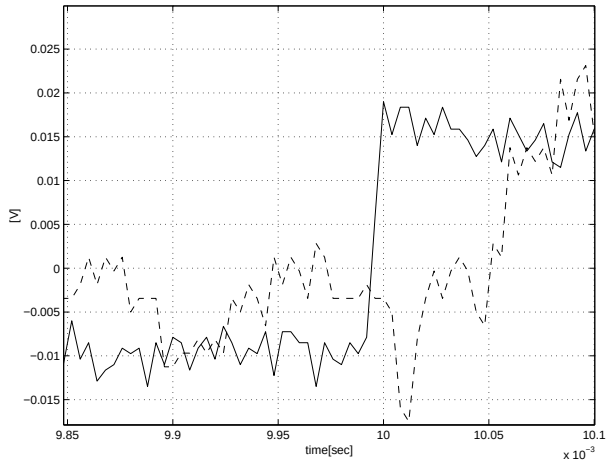

Figure 4.15: Measured step response in closed-loop. Input step (solid line) and controller output (dash line).

t_r usually verifies the following equation [51] :

$$t_r \simeq \frac{2.3}{2\pi f_t} = 0.104\, ms \tag{4.25}$$

This relation is usually valid for a second order system, according to the fact that the main plant dynamic is given by eq.(3.32) (see section 3.7 of page 113). eq.(4.25) has been checked experimentally, on the experimental bench, injecting a step signal v and measuring the controller output signal u. Results confirm that the closed-loop system responds with a rise time equal to about 0.1 ms, as shown on fig.4.15.

4.8.2 Disturbance rejection

The bandwidth of the output Sensitivity function $S(j\omega)$, defined as the frequency f_S where $|S(j\omega)|$ crosses, the first time, $-3dB$ from below, can be deduced from fig.4.7 and 4.8, where it can seen that $f_S = 1.4KHz$. For a generic SISO system, f_S gives an indication on the value of the frequency until the output disturbances are attenuated. In our case disturbances are attenuated for $f \leq f_S$. In addition f_S has to be smaller than f_t [51], and this is proved by experimental data.
However, from table 2.3, we know that to avoid loosing the track, the maximum allowable tracking position error should be $h_{max} = \pm 0.022\mu m$ and this level should be attained in the presence of eccentricity of the tracks. Since the max eccentricity should not be greater than $x_{max} = \pm 50\mu m$, a time-domain attenuation of the disturbances of a factor equal to $67dB$ should be achieved at low frequencies.
This is confirmed by the assessment of section 2.9, where bounds fixed in eq.(2.14) are verified by the experimental radial track spectrum, but they represent only a necessary condition on the maximum value that the track

error e has to satisfy on the time-domain.
From experimental results, shown in fig.4.7 and fig.4.16, it appears that the desired low frequency attenuation level of $-67dB$ is not guaranteed by the actual controller, One possible cause of this behavior is that, even though we have chosen the best setting of the dynamic signal analyzer, the input-output SNR level provided by measurements is not sufficient.

4.8.3 Robustness

The sensitivity peak criteria typically requires that $|S|_{max} \leq 6dB$ to have a robust control scheme respect with modelling errors (this guarantees a minimal distance from the Nyquist curve to the critical point -1) *i.e.* a modulus margin $M_\varphi \geq 0.5$.
Another robustness criterion is given by the peak value of $|T(j\omega)|$, that usually should be lower than 2 dB.
Robustness indicators can be achieved from the measured sensitivity functions of fig.4.7, where it can seen that $|\hat{S}(j\omega)|_{max} = 5.1dB$ and $|\hat{T}(j\omega)|_{max} = 3dB$. This confirms that the sensitivity peaks, obtained with the actual industrial solution, are satisfactory.

Nevertheless, experiments performed with test discs having nominal eccentricity $\epsilon > 0\ \mu m$, show that the measured sensitivity function $\hat{S}(j\omega)$ presents lower attenuation levels at the rotational frequency, $f_{rot} = 33Hz$, as it is shown in fig.4.16.
Hence, even though the actual control scheme is robust against model parameters variations, it does not guarantee robustness with respect to discs having different nominal eccentricity ϵ. In fact, disc eccentricity is considered as periodic disturbance entering at the plant output. We therefore consider that, due to the desired attenuation of $S(s)$, it should be rejected at low frequencies.

4.9 Analysis of the Coupling Phenomena

Usually, the CD and DVD player servo systems are composed by two independent SISO control loops. It is assumed that in the frequency range of interest for control (from low frequencies to the desired closed-loop bandwidth), the dynamic interaction between the focus and the radial loop is relatively low, as stated in Steinbuch et al. [55], Dettori [10], Dettori et al. [11], and Stan [54].

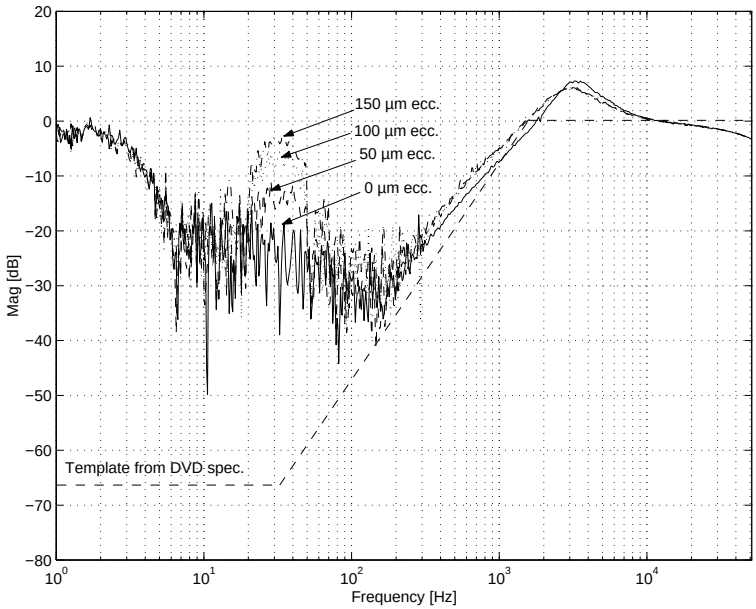

Figure 4.16: $|\hat{S}(j\omega)|$ for test discs having different nominal eccentricities.

It is interesting then to see if this assumption is also valid for the industrial DVD-video player, implemented in the STMicroelectronics laboratory. Hence, in this last section we present the analysis of the eventual coupling phenomena, between the two control loops, by using the measured frequency responses of the system closed-loop transfer functions $\hat{T}(j\omega)$, $\hat{S}(j\omega)$, and $\widehat{SP}(j\omega)$.

The experimental set-up used for experiments is the same depicted in fig.4.1, where the test signal are considered as bi-dimensional vectors having two components, one for focus and one for radial loop, respectively.
For measurements, both the loops are closed (play-back mode), and two sinusoidal signals v_1 and v_2, having same amplitude and swept at the same frequencies, are injected independently in each loop. Note that the dynamic signal analyzer do not allow to use two different excitation signals at the same time, during frequency response measurements.
In what follows, with the index 1 we denote the focus loop channel, and with the index 2 the radial loop channel. v_1 is the swept sine injected on channel 1, as v_2 is the one injected on channel 2.
Under these conditions, the measured closed-loop transfer functions can be represented as diagonal transfer matrices, having on the main diagonal the ratio between measured channel 1 and v_1 or measured channel 2 and v_2, and on the secondary diagonal, cross-terms given by the ratio of measured channel 1 and v_2 or measured channel 2 and v_1. These cross-terms give information about dynamical interactions between the two control loops.

The closed-loop transfer matrix is given by :

$$\overline{T}(j\omega) = \begin{bmatrix} T_{11}(j\omega) & T_{12}(j\omega) \\ T_{21}(j\omega) & T_{22}(j\omega) \end{bmatrix} \tag{4.26}$$

where, from measurements :

$$\begin{aligned} \widehat{T}_{11}(j\omega) &= \left(\frac{u_1}{v_1}\right)_{v_1\neq 0, v_2=0}, \quad \widehat{T}_{12}(j\omega) = \left(\frac{u_1}{v_2}\right)_{v_1=0, v_2\neq 0} \\ \widehat{T}_{21}(j\omega) &= \left(\frac{u_2}{v_1}\right)_{v_1\neq 0, v_2=0}, \quad \widehat{T}_{22}(j\omega) = \left(\frac{u_2}{v_2}\right)_{v_1=0, v_2\neq 0} \end{aligned} \tag{4.27}$$

Similarly, for the output sensitivity transfer matrix we have :

$$\overline{S}(j\omega) = \begin{bmatrix} S_{11}(j\omega) & S_{12}(j\omega) \\ S_{21}(j\omega) & S_{22}(j\omega) \end{bmatrix} \tag{4.28}$$

where :

$$\begin{aligned} \widehat{S}_{11}(j\omega) &= \left(\frac{u_1+v_1}{v_1}\right)_{v_1\neq 0, v_2=0}, \quad \widehat{S}_{12}(j\omega) = \left(\frac{u_1+v_1}{v_2}\right)_{v_1=0, v_2\neq 0} \\ \widehat{S}_{21}(j\omega) &= \left(\frac{u_2+v_2}{v_1}\right)_{v_1\neq 0, v_2=0}, \quad \widehat{S}_{22}(j\omega) = \left(\frac{u_2+v_2}{v_2}\right)_{v_1=0, v_2\neq 0} \end{aligned} \tag{4.29}$$

and for the input sensitivity transfer matrix :

$$\overline{SP}(j\omega) = \begin{bmatrix} SP_{11}(j\omega) & SP_{12}(j\omega) \\ SP_{21}(j\omega) & SP_{22}(j\omega) \end{bmatrix} \tag{4.30}$$

where :

$$\begin{aligned} \widehat{SP}_{11}(j\omega) &= \left(\frac{e_1}{v_1}\right)_{v_1\neq 0, v_2=0}, \quad \widehat{SP}_{12}(j\omega) = \left(\frac{e_1}{v_2}\right)_{v_1=0, v_2\neq 0} \\ \widehat{SP}_{21}(j\omega) &= \left(\frac{e_2}{v_1}\right)_{v_1\neq 0, v_2=0}, \quad \widehat{SP}_{22}(j\omega) = \left(\frac{e_2}{v_2}\right)_{v_1=0, v_2\neq 0} \end{aligned} \tag{4.31}$$

To verify if the signal injected on channel 1 has relevant effects on the measurements done on the channel 2 (and viceversa), two measurements are performed, for each diagonal element of the three previous sensitivity functions (see eq.(4.26), (4.28) and (4.30)).
A first measurement is done on channel 1, when $(v_1, v_2) \neq 0$. Then, a second measurement is done when $v_1 \neq 0$ and $v_2 = 0$. The reciprocal is done on channel 2. This procedure is not applied to terms belonging to the other

diagonal, since it is senseless to apply at the same time v_1 and v_2, when measuring cross-related transfer functions.

Experimental results, obtained for the *pick-up 1*, are shown in fig.4.17, fig.4.18 and fig.4.19, as well as in fig.4.20, fig.4.21 and fig.4.22, for the *pick-up 2*. From these figures, we can conclude that :

- The frequency response of the cross-terms $\widehat{T}_{ij}(j\omega)$, $\widehat{S}_{ij}(j\omega)$ and $\widehat{SP}_{ij}(j\omega)$ $\forall\, i,j = 1,2,\ i \neq j$ present, in the full measurement frequency span, a low value of gain and an incoherent phase. This confirms that the cross coupling phenomena between focus and radial loop have a negligible impact on the whole control system behavior.

- The frequency responses of the main diagonal elements $\widehat{T}_{ij}(j\omega)$, $\widehat{S}_{ij}(j\omega)$ and $\widehat{SP}_{ij}(j\omega)$ $\forall\, i,j = 1,2,\ i = j$ show that there are no differences between measurements acquired when both the external stimulus are used, and when only one of them is applied. So, also for the elements of the main diagonal, the influence of coupling phenomena is not relevant.

- For the *pick-up 2*, it seems that the external signal v_1, injected on the focus loop, affects the radial loop control signal u_2 in frequencies higher than the desired closed loop bandwidth, as shown in fig.4.20 (see $\widehat{T}_{21}$) and fig.4.21 (see $\widehat{S}_{21}$). This phenomenon is not noticed from measurements obtained for the *pick-up 1*. It means that the *pick-up 2* radial actuator presents a higher sensitivity to disturbance entering on the focus loop at frequencies where normally the radial controller stops its filtering action. This can clearly seen in fig.4.6, where the gain of the radial loop controller is of about 13 dB at $f = 10\ KHz$.
  From the analysis of the main diagonal elements of the closed-loop frequency response $\widehat{T}_{11}$ and $\widehat{T}_{22}$, it can finally be noticed that *pick-up 2* is more sensitive to measurement noise than *pick-up 1* up to 10 KHz, as it can seen from fig.4.17 and fig.4.20.

We can therefore conclude that for both controllers and pick-ups coupling phenomena existing between the focus and the radial loops are negligible in the frequencies of interest for control. Experimental results confirm that the spot position along the radial and the vertical directions can be controlled using two independent SISO schemes.

4.10 Conclusions

In this Chapter we have presented the frequency-domain procedure used to identify the plant model of an industrial DVD-video player servo system. We have derived a SISO local linear model of the moving lens radial actuator, which is valid around a certain track location, through closed-loop frequency response measurements obtained with a Dynamic Signal Analyzer and curve fitting procedure.
After model validation, we have presented the performance analysis of the actual industrial solution. Robustness against model parameter variations is then evaluated through typical sensitivity peak criteria. Experimental results show that the actual implemented controller is robust against model parameters variations, but it does not guarantee robustness with respect to discs having different nominal eccentricity.
Finally, in the last part of this chapter, we have analyzed eventual coupling phenomena existing between the two control loops, by using the measured frequency responses of the system closed-loop transfer functions.
We have pointed out that, in the frequency range of interest for control, the dynamic interaction between the both loops remains relatively weak.

In the next chapter results obtained from the described plant identification procedure will be used for designing a low complexity radial loop controller based on the computed plant model. The new controller achieves enhanced track following performance and guarantees robustness with respect to system parametric uncertainty.

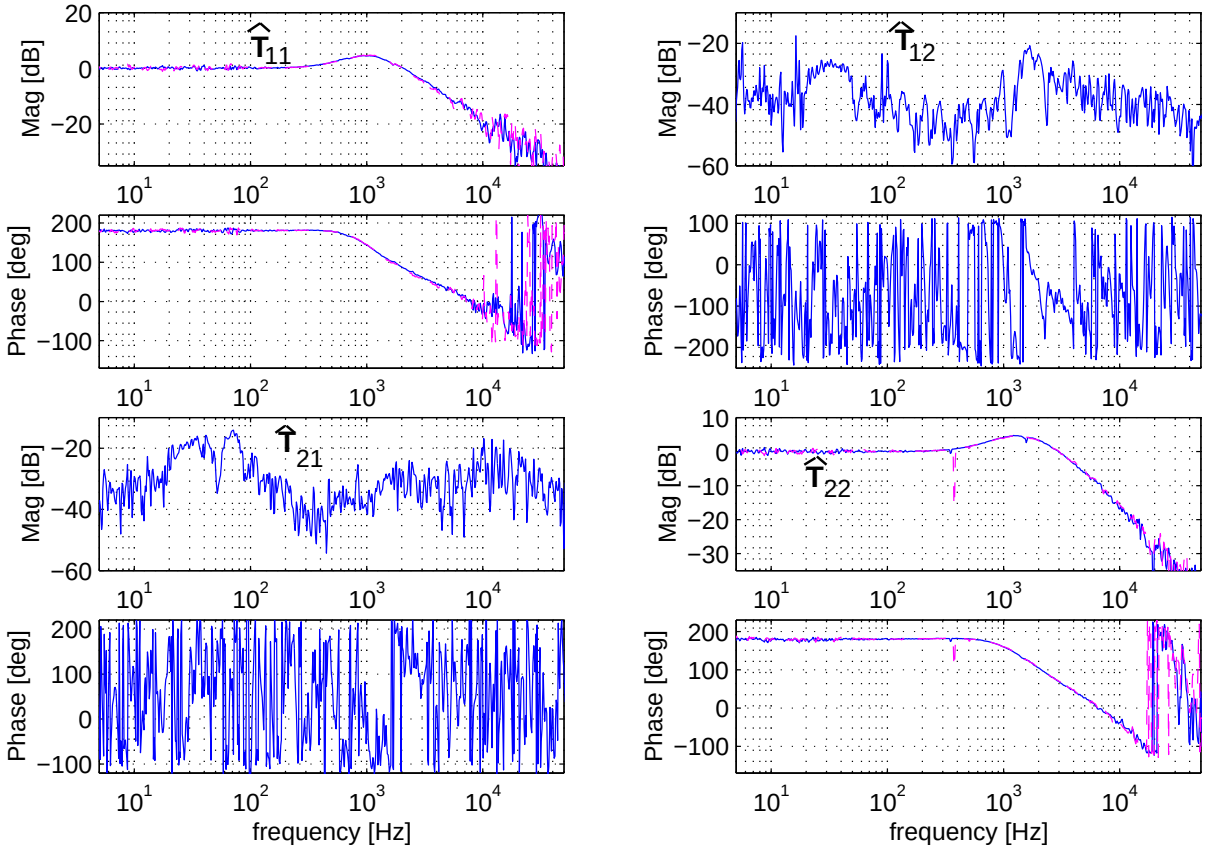

Figure 4.17: $\widehat{T}_(j\omega)$ measured for *pick-up 1*. $v_i = v_j \neq 0 \ \forall i, j = 1, 2$ (solid line), $v_i \neq 0 \ \forall i = 1, 2$ and $v_j = 0 \ \forall j = 1, 2$ (dashed line).

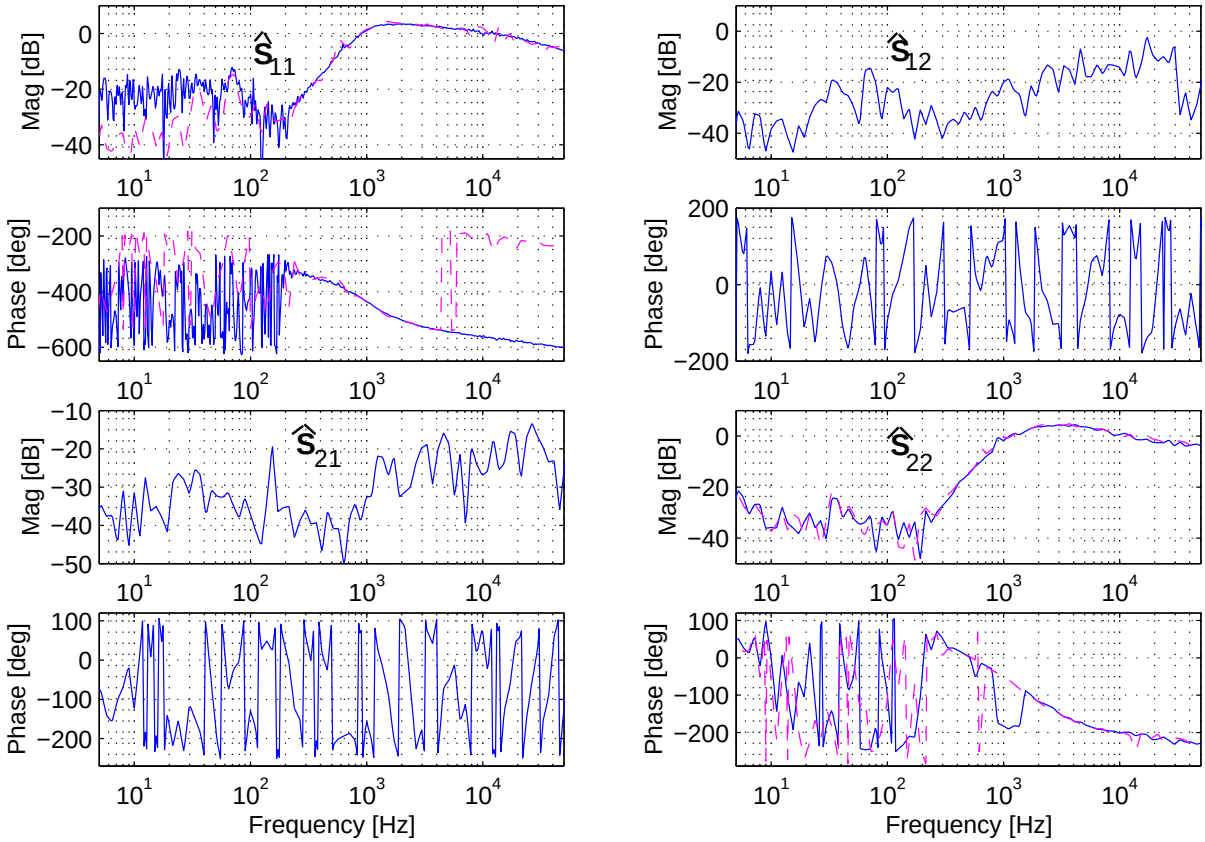

Figure 4.18: $\widehat{S}(j\omega)$ measured for *pick-up 1*. $v_i = v_j \neq 0 \ \forall i, j = 1, 2$ (solid line), $v_i \neq 0 \ \forall i = 1, 2$ and $v_j = 0 \ \forall j = 1, 2$ (dashed line).

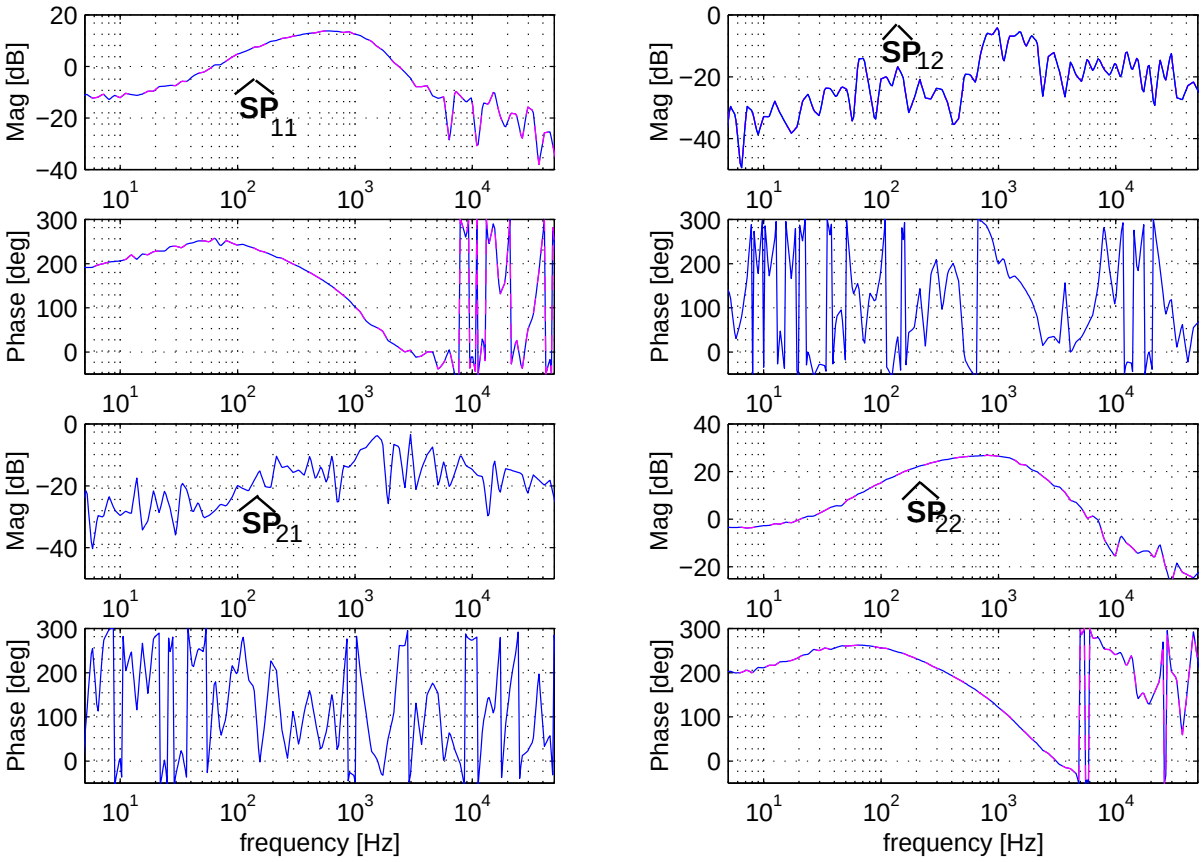

Figure 4.19: $\widehat{SP}_{(}j\omega)$ measured for *pick-up 1*. $v_i = v_j \neq 0 \ \forall i, j = 1, 2$ (solid line), $v_i \neq 0 \ \forall i = 1, 2$ and $v_j = 0 \ \forall j = 1, 2$ (dashed line).

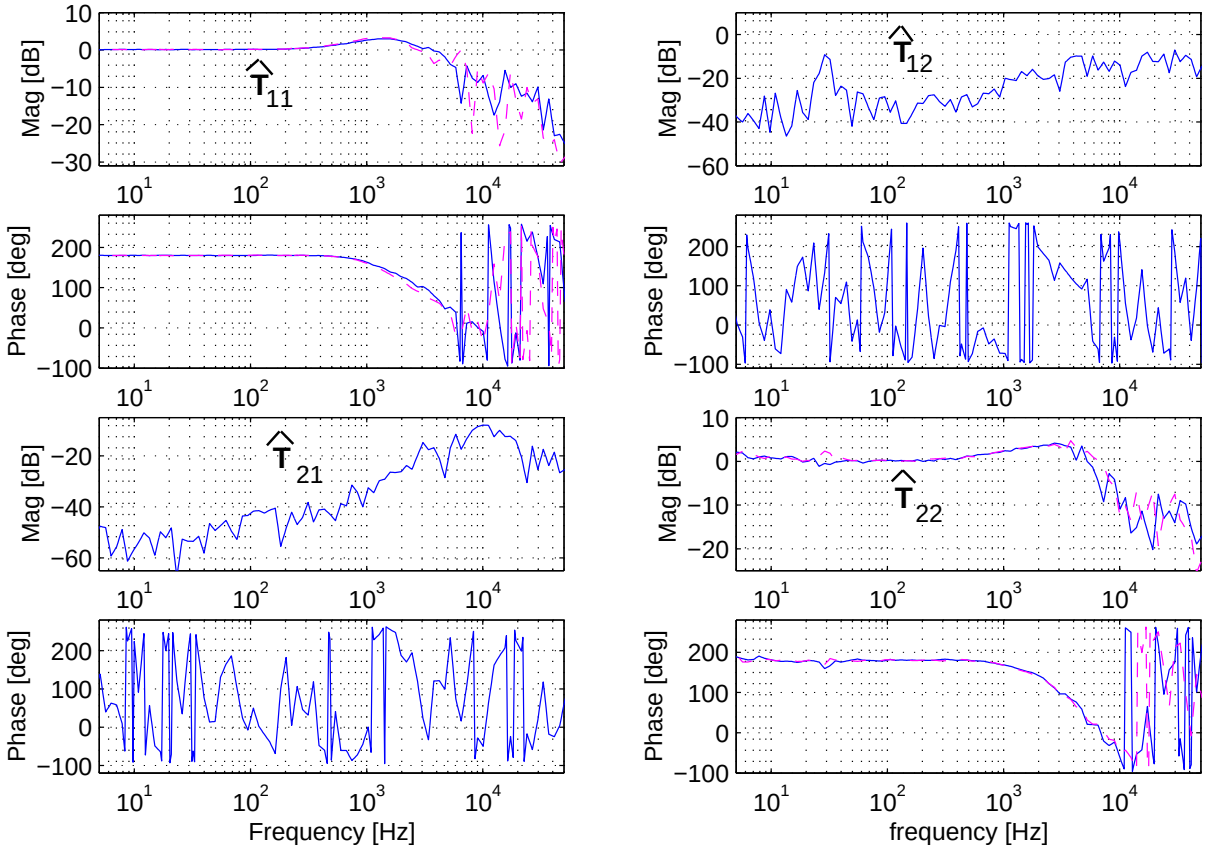

Figure 4.20: $\widehat{T}(j\omega)$ measured for *pick-up 2*. $v_i = v_j \neq 0 \ \forall i, j = 1, 2$ (solid line), $v_i \neq 0 \ \forall i = 1, 2$ and $v_j = 0 \ \forall j = 1, 2$ (dashed line).

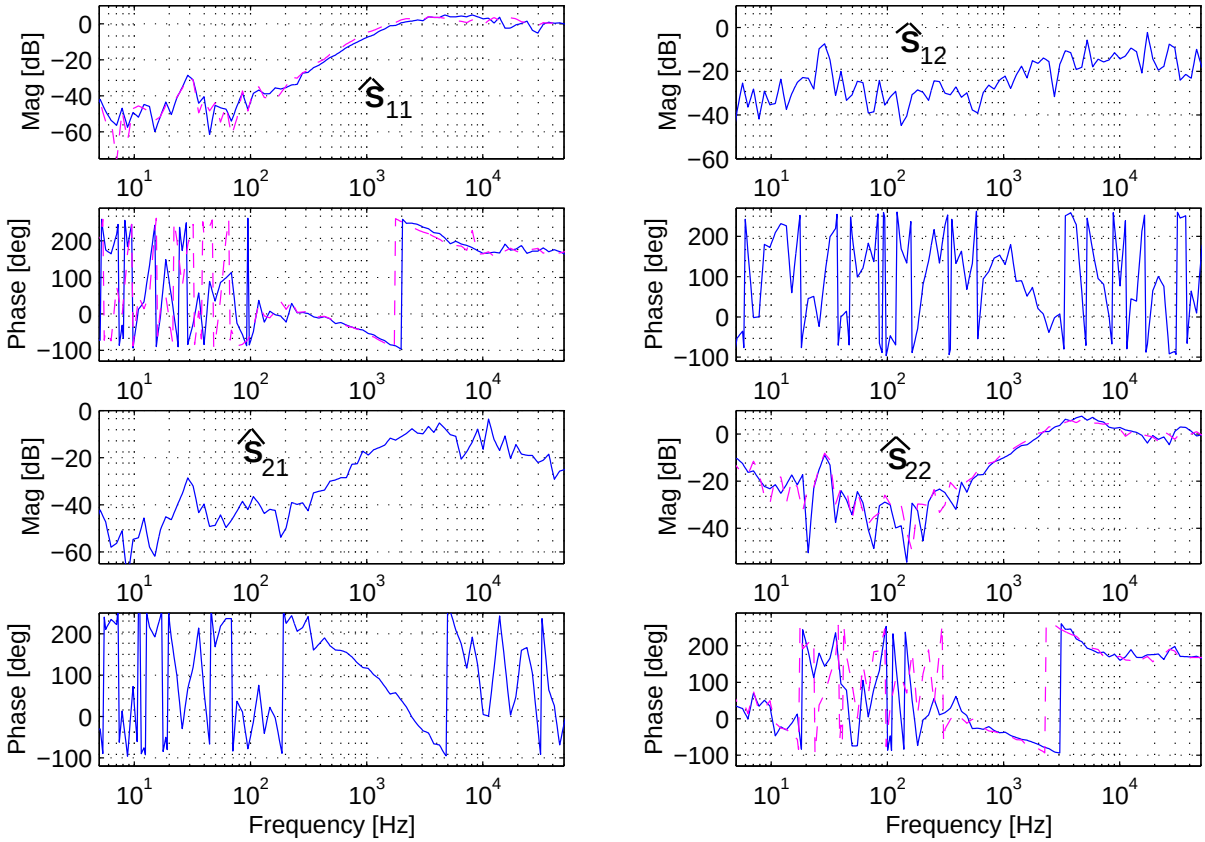

Figure 4.21: $\widehat{S}_(j\omega)$ measured for *pick-up 2*. $v_i = v_j \neq 0 \ \forall i,j = 1,2$ (solid line), $v_i \neq 0 \ \forall i = 1,2$ and $v_j = 0 \ \forall j = 1,2$ (dashed line).

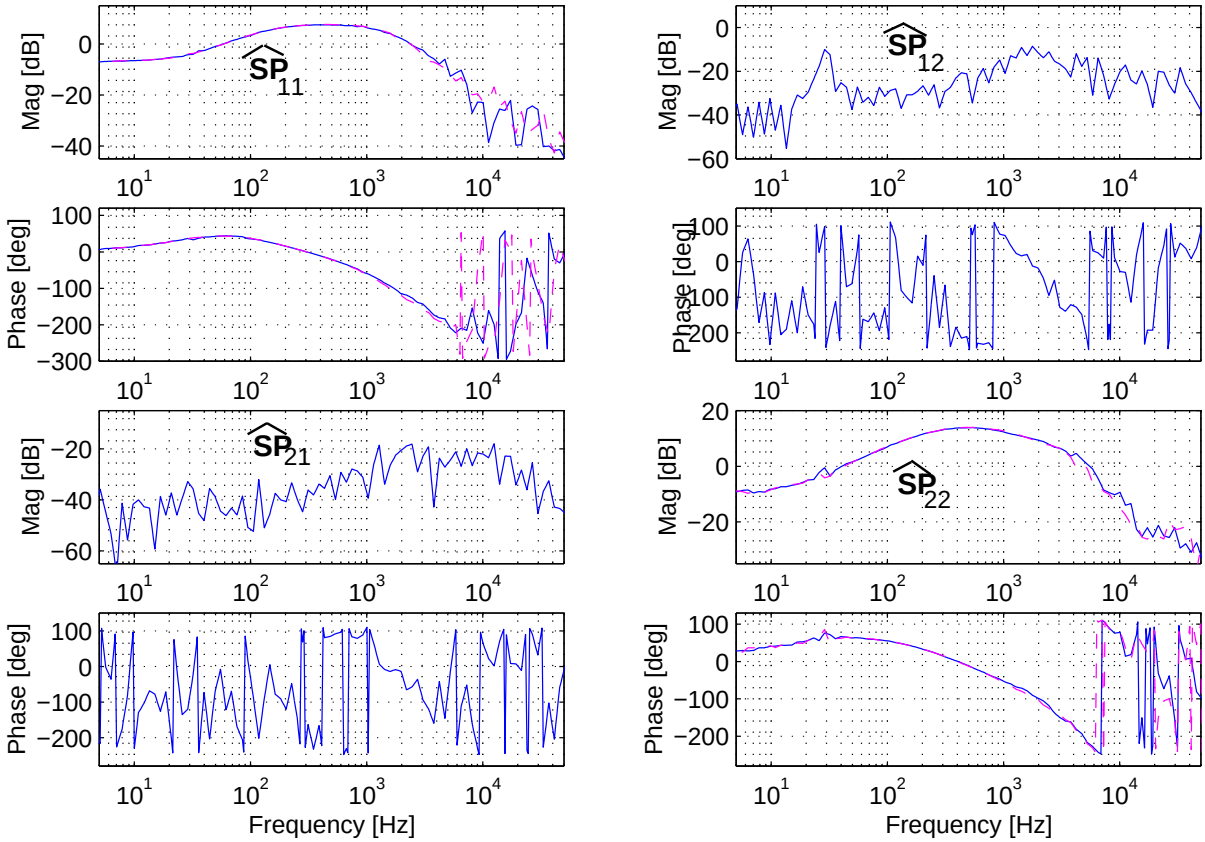

Figure 4.22: $\widehat{SP}_{(}j\omega)$ measured for *pick-up 2*. $v_i = v_j \neq 0 \ \forall i, j = 1, 2$ (solid line), $v_i \neq 0 \ \forall i = 1, 2$ and $v_j = 0 \ \forall j = 1, 2$ (dashed line).

Chapter 5

Robust Control Design for the DVD Video Player

5.1 Introduction

A model-based control design procedure is proposed in this chapter for construction of a low complexity controller, that achieves an enhanced track following performance for the DVD-video player. As stated in section 3.4, low complexity controllers are motivated by the need of keeping the design cost low, and to make digital controllers implementation feasible in the actual industrial solution.
In the H_∞ approach, model-based controllers are solutions of optimization problems, based on mathematical models of the system and some weighting functions that represent performance specifications. The resulting controllers have a complexity similar to that of the model and weighting functions that are used for the design. Due to industrial constraints, here complex models and high-order weighting functions are avoided, since this would lead to controllers of unacceptably high orders.
Usually, it is assumed that the model used for the synthesis is equivalent to the system for which the compensator primarily is designed. However, a model generally provides an approximate system description so that controllers, designed on the basis of this model, will exhibit a different performance for the nominal model and the actual system. This mainly depends on system physical parameters variations, due to tolerances present along the manufacturing process and actuators aging.
In the case of DVD-video players, even though improvements are observed in obtaining shorter data time access, higher storage capacity and information

density on the disc, little has been done to improve control system performances with respect to different systems behaviors, variable from player to player, and manufacturing tolerances of optical pick-ups, present in mass-production. This explains the need for robustness of the achieved controllers.

In this chapter we will study the possible improvements of the track-following behavior of a DVD-video player, using robust control design techniques. Hence, a standard H_∞ control design approach is proposed, to design a SISO controller able to drive the linear displacement of the optical head actuator along the disc radius, which reduces the effect of external disturbances like eccentricity and vertical deviations.
After controller order reduction the achieved solution is implemented on the industrial system. Then, an uncertainty model set, based on a parametric description of the DVD mechanism, is considered in order to analyze the influence of the actuator parameter variations on the system performances. Firstly, we assume unstructured parametric uncertainties and the small gain theorem is applied to evaluate robust stability and performance. Then, structured parametric uncertainties are taken into account, and robustness analysis is performed by mean of RS and RP μ-analysis. In both cases, system parameters variations are assumed as norm-bounded real perturbations affecting the plant nominal model.

Our contribution consists of providing a general and simple methodology for control design of a DVD-video servo system, that is more suitable for unknown parameter variations and real-time implementation. This methodology leads to development of controllers which are potentially more accurate, powerful and simpler to implement. Performance and robustness analysis of the achieved controller are also performed, to point out the interactions existing between the DVD-drive design and the controller synthesis, as presented in Filardi et al. [22] and [23].

This chapter is organized as follows. In section 5.2 a brief state of the art is presented. Some theoretical background on the general H_∞ control problem is given in section 5.3. The choice of the control scheme to apply to the DVD-video player, together with the controller order reduction procedure and simulation and experimental results, are presented in section 5.4. In section 5.5 we give a representation of the system uncertainty, and in section 5.6 we show how unstructured uncertainty can be represented in the frequency-domain framework. Here, a frequency analysis is proposed to point out improvements due to the resulting controller. Robust stability and

performances are analyzed in section 5.7 for system structured parametric uncertainty, by means of μ-analysis tools. Finally, in section 5.8 we draw some conclusions.

5.2 State of the Art

There exist in the literature several studies concerning application of norm-based control synthesis applied to Compact Disk mechanism. In what follows we briefly summarize, by author, the subjects treated in the previous researches.

Linear Matrix Inequalities (LMI)-based mixed and multi-objectives design techniques applied to a CD player mechanism, are presented in Dettori [10], [11], [12], [14] and [15] to investigate the possibility of enhancing the system track-following and focusing behavior. The design of robust controllers is performed by identifying, in the H_∞ and H_2 norms, suitable measures to represent performance specifications, as also presented in section 2.9. The advantage of using mixed objective design is that different performance specifications can be posed on different channels of the plant, such as the transient and the steady-state behavior, disturbance rejection and robustness against structured and unstructured plant uncertainty.
Something new is presented in these latter works, if compared to other papers appeared in the literature, where LMI control techniques have only been tested on academic idealized models of small order which prevent numerical problems. These works concern for instance, the mixed objective example in [46], the H_∞ design applied to an underwater vehicle in [33], a pressurized water reactor in [1], flight control in [47], and missile autopilot in [37]. None of these works focus on the application of the LMI algorithms on actual industrial systems, and solutions are not validated through real implementation.
An evaluation of the performance achieved by a Linear Parametric Varying (LPV) control design for a CD player servomechanism is presented in Dettori [10] and [13]. Experimental results show that LPV techniques allow to obtain a non conservative design, and better performance than standard Linear Time Invariant (LTI) algorithms. Nevertheless, using these methodologies complex and high-order controllers, impossible to implement on our industrial solution, are obtained.

In Steinbuch et al. [55] the analysis of a robust controller designed for a

CD mechanism is performed by using D-K iterations (i.e. μ-synthesis). After control order reduction, the solution is implemented using two parallel DSPs.

Another approach, used to design the positioning controllers of a CD player is presented in Vidal et al. [62]. An algorithm is suggested to detect defects of the disc surface without using additional sensors, and an observer combined with a Linear Quadratic Regulator allows to enhance the disc playability. In Vidal and Karlsson [63], two focus loop H_∞ controllers are designed and applied on an industrial CD player, to suppress external disturbance and defect on the disk, when norm-bounded system uncertainties are assumed.

Only recently Sliding Mode Control (SMC) techniques have been used to design a more robust servo control system, able to handle external shocks and vibrations disturbances for optical disk drive systems, as presented in Zohu and Steinbuch [70]. An estimator-based SMC controller is used in the radial servo loop, and simulation and experimental results show a significant improvement of drive's anti shock performance.

As exposed in section 5.1, the system knowledge, available from the modelling step and frequency response measurements, constitutes an idealized description of the dynamical behavior of the plant. Therefore, any model-based control design procedure should account for inaccuracies of available system knowledge, in order to ensure robustness of the design, as stated in Dötsch [18] and Skelton [50].

There exist in the literature studies concerning deterministic methods for obtaining nominal and uncertainty models of optical disc drives. Particularly, in Vidal et al. [64] and [66] model-based design is developed for the focus loop in a CD player. Models are based on parameter identification and measurement of actual CD drives, that differ by having worst case behaviors with respect to various properties. This methodology allow to derive nominal model as well as a structured multiplicative input uncertainty model, and mixed μ-synthesis is then applied, by assuming only parametric uncertainty representation and real perturbations, to design a model-based controller meeting robust performance criteria.
However, none has been published about robust stability and performance analysis of the radial loop control system in DVD players (for which tougher performance specifications have to be satisfied), when plant structured and unstructured parametric uncertainty representations are considered, and

perturbations are restricted to be real.
In this chapter, we will assume such plant uncertainty representations, and we will apply to a DVD drive a similar methodology exposed in Sename and Dugard [49], to perform a single-objective controller design and study the system steady-state behavior, its disturbance rejection properties, and robustness against parametric uncertainty.

5.3 H_∞ Control Design : theoretical background

In this paragraph the standard H_∞ control problem is stated in a way similar to Skogestad and Postlethwaite [51], where more details can be found.

The general H_∞ control problem is formulated using the general control configuration (I) in fig.5.1, where $P(s)$ is the generalized plant model, composed by the plant model $G(s)$ and the performance weighting functions $W_p(s)$ and $W_u(s)$, w is the exogenous input vector, u is the control output vector, z is the controlled output vector, e is the measurement vector.
The generalized plant $P(s)$ of fig.5.1 (II) is usually denoted as :

$$\begin{pmatrix} z \\ e \end{pmatrix} = P(s) \begin{pmatrix} w \\ u \end{pmatrix} = \begin{pmatrix} P_{11}(s) & P_{12}(s) \\ P_{21}(s) & P_{22}(s) \end{pmatrix} \begin{pmatrix} w \\ u \end{pmatrix} \tag{5.1}$$

where $u = K(s)e$, and a state-space realization of $P(s)$ is given by :

$$P \doteq \left(\begin{array}{c|cc} A & B_1 & B_2 \\ \hline C_1 & D_{11} & D_{12} \\ C_2 & D_{21} & D_{22} \end{array}\right) \tag{5.2}$$

As shown in Skogestad and Postlethwaite [51], the system closed-loop transfer function from w to z is given by the following linear fractional transformation :

$$z = F_l(P, K)w \tag{5.3}$$

where :

$$F_l(P, K) = P_{11} + P_{12}K(I - P_{22}K)^{-1}P_{21} \tag{5.4}$$

5.3.1 H_∞ Performance

In this section we recall some property the H_∞ norm, useful for deriving relevant system performance indicators.

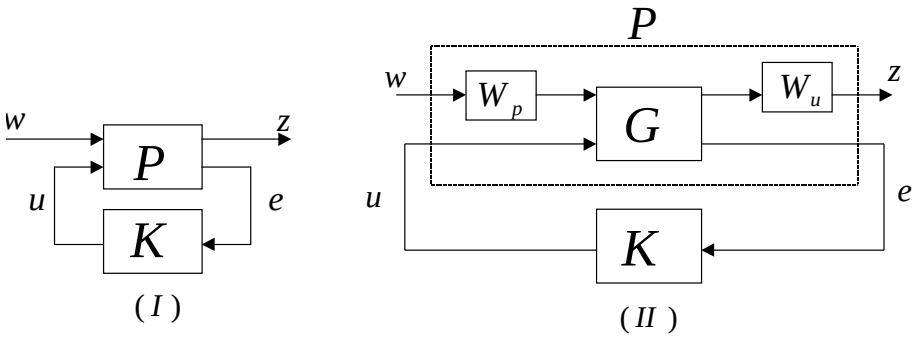

Figure 5.1: General control configuration.

With reference to fig.5.1, the transfer function associated to the plant $P(s)$ is given by :

$$P(s) = C(sI - A)^{-1}B + D \tag{5.5}$$

We remind that the spectral norm of a matrix M $\in \mathbb{C}^{p\times m}$ is defined as :

$$\|M\| \doteq \overline{\sigma}(M) \tag{5.6}$$

where $\overline{\sigma} = \sqrt{\lambda_{max}(M^*M)} = \sqrt{\lambda_{max}(MM^*)}$ denotes the maximum singular value of M (see [51]). Let us consider the transfer function matrix given by eq.(5.5) associated with an asymptotically stable system. If the system is stable, $P(s)$ is analytic in $\mathbb{C}^+$, where its spectral norm is also bounded. The set of these functions is a space vector which is denoted by H_∞, and which is associated with the H_∞ norm defined as :

$$\|P\|_\infty \doteq \sup_{s\in\mathbb{C}^+} \|P(s)\| \tag{5.7}$$

Using the Fatou Lemma, it can be shown that [10] :

$$\|P\|_\infty \doteq \sup_{\omega\in\mathbb{R}} \|P(j\omega)\| \tag{5.8}$$

i.e the H_∞ norm of a system is equal to the superior of the maximum singular value of its frequency response.

This property is known as *frequency domain interpretation of the H_∞ norm*, defined as follows : **The H_∞ norm of a SISO system is equal to the maximum steady-state amplification for pure sinusoidal inputs.**

Another interpretation of the H_∞ performance can be obtained if input and output signals of finite energy are considered inside the induced L_2 norm vector space, which is defined as follows :

$$L_2 \doteq \{x : [0,\infty) \to \mathbb{R}^m \ \mid \ \|x\|_2 < \infty\} \tag{5.9}$$

where :

$$\|x\|_2 \doteq \left(\int_0^\infty x(t)' x(t) dt \right)^{1/2} \tag{5.10}$$

it holds that [10] :

$$\|P\|_\infty = \sup_{\omega \in L_2, \omega \neq 0} \frac{\|z\|_2}{\|w\|_2} \tag{5.11}$$

$\|P\|_\infty$ is therefore an upper bound of the L_2 gain.

This property is known as *time domain interpretation of the H_∞ norm*, defined as follows : **The H_∞ norm of an LTI system is equal to the maximum energy amplification for all signals of finite energy.**

A third important interpretation of the H_∞ norm is related to the amplification of power signals. We remind that a signal x is called a power signal if the limit :

$$\lim_{T \to \infty} \frac{1}{T} \int_0^T x^{'}(t) x(t) dt \tag{5.12}$$

exists and it is finite. In this case the power of the signal is defined as :

$$pow(x) \doteq \left(\lim_{T \to \infty} \frac{1}{T} \int_0^T x^{'}(t) x(t) dt \right)^{1/2} \tag{5.13}$$

Since the set of power signals contains the set of finite energy signals L_2, the following property holds, as stated in Doyle et al. [20] :

Interpretation in terms of power amplification : **The H_∞ norm of an LTI system is equal to the maximum power amplification for all signals of finite nonzero power, i.e :**

$$\|P\|_\infty = \sup_{pow(w) \neq 0} \frac{pow(z)}{pow(w)} \tag{5.14}$$

As a last performance criterion, we consider the so-called peak-to-peak gain, which measures the peak amplification of the output for inputs bounded in amplitude.

The peak-to-peak norm of the system (5.2) is equal to the induced gain of the system considered as a mapping from L_∞ to L_∞, i.e [10] :

$$\|P\|_{\infty \to \infty} = \sup_{\omega \in L_\infty, \omega \neq 0} \frac{\|z\|_\infty}{\|w\|_\infty} \tag{5.15}$$

This definition of the peak-to-peak gain is different from the so-called L_1 norm considered in the literature.

5.3.2 H_∞ Optimal Control

With reference to the general control configuration of fig.5.1, the standard H_∞ optimal control problem consists in finding all stabilizing controllers which minimize the following quantity :

$$\|F_l(P,K)\|_\infty = \sup_\omega \overline{\sigma}[F_l(P,K)(j\omega)] \tag{5.16}$$

Typically, in the H_∞ framework, with reference to eq.(5.2) the following assumption are made [51] :

1. (A, B_2, C_2) is stabilizable and detectable
2. D_{12} and D_{21} have full rank
3. $\begin{pmatrix} A - j\omega I & B_2 \\ C_1 & D_{12} \end{pmatrix}$ has full column rank $\forall\ \omega$
4. $\begin{pmatrix} A - j\omega I & B_1 \\ C_2 & D_{21} \end{pmatrix}$ has full row rank $\forall\ \omega$
5. $D_{11} = 0$ and $D_{22} = 0$
6. $D_{12} = \begin{pmatrix} 0 \\ I \end{pmatrix}$ and $D_{21} = \begin{pmatrix} 0 & I \end{pmatrix}$

Assumption 1) is required for the existence of a stabilizing controller K, and assumption 2) is sufficient to ensure the controller is proper and hence realizable. Assumptions 3) and 4) ensure that the optimal controller does not cancel poles or zeros on the imaginary axis, which would result in closed-loop instability. $D_{11} = 0$ and $D_{22} = 0$ in assumption 5) significantly simplify the H_∞ control problem solution formulas. For simplicity it is also assumed that D_{12} and D_{21} are given by assumption 6).

For the general control configuration of fig.5.1 described by eq.(5.4), with the assumptions 1) to 6) listed above, there exists a stabilizing controller $K(s)$ such that $\|F_l(P,K)\|_\infty < \gamma$ if and only if :

i) $X_\infty \geq 0$ is a solution to the algebraic *Riccati* equation :

$$A^T X_\infty + X_\infty A + C_1^T C_1 + X_\infty(\gamma^{-2} B_1 B_1^T - B_2 B_2^T) X_\infty = 0 \tag{5.17}$$

such that $\Re\{\lambda_i[A + (\gamma^{-2} B_1 B_1^T - B_2 B_2^T) X_\infty]\} < 0\ \forall i$

ii) $Y_\infty \geq 0$ is a solution to the algebraic *Riccati* equation :

$$AY_\infty + Y_\infty A^T + B_1 B_1^T + Y_\infty(\gamma^{-2} C_1^T C_1 - C_2^T C_2) Y_\infty = 0 \qquad (5.18)$$

such that $\Re\{\lambda_i[A + Y_\infty(\gamma^{-2} C_1^T C_1 - C_2^T C_2)]\} < 0 \ \forall i$

iii) $\rho(X_\infty, Y_\infty) < \gamma^2$

The family of all admissible controllers is given by $K = F_l(K_c, Q)$, where :

$$K_c \doteq \left(\begin{array}{c|cc} A_\infty & -Z_\infty L_\infty & Z_\infty B_2 \\ \hline F_\infty & 0 & I \\ -C_2 & I & 0 \end{array}\right) \qquad (5.19)$$

$$F_\infty = -B_2^T X_\infty, \quad L_\infty = -Y_\infty C_2^T, \quad Z_\infty = (I - \gamma^{-2} Y_\infty X_\infty)^{-1} \qquad (5.20)$$

$$A_\infty = A + \gamma^{-2} B_1 B_1^T X_\infty + B_2 F_\infty + Z_\infty L_\infty C_2 \qquad (5.21)$$

and $Q(s)$ is a stable proper transfer function such that $\|Q\|_\infty < \gamma$. For $Q(s) = 0$ we get :

$$K(s) = -Z_\infty L_\infty (sI - A_\infty)^{-1} F_\infty \qquad (5.22)$$

$K(s)$ is called the *central* controller and has the same number of states as the generalized plant $P(s)$.

As discussed in section 5.3.1, the H_∞ norm has several interpretations in terms of performance. In practice, it is usually not necessary to obtain an optimal controller for the H_∞ problem, and it is simpler to design a sub-optimal one, which is close to the optimal controller, in the sense of the H_∞ norm.
Let assume γ_{min} be the minimum value of $\|F_l(P, K)\|_\infty$ over all stabilizing controllers K. Then, the H_∞ sub-optimal control problem consists in finding, given a $\gamma > \gamma_{min}$, all stabilizing controllers K such that [51] :

$$\|F_l(P, K)\|_\infty < \gamma \qquad (5.23)$$

In this work the problem described by eq.(5.23) is solved using the algorithm presented in Glover and Doyle [24] and [21], where a solution to the optimal H_∞ control design problem is provided as best solution of the Riccati equations.
If it is desired a controller that achieves γ_{min}, to within a specified tolerance, then a bisection algorithm can be applied on γ until its value is sufficiently

accurate. Note that this problem can also be solved using Linear Matrix Inequalities (LMI).

Usually, some weights are considered on the controlled outputs (including the actuator force and some external input). They represent the performance specifications in the frequency-domain. P thus includes the plant model G and the considered input and output weights (W_p, W_u) as in figure 5.1 (II). The H_∞ control problem is then referred to as a mixed sensitivity problem, W_p and W_u thus appearing in eq.(5.23) as weights on the sensitivity functions.

There exist two methodologies for H_∞ controller design : the signal-based approach and the loop shaping approach. The first approach is based on the minimization of the energy of error signals, given a set of exogenous input signals. This methodology is very general and more appropriate for multivariable problems in which several objectives must be taken into account simultaneously.
The transfer function shaping approach uses H_∞ optimization to shape the singular values of specified closed-loop transfer functions, over frequency. The maximum singular values are easy to shape by forcing them to lie below user defined bounds, thereby ensuring desirable bandwidths and roll-off rates.
For these reasons, we have chosen to use the loop shaping approach to compute a H_∞ compensator able to control, in DVD drives, the fine displacement of the spot along the radial direction.

5.3.3 Mixed-Sensitivity H_∞ Control

Mixed-sensitivity is the name given to transfer function shaping problems in which the sensitivity function $S = (I + GK)^{-1}$ is shaped along with one or more other closed-loop transfer functions such as KS or the complementary sensitivity function $T = I - S$. We remind that S is the transfer function between a disturbance, entering at the plant output, and the output of the system to control. KS is the transfer function between the reference and the control signal, and T the transfer function between the output and the reference signal.
In regulation problems, it is usually required to reject a disturbance entering at the plant output (eccentricity or vertical deviations) assuming that the measurement noise is relatively insignificant. Moreover, the actuator constraints should be taken into account in the design step. Hence, it makes

sense to shape the closed-loop transfer functions S and KS. The disturbance is usually a low frequency signal, and it is well rejected if the maximum singular value of S is made small over the same low frequencies. For this objective it can be chosen a low pass filter $W_1(s)$ with a bandwidth equal to that of the disturbance, and then a stabilizing controller $K(s)$ that minimizes $\|W_1 S\|_\infty$ may be found.
In practice it is more useful to use a second weighting function $W_2(s)$ to guarantee that the optimal controller has finite gain if the plant has not right-half plane zeros.
Usually $W_2(s)$ is a scalar high-pass filter having a cross-over frequency equal to that of the desired closed-loop bandwidth. Moreover, the ability to shape the complementary sensitivity function T and SG is desirable for enhancing track following, reducing measurement noise, as well as for guaranteing robust stability with respect to multiplicative perturbations acting at the system output.

For all these reasons, we have decided to solve a full mixed-sensitivity minimization problem, in a one degree of freedom setting.
Such a problem is usually formulated by using an additional weighting function $W_d(s)$ on the exogenous input w_1, which adds a degree of freedom in the design allowing to shape the SG and T transfer functions independently from $W_1(s)$ and $W_2(s)$. We have not used such a formulation since the desired shape of SG and T can be obtained using only two weights. Hence, our considered problem consists in finding a stabilizing controller $K(s)$ which minimizes the following quantity :

$$\left\| \begin{array}{cc} W_1 SG & W_1 S \\ W_2 T & W_2 KS \end{array} \right\|_\infty \tag{5.24}$$

The closed-loop transfer functions shaping approach, discussed above, is also valid for MIMO systems. In this case, the scalar weighting functions $W_1(s)$ and $W_2(s)$ are replaced by weighting matrices which contain different scalar weights for each channel of the system.
We would stress that the choice of the weighting functions $W_i(s)$ is crucial to carry out the required shaping and trade-offs. For SISO systems, like the spot position control loops of DVD players, the shaping of the closed-loop transfer function is relatively easy if no more than two weighting functions are considered. They should be simple, stable low-pass and high-pass filters, and their complexity should be limited to avoid that the order of the synthesized controllers grows drastically.
In industrial applications, this represents another crucial point to consider

during the design since implementation constraints often limit the maximum order of the achieved controllers.

In the following sections a full mixed-sensitivity minimization problem is applied to a DVD-video player, to compute a finite-dimensional stabilizing controller which guarantees enhanced spot track following and periodic disturbance rejection along the disc radial direction.

5.4 H_∞ Control Design applied to a DVD Player

Our goal in this chapter is to see how performances and robustness of the control system already implemented on the actual industrial solution, and presented in section 3.5, can be improved by using H_∞ norm-based design. Since the disc eccentricity represents the main source of disturbance affecting the spot position during playback, we focus more on periodic disturbance rejection rather than on track following problems. Hence, a LTI control design, based on a mixed-sensitivity minimization problem, is applied to the radial loop servo mechanism of the industrial DVD-video player, by taking into account industrial implementation constraints (see section 3.4). It means that the synthesized controller will work properly around a certain track location where the disc rotational frequency f_{rot} remains constant. To get a controller that works properly on the whole disc, it is sufficient for instance to couple this methodology with an adaptive algorithm, able to "change" one of the controller synthesis parameters (i.e. f_{rot}) with respect to the actual track location.

From previous chapters (see section 2.8) we know that the main specifications for the DVD-video player servomechanism is to limit the time-domain amplitude of the tracking errors e_{F} and e_{R} along the vertical and the radial directions, respectively. These specifications are usually translated in the frequency domain by shaping the system output sensitivity function S, according to fig.3.8. We recall that in DVD players, the output sensitivity function S is the transfer function from the track disturbance r to the actuator displacement h, as shown in fig.4.1. Weighting the sensitivity function allows to reduce the tracking error in correspondence with the disturbance model described through the weighting function. In addition, via weighting it is also possible to bound the peak of the sensitivity function, for robustness requirements.
Through sensitivity weighting, a lower bound for the closed loop bandwidth

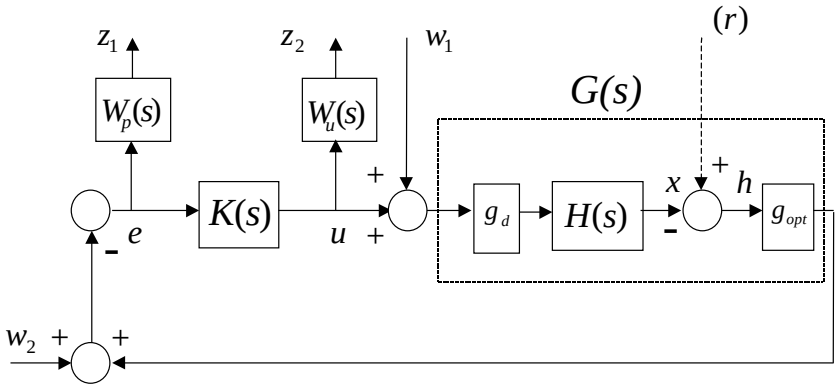

Figure 5.2: Control scheme used for the H_∞ controller design applied to a DVD player.

can be determined indirectly, to prevent it from coming too close to the plant parasitic resonances. These resonances can, in fact, affect the performance of the system and since their location vary from player to player (due to manufacturing tolerances), the behavior of a controller that achieves a too high bandwidth can exhibit large differences on different players. A way to limit the system closed-loop bandwidth is to impose an upper bound on the KS sensitivity function, which is the transfer function from the track disturbance r to the plant input u, as shown in fig.4.1.

Through KS, the following two design specifications can be expressed :

- The high-frequency roll-off of the controller can be imposed in order to reduce the controller amplification in the region where the plant parasitic resonances appear.
- The controller action can be kept bounded to prevent that too large values of the plant input u can saturate the actuator or damage the system.

From specifications given on the closed-loop transfer functions S, KS, T and SG the controller is the outcome of a minimization of the H_∞ norm of a system matrix, which groups two different performance channels.

5.4.1 Choice of the Control Scheme

In the case of DVD players, robustness aspects and shape of some of the relevant closed-loop transfer functions are taken into account to specify an H_∞ criterion to be minimized.
In fig.5.2 the scheme of the generalized servo loop considered for this design is shown. The transfer functions W_p and W_u represent the design weighting functions, w_1 and w_2 are the exogenous inputs, z_1 and z_2 the performance outputs, e is the measurement output and u is the control input. $H(s)$ denotes the moving lens actuator transfer function, g_d the power driver gain,

g_{opt} the optics gains, and $G(s) = g_{opt} g_d H(s)$ is the complete plant transfer function (already indicated with $P(s)$ in section 2.8 and 4.5.3).
We remind that the closed-loop transfer functions can be expressed as follows (see eq.(4.15) and (4.16)) :

$$T(s) = -\frac{g_d g_{opt} K(s) H(s)}{1 + g_d g_{opt} K(s) H(s)}, \quad S(s) = -\frac{1}{1 + g_d g_{opt} K(s) H(s)}$$

In the configuration shown in fig.5.2, the objective is to minimize a suitable norm of the transfer function from the performance-input vector $w = (\, w_1^T \quad w_2^T \,)^T$ to the performance-output vector $z = (\, z_1^T \quad z_2^T \,)^T$, that is :

$$\begin{pmatrix} z_1 \\ z_2 \end{pmatrix} = \begin{pmatrix} -W_p SG & -W_p S \\ -W_u [I + GK]^{-1} GK & -W_u KS \end{pmatrix} \begin{pmatrix} w_1 \\ w_2 \end{pmatrix} \tag{5.25}$$

The objective is to find a $\gamma > 0$ and a controller $K(s)$ that ensures closed-loop internal stability, i.e :

$$\|F_l(P, K)\|_\infty = \left\| \begin{array}{cc} W_p SG & W_p S \\ W_u T & W_u KS \end{array} \right\|_\infty \leq \gamma \tag{5.26}$$

and which minimizes the H_∞ norm of the transfer function from the performance inputs w_1 and w_2 to the performance outputs z_1 and z_2.
The weighting functions (W_p, W_u) should be chosen to reflect the design objectives (performance specifications) and knowledge of the disturbances and sensor noise. W_u is the weight on the control input, that can be affected by by sensor noise w_2, and W_p represents the weight on the error signal, that is affected by disc eccentricity or defects w_1.
In eq.(5.26) the goal is to minimize the amplitude of the error signal limiting the effort of the controller. Hence, the advantage of solving (5.26) is that using only two weights W_p and W_u, we force the frequency response of all the closed-loop transfer functions T, S, KS and SG to stay below pre-specified templates, in order to achieve performance specification and robustness objectives.

In fig.5.3 the general control configuration used for DVD-video player (see fig.5.2) is shown in LFT (Linear Fractional Transformation) form, where the plant $G(s)$ and the weighting functions $W_p(s)$ and $W_u(s)$ are included in the generalized plant $P(s)$.

The weighting functions have been chosen according to industrial performance specifications. Notice that, due to implementation constraints, low order weighting functions are considered to limit the order of the controller.

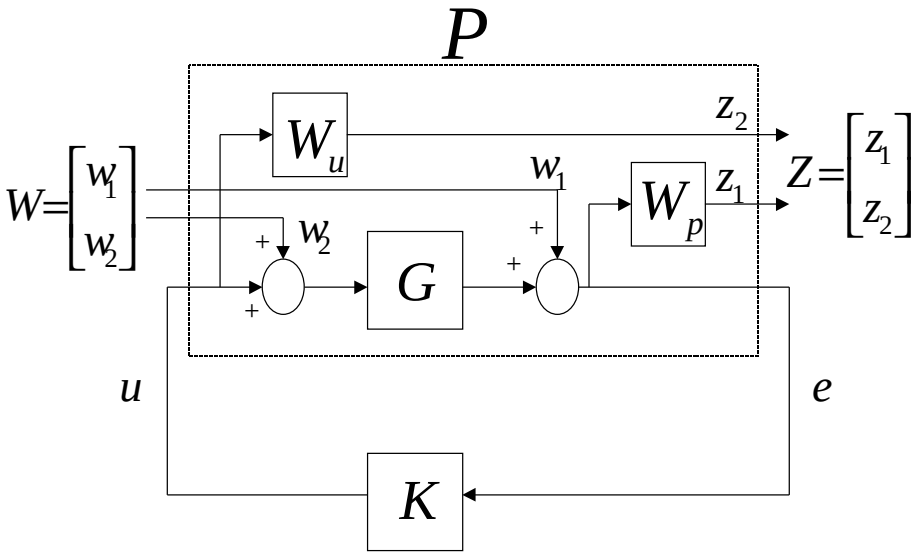

Figure 5.3: LFT form of the general control configuration applied to a DVD player.

$\mathbf{W}_p$: is used to impose a performance specification in terms of the sensitivity function S. We choose :

$$W_p(j\omega) = \frac{(j\omega/M_s + \omega_b)}{(j\omega + \omega_b A_s)} \tag{5.27}$$

where $M_s = 2.8$ to introduce a margin of robustness limiting the peak of S, $\omega_b = 2\pi 250$ $[rad/sec]$ to have a sensible attenuation of disturbances from low frequencies up to $250Hz$, and $A_s = 2.2 * 10^{-2}$ to reduce the steady-state error.

$\mathbf{W}_u$: is used to weight the output of the controller u according to the actuator limitations and it is set equal to :

$$W_u(j\omega) = \frac{(j\omega + \omega_{bc}/M_u)}{(j\omega\varepsilon + \omega_{bc})} \tag{5.28}$$

where $M_u = 0.63$ to impose limitations on the maximum value of the controller output signal up to 30 kHz, $\omega_{bc} = 2\pi 30e^3$ $[rad/sec]$ to limit the effect of measurement noise and plant uncertainties at high frequencies, and $\varepsilon = 0.01$ to ensure a high-frequency controller roll-off of $-40dB/$decade.

The amplitude of the inverse of the weighting functions $W_p(s)$ and $W_u(s)$ we have used for the control design is presented in fig.5.4.
Using the chosen weighting functions, we have designed a controller by minimizing the H_∞ norm of the closed-loop transfer functions S, T, KS and

SG. The synthesis has been performed for a fixed disc rotational frequency $f_{rot} \simeq 36\ Hz$, which corresponds to the innermost position $x_{in} \simeq 23\ mm$ of the actuator optical head when an over-speed factor $N = 1.5$ is chosen. The achieved optimal value of γ is $\gamma_\infty = 2.868$, and a 5^{th} order controller is obtained.

The amplitude and phase plots of the standard controller and of the synthesized H_∞ one are presented in fig.5.5. From this figure it appears that the poles of the chosen weighting functions W_p and W_u becomes poles of the synthesized controller, as required by the design. In fact, the H_∞ controller presents a higher low-frequency gain than the actual one, and this is due to the additional low-frequency pole introduced by the weighting function W_p at $\omega = -\omega_b A_s = 34.5\ rad/sec$, to reduce the steady state error and attenuate the low-frequency disturbances entering at the plant output. It can be also noticed the presence of a second additional high-frequency pole introduced by W_u at ω_{bc}, to reduce the effect of measurement noise, and to ensure that the controller gain decreases with a slope of $-40\ dB/dec$ after this frequency. Moreover, since the synthesized controller allows to get a phase margin $m_\varphi \simeq 40°$, it still guarantees nominal stability of the loop.

In fig.5.6 the singular values of the closed-loop sensitivity functions achieved for the actual controller and for the synthesized H_∞ one are shown. We notice that the closed loop sensitivity functions S and KS of both controllers stay within the chosen $1/W_p$ and $1/W_u$ templates.
From the upper left-hand corner plot it can be seen that the DVD disc specifications are satisfied, and that the synthesized controller gives a smaller low-frequency gain of S, due to its low-frequency behavior (see fig.5.5). Hence, we expect that low-frequency periodic disturbances will be better suppressed on the control signal u, by the designed controller.
From the upper right-hand corner plot, it can noticed that the closed loop transfer functions T match up to the desired closed-loop bandwidth. This is due to the additional high-frequency pole introduced in the H_∞ controller by the weight W_u, at above $30Khz$. The extra-pole is also responsible for the different behavior of the KS transfer functions, as it can seen from the lower left-hand corner plot. The control output signal is kept bounded to the level of M_u up to this pole, and then a controller roll-off of $-40\ dB/dec$ is guaranteed by the new design, which limits the actuator efforts up to frequencies where the measurement noise becomes relevant. As it can observed, this is not guaranteed by the actual implemented controller.

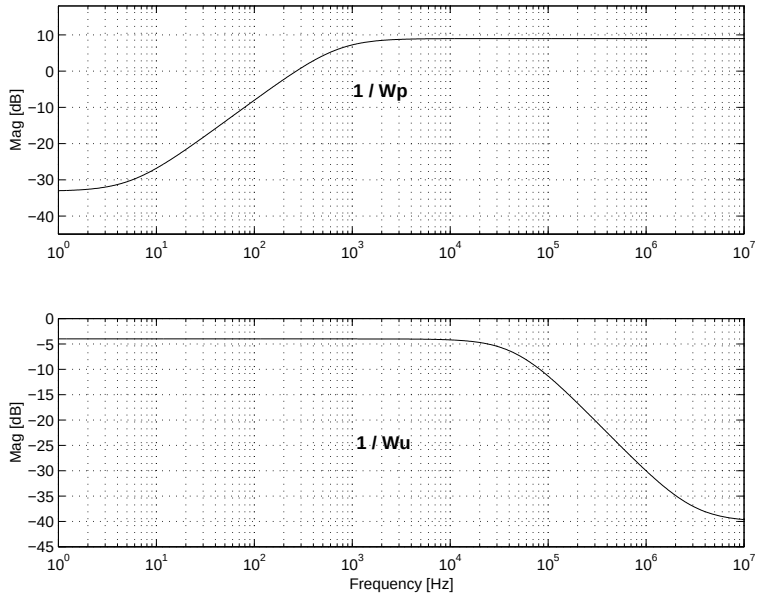

Figure 5.4: Amplitude of the inverse of the weight $W_p(s)$ and $W_u(s)$.

Finally, by looking at the lower right-hand corner plot, it can been seen that the SG transfer functions of both controllers are quite similar. We remind that the SG transfer function discloses the influence of w_1 (i.e. periodic disturbances see fig.5.2) entering at the plant input on the position error signal. Hence, the designed controller allows to obtain a better low-frequency disturbance attenuation on the position error signal e than the actual implemented controller, and this is always due to its high DC gain. Then, both controllers exhibit the same behavior with a slight amplification of disturbances on e up to the desired bandwidth, and a definitive suppression from the bandwidth to higher frequencies.

In Vidal et al. [66] and Dettori and Scherer [14] high-order weighting functions W_p and W_u are chosen, in order to achieve a very performing H_∞ controller and fulfill system performance specifications. However, due to implementation constraints, we have limited to $n = 3$ the maximum order of the synthesized controller, as explained in the following section.

5.4.2 Controller Order Reduction

Modern controller design methods such H_∞, produce controllers of order at least equal to that of the plant, and usually higher because of the inclusion of weighting functions during the synthesis.
These control laws may be too complex with regards to its practical implementation, and simpler designs are then needed. For this purpose, one can either reduce the order of the plant model prior to controller design, or

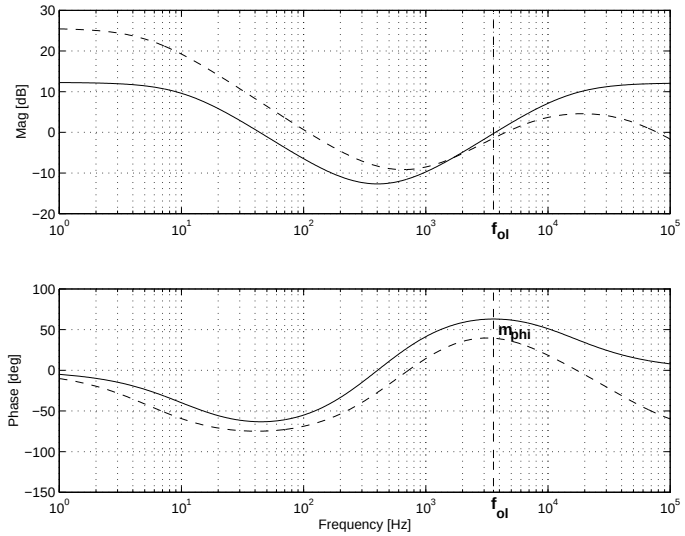

Figure 5.5: Amplitude and phase plots of the radial loop controllers. Actual controller (solid line), H_∞ full-order controller (dashed line).

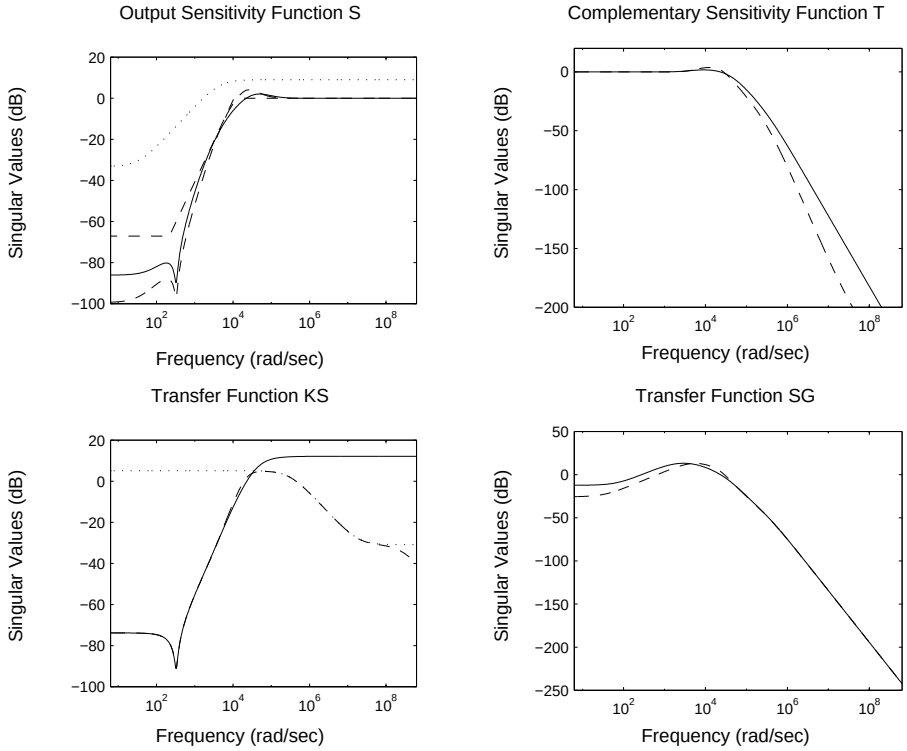

Figure 5.6: Singular values of the closed-loop sensitivity functions computed for the actual (solid line) and of the synthesized H_∞ (dashed line) controllers.

reduce the controller in the final stage.
As already exposed in section 3.7 and section 4.6, in a DVD-video players, the electro-mechanical behavior of the objective lens actuators can be represented by a simple third order model (see eq.(3.34)). Since no need of further model order reduction is required, we have preferred to reduce the order of the synthesized controller because, in our industrial benchmark, the size of the controller is limited by the dedicated hardware, used to implement digital filters (see section 3.3.1 and section 3.4), and by the micro-controller computational time.
It is essential that the controller order reduction procedure preserves the required closed-loop properties as far as possible.
One useful methodology is the one exposed in Skogestad and Postlethwaite [51], and based on balanced reductions obtained by using the Grammian of the controller balanced state-space realization.

By applying this algorithm, we have obtained a reduced-order controller of order $n = 3$, which has been implemented in discrete-time on the industrial benchmark. The applied order reduction procedure gives a reduced-order controller by :

- suppression of the polynomials $(1+s/3.611\cdot10^5)$ and $(1+s/3.721\cdot10^5)$ of the numerator and denominator of $K(s)$. The suppressed zero and pole are located at about 57.4 Khz and 59.2 Khz, respectively.

- suppression of the high-frequency pole located at about 37 Mhz, and given by the polynomial $(1+s/2.366\cdot10^8)$ of the denominator of $K(s)$.

These operations, which suppress a zero and two poles located quite far from the desired closed-loop bandwidth, reduces the order of the controller without changing its performances.

In fig.5.7 the amplitude and phase plots of the radial loop controllers is presented. From this figure it can be seen that the reduced-order controller exhibits, at low frequencies, a different behavior from the full-order H_∞ controller. Implementation constraints, given in terms of rounding errors, quantization noise, and overflows can in fact give rise to finite precision of digital computation. As already said in section 3.4, the high sampling frequency (f_s) used by the dedicated DSP, makes hard to implement digital filters having very low cut-off frequencies, since rounding and truncation phenomena do not allow to represent coefficients with necessary accuracy. Hence, we had to reduce the controller low-frequency gain to allow its im-

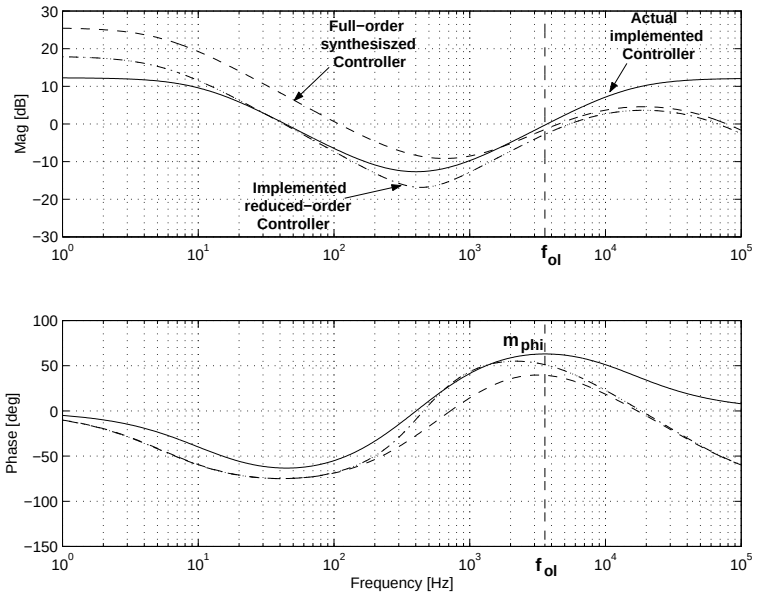

Figure 5.7: Amplitude and phase plots of the radial loop controllers. Actual controller (solid line), H_∞ full-order controller (dashed line), H_∞ reduced-order controller (dash-dot line) implemented in the industrial system.

plementation on the test benchmark. At higher frequencies the full and the reduced-order controllers present the same behavior.

In the following sections we will present the performance and robustness analysis obtained with both the full and the reduced-order synthesized controllers, showing that controller order reduction preserves the desired closed-loop properties.

5.4.3 Simulation and Experimental results

In fig.5.8 - 5.11 the measured and the simulated closed-loop transfer functions, obtained for both the full and reduced-order H_∞ controllers are presented. Here, as term of comparison, we present also the measured and the simulated closed-loop transfer function computed with the actual implemented controller. Experimental results are obtained by implementing the reduced order H_∞ controller on the industrial benchmark.
The system frequency responses have been measured for a fixed disc rotational frequency $f_{rot} \simeq 36\ Hz$. As done for closed-loop identification (see section 4.5), we have set a sweep resolution of $R_{sw} = 100$ points/sweep. The integration time has been fixed equal to $T_{in} = 5$ swept sine cycles. $N_{sw} = 400$ is the number of resolution lines considered during acquisitions, and a rms (root mean square) averaging mode has been selected with $N_{av} = 4$ averaging per frequency point, to reduce the measurement noise to its mean value. The maximum peak amplitude of the injected swept sine has been set equal to $A_{sw} = 30\ mV_{pk}$, and its DC offset of $\overline{A_{sw}} = 1\ V$.

From these figures it can be seen that closed-loop measurements are very ill-conditioned since the high attenuation level needed at low frequencies to suppress external disturbances reduces the output signal-to-noise ratio (SNR) and affect the control loop, as already explained in section 4.5.3. This is true when both designed and actual controllers are used. This explains why, in fig.5.8, the measured frequency response of S, obtained for the reduced-order H_∞ controller, lies above $1/W_p$ up to 500 Hz, and matches with the simulated curve obtained with the same controller only after this frequency.
From simulation results we remark that at low frequencies the same characteristic differs from the one plotted for the full-order controller. This is mainly due to the need of imposing a lower DC gain for implementing a reduced-order controller on the real system. At higher frequencies both characteristics match, confirming that closed-loop robustness properties are hold by the implemented controller.

From fig.5.9 it can be seen that the complementary sensitivity function T of both controllers matches on the whole measurement span, and they fit the measured frequency response of T till about 20 Khz, where measurement noise become to high. This confirm that also closed-loop performance are hold by the reduced-order controller.

The fact that closed-loop robustness and performance properties are hold by the implemented reduced-order H_∞ controller is also confirmed by the measured frequency responses of KS and SG, as presented in fig.5.10 and fig.5.11 respectively.
Also here because of noise entering on the measurement channel, simulations match with the measured frequency response up to 500 Hz. At higher frequencies the correspondence between simulations and real time results is quite satisfactory.

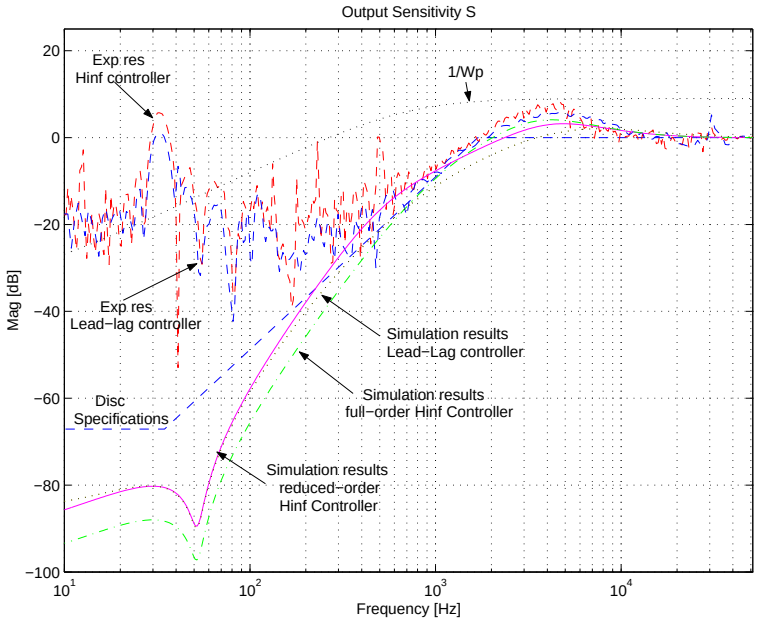

Figure 5.8: Amplitude plots of the output sensitivity function S.

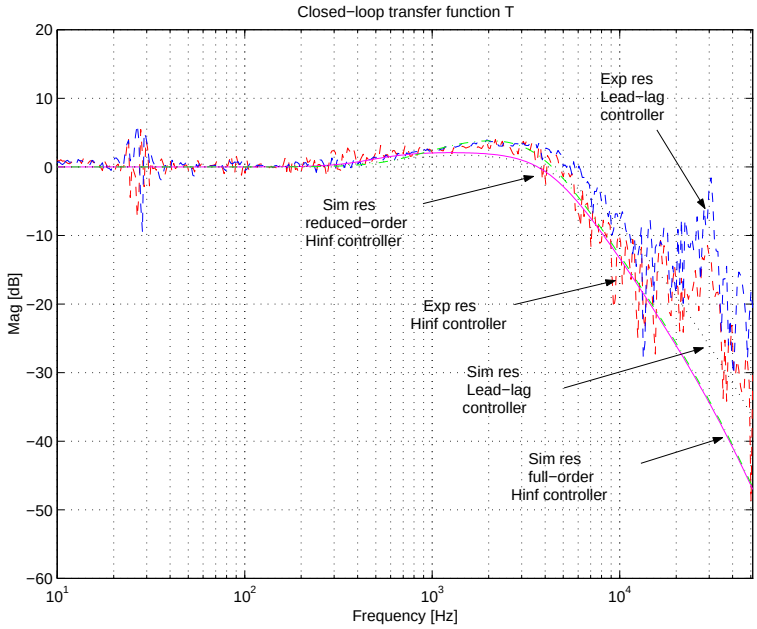

Figure 5.9: Amplitude plots of the complementary sensitivity function T.

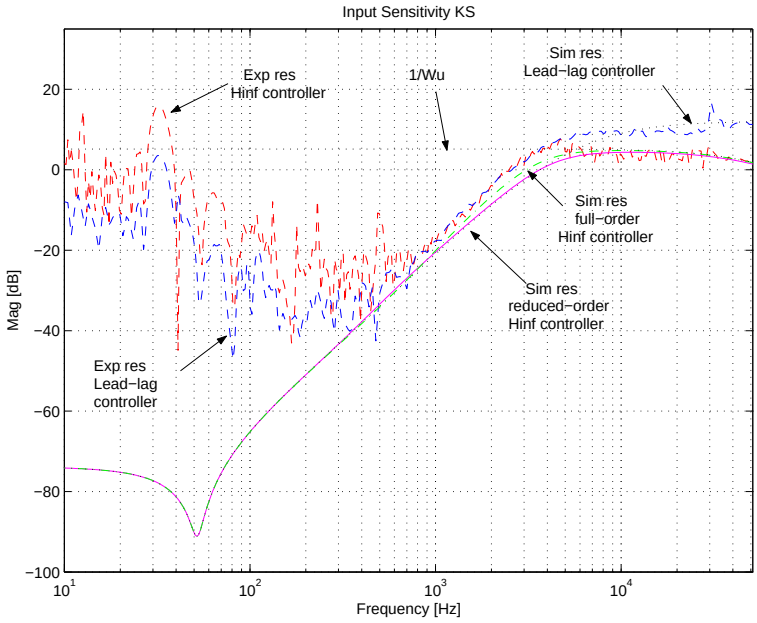

Figure 5.10: Amplitude plots of the input sensitivity function KS.

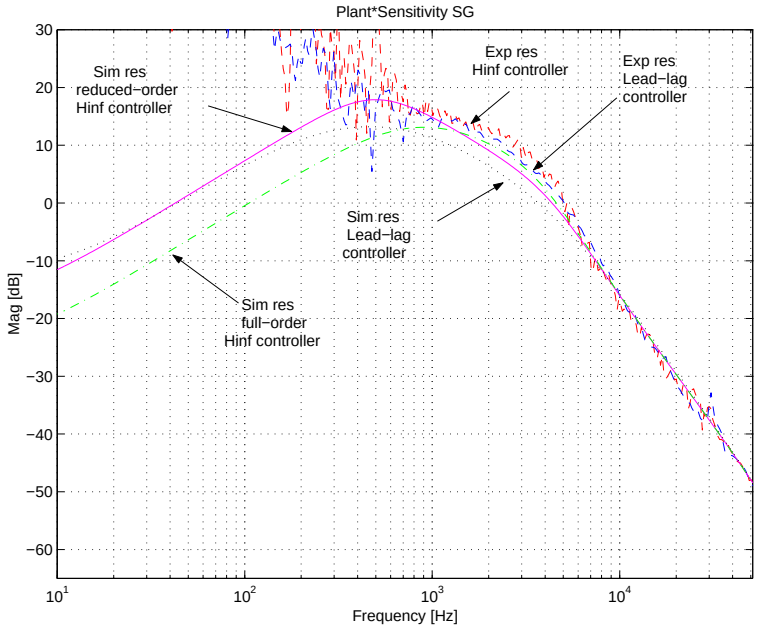

Figure 5.11: Amplitude plots of the SG sensitivity functions.

5.5 System parametric uncertainties : theoretical background

In this section our aim is to show how to represent system uncertainty by real perturbations, and to analyze robust stability (RS) and robust performance (RP) of the DVD-video servo system.
Usually, a control system is robust if it is insensitive to differences between the actual system and the model of the system which has been used to design the controller. These differences are referred to as model uncertainties.
To account for model uncertainty we assume that the dynamic behavior of the plant is described not by a single linear time invariant model $G(s)$, but by a set Π of possible linear time invariant models $G_\Delta(s) \in \Pi$, denoted as "uncertainty set".
We use a norm-bounded uncertainty description, where the set Π of possible LTI models is generated by allowing H_∞ norm-bounded perturbations to the nominal plant $G(s)$.
Let Δ denote a normalized perturbation with H_∞ norm less than one, i.e :

$$\|\Delta\|_\infty < 1 \tag{5.29}$$

Uncertainty in the plant model may have several origins :

- There always exist parameters in the LTI model that are known approximatively.
- The parameters in the LTI model can vary due to non-linearities or changes in the operating conditions.
- Imperfections of measurement devices can give rise to uncertainty on the measured inputs to the LTI model.
- At high frequency the structure and the order of the model are often badly known.
- When a very detailed model is available, it is often preferred to work with a simpler nominal model and represent the neglected dynamics as uncertainty.
- The implemented controller can differ from the one obtained by solving the synthesis problem. Uncertainty can be included to allow for controller order reduction and implementation inaccuracies.

As stated in Skogestad and Postlethwaite [51], these sources of model uncertainty may be grouped in three main classes :

I) Parametric uncertainty : the structure and the order of the model are known, but some of the parameters are uncertain.

II) Neglected and un-modelled dynamics uncertainty : the model is in error because of missing dynamics, usually present at high frequencies.

III) Lumped uncertainty : the uncertainty description represent one or several sources of parametric or un-modelled dynamics uncertainty.

Parametric uncertainty is often called *structured uncertainty* as it models the uncertainty in a structured manner. Lumped dynamics uncertainty is also called *unstructured uncertainty*. In this chapter, parametric unstructured and structured uncertainties will be handle by using a H_∞ frequency-domain approach.

In addition to nominal stability and performance, the objectives of any control system include :

Nominal Stability (NS). Nominal stability (NS) is achieved if the nominal system is internally stable.

Nominal Performance (NP). Nominal performances (NP) are obtained if the nominal system performances hold, and if the (NS) is achieved.

Robust Stability (RS). The system is stable for all perturbed plants around the nominal model up to the worst-case model uncertainty.

Robust Performance (RP). The system satisfies the (NS) and the (NP) conditions. It also guarantees that performance specifications are meet for all perturbed plants about the nominal model up to the worst-case model uncertainty.

5.6 Unstructured Uncertainty

This section deals with unstructured parametric uncertainties. In section 5.6.1 a theoretical background on unstructured parametric uncertainty is presented. Then, in section 5.6.2 a simple frequency-domain representation of parametric uncertainty affecting the DVD-video servo mechanism is proposed. In section 5.6.3 we derive general conditions for RS and RP analysis when perturbations are restricted to be real, and in section 5.6.4 we present simulation and experimental results obtained for the industrial system.

5.6.1 Modelling unstructured uncertainty

Unstructured uncertainty can be represented in or frequency-domain framework, if we restrict the perturbations Δ to be real.
From the nominal plant model $G_0(s)$, the set Π of possible linear time invariant models $G_\Delta(s)$ can be built by varying the model parameters inside a given range of values. Hence, parametric uncertainties can be represented as frequency-domain uncertainties, by considering the Nyquist plot generated by the set Π as follows :

- At each frequency, an uncertainty region is generated by varying the parameters of $G_\Delta(s)$ in a given range of values, and by computing region of complex numbers $G_\Delta(s)$.
- This complex region can be approximated as disc-shaped regions, resulting in a complex additive or multiplicative uncertainty model description.

These disc-shaped regions may be generated by additive complex norm-bounded perturbations (*additive uncertainty*) around the nominal plant $G_0(s)$ as follows :

$$G_\Delta(s) = G_0(s) + W_A(s)\Delta_A(s), \quad |\Delta_A(j\omega)| \leq 1 \ \ \forall\omega \tag{5.30}$$

where $\Delta_A(s)$ is any stable rational transfer function which at each frequency is no larger than one in magnitude. At each frequency $\Delta_A(j\omega)$ generates a disc-shaped region with radius 1 centered at 0, so $G_0(s) + W_A(s)\Delta_A(s)$ generates at each frequency a circular region of radius $|W_A(j\omega)|$ centered at $G_0(s)$. Hence, $W_A(s)$ can be seen as a weight introduced to normalize the perturbation to be less than 1 in magnitude at each frequency.
The disc-shaped regions may also be represented by a *multiplicative uncertainty* description as follows :

$$G_\Delta(s) = G_0(s)[1 + W_I(s)\Delta_I(s)], \quad |\Delta_I(j\omega)| \leq 1 \ \ \forall\omega \tag{5.31}$$

From eq.(5.30) and (5.31) it appears that for SISO systems the additive and multiplicative uncertainty descriptions are equivalent if at each frequency the following relation holds :

$$|W_I(j\omega)| = |W_A(j\omega)|/|G_0(j\omega)| \tag{5.32}$$

The problem is how to find the weights for system parametric uncertainty.

Let consider a set Π of possible plants resulting from parametric uncertainty. If we want to describe this set of plants by a single real perturbation $\Delta_A(s)$ or $\Delta_I(s)$, this uncertainty description can be generated as follows :

- Select the nominal model $G_0(s)$, by considering, for example, a model of mean parameters values $G_0(s) = \overline{G(s)}$.
- *Additive uncertainty :* at each frequency find the smallest radius $l_A(\omega)$ which includes all the possible plants Π :

$$l_A(\omega) = \max_{G_\Delta \in \Pi} |G_\Delta(j\omega) - G_0(j\omega)| \tag{5.33}$$

  the rational transfer function $W_A(j\omega)$ is chosen as follows [51] :

$$|W_A(j\omega)| \geq l_A(\omega) \ \ \forall\omega \tag{5.34}$$

- *Multiplicative uncertainty :* at each frequency find the smallest radius $l_I(\omega)$ which includes all the possible plants Π :

$$l_I(\omega) = \max_{G_\Delta \in \Pi} \left| \frac{G_\Delta(j\omega) - G_0(j\omega)}{G_0(j\omega)} \right| \tag{5.35}$$

  and with rational weight $W_I(j\omega)$ is chosen as follows [51] :

$$|W_I(j\omega)| \geq l_I(\omega) \ \ \forall\omega \tag{5.36}$$

In order to check robust stability (RS) and performance (RP) on the industrial benchmark, we have chosen a multiplicative uncertainty model of the DVD-video player servo mechanism. In fact, multiplicative weights are usually preferred because their numerical value is more informative giving an upper bound on the complementary sensitivity function T, as stated in Skogestad and Postlethwaite [51].

5.6.2 Choice of the uncertainty models

In order to allow an accurate and non conservative representation of the actual DVD system, and to increase performance, a simple frequency-domain representation of real parametric uncertainty is chosen by using real norm-bounded perturbations, as done in Vidal et al. [64] and [66].

The nominal model of the plant is obtained considering the average values of physical parameters of three DVD pick-ups, which are used in industrial applications. Then, the worst-case behavior is analyzed by taking into account the variation of each parameter in the largest interval of values taken from the pick-ups data-sheet. The values of the physical parameters characterizing the radial actuator nominal model together with their maximum and percentage variations is presented in table 5.1. Here where f_0 and DC are the values of the actuator resonance frequency and DC sensitivity, that are used to compute the values of the elastic constant k, of the mass spring dumping factor D and of the electro-magnetic constant K_e, as follows (see eq.(3.38)-(3.40) in section 3.7) :

$$k = (2\pi f_0)^2 M, \;\; K_e = kRDC \;\; and \;\; D = \sqrt{2f_0^2(1 - \sqrt{1 - 1/p^2})}$$

and p is the value of the actuator transfer function peak, at the resonance frequency f_0.

Table 5.1: *Values of the physical parameters characterizing the radial actuator nominal (average from 3 pick-ups) model together with their maximum and % variations.*

Parameters	Nominal value	Maximum variation	% Variation
$R\ [\Omega]$	4.83	[4.11, 5.55]	15 %
$L\ [\mu H]$	12	[8, 16]	33 %
$M\ [g]$	0.30	[0.27, 0.33]	10%
$f_0\ [Hz]$	59	[56, 62]	5%
$DC\ [dB]$	-65.14	$[-67.08, -63.55]$	20%
$k\ [N/m]$	45.350	[36.769, 55.087]	20 %
$K_e\ [Wb/m]$	0.1212	[0.0897, 0.1528]	26 %
$D\ [Ns/m]$	0.0160	[0.0136, 0.0185]	15 %

Let us consider $G_0(j\omega) = g_{opt}H(j\omega)$ as the nominal plant transfer function, where g_{opt} is chosen in a way that the system bandwidth f_t matches the

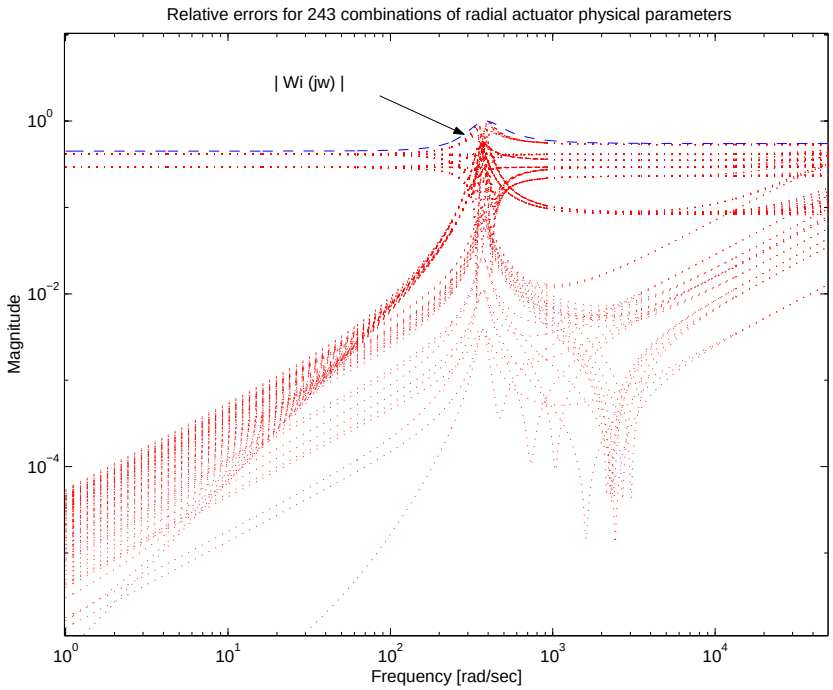

Figure 5.12: Relative plant errors $l_I(j\omega)$ (dotted line) and rational weight $W_I(j\omega)$ (dashed line) for 243 combination of the radial actuator physical parameters.

value prescribed in [59].

Then, the multiplicative uncertainty model $G_\Delta(j\omega)$ described by eq.(5.31) is considered for describing uncertainty acting on the DVD-video player servo mechanism.

The dependency of the plant model from the variation of each of its physical parameters is analyzed, and we compute the relative error function given by eq.(5.35). Finally, the rational weight $W_I(j\omega)$ is found in by using eq.(5.37). The relative errors $l_I(j\omega)$, together with the rational weight $W_I(j\omega)$, are plotted in fig.5.12.

The chosen weighting function $W_i(j\omega)$ has the following form :

$$W_I(j\omega) = g_{W_I} \frac{(s^2 + 2\zeta_1\omega_{n_1}s + \omega_{n_1}^2)(s^2 + 2\zeta_2\omega_{n_2}s + \omega_{n_2}^2)}{(s^2 + 2\zeta_3\omega_{n_3}s + \omega_{n_3}^2)(s^2 + 2\zeta_4\omega_{n_4}s + \omega_{n_4}^2)} \tag{5.37}$$

where the values of g_{W_I}, ζ_i and ω_{n_i}, $\forall\ i = 1 \ldots 4$ are found by trial and errors. As it can seen form fig.5.12, this function has order four and it gives an upper bound on the system uncertainty description including the set of all possible plant models $G_\Delta(s)$.

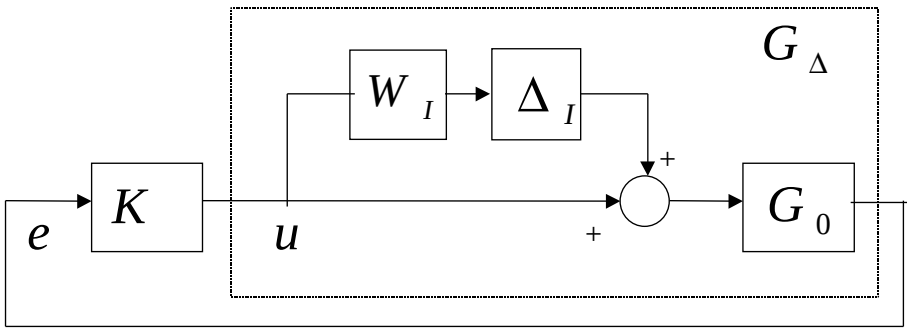

Figure 5.13: The DVD-video player servo system with multiplicative parametric uncertainty.

5.6.3 Robust Stability and Robust Performance with Unstructured Uncertainty

In this section we want derive conditions which ensure that the system remains stable and that closed-loop performance are achieved for all perturbation in the uncertainty set Π.

The scheme of a general uncertain feedback system with input multiplicative uncertainty is presented in fig.5.13.
The multiplicative uncertainty is assumed to have magnitude $|W_I(j\omega)|$. The quantities L_Δ and L_0 represent the uncertain and the nominal open-loop transfer function, respectively, as well as G_Δ and G_0 denote the uncertain and the nominal plant transfer functions. Similarly, T_0 and S_0 represent the closed-loop complementary and output sensitivity transfer functions, computed using the nominal plant model G_0, as well as T_Δ and S_Δ the same functions obtained with the uncertain plant transfer function G_Δ. Δ_I are the perturbations acting on the plant.
With uncertainty the loop transfer function becomes :

$$L_\Delta = G_\Delta K = G_0 K(1+W_I\Delta_I) = L_0 + W_I L_0 \Delta_I, \quad |\Delta_I(j\omega)| \leq 1 \ \ \forall\omega \quad (5.38)$$

We assume stability of the nominal closed-loop system, and for simplicity that L_Δ is stable. Using the *small gain theorem* (i.e.the Nyquist stability condition) to test for Robust Stability (RS) of the closed-loop system, we obtain [51] :

$$RS \Leftrightarrow |W_I L_0| < |1 + L_0| \Leftrightarrow \left|\frac{W_I L_0}{1 + L_0}\right| < 1 \Leftrightarrow |W_I T_0| < 1, \ \ \forall\omega \qquad (5.39)$$

Thus, the requirement for robust stability (RS) for the case with multiplicative parametric uncertainty gives an upper bound on the nominal system complementary sensitivity function, as follows :

$$RS \Leftrightarrow |T_0| < \frac{1}{|W_I|}, \quad \forall\omega \qquad (5.40)$$

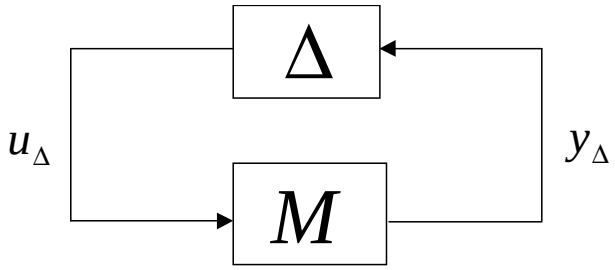

Figure 5.14: $M\Delta$ Structure.

Eq.(5.40) gives a necessary and sufficient condition provided that there exist uncertain plants such that at each frequency all perturbations satisfying $|\Delta_I(j\omega)| < 1$ are possible.

The Nyquist stability condition can also be applied to an alternative loop transfer function M_Δ rather than L_Δ. In fact, if the nominal feedback system is stable then stability of system in fig.5.13 is equivalent to stability of the $M\Delta$ form presented in fig.5.14, where $\Delta = \Delta_I$ and [51] :

$$M = W_I K(1 + G_0 K)^{-1} G_0 = W_I T_0 \tag{5.41}$$

is the transfer function from u_Δ to y_Δ.

By applying the Nyquist stability condition to the system of fig.5.14 we obtain :

$$RS \Longleftrightarrow |1 + M\Delta| > 0 \Longleftrightarrow |M| = |W_I T_0| < 1, \ \forall\omega, \ \forall|\Delta| \leq 1 \tag{5.42}$$

The $M\Delta$ structure provides a very general way of handling robust stability, since eq.(5.42) is essentially an application of the small gain theorem where usual conservatism is avoided, since any phase in $M\Delta$ is allowed.

Considering the performance specifications in term of the weighted sensitivity functions, for Robust Performance (RP) we require that the conditions for nominal performance (NP) i.e :

$$NP \Leftrightarrow |W_p S_0| < 1 \Leftrightarrow |W_p| < |1 + L_0|, \ \forall\omega \tag{5.43}$$

are satisfied for all possible plants, including the worst-case uncertainty, which can be re-written as follows [51] :

$$RP \Leftrightarrow \max_\omega(|W_p S_\Delta| + |W_I T_\Delta|) < 1, \ \forall\omega \tag{5.44}$$

The RS and the RP conditions of eq.(5.40) and eq.(5.44), given for multiplicative parametric uncertainty, can be closely approximated by the following mixed-sensitivity H_∞ condition [51] :

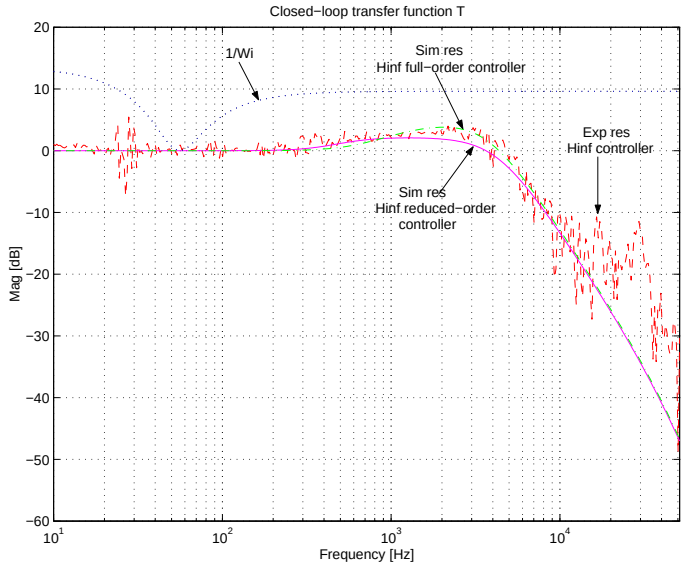

Figure 5.15: Measurements (dotted line), simulation with the 3rd order controller (solid line), simulation with the 5th order controller (dash-dotted line), weighting functions (dotted line).

$$\left\| \begin{pmatrix} W_p S_0 \\ W_I T_0 \end{pmatrix} \right\|_\infty = \max_\omega \sqrt{|W_p S_0|^2 + |W_I T_0|^2} < 1 \tag{5.45}$$

Since eq.(5.45) is within a factor of at most $\sqrt{2}$ to condition (5.44), for SISO systems the RS and the RP-conditions can be approximated in terms of an H_∞ problem.

5.6.4 Simulation and experimental results

In this section we present simulation and experimental results obtained when the nominal model of the DVD-video player servo mechanism is subjected to parametric unstructured uncertainties and real norm bounded perturbations are considered.
Usually, in the optical pick-up the values of the resistance, of the inductance and of the mass of the voice coil motor are badly known. As it can seen in table 5.1, the first two are the most varying parameters, depending on environmental conditions (temperature and humidity) and on device's aging. The other parameters will vary due to industrial manufacturing only.

In fig.5.15 the simulated closed-loop transfer functions, obtained for both the full and reduced-order H_∞ controllers are presented. Experimental results are obtained by implementing the reduced order H_∞ controller on the industrial benchmark.
In this figure we present the same results shown by fig.5.9. Moreover, in the upper right-hand corner plot, the frequency response of the inverse of the

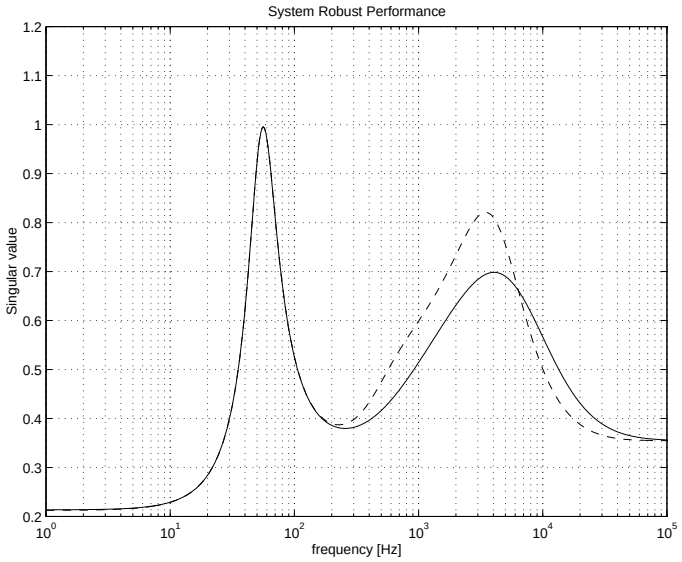

Figure 5.16: System robust performance, given by (5.44) Reduced-order H_∞ controller (solid line), actual implemented controller (dashed line).

uncertainty weight $W_I(j\omega)$ is drawn together with the closed-loop transfer function T.

From this figure it is easy to verify that the robust stability (RS) property of eq.(5.40) is satisfied for this design, i.e. that the closed-loop system remains stable for all perturbed plants around the nominal model up to the chosen worst-case model uncertainty.

Figure 5.16 shows the robust performance (RP) achieved with the reduced-order H_∞ and the actual implemented controllers. It is clear that in both cases (RP) condition of eq.(5.44) is satisfied, and that the designed controller guarantees better system robustness properties with respect to parametric uncertainties.

Finally, in fig.5.17 are presented the measured power spectral densities (PSD) of the the tracking error signals, obtained for the reduced-order H_∞ controller and for the actual controller implemented in the current industrial solution. Measurements have been acquired by using the worst-case disc (test disc having nominal eccentricity of $\epsilon = 150\ \mu m$) and for a disc rotational frequency of about $f_{rot} = 33Hz$. From this figure it appears that the H_∞ controller provides the same level of periodic disturbance rejection as the standard controller, for a fixed rotational frequency.

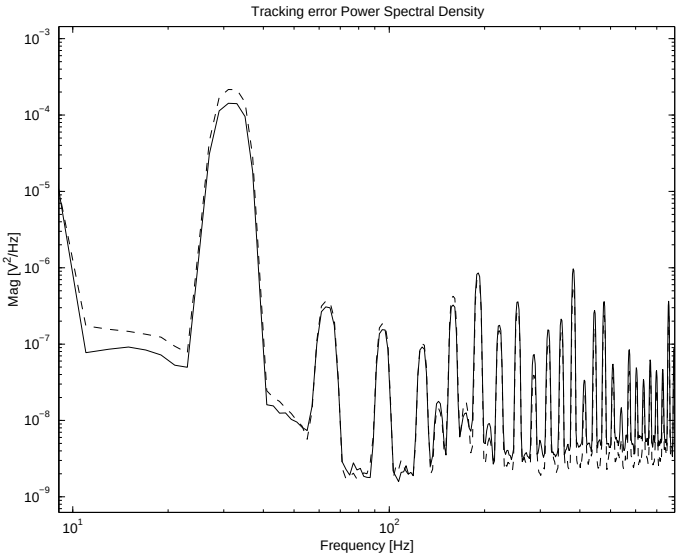

Figure 5.17: Measured Power Spectral Density of the tracking error signal. Reduced-order H_∞ controller (solid line), actual implemented controller (dashed line).

5.7 μ-Analysis : System Structured Uncertainty

Usually, the models used for control design are computed whether by using identification algorithms, or by knowledge of physical principles that govern the system behavior. Nevertheless, the real system parameters are not always well known and they can vary during its life.

The main property required to a control system is to maintain closed-loop stability, also when system parametric or neglected dynamics uncertainties are considered. The robust stability problem can be analyzed by considering the smallest uncertainty that makes the system unstable. The small gain theorem [69] can be applied to quantify the H_∞ norm of the maximum allowable uncertainty, by measuring the H_∞ norm of some relevant closed-loop sensitivity function. Nevertheless, a conservative idea of the uncertainty tolerances intervals may be obtained if the uncertainty upper bound includes a set of models which do not have any plausible correspondence with the real system.

The μ-analysis is an alternative tool which allows to study the robust stability problem of a system subject to uncertainty, by using the structured singular value μ of a system matrix. The advantage of using the structured singular value is that it takes into account the structure of such matrix, giving thus a "less pessimistic" or less conservative idea of the uncertainty tolerances intervals than the H_∞ norm-based method. As drawback, the structured singular value can not be computed analytically. Only upper or

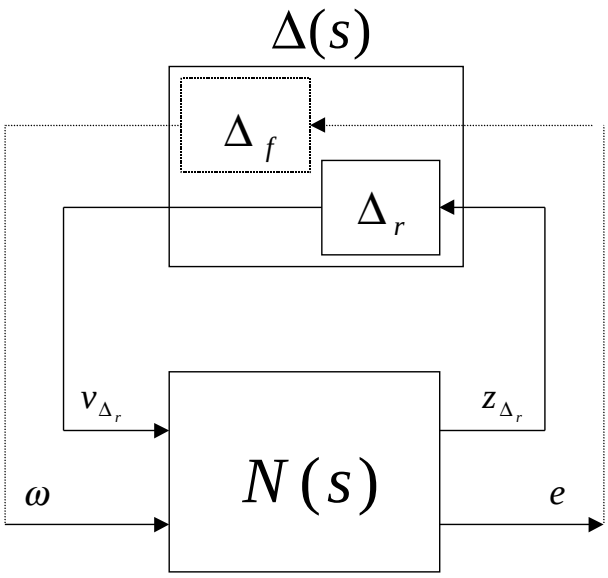

Figure 5.18: $N\Delta$ configuration.

lower bounds of μ can be obtained to estimate more or less exactly its final value.

5.7.1 Theoretical background on μ-Analysis

The starting point of the robustness analysis is the block-diagonal representation of the uncertainties set considered for the system closed-loop stability analysis, and formed by the set $\underline{\Delta}$ of the following complex matrices :

$$\underline{\Delta} = \text{diag}\{\Delta_1, \cdots, \Delta_q, \delta_1 I_{r_1}, \cdots, \delta_r I_{r_r}, \epsilon_1 I_{c_1}, \cdots, \epsilon_c I_{c_c}\} \in \mathbb{C}^{k \times k} \qquad (5.46)$$

where :

$$\Delta_i \in \mathbb{C}^{k_i \times k_i}, \;\; \delta_i \in \mathbb{R}, \;\; \epsilon_i \in \mathbb{C}$$

and $\Delta_i(s), \forall\, i = 1, \ldots, q$ represent the full block complex uncertainties, $\delta_i(s)$, $\forall\, i = 1, \ldots, r$ the real parametric uncertainties, and $\epsilon_i(s)$, $\forall\, i = 1, \ldots, c$ the complex parametric uncertainties.

Usually, parametric or neglected dynamics uncertainty can be drawn as a block separated from the system, as shown in fig.5.18, where the model uncertainty are represented by using an upper Linear Fractional Transformation (LFT) form. This figure represents the nominal system transfer matrix $N(s)$ as well as the uncertainty matrix $\Delta(s)$ which can be divided in two sub-blocks : Δ_r which contains model and parametric uncertainties, and Δ_f which is a fictive full block complex uncertainty connecting the output signals to control e to the exogenous inputs w.

Note that the nominal system transfer matrix has the following form :

$$N(s) = \begin{bmatrix} N_{zv}(s) & N_{zw}(s) \\ N_{ev}(s) & N_{ew}(s) \end{bmatrix} \tag{5.47}$$

and the closed-loop transfer matrix from the output e and the inputs w is given by :

$$T_{ew}(s) = N_{ew}(s) + N_{ev}(s)\Delta(s)(I - N_{zv}(s))^{-1}N_{zw}(s) \tag{5.48}$$

This scheme is also called $N\Delta$ configuration, and it is useful to perform nominal stability (NS), nominal performance (NP), robust stability (RS) and robust performance (RP) analysis from the values of the structured singular value μ of different transfer matrices.

As seen from eq.5.46, $\Delta(s)$ is formed by q transfer matrices, r real blocks containing real scalar factors δ_i repeated r_i times, and c complex scalar factors ϵ_i repeated c_i times. Parametric uncertainty are usually represented by blocks of repeated real scalar factors. Models uncertainties, as neglected dynamics, are often represented by transfer matrices [51] and [69]. As we tackle real parametric uncertainties, we consider structured uncertainties, associated to μ-analysis for RS and RP, and real parametric uncertainties block Δ_r is considered for RS analysis. The RP analysis also needs the fictive full block complex uncertainty Δ_f.

Let now consider a generic matrix $M \in \mathbb{C}$ having same dimension as Δ. The structured singular value of M with respect to the set $\underline{\Delta}$, is defined as follows :

$$\mu_{\underline{\Delta}}(M)^{-1} := \min\{\overline{\sigma}(\Delta) : \Delta \in \underline{\Delta},\ \det(I - \Delta P) \neq 0\} \tag{5.49}$$

$\mu_{\underline{\Delta}}(M)^{-1}$ is as the minimum value of the norm of Δ which makes $(I - \Delta P)$ singular. For RS, we shall determine how large values Δ (in terms of H_∞ norm) can assume, without destabilizing the feedback system.
Since the closed-loop poles are given by $det(I - N_{zv}(s)) = 0$, the feedback system becomes unstable if $det(I - N_{zv}(s)) = 0$ for some $s \in \mathbb{C}, \Re(s) \geq 0$.

The result is then given by the following theorem [51] :

Theorem 1 *Assume that the nominal system $M(= N_{ew})$ and the perturbations Δ are stable. Then the feedback system is stable for all allowed perturbations Δ such that, $\forall\ \overline{\mu} \in \mathbb{R}$:*

$$||\Delta(s)|\,|_\infty < 1/\overline{\mu} \tag{5.50}$$

if and only if :

$$\forall \omega \in \mathbb{R}, \quad \mu_{\underline{\Delta}}(M(j\omega)) \leq \overline{\mu} \tag{5.51}$$

Since μ can not be computed analytically, the idea which is at the basis of μ-analysis is to find the smallest upper bound $\overline{\mu}$ of $\mu_{\underline{\Delta}}(M)$. To do this, the upper bound $\overline{\mu}$ is computed by taking, through a set of "sufficiently near" frequencies ω_i, the biggest of the bounds $\mu_{\underline{\Delta}_i}(M)$ computed at each frequency. Hence, the robust stability (RS) condition holds for each $\Delta(s)$ having norm smaller or equal to $\overline{\mu}^{-1}$. If real uncertainties δ_i are taken into account, the (RS) condition holds for every δ_i whose absolute value is smaller or equal to $\overline{\mu}^{-1}$. In this way it is possible to determine an allowable range of values for every single parameter.

The nominal system performances (NP) are tested by using the system stability μ-analysis and considering only the complex uncertainty fictive block Δ_f, as stated in Skogestad and Postlethwaite [51] and Zhou [69]. The quantity $\mu_{\underline{\Delta}}(N_{ew}(s))$ gives us information on the nominal system NP.
The perturbed system stability is tested by using the μ-analysis tools and taking into account only real uncertainty block Δ_r. If $\mu_{\underline{\Delta}}(N_{zv}(s)) < 1$, then the system robust stability (RS) is guaranteed, and robustness margins can be computed for each considered real uncertainty.
The system robust performance (RP) are studied by considering both real Δ_r and fictive Δ_f uncertainties, which are contained in $\Delta(s)$. Hence, the value of $\mu_{\underline{\Delta}}(N(s))$ gives information about the system robust stability (RP).

To summarize, assuming that the perturbation diagonal block $\Delta(s)$ satisfies $\|\Delta(s)\|_\infty < 1$ and that the required nominal performance corresponds to $\|T_{ew}(s)\|_\infty \leq 1$ for all considered perturbations, we have :

$$\text{NS} \quad \Leftrightarrow \quad N \textit{ is internally stable} \tag{5.52}$$

$$\text{NP} \quad \Leftrightarrow \quad \overline{\sigma}(N_{ew}) = \mu_{\underline{\Delta}_f}(N_{ew}) < 1, \ \forall \omega \textit{ and } \text{NS} \tag{5.53}$$

$$\text{RS} \quad \Leftrightarrow \quad \mu_{\underline{\Delta}_r}(N_{zv}) < 1, \ \forall \omega \textit{ and } \text{NS} \tag{5.54}$$

$$\text{RP} \quad \Leftrightarrow \quad \mu_{\underline{\Delta}}(N) < 1, \ \forall \omega, \ \Delta = \begin{bmatrix} \Delta_f & 0 \\ 0 & \Delta_r \end{bmatrix} \textit{ and } \text{NS} \tag{5.55}$$

Depending on the considered uncertainty (Δ_f, Δ_r or Δ), the μ-analysis allows to analyze nominal performance (NP), robust stability (RS) and robust performance (RP) of a perturbed nominal system.

5.7.2 Application to the DVD player servo mechanism

As we have seen in the previous section, μ-analysis is a powerful tool which allows to analyze stability and performance properties of a nominal system subjected to uncertainty.
In our case, we wish to compute confidence intervals for the different physical parameters (the moving lens mass M, the voice coil resistance R and inductance L, the elastic constant k, the mass spring dumping factor D and the electro-magnetic constant K_e) of the system, for which the robust stability and performance are guaranteed.
Hence, the first step consists in defining parametric uncertainties, then we determine the nominal system transfer matrix $N(s)$ and the structure of uncertainties, i.e.$\Delta_r(s)$. This allows to compute an upper bound of μ, corresponding to the considered problem (NS, RP or RP), which will give the allowable confidence intervals for every parametric uncertainty.

In fig.5.19 are shown the NΔ-structure block-schemes used to apply μ-analysis on the DVD player control design scheme, where u and e denotes the controller input and the system measured output respectively, $W = (\, w_1, \quad w_2 \,)^T$ are the exogenous inputs, $Z = (\, z_1, \quad z_2 \,)^T$ the controlled outputs, and u_Δ and y_Δ the uncertainty block inputs and outputs.

The weighting functions $W_p(s)$ and $W_u(s)$ are used to define frequency-domain templates corresponding to the desired closed-loop nominal performance, in a way that $\|N_{ew}\|_\infty < 1$ if the desired performance are achieved. We have chosen as weighting functions those used for H_∞ control design (see eq.(5.27) and (5.28) in section 5.4) and we have divided them by γ_∞, in order to let the desired performance of the closed-loop transfer matrix N_{ew} correspond to those of the obtained with the designed H_∞ controller.

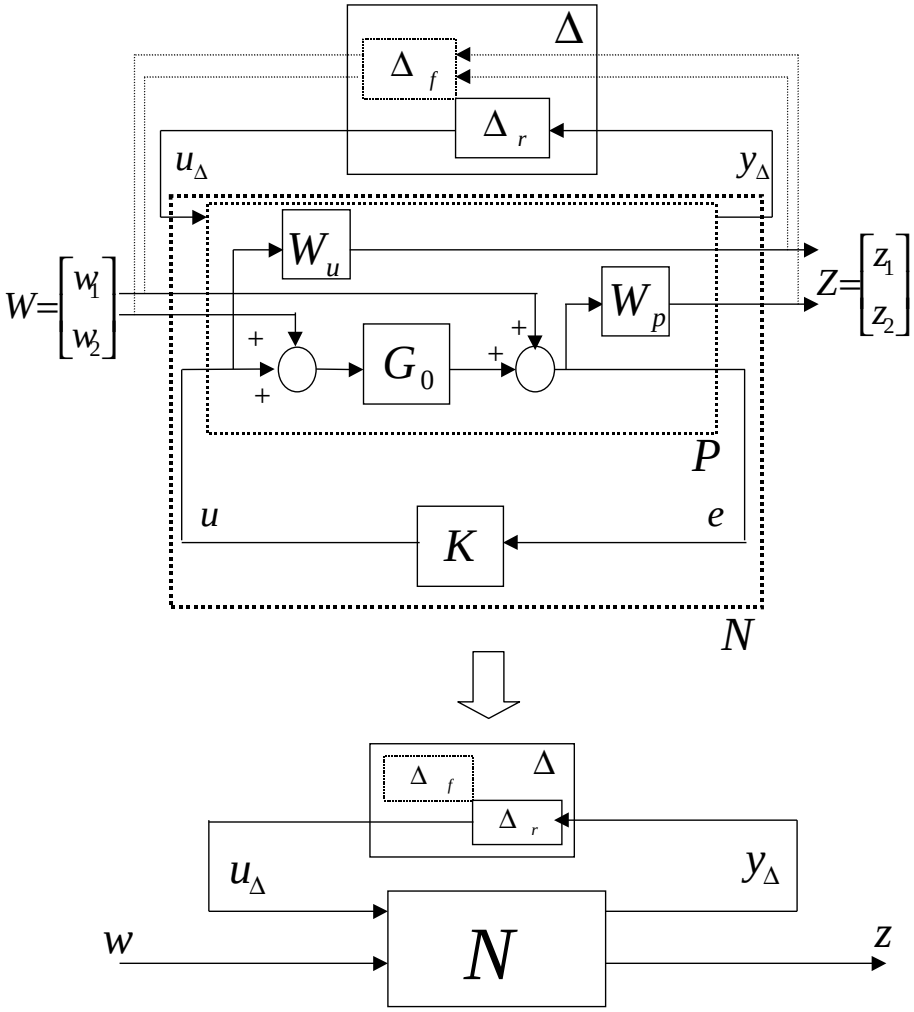

Figure 5.19: Block-schemes used to compute the NΔ-structure of the DVD player servo mechanism.

5.7.3 Choice and Representation of Uncertainty

In this work we consider only system parametric uncertainties, while in [51] and [69] it is shown how other types of uncertainties can be represented. According to table 5.1, the nominal model parametric uncertainties can be represented as follows :

$$\overline{R} = R(1 + p_R\delta_R),\ p_R = 15\%,\ \delta_R \in [-1; 1] \quad (5.56)$$
$$\overline{L} = L(1 + p_L\delta_L),\ p_L = 33\%,\ \delta_L \in [-1; 1] \quad (5.57)$$
$$\overline{M} = M(1 + p_M\delta_M),\ p_M = 10\%,\ \delta_M \in [-1; 1] \quad (5.58)$$
$$\overline{k} = k(1 + p_k\delta_k),\ p_k = 20\%,\ \delta_k \in [-1; 1] \quad (5.59)$$
$$\overline{K_e} = K_e(1 + p_{K_e}\delta_{K_e}),\ p_{K_e} = 26\%,\ \delta_{K_e} \in [-1; 1] \quad (5.60)$$
$$\overline{D} = D(1 + p_D\delta_D),\ p_D = 15\%,\ \delta_D \in [-1; 1] \quad (5.61)$$

where, for instance, $\overline{R}$ denotes the parameter real value, R its nominal value, p_R its percentage variation and δ_R a scalar factor representing real uncertainty.

The nominal model of the plant is obtained by considering the average value of physical parameters of three DVD-video players actuators used in industrial applications. Then its worst-case behavior is analyzed by taking into account the variation of each parameter in a specified range, as shown in table 5.1.

In the current application, the class of uncertainties we are interested in is real parametric uncertainties. In particular, the resistance R, the inductance L of the voice coil motor and the mass M of the objective lens are badly known. The first two are the most varying parameters, depending on the temperature and number of hours of the device life. The magnetic flux density K_e, the spring dump D and elastic constant k, will vary due to industrial manufacturing only.

Using ad hoc LFT representations of uncertainties we can pull out the parametric perturbations in a 6×6 diagonal block, as shown in Zhou [69] :

$$\Delta_r = \text{diag}\{\delta_R, \delta_L, \delta_M, \delta_k, \delta_{K_e}, \delta_D\} \quad (5.62)$$

The fictive complex uncertainty block Δ_f has dimension 2×2, since it connects the output to control $Z = (\, z_1, \quad z_2\,)^T$ to the system exogenous inputs $W = (\, w_1, \quad w_2\,)^T$, and it has the following form :

$$\Delta_f = \text{diag}\{\Delta_1\},\ \ \Delta_1 \in \mathbb{C}^{2\times 2} \quad (5.63)$$

To analyze the robust stability and performance properties of the designed control system by means of μ-analysis tools, we need to represent the perturbed plant model in a structured way. To this end, we have used a state-space representation of the whole nominal plant G_0, formed by nominal model of the objective lens actuator $H(s)$ and the optical gain g_{opt}, as explained in what follows.

We remind that the behavior of the objective lens actuator is described by the following equations (see eq.(3.28), (3.30) and (3.32) in section 3.7) :

$$\begin{cases} L\frac{\partial i(t)}{\partial t} + Ri(t) = v(t) - K_e\frac{\partial x(t)}{\partial t} \\ \\ f(t) = K_e i(t) \\ \\ M\frac{\partial^2 x(t)}{\partial t^2} + D\frac{\partial x(t)}{\partial t} + kx(t) = f(t) \end{cases} \tag{5.64}$$

If we assume that the state vector $\xi^T = (\,\xi_1, \quad \xi_2, \quad \xi_3\,)^T = (\,x, \quad i, \quad \dot{x}\,)^T$, that the input to the system $V = u$, that the output to the system $y = g_{opt}x$, the state-space representation of the plant nominal model is given by :

$$G_0 = \begin{cases} \begin{pmatrix} \dot{x} \\ \frac{di}{dt} \\ \ddot{x} \end{pmatrix} = \begin{pmatrix} 0 & 0 & 1 \\ 0 & -\frac{R}{L} & -\frac{K_e}{L} \\ -\frac{k}{M} & \frac{K_e}{M} & -\frac{D}{M} \end{pmatrix} \begin{pmatrix} x \\ i \\ \dot{x} \end{pmatrix} + \begin{pmatrix} 0 \\ \frac{1}{L} \\ 0 \end{pmatrix} V \\ \\ y = \begin{pmatrix} g_{opt} & 0 & 0 \end{pmatrix} \begin{pmatrix} x \\ i \\ \dot{x} \end{pmatrix} \end{cases} \tag{5.65}$$

which are represented by the block-scheme of fig.5.20.

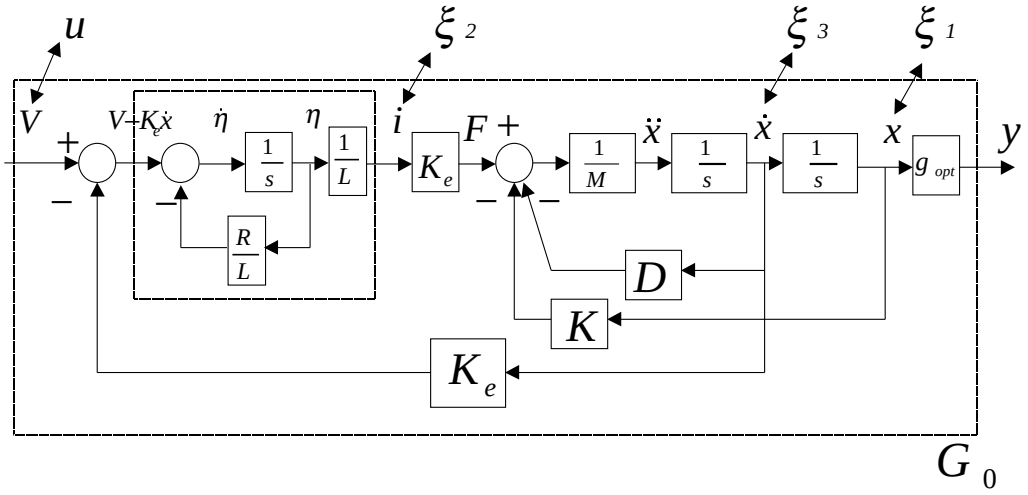

Figure 5.20: State-space representation of the plant nominal model, corresponding to eq.(5.65).

From eq.(5.56)-(5.61) and eq.(5.65) we derive :

$$\overline{L}\frac{di}{dt} = -\overline{R}i + V - \overline{K_e}\dot{x} \Rightarrow L\frac{di}{dt}(1 + p_L\delta_L) = -\overline{R}i + V - \overline{K_e}\dot{x} \qquad (5.66)$$

which gives :

$$L\frac{di}{dt} = -\overline{R}i + V - \overline{K_e}\dot{x} - p_L L\delta_L\frac{di}{dt} = -\overline{R}i + V - \overline{K_e}\dot{x} - p_L y_{\Delta_L} \qquad (5.67)$$

Similarly we compute :

$$\overline{M}\ddot{x} = -\overline{k}x + \overline{K_e}i - \overline{D}\dot{x} \Rightarrow M\ddot{x}(1 + p_M\delta_M) = -\overline{k}x + \overline{K_e}i - \overline{D}\dot{x} \qquad (5.68)$$

which gives :

$$M\ddot{x} = -\overline{k}x + \overline{K_e}i - \overline{D}\dot{x} - p_M M\delta_M\ddot{x} = -\overline{k}x + \overline{K_e}i - \overline{D}\dot{x} - p_M y_{\Delta_M} \qquad (5.69)$$

If we assume that :

- The quantities α_1 and α_2 are :

$$\alpha_1 = -\overline{R}i + V - \overline{K_e}\dot{x} \quad and \quad \alpha_2 = -\overline{k}x + \overline{K_e}i - \overline{D}\dot{x} \qquad (5.70)$$

- The uncertainty blocks outputs are :

$$y_{\Delta_L} = L\delta_L\frac{di}{dt} \quad and \quad y_{\Delta_M} = M\delta_M\ddot{x} \qquad (5.71)$$

- The uncertainty blocks inputs are :

$$u_{\Delta_L} = \alpha_1 - \frac{p_L}{L}y_{\Delta_L} \quad and \quad u_{\Delta_M} = \alpha_2 - p_M y_{\Delta_M} \qquad (5.72)$$

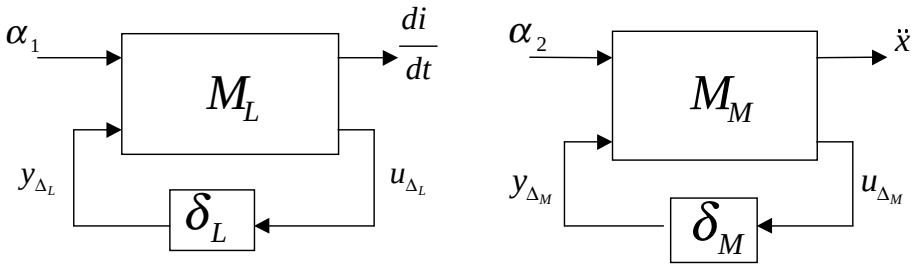

Figure 5.21: Parametric uncertainties block-scheme, corresponding to eq.(5.67) and (5.69).

Then, the real parameters with their average values and uncertainties can be represented as shown in fig.5.21, where :

$$M_L = \begin{pmatrix} \frac{1}{L} & -\frac{p_L}{L} \\ 1 & -p_L \end{pmatrix} \quad and \quad M_M = \begin{pmatrix} \frac{1}{M} & -\frac{p_M}{M} \\ 1 & -p_M \end{pmatrix} \tag{5.73}$$

From eq.(5.70) we have for α_1 :

$$\alpha_1 = -\overline{R}i + V - \overline{K_e}\dot{x} = (V - Ri - K_e\dot{x}) + \delta_R(-Rp_Ri) + \delta_{K_e}(-K_ep_{K_e}\dot{x}) \tag{5.74}$$

which gives :

$$\alpha_1 = (V - Ri - K_e\dot{x}) - y_{\delta_R} - y_{\delta_{K_e}} \tag{5.75}$$

and for α_2

$$\alpha_2 = -\overline{k}x - \overline{K_e}i + \overline{D}\dot{x} = (-kx + K_ei - D\dot{x}) + \delta_k(-kp_kx) + \delta_{K_e}(-K_ep_{K_e}i) + \delta_D(-Dp_D\dot{x}) \tag{5.76}$$

which gives :

$$\alpha_2 = (-kx + K_ei - D\dot{x}) - y_{\delta_k} - y_{\delta_{K_e}} + y_{\delta_D} \tag{5.77}$$

By substituting eq.(5.75) in eq.(5.67) and eq.(5.77) in eq.(5.69) we finally obtain :

$$\frac{di}{dt} = \frac{1}{L}(-Ri - K_e\dot{x} + V) - \frac{y_{\Delta_R}}{L} + \frac{y_{\Delta_L}}{L}p_L - \frac{y_{\Delta_{K_e}}}{L} \tag{5.78}$$

and

$$\ddot{x} = \frac{1}{M}(-kx + K_ei - D\dot{x}) - \frac{y_{\Delta_k}}{M} + \frac{y_{\Delta_{K_e}}}{M} - \frac{y_{\Delta_D}}{M} - p_My_{\Delta_M} \tag{5.79}$$

Finally, considering eq.(5.65), (5.72), (5.75), (5.77), (5.78) and (5.79) we obtain the transfer matrix N, which links the inputs W and u_Δ to the outputs Z and y_Δ (see fig.5.19), by using the following equations :

$$N = \begin{cases} \dot{x} = \dot{x} \\ \frac{di}{dt} = \frac{1}{L}(-Ri - K_e\dot{x} + V) - \frac{y_{\Delta_R}}{L} + \frac{y_{\Delta_L}}{L}p_L - \frac{y_{\Delta_{K_e}}}{L} \\ \ddot{x} = \frac{1}{M}(-kx + K_e i - D\dot{x}) - \frac{y_{\Delta_k}}{M} + \frac{y_{\Delta_{K_e}}}{M} - \frac{y_{\Delta_D}}{M} - p_M y_{\Delta_M} \\ u_{\Delta_R} = -Rp_R i \\ u_{\Delta_L} = (V - Ri - K_e\dot{x}) - y_{\Delta_R} - y_{\Delta_L}p_L - y_{\Delta_{K_e}} \\ u_{\Delta_M} = (-kx + K_e i - D\dot{x}) - p_M y_{\Delta_M} - y_{\Delta_k} - y_{\Delta_{K_e}} - y_{\Delta_D} \\ u_{\Delta_k} = -kp_k x \\ u_{\Delta_{K_e}} = K_e p_{K_e} i - K_e p_{K_e}\dot{x} \\ u_{\Delta_D} = -Dp_D\dot{x} \\ z_1 = V \\ z_2 = g_{opt}x + w_1 \\ e = -g_{opt}x - w_1 \end{cases} \tag{5.80}$$

The system parametric uncertainties are grouped in an uncertainty block $\Delta_r = diag\{\delta_R, \delta_L, \delta_M, \delta_k, \delta_{K_e}, \delta_D\}$, which is separated from N. By describing the output :

$$y_{\Delta_r}^T = (\, y_{\Delta_R}, y_{\Delta_L}, y_{\Delta_M}, y_{\Delta_k}, y_{\Delta_{K_e}}, y_{\Delta_D}\,)^T$$

as function of the input :

$$u_{\Delta_r}^T = (\, u_{\Delta_R}, u_{\Delta_L}, u_{\Delta_M}, u_{\Delta_k}, u_{\Delta_{K_e}}, u_{\Delta_D}\,)^T$$

we obtain a transfer matrix N_{11}, which is used to compute the measure of $\mu_{\underline{\Delta_r}}(N_{11})$. This value allows to evaluate the system robust stability (RS) with respect to parametric uncertainties. We group the matrices Δ_r and Δ_f into a matrix $\Delta = diag\{\Delta_r, \Delta_f\}$, and the set $\underline{\Delta}$ of complex matrices having the same structure as Δ is defined by :

$$\underline{\Delta} = diag\{\delta_R, \delta_L, \delta_M, \delta_k, \delta_{K_e}, \delta_D\, \Delta_1\} \quad \Delta_1 \in \mathbb{C}^{2\times 2}, \quad \delta_i \in \mathbb{R} \tag{5.81}$$

The system robust performance (RP) can be evaluated by computing the upper bound of the measure of $\mu(N)$, with respect to $\underline{\Delta}$.

5.7.4 RS and RP analysis applied to the H_∞ controller

In this section we present, for both the actual implemented and the designed reduced-order H_∞ controllers, results obtained when nominal performance (NP), robust stability (RS) and robust performance (RP) problems are analyzed. We consider the parametric uncertainties presented in table 5.1.

1. **NP Problem**

   The NP problem does not depend on the chosen parametric uncertainties. Upper and a lower bounds of μ for NP are given on fig.(5.22). Since $\overline{\sigma}(N_{ew}) = \mu_{\underline{\Delta}_f}(N_{ew}) = 0.1788 < 1$, for the designed H_∞ controller, and $\overline{\sigma}(N_{ew}) = \mu_{\underline{\Delta}_f}(N_{ew}) = 0.4727 < 1$ for the actual implemented controller, from eq.(5.53) it can easily seen that nominal performances are achieved by both solutions. It appears also that at high frequencies the designed controller guarantees better nominal performances than the actual one.

2. **RS Problem**

   Upper bounds of μ for RS are given in fig.(5.23). As $\mu_{\underline{\Delta}_r}(N_{zv}) = 0.60 < 1$, for both controllers, from eq.(5.54) RS is satisfied. Hence the actual implemented and the designed H_∞ controllers keep stability for the following larger parametric uncertainties, i.e :

   $R = 4.83\Omega \pm (15/0.60) = 4.83\Omega \pm 24.99\%$
   $L = 12\mu H \pm (33/0.60) = 12\mu H \pm 54.99\%$
   $M = 0.33g \pm (10/0.60) = 0.33g \pm 16.66\%$
   $k = 45.350N/m \pm (20/0.60) = 45.350N/m \pm 33.33\%$
   $K_e = 0.1212Wb/m \pm (26/0.60) = 0.1212Wb/m \pm 43.33\%$
   $D = 0.0160Ns/m \pm (15/0.60) = 0.0160Wb/m \pm 25\%$

3. **RP Problem**

   Upper and a lower bounds of μ for RP are given on fig.(5.24). As $\mu_{\underline{\Delta}}(N) = 0.6016 < 1$, for both controllers from eq.(5.55) we can conclude on robust performance (RP) in this uncertainty case.
   This also means that larger uncertainties may not deteriorate the system closed-loop performance.

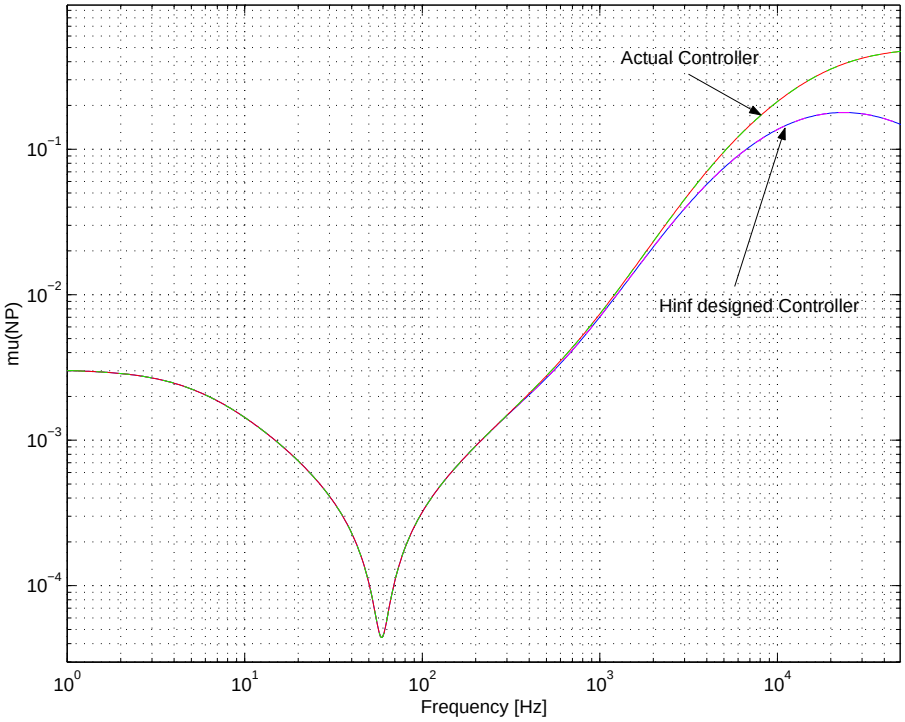

Figure 5.22: Upper (solid line) and lower (dashed line) bounds for NP obtained for the designed H_∞ (blue and magenta curves) and for the actual implemented controllers (red and green curves).

In fig.5.25 we show the frequency plot of the open-loop system, when the physical parameters vary in the range of values presented in table 5.1.
These results show that the synthesized control scheme remains stable and ensures good performance for large variations of the DVD-drive parameters.

5.8 Conclusions

In this chapter we have presented a model-based control design methodology applied to an industrial DVD-video player, to enhance track following and improve control performances with respect to different behaviors and manufacturing tolerances of optical pick-ups. By minimizing the H_∞ norm of some relevant closed-loop transfer function, a robust SISO regulator is designed to control the linear displacement of the optical head actuator along the disc radius, and to reduce the effect of external disturbances, like eccentricity and vertical deviations. Control order reduction is performed to make the digital implementation feasible on the industrial benchmark.

An uncertainty model set, based on a parametric description and norm-bounded real perturbations, is considered to analyze how the variations of the plant physical parameters influence performances and robustness of the

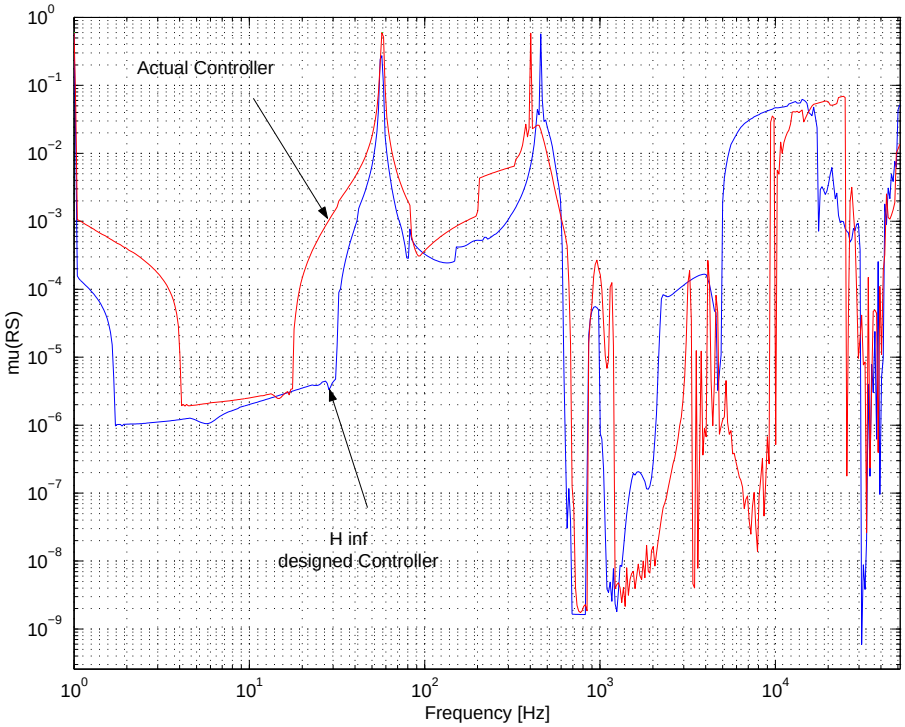

Figure 5.23: Upper bound for RS obtained for the designed H_∞ (blue curve) and for the actual implemented controllers (red curve).

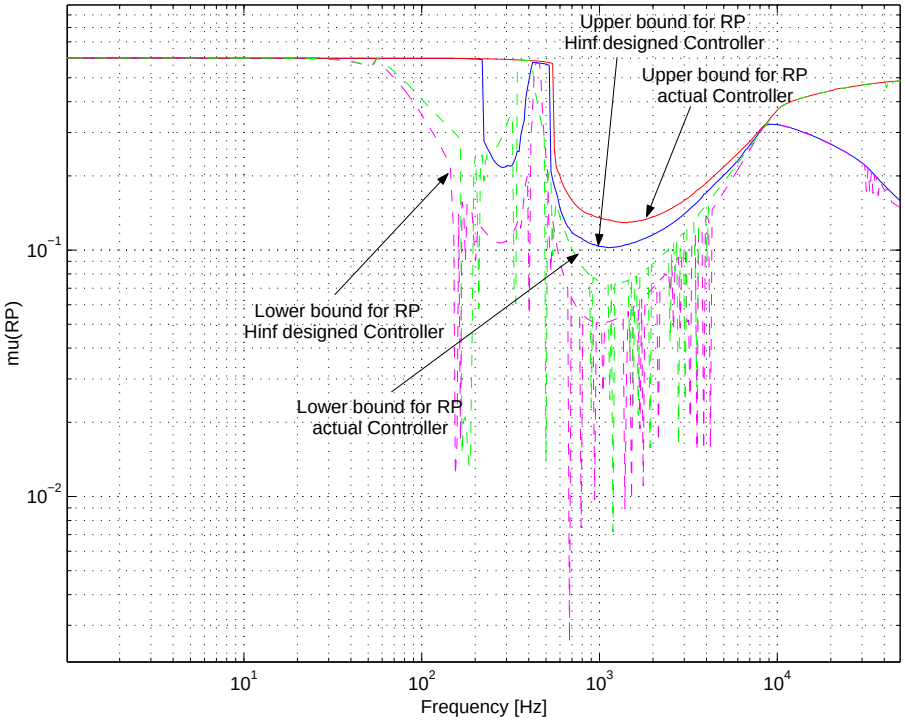

Figure 5.24: Upper (solid line) and lower (dashed line) bounds for RP obtained for the designed H_∞ (blue and magenta curves) and for the actual implemented controllers (red and green curves).

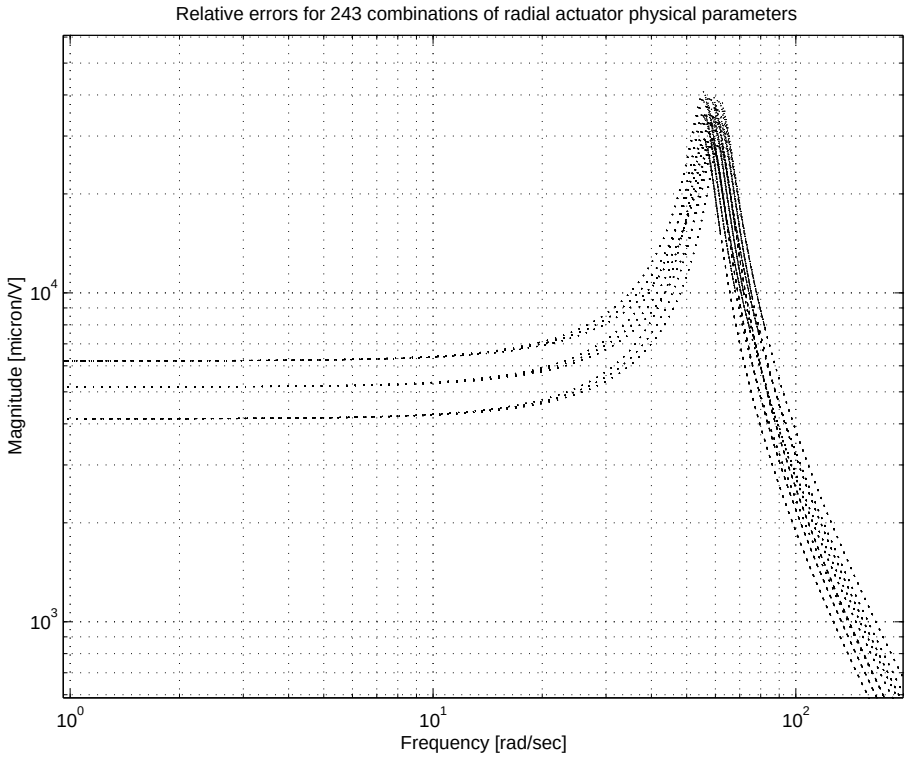

Figure 5.25: Open-loop system under parametric uncertainties.

achieved solution.
First, an upper-bound of the plant multiplicative uncertainties is computed and, by applying the small gain theorem, it is verified that (RS) and (RP) are achieved for large variation of plant physical parameters. Nevertheless, this approach leads to conservative results, either because it takes into account the plant worst-case uncertainty, either because it does not allow to determine which physical parameter (varying in a given interval of admissible values) can be "critical" for the control system stability and performance achievement.

Hence, structured parametric uncertainties and real perturbations, are considered and μ-analysis is applied. Simulation and experimental results show that the implemented H_∞ controller remains stable for large parameters uncertainty, and that performance specifications are achieved in a large uncertainty case.

In this chapter, we have pointed out the importance of the interaction between the design of the DVD-drive, and the synthesis of the control system. The pick-up design should indeed take into account the robustness and performance of the usually considered controllers, to reduce the global time duration of any OPU design and guarantee nominal and robust performance. This methodology can be applied to other families of DVD players.

Chapter 6

Conclusions and Perspectives

6.1 Review

The main motivation for the research reported in this thesis is to apply advanced automatic control methodology, in order to develop plant identification and model-based control design for an industrial optical disc drive system.

The aim of this work is twofold. Firstly, since the limitations of present feedback control design technics are mainly determined by the lack of model accuracy, an identification procedure is performed by measuring the frequency responses of the closed-loop transfer functions, for constructing a plant nominal model, as presented in Chapter 4.
Secondly, tough specifications on tracking performance in optical disc drive systems require an enhanced strategy for designing feedback controllers able to guarantee high performance and robustness properties.
As measure of performance, we choose the ability of the controller to guarantee correct track following under the presence of periodic disturbances (eccentricity and vertical deviation). For testing robustness, after the design, we evaluate if closed-loop stability hold when system parametric uncertainties are considered.

Our problem statement hence is to show to what extent a "combined" plant identification and model-based control design procedure can improve performance and robustness of an industrial control system, which is usually tuned by trial and errors techniques.

The approach adopted to tackle our problem is due to the following two observations :

- Actual feedback control of optical disc drives is hold up by the fact that models used for the design are not sufficiently accurate to comply with tough performance specifications and robustness requirements. This is particularly true for DVD discs servo system, for whom technical specifications establish stricter requirements than for CD discs.
- Available system identification techniques provide very accurate but complex models of optical disc drive actuators, resulting in controllers that are too complex to be implemented on industrial solutions.

A low order nominal model of the plant is used for control design, to keep the control order limited, during the subsequently synthesis. Robustness with respect to system parametric uncertainty is analyzed by taking into account a model uncertainty set for analysis of performance achieved with the designed controller. Performances are evaluated in terms of the magnitude of the closed-loop transfer functions, which give indications about disturbance attenuation, control reaction speed , power consumption and reproducible noise, as discussed in Chapter 5.

6.2 Contributions of this research

In the context of the outlined strategy, for a restricted complexity control design and an a posteriori robustness analysis, the following points have been elaborated in this work :

- As established by the *C.I.F.R.E.* (*Contrat Industriel de Formation et Recherche*) PhD agreement, a development activity has been accomplished at the beginning of this thesis. To let the author acquire practical experience with the real system and its associated software, the digital filters, used to realize the spot positioning control loops, have been implemented in a dedicated DSP. This part of the work has allowed to evaluate performance and robustness of the original industrial solution, as well as to understand and handle implementation problems. We have thus carried out the laser spot fine displacement control systems, used in DVD-video players already present on the consumer market (*PIONEER DV350-DV351* and series).
- Modelling physically the radial actuator of two industrial DVD-video player servo mechanism is found to be not insufficiently accurate to

provide a reliable model useful for high performance control design. The real system has been identified to verify if the computed model represent accurately the plant dynamics and to estimate the optical gain.

- Plant identification is performed by measuring with a Dynamic Signal Analyzer the frequency response of the closed-loop transfer functions, for two commercial radial DVD servo actuator (*PIONEER M1* and *SANYO DV33*). Experimental results, obtained by comparing the measured plant frequency response with the physical model characteristics, show that the plant dynamics are described satisfactory by a third order transfer function. The optical gain is then estimated imposing that the amplitude open-loop characteristic has unitary value at the desired closed-loop bandwidth.

- Performance analysis of the actual industrial solution shows that the implemented controller allows to achieve both the desired closed-loop bandwidth (for a fixed over-speed factor N) and rise time, established in [59]. It also guarantees disturbance rejection, from the disc rotational frequency up to higher frequencies. Nevertheless, it appears from measurements that the desired low frequency attenuation level is not achieved (since the DSA does not provide a sufficient input-output signals SNR in this region) and that high-frequency noise may additionally corrupt acquisitions.

- Robustness indicators confirm that the actual control scheme is robust against model parameters variations, even though experiments reveal that it does not guarantee robustness with respect to discs having different nominal eccentricity. This is due to the fact that variations of the radial disc deviations have not been taken into account during the plant modelling step. Coupling phenomena existing between the two control loops point out that, in the frequency range of interest for control, the dynamic interaction between both focus and radial loops remains relatively weak.

- An H_∞ norm-based control design procedure is proposed for construction of a low-complexity controller, able to achieve an enhanced track following performance and periodic disturbance rejection. Application to the experimental DVD-video player has shown that :

  - the identified plant model enables a reliable and useful evaluation of robust stability and performance properties in terms of magni-

tude bounds on the closed-loop transfer functions, provided that the order of the computed controller is reduced and that it not differ too much from the actual implemented solution.

- a critical issue in designing an enhanced robust controller is represented by the choice of the performance weighting functions used to solve the H_∞ sub-optimal control problem. Due to industrial constraints, low-order weighting functions are chosen, to avoid that the resulting controller has unacceptably high order.
- the advantage of solving a mixed-sensitivity H_∞ problem is that using only two performance weights, all the system closed-loop frequency responses have to lie below pre-specified templates, in order to achieve performance and robustness objectives.
- the synthesized controller guarantees nominal stability of the loop and performance specifications are met. As difference with the actual controller, the new design allows to limit the actuator efforts up to frequencies where the measurement noise becomes relevant. It also provides an enhanced low-frequency disturbance attenuation on the position error signal.

- Robust stability and performance, obtained with the new controller are analyzed, when system parametric uncertainty and norm-bounded real perturbations are considered. Two methodologies for evaluating the influence of parametric uncertainty on the real system, have been applied as follows :

  - An uncertainty model set is build by varying parameters of an "average" model inside a given range of values. Hence, the system worst-case behavior is analyzed by mean of a weighting function which provides in the frequency domain an upper bound on the system uncertainty including the set of all possible plant models. Results show that the closed-loop system is stable and satisfies the performance specifications, for all perturbed plants about the nominal model up to the worst-case model uncertainty.
  - To compute confidence intervals of the DVD drive physical parameters, for which the closed-loop robust stability and performance are guaranteed, μ-analysis is applied by using the system structured singular value. The advantage of using this approach is that it takes into account the closed-loop matrix structure, giving a

less conservative idea of the tolerance intervals than the uncertainty frequency-domain representation method. Experimental results show that the designed control scheme remains stable for large parameters uncertainty, and that performance specifications are achieved in a large uncertainty case.

These methodologies point out the importance of the interaction between the DVD-drive design and the control system synthesis.

6.3 Perspectives

This research has shown that model-based control design applied to a physical system requires the understanding of model uncertainty for evaluating the system robust performance and the need of a systematic methodology useful to perform robust controllers design. We have considered in this work uncertainty due to inaccurate modelling of an optical disc drive electromechanical actuator.
Hovewer the system tracking performance is also determined by the limited accuracy of knowledge of the controller which operates in the feedback loop. Usage of data-based and error bound models in the control synthesis step should therefore be extended to modelling of system and controller.

Another phenomenon that has received not attention in this work, but which is nevertheless important for evaluating system robustness with respect to discs having different nominal eccentricity, is the influence that the variation of disc radial deviations may have during plant modelling.
Indeed, it is worth to give attention to whether plant uncertainties due to disc eccentricity are informative with respect to the nature and extent of periodic disturbances which affect the feedback system. Moreover the availability of accurate models that account for such disturbances, in a model-based control design approach, may contribute to an enhanced tracking performance. This aspect can be relevant for designing high-rotational speed robust controllers, for whom a higher target bandwidth may lead to an increasing effect of disturbances on the position error signal.

Finally, a problem often encountered in consumer optical disc drives mass production is the variability of dynamical behavior, due to variation environmental conditions and system aging. There is a clear need for models that accurately describe this variable dynamical behavior for a *large* number

of systems in view of an enhanced robust tracking performance and disturbance rejection control design.

In this work we have presented a simple approach useful to derive a reliable model uncertainty set based on technical specifications of two industrial DVD-video radial actuators. However, the utility of this approach in view of a *large* number of pick-ups demand a more detailed analysis of parametric uncertainty acting on DVD-video players, and it requires a thorough investigation of alternative modelling techniques.

Appendix A

Modelling the error signals generation

A.1 Introduction

For applications such as the reading or writing digital information from or on an optical medium as the DVD, the need for a real-time control of the position of the focus objective is imperative. As exposed in section 3.5, in order to retrieve the data correctly, the laser beam must be focused on the data layer surface of the disk, and must follow the track.
In the literature many methods have been developed to obtain analytical or numerical models of the focus and tracking error signal generation, as in Bouwhuis et al. [4], Braat et al. [6], Isaloilović [34], Pohlmann [44], and Stan [54]. Particularly, in focus search procedures, one very important element is the dependence between the focus error signal e_{F} and the vertical disk displacement Δz, which is a non-linear function, known under the name S-curve. In radial track seek procedures, the DPD (Differential Phase Detection) method is the most widely used for obtaining a non-linear dependence between the tracking error signal e_{R} and the radial disk displacement Δx in DVD players.
However, despite their practical importance, at present, no simple analytical or numerical models describing these dependencies are available for industrial applications, since only rough approximations of these functions are used. Indeed, the development of an analytical or numerical models involves the application of a large amount of optical theory and heavy computations. Our aim is to shortly present two methodologies useful for obtaining models for focus and radial error signals generation, by means of basic optical principles. More details can be found in Hnilička et al. [26] and [28].

A.2 Modelling the Focus error signal generation

The focus error signal e_{F} is obtained when some asymmetry is present in the optical path. Numerous optical properties have been used to generate focus error signal from small displacement Δz in CD players, as in Bouwhuis et al. [4] and Stan [54], but for DVD optical pick-ups, the astigmatic method is the most widely used.
In section 2.6 we have already described a simplified arrangement of the optical pick-up unit (see fig.2.9), and in section 2.6.2 we have illustrated the astigmatism method used, in a DVD player, to generate the focus S-curve which describes the dependency of e_{F} from Δz (see fig.2.13 and fig.2.14).
Hence, our aim here is to present how to compute analytical or numerical models $\hat{e}_{\mathrm{F}}(\Delta z, \theta)$ of this non-linear characteristic, and to identify the unknown or hardly measurable parameters θ characterizing them.
A detailed model description based on the opto-geometrical analysis is described in [28]. We remind only that the main idea consists in assuming that, for simplicity, the whole optical system is formed by two subsystems having thin lenses. The separation of the whole optical system in the two orthogonal planes yz and xz allows to use the theory of a system formed by two centered thin lenses, as described in Born and Wolf [3]. Figs. A.1 and A.2 show the separated optical system with thin lens approximation at planes yz and xz where :

- f_{obj}: objective focal length of the objective lens
- z_{obj}: distance between the disk and the objective lens
- d_3: distance between the objective lens and the collimator
- d_4: distance between the collimator and the cylindrical lens
- z_{det}: distance between the collimator and the photo-detector
- z_1: distance between the collimator and the second focal line
- z_2: distance between the collimator and the first focal line
- f_{L1}: distance between the collimator and the first focal line if disk is in focus
- f_{L2}: distance between the collimator and the second focal line if disk is in focus

Without loss of generality, we consider a diverging cylindrical lens, since it is the more used in DVD players. Fig. A.3 illustrates the laser beam, the detector position, the laser spot shape on photo-detector when the disk is

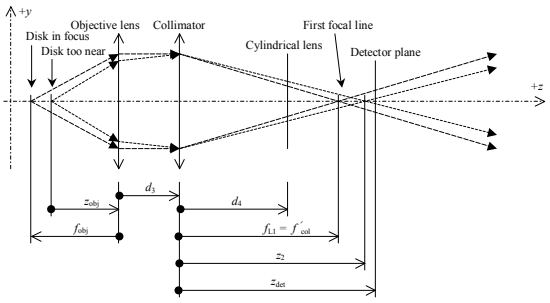

Figure A.1: Arrangement in yz plane. The diverging cylindrical lens is approximated by air.

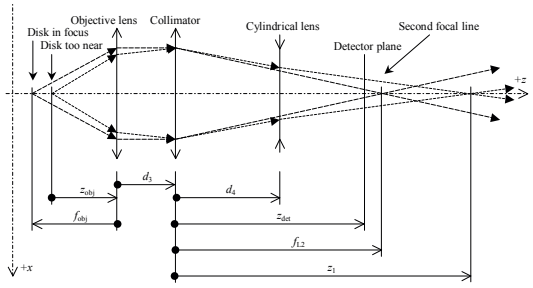

Figure A.2: Arrangement in xz plane. The diverging cylindrical lens is approximated by diverging thin lens.

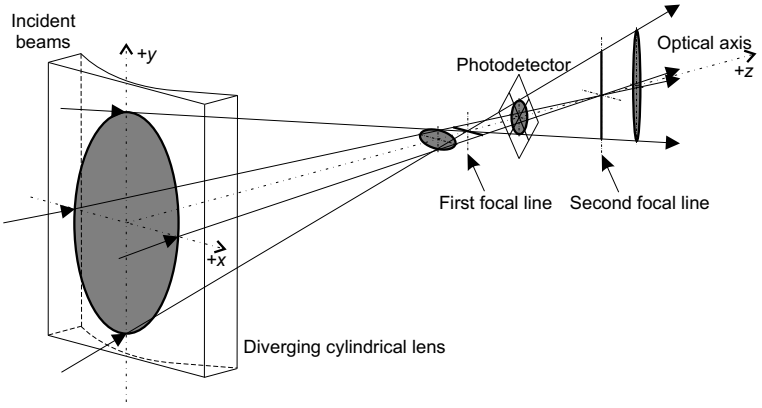

Figure A.3: The marginal rays of the cylindrical diverging lens if light source (disk) is in focus.

in focus. There are two distances z_1, z_2 in the image space of collimator where the focal lines could be found, (see figs. A.1 and A.2). Therefore, the focal lines could be defined as light lines that can be observed on the screen in the image space of the cylindrical lens. The knowledge of the focal lines positions $z_1(z_{\text{obj}})$, $z_2(z_{\text{obj}})$ is the first information needed to compute the S-curve model, because it allow to establish the size of the laser spot on the photo-detector (see figs. A.1 and A.2).
Firstly, a dependence between distance z_2 and z_{obj} is derived in yz plane. Fig. A.4 shows a solution in yz plane where the notation has the following meaning :

- $F'_{\text{obj}}, F_{\text{col}}$: focal points

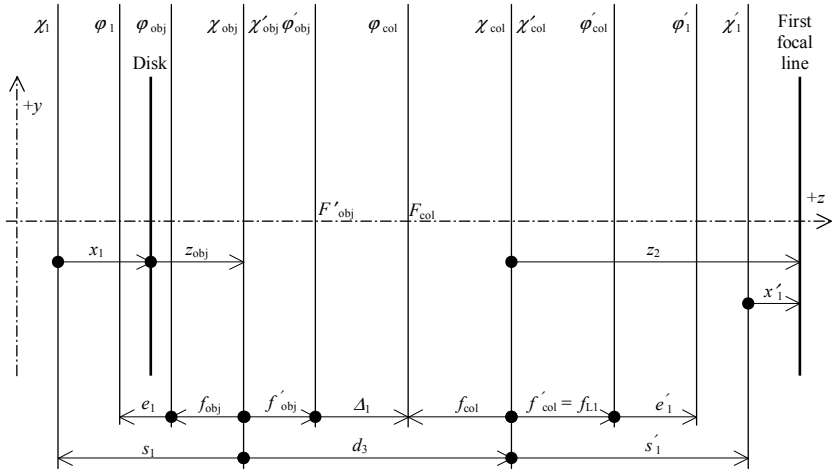

Figure A.4: System formed by two centered thin lens in yz plane.

- $\chi_{\text{obj}}, \chi'_{\text{obj}}$: unit planes of the objective lens
- $\chi_{\text{col}}, \chi'_{\text{col}}$: unit planes of the collimator
- χ_1, χ'_1: unit planes of the *resulting* lens
- $\varphi_{\text{obj}}, \varphi'_{\text{obj}}$: focal planes of the objective lens
- $\varphi_{\text{col}}, \varphi'_{\text{col}}$: focal planes of the collimator
- φ_1, φ'_1: focal planes of the *resulting* lens
- Δ_1 : optical interval
- e_1: distance of the *resulting* focal plane φ_1 from objective focal plane φ_{obj} of the first lens
- e'_1: distance of the *resulting* focal plane φ'_1 from image focal plane φ'_{col} of the second lens
- s_1: distance of the *resulting* first unit (principal) plane χ_1 from first unit plane χ_{obj} of the first lens
- s'_1: distance of the *resulting* second unit (principal) plane χ'_1 from last unit plane χ'_{col} of the second lens
- x_1, x'_1: objective and image distance of the "resulting" lens
- f'_1: *resulting* objective focal length in yz plane

Let assume the objective lens focal length $f'_{\text{obj}} = -f_{\text{obj}}$ and the collimator focal length $f_{\text{col}} = -f'_{\text{col}} = f_{\text{L1}}$. Then, the model parameters are given by :

$$\Delta_1 = d_3 - f'_{\text{obj}} + f_{\text{col}} = d_3 + f_{\text{obj}} - f'_{\text{col}}, \tag{A.1}$$

$$s_1 = \frac{d_3 f'_{\text{obj}}}{f'_{\text{obj}} + f'_{\text{col}} - d_3}, \tag{A.2}$$

$$s'_1 = -\frac{d_3 f'_{\text{col}}}{f'_{\text{obj}} + f'_{\text{col}} - d_3}, \tag{A.3}$$

$$e_1 = -\frac{{f'_{\text{obj}}}^2}{\Delta_1}, \tag{A.4}$$

$$e'_1 = \frac{{f'_{\text{col}}}^2}{\Delta_1}, \tag{A.5}$$

$$f'_1 = -\frac{f'_{\text{obj}} f'_{\text{col}}}{\Delta_1}. \tag{A.6}$$

The Lensmaker's equation [3] can be used :

$$\frac{1}{-s'_1 + z_2} - \frac{1}{-s_1 - z_{\text{obj}}} = \frac{1}{f'_1}. \tag{A.7}$$

and the dependence between distances z_2 and z_{obj} after modification of eq.(A.7) is given by :

$$\boxed{z_2 = \frac{1}{\frac{1}{f'_1} + \frac{1}{-s_1 - z_{\text{obj}}}} + s'_1} \tag{A.8}$$

Fig.A.5 shows the solution in xz plane (a dependence between distance z_1 and z_{obj}) [28] where the remained variables have the following meaning :

- f_{cyl}: objective focal length of the cylindrical lens
- f'_{cyl}: image focal length of the cylindrical lens
- F'_{cyl}, F'_1: focal points
- v_2: distance between two lenses
- Δ_2: optical interval
- $\chi_{\text{cyl}}, \chi'_{\text{cyl}}, \chi_2, \chi'_2$: unit (principal) planes of lenses
- $\varphi_{\text{cyl}}, \varphi'_{\text{cyl}}, \varphi_2, \varphi'_2$: focal planes of lenses

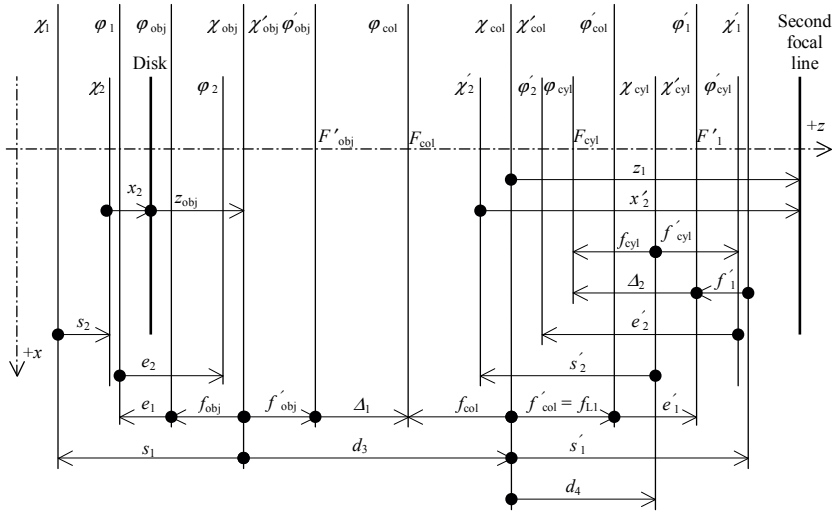

Figure A.5: System formed by two centered thin lens in xz plane.

- e_2: distance of the *resulting* focal plane φ_2 from the objective focal plane φ_1 of the first lens
- e'_2: distance of the *resulting* focal plane φ'_2 from image focal plane φ'_{cyl} of the second lens
- s_2: distance of the *resulting* first unit (principal) plane χ_2 from the first unit plane χ_1 of the first lens
- s'_2: distance of the *resulting* second unit (principal) plane χ'_2 from last unit plane χ'_{cyl} of the second lens
- x_2, x'_2: objective and image distance of the "resulting" lens approximation
- f'_2: "resulting" objective focal length in xz plane

The focal length f'_{cyl} is calculated when the disk is in focus, by the following equation :

$$\text{if } (z_{\text{obj}} = -f_{\text{obj}}) \text{ then } (z_1 = f_{\text{L2}}), \tag{A.9}$$

Let $f'_{\text{cyl}} = -f_{\text{cyl}}$, then :

$$\Delta_2 = -e'_1 - f'_{\text{col}} + d_4 + f_{\text{cyl}} = -e'_1 - f'_{\text{col}} + d_4 - f'_{\text{cyl}}, \tag{A.10}$$

$$v_2 = \Delta_2 + f'_1 - f_{\text{cyl}} = -e'_1 - f'_{\text{col}} + d_4 + f'_1, \tag{A.11}$$

$$s_2 = \frac{v_2 f'_1}{f'_1 + f'_{\text{cyl}} - v_2}, \tag{A.12}$$

$$s'_2 = -\frac{v_2 f'_{\text{cyl}}}{f'_1 + f'_{\text{cyl}} - v_2}, \tag{A.13}$$

$$e_2 = -\frac{{f'_1}^2}{\Delta_2}, \tag{A.14}$$

$$e'_2 = \frac{{f'_{\text{cyl}}}^2}{\Delta_2}, \tag{A.15}$$

$$f'_2 = -\frac{f'_1 f'_{\text{cyl}}}{\Delta_2}. \tag{A.16}$$

The Lensmaker's equation [3] gives :

$$\frac{1}{x'_2} - \frac{1}{x_2} = \frac{1}{f'_2}. \tag{A.17}$$

and if

$$\frac{1}{-s'_2 - d_4 + z_1} - \frac{1}{-s_2 - s_1 - z_{\text{obj}}} = \frac{1}{f'_2}. \tag{A.18}$$

the dependence between the distance z_1 and z_{obj} can be obtained from eq.(A.18), thus :

$$\boxed{z_1 = \frac{1}{\frac{1}{f'_2} + \frac{1}{-s_2 - s_1 - z_{\text{obj}}}} + s'_2 + d_4.} \tag{A.19}$$

Eq.(A.9) is used to derive the unknown variable f'_{cyl} by substitution to the eq.(A.18) :

$$\frac{1}{-s'_2 - d_4 + f_{\text{L2}}} - \frac{1}{-s_2 - s_1 - f'_{\text{obj}}} - \frac{1}{f'_2} = 0. \tag{A.20}$$

There is an explicit solution of eq.(A.20) for the quantity f'_{cyl}. In the xz plane the approximation by the diverging thin lens is used because we have assumed diverging cylindrical lenses and their focal length of f'_{cyl} is negative. It means that $f'_{\text{cyl}} < 0$, which allows to derive roots of eq.(A.20). Thus, f'_{cyl} is given by :

$$\boxed{f'_{\text{cyl}} = \frac{f_{\text{L1}} f_{\text{L2}} - f_{\text{L1}} d_4 - f_{\text{L2}} d_4 + d_4^2}{f_{\text{L1}} - f_{\text{L2}}}.} \tag{A.21}$$

The determination of the reflected light spot shape on the photo-detector allows to obtain the relation linking the half-axes sizes of the elliptic laser spot a, b and the focal lines distances z_1, z_2, respectively.

Usually it is not evident to define the light intensity distribution on the photo-detector analytically, thus rough approximations have been used, like the *uniform* and the *paraboloid* light intensity distribution (in the case of analytical models) or the *Gaussian* intensity distribution (in case of numerical model). This avoid to assume more complicated light distributions, such as those described by Rayleigh-Sommerfeld and Kirchhoff diffraction integrals (see Stamnes [52]).

In what follows we shortly present some simulation and experimental result, obtained during focus search procedure. A complete description of analytical and numerical models of the light intensity distribution on the photo-detector can be found in Hnilička et al. [28].

Fig.A.6 shows the effect of varying Gaussian intensity distribution ratio H_{R} (height ratio). This ratio defines the quantity of light intensity of the normalized Gaussian intensity distribution, along the elliptic laser spot half-axis. In general, as the ratio H_{R} increases, the *acquisition range* increases, nevertheless the sensitivity of photo-detector and its *lock-on range* remain without radical changes. We remind that the *acquisition range* is the distance from the disc layer at which $e_{\mathrm{F}}(\Delta z)$ is large enough to allow the system to acquire focus, and that the *lock-on range* defines the area between peaks of the S-curve.
The influence of the varying distance between the collimator and the second focal line f_{L2} on $\hat{e}_{\mathrm{F}}(\Delta z, \theta)$ is shown in fig. A.7.
Fig.A.8 shows the *nominal* focus error characteristic $e_{\mathrm{F}}(\Delta z)$, obtained after having preprocessed data and computed the focus error characteristic $e_{\mathrm{F}}(\Delta z)$ from the measured $e_{\mathrm{F}}(t)$.

Summary :

In order to compare results achieved with the computed models, paraboloid light distribution is skipped, since it has been seen in [28] that it gives worse results in term of curve fitting than the other models.
Hence, two models have been used : the first uses the uniform intensity distribution of the laser beam on the photo-detector, while the second uses the Gaussian intensity distribution.
Since not all optical parameters are measurable on the real system, their values have been identified by using a curve fit procedure, by using *nominal* characteristic $e_{\mathrm{F}}(\Delta z)$. Curve fitting has been based on the following

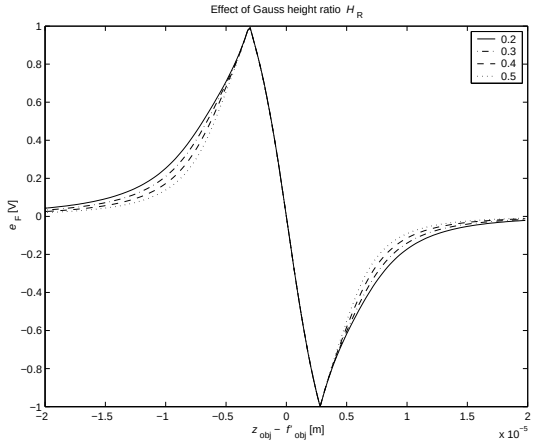

Figure A.6: Effect of Gauss height ratio H_R.

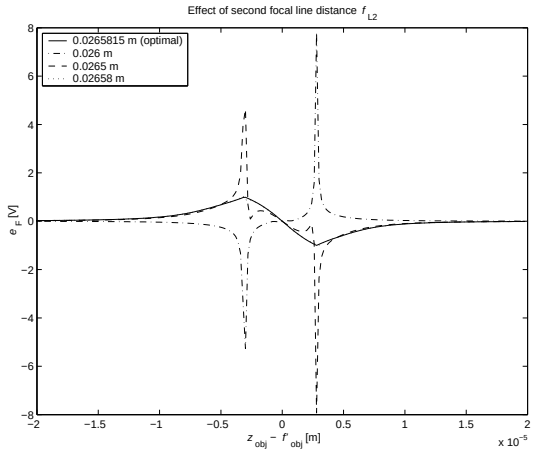

Figure A.7: Effect of second focal line distance f_{L2}.

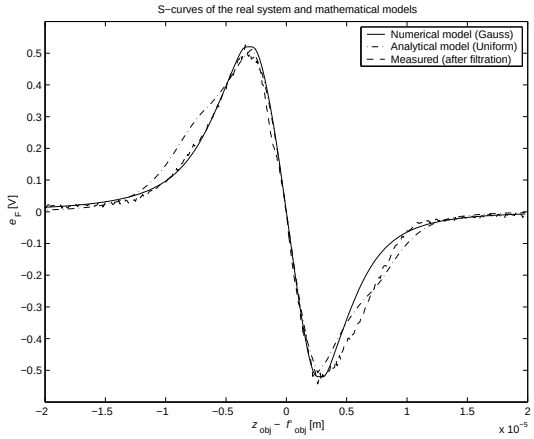

Figure A.8: S-curves of the real system and mathematical models.

Table A.1: *Models statistic parameters obtained from curve-fitting procedure.*

Model	$J(\theta)_{\min}$	$\bar{\sigma}$	$\bar{\nu}$
Analytical	0.2262	$\pm$0.03067	0.00094
Numerical	0.1615	$\pm$0.02821	0.00076

weighted nonlinear least-squares criterion :

$$J(\theta) = \sum_{\Delta z=\Delta z_{ini}}^{\Delta z_{fin}} w\,[e_{\mathrm{F}}(\Delta z) - \hat{e}_{\mathrm{F}}(\Delta z, \theta)]^2, \tag{A.22}$$

where the highest weight, given by a vector w, has been set on the *lock-on range* of the S-curve, and the smaller weight on the remaining parts.
$e_{\mathrm{F}}(\Delta z)$ stands for measured error signal from the real system ("nominal" characteristic) while $\hat{e}_{\mathrm{F}}(\Delta z, \theta)$ is the error signal calculated from the model.

$J(\theta)_{\min}$, the standard deviation $\bar{\sigma}(e_{\mathrm{F}}(\Delta z) - \hat{e}_{\mathrm{F}}(\Delta z, \theta))$ and the variance $\bar{\nu}(e_{\mathrm{F}}(\Delta z) - \hat{e}_{\mathrm{F}}(\Delta z, \theta))$ of the estimated models are used for evaluating performances of the different models, and they are presented in table A.2.

Fig.A.8 and table A.2 show the good match of the numerical model (Gaussian intensity distribution) with the real system.
It can be noticed that the analytical model provides worse performances than the numerical one, even though it represents a *complete* optics mathematical model, which can be very useful for identification of the optical system. In fact, it has been proved (see Hnilička et al. [28]) that hardly or non measurable optical parameters can be estimated easier and faster when the analytical model is used, and that it allows to reduce computational time when system closed-loop simulations are performed. These properties could be advantageous for future improvements of photo-detectors manufacturing.

A.3 Modelling the Tracking error signal generation

To understand principles that define image generation in optical systems it is necessary to have a clear understanding of how the light electro-magnetic field propagates through the optical system. This requires the knowledge of scalar diffraction theory and Fourier imaging.

In this section we will not go further in describing the wave nature of light, and how it can be used to derive the propagation of the optical field between two arbitrary planes. In fact, a complete and exhaustive analysis of these phenomena is already presented in Hnilička et al. [26], where a description of Huygens' principle as a solution to the scalar wave equation, and Kirchhoff's formula are given, to develop an expression describing the far-field diffraction pattern for a propagating optical field. Our aim is to briefly expose a simple mathematical analysis useful for understanding how the tracking error signal is generated in current DVD-video players. Due to the complexity of far field diffraction theory, and to the excessive computational time required to test optical devices models, no simulation results are provided in this section. More details can be found in [26] where final results are presented.

There exist in the literature some work treating the tracking error signal modelling in CD and DVD players, as in Bouwhuis et al. [4], Hnilička et al. [26], Pohlmann [44] and Stan [54]. Nevertheless the DPD (Differential Phase Detection) method, widely used in DVD-video player, is not explained more precisely anywhere.

As already discussed in section 2.6.3, there exist two ways of computing the tracking error signal in DVD players :

- A first method is based on the delay differences of the signals from the detectors A, B, C, D (see fig.2.15 of page 77). By summing the signals from the diagonal pairs of detectors $V_{\mathrm{A}} + V_{\mathrm{C}}$ and $V_{\mathrm{B}} + V_{\mathrm{D}}$, and by measuring the time difference between its rising and falling edges the tracking error signal e_{R} can be computed.

- A second method consists in measuring the delay differences between adjacent pairs of detectors A, B and C, D respectively. This will give two intermediate track error signals, which are then added to give the final tracking error. In the case of DVD-video systems, this DPD method is used to generate the tracking error signal.

A situation useful for understanding the differential phase detection method is obtained when the information in the tangential direction is replaced by a single frequency, so that, together with the radial periodicity, a purely two-dimensional grating is present on the disk.
Fig.A.9 shows a typical far field pattern generated by an optical disk with a regular diffracting structure on it. Although such a regular pattern is more

representative for the former analog video disks, the *harmonic* analysis with a periodic pattern also gives the correct trends for digital CD and DVD disks.

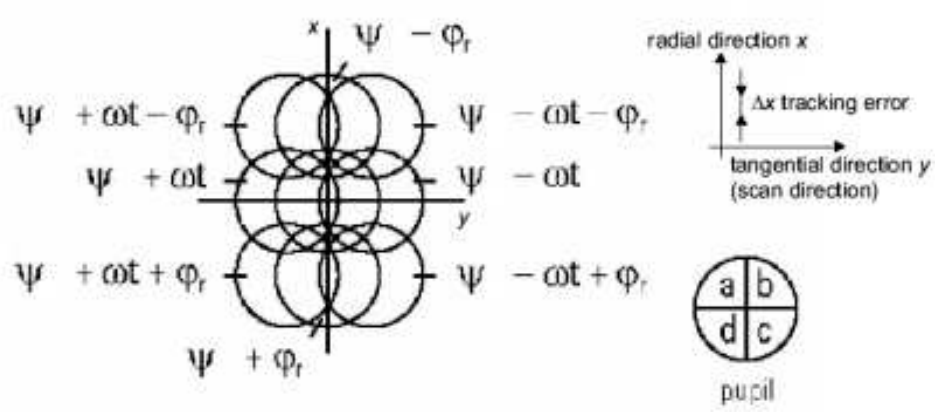

Figure A.9: Far field pattern generated by an optical disk.

Each modulation term depends on the diffraction direction.
The radially diffracted zeroth-order overlapping regions show a varying intensity level that is proportional to $\cos(\psi \pm \phi_{\rm r})$. The reference phase $\psi = \psi_{10} - \psi_{00}$ between the first and zeroth orders is determined by the disc structure and it can vary from $\pi/2$ for very shallow structures to π if the phase depth $\Delta\phi$ of the optical effects attains the value of π. The quantity $\phi_{\rm r} = 2\pi\Delta x/q$ is proportional to the tracking error Δx, and $q = 0.74$ μm is the track pitch. The sign of $\phi_{\rm r}$ depends on the order number ± 1 of the diffracted order.
Similarly, the overlapping regions along the tangential direction show an intensity variation proportional to $\cos(\psi \pm 2\pi f_{\rm pit} t)$, due to the scanning of the tangentially stored periodic pattern at the uniform speed $v_{\rm a}$.

The quantity :

$$f_{\rm pit} = \frac{v_{\rm a} N}{p}$$

denotes a temporal frequency generated by the spiral track scanning (N is an over-speed factor and p is a real distance between periodic pits on a track). Obliquely diffracted orders show a mixed phase contribution and carry interesting information for deriving the tracking error signal.

The objective lens signal high-frequency content, generated by the photo-detector quadrant 'a' has the following expression [4] :

$$\begin{aligned} S_{\mathrm{a}}(t) &= W_{00,10}\,\cos(\psi + 2\pi f_{\mathrm{pit}} t) && (1 \\ &+ W_{01,11}\,\cos(2\pi f_{\mathrm{pit}} t) && (2 \\ &+ W_{00,11}\,\cos(\psi + 2\pi f_{\mathrm{pit}} t - \phi_{\mathrm{r}}) && (3 \\ &+ W_{01,10}\,\cos(2\pi f_{\mathrm{pit}} t - \phi_{\mathrm{r}}) && (4 \end{aligned} \qquad \text{(A.23)}$$

where the weighting factors W are proportional to the product of the diffracted orders amplitudes and to the size of the interfering regions on the photo-detector quadrant. Similar expressions are obtained for the signals from the quadrants b, c and d with the appropriate algebraic signs in the phase terms $(2\pi f_{\mathrm{pit}} t)$ and ϕ_{r}.

The Hopkins theory, presented in [31], is used to compute the phase terms ψ in eq.(A.23). These values are evaluated to be $\psi_{00} = 8\,^{\circ}$ while $\psi_{10} = \psi_{01} = \psi_{11} = 160\,^{\circ}$. As it can seen, the main contributions to the high-frequency signal come from the components (1 and (3 of eq.(A.23), so to simplify the analysis, in the four quadrants we have considered only to the main phase contributions 1 and 3 from eq.(A.23).

Hence, for each photo-detector quadrant (see fig.A.9), we can write :

$$\begin{aligned} S_{\mathrm{a}}(t, \phi_{\mathrm{r}}) &= \cos(2\pi f_{\mathrm{pit}} t + \psi) + \alpha_3\,\cos(2\pi f_{\mathrm{pit}} t - \phi_{\mathrm{r}} + \psi) \\ S_{\mathrm{b}}(t, \phi_{\mathrm{r}}) &= \cos(2\pi f_{\mathrm{pit}} t - \psi) + \alpha_3\,\cos(2\pi f_{\mathrm{pit}} t + \phi_{\mathrm{r}} - \psi) \\ S_{\mathrm{c}}(t, \phi_{\mathrm{r}}) &= \cos(2\pi f_{\mathrm{pit}} t - \psi) + \alpha_3\,\cos(2\pi f_{\mathrm{pit}} t - \phi_{\mathrm{r}} - \psi) \\ S_{\mathrm{d}}(t, \phi_{\mathrm{r}}) &= \cos(2\pi f_{\mathrm{pit}} t + \psi) + \alpha_3\,\cos(2\pi f_{\mathrm{pit}} t + \phi_{\mathrm{r}} + \psi) \end{aligned} \qquad \text{(A.24)}$$

where α_3 is a factor that takes into account the phase contribution of the diagonal orders. Since this quantity is relatively smaller than the one coming from the tangential orders, it is assumed that $|\alpha_3| < 1$.

The standard DTD-signal is derived by firstly summing the light intensities on a diagonal pair of detector, then detecting the signals relative time shift. It is also possible to compare the phase difference between signals delivered by each single photo-detector quadrant.

Thus, we can summarize all the possible set of tracking error signal detection methods as follows :

1. $\Delta t_2(t) = t_{\mathrm{a+c}} - t_{\mathrm{b+d}}$: The time difference between the sum of signals from quadrants 'a+c' and the sum of signals from quadrants 'b+d' is taken. This is the standard DTD-method based on the difference of diagonal quadrant signals, and it is called DTD2 method.

2. $\Delta t_4(t) = t_{\mathrm{b-c}} + t_{\mathrm{d-a}}$: This difference requires four independent high-frequency detectors to be computed. When the laser spot is on the track, each difference signal 'd-a' and 'b-c' is identical zero. The common denomination is DTD4-method.

3. $\Delta t_{4a}(t) = t_{\mathrm{b-a}} + t_{\mathrm{d-c}}$: This signal is comparable to the previous one. The time differences 'b-a' and 'd-c' are not null zero when the laser spot is on the track, since these differences depend among other factors on the optical pit depth. The common denomination is DTD4a-method.

It is proved that the DTD4-method remains unaffected by de-focusing less than the DTD2-method [4]. In particular, the slope at the central zero set-point of the servo system remains unaltered by de-focusing effects. Therefore, the DTD4 method the one commonly used in DVD players for tracking error signal generation.

After the time differences $\Delta t_4(t)$ being generated, a IIR low-pass filter is used to integrate it to give the final tracking error signal $e_{\mathrm{R}}(t)$. This filter can be approximated by a simple RC low-pass filter, as follows :

$$\Delta t_4(t) = \frac{1}{K}\left(e_{\mathrm{R}}(t) + \frac{1}{2\pi f}\frac{\partial e_{\mathrm{R}}}{\partial t}\right) \tag{A.25}$$

where f is the filter cut-off frequency and K is a gain which gives the value of a total gain form the time difference $\Delta t_4(t)$ to the tracking error signal e_{R}.

With this assumptions, the tracking error signal generation model can be split-up in two different parts : a first part which is non-linear (NP) and a second part, considered as linear (LP). In fig.A.10 a block-scheme of the tracking error generation model is shown.

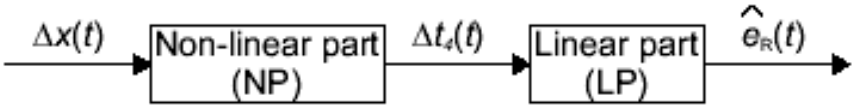

Figure A.10: Block-scheme of the tracking error generation model.

The model output is the estimated tracking error signal $\hat{e}_{\mathrm{R}}(t)$, which is given by the following expression :

$$\Delta t_4(\Delta x, \theta, \varrho, t) = \frac{1}{K}\left(\hat{e}_{\mathrm{R}}(\Delta x, \theta, \varrho, t) + \frac{1}{2\pi f}\frac{\partial \hat{e}_{\mathrm{R}}(\Delta x, \theta, \varrho, t)}{\partial t}\right) \qquad \text{(A.26)}$$

where the model input $\Delta x(t)$, the unknown parameters vector θ and the known parameters vector ϱ are emphasized.
Eq.(A.26) describes the linear part of fig.A.10. Its non-linear part, which gives the dependency of $\Delta t_4(t)$ from the track displacement along the disc radius $\Delta x(t)$ is instead described by :

$$\Delta t_4(\Delta x, \theta, \varrho, t) = \Big(S_b(\Delta x, \theta, \varrho, t) - S_c(\Delta x, \theta, \varrho, t)\Big) + \Big(S_d(\Delta x, \theta, \varrho, t) - S_a(\Delta x, \theta, \varrho, t)\Big) \qquad \text{(A.27)}$$

where S_a, S_b, S_c and S_d (see eq.(A.24)) represent the phase contributions of the pupil quadrants a, b, c and d respectively.

Hence, the model is characterized by the following parameters :

- The input track displacement $\Delta x(t)$ along the disc radial direction
- The estimated output tracking error $\hat{e}_{\mathrm{R}}(\Delta_x, \theta, \varrho, t)$
- The unknown parameters vector $\theta = [\alpha_3, K]$
- The known parameters vector $\varrho = [f_{obj}, NA, \psi_{00}, \psi_{10}, \lambda, q, T_{pit}, p, v_a, N, f]$

Summary :

Modelling the tracking error signal generation in optical disk drives is hard task since :

- liner models can be computed only by measuring the tracking *S-curves* in open-loop (radial loop opened, focus loop closed). In this condition it is possible to correctly focus the laser spot with respect to the disc layer, but the radial displacement of the objective lens is affected by disc eccentricity. This perturbation makes the laser cross tracks inward and outward with respect to the center of the track, resulting in not very reliable time acquisitions.
- characteristics of the periodic perturbation entering at the plant output are not known exactly. Particularly, it is hard to know accurately

the values of its phase and amplitude when tracking *S-curves* measurements start. This makes difficult to estimate unknown parameters vector $\theta = [\alpha_3, K]$ of mathematical models.

- sensor noise and quantization effects introduced by the D/A converters, at the output of the control chain, lead to very ill conditioned measurements which amplify inaccuracy of model parameters estimation algorithms.

Appendix B

The DVD Forum

The DVD specifications have been produced and published by the DVD Forum, which represents the DVD industry.
The DVD Forum was originally called the DVD Consortium and comprised the following 10 members who were responsible for developing the DVD standards and specifications :

- AOL Time Warner
- Philips
- Hitachi
- Pioneer
- JVC
- Sony
- Matsushita
- Thomson
- Mitsubishi
- Toshiba

Seven new members were added to these to form the DVD Steering Committee:

- IBM Corporation

- LG Electronics
- Industry Technology Research Institute of Taiwan
- NEC Corporation
- Samsung Electronics
- Intel Corporation
- Sharp Corporation

The DVD Forum now has about 230 members, 12% of which are in Europe. General Meetings of the DVD Forum are held annually and members are entitled to attend. There are two categories of DVD Forum membership:

- Principal (or 'A') members who can vote at General Meetings
- Associate (or 'B') members who can attend but cannot vote at General Meetings

In December 2001 all 17 of the companies mentioned above were re-elected to the Steering Committee by Principal Members of the DVD Forum.

The DVD Forum continues to maintain and improve the specifications describing the various standards and to carry out other related work in support of the formats. This work is carried out by a number of working groups under the Technical Coordination Group (TCG), as listed below :

Table B.1: *DVD Working Groups coordinated by the TCG .*

WG	Company	Field
WG1	Toshiba	Video application specifications
WG2	Pioneer	DVD Read-Only Disc specifications
WG3	Matsushita	File system specifications
WG4	JVC	Audio application specifications
WG5	Hitachi	Physical specifications for the DVD-R Disc Format
WG6	Pioneer	Physical specifications for the DVD-Recordable Disc
WG9	Toshiba	Copy Protection review and proposals to TCG
WG10	Pioneer	DVD application formats for broadcasting and industrial use

Curriculum Vitae

Giampaolo FILARDI was born on the 9^{th} of March 1972 in Alatri, Italy.

Education :

1986-1991 Pre-University education.Diploma di Maturita'Scientifica with 60/60 from the Liceo Scientifico "G.Sulpicio", Alatri (FR), Italy.

1991-1999 M. Sc. student in Electrical Engineering at the University of Rome "La Sapienza", Italy.
Gratuated (102/110) with a final thesis, carried out at the *Laboratoire d'Automatique de Grenoble* - INPG/ENSIEG (France), on optimal control design strategies applied to an electro-pneumatic actuator.

1999-2003 Ph.D. student at the *Systemes Avancés de Régulation et Commande* Group, *Laboratoire d'Automatique de Grenoble* - INPG/ENSIEG, (France), sponsored by STMicroelectronics Consumer and Microcontroller Group, DVD division Research Laboratories, Grenoble (France).

Publications :

First Author :

2001 G. Filardi, A. Besançon-Voda, D. Rey and A. Franco.
LQG Optimal Control Design Strategies applied to an electro-pneumatic actuator. IEEE European Control Conference, Porto, Portugal.

2002 G. Filardi, A. Besançon-Voda, O. Sename and H.J. Schroeder.
Modeling, Identification and Performance Analysis of a DVD player. IEEE International Conference On Control Applications, Glasgow, Scotland.

2003 G. Filardi, O. Sename and A. Besançon-Voda.
Structured Robust Stability and Performance Analysis with real perturbation of a DVD-drive $\mathcal{H}_\infty$ Controller. Computational Engineering in Systems Applications multiconference (CESA), Lille France.

2003 G. Filardi, O. Sename, A. Besançon-Voda and H.J. Schroeder.
Robust $\mathcal{H}_\infty$ control of a DVD drive under parametric uncertainties.
IEEE European Control Conference, Cambridge, U.K.

Co-Author :

2002 B. Hnilička, A. Besançon-Voda and G.Filardi.
Modelling the focus error characteristic of a DVD player. IEEE International Conference On Control Applications, Glasgow, Scotland.

2003 B. Hnilička, A. Besançon-Voda, G.Filardi and H.J.Schroeder
Poles placement sensitivity function shaping and controller order reduction in DVD players (Radial Control loop).
Computational Engineering in Systems Applications multiconference (CESA), Lille France.

2003 B. Hnilička, A. Besançon-Voda and G.Filardi
Poles placement sensitivity function shaping and controller order reduction in DVD players (Focus Control loop).
IEEE European Control Conference, Cambridge, U.K.

Bibliography

[1] G. Becker, P. Bendotti, P. Gahinet, and C.M. Falinower. Analysis and controller synthesis for a pressurized water reactor using linear parameter varying systems. In *IEEE Conference on Decision and Control*, pages 1676–1681, 1996.

[2] S. Bittanti, F. Dell'Orto, A. Di Carlo, and S. Savaresi. Radial Tracking in High-Speed DVD Players. In *40th IEEE Conference on Decision and Control*, pages 4705–4710, Orlando, Florida, 2001.

[3] M. Born and E. Wolf. *Principles of Optics*. Pergamon, New York, 6th edition, 1987.

[4] G. Bouwhuis, J. Braat, J. Huijser, and A. Pasman. *Principles of Optical Disc Systems*. Adam Hilger Ltd, Bristol and Boston, 1985.

[5] J. Braat. Differentail time detection for radial tracking of optical discs. *Applied Optics*, 37(29):6973–6982, 1998.

[6] J. Braat, P. Dirksen, et al. Diffractive read-out of optical discs. *Focus on Microscopy*, June 2002.

[7] R. De Callafon, P.M.J. Van den Hof, and D.K. De Vries. Identification and Control of a CD Mechanism using fractional representation. In *Proc. 10th IFAC Symposium on System Identification*, volume 2, pages 121–126, Copenhagen, Denmark, 1994.

[8] R. De Callafon and P.M.J. Van den Hof. Freqid-frequency domain identification toolbox for use with matlab. *Selected Topics in Identification, Modelling and Control*, 9:129–134, 1996.

[9] M. Dettori. *LMI techniques for control with application to a Compact Disc player mechanism*. PhD thesis, Technische Universiteit Delft, 2001.

[10] M. Dettori. *LMI techniques for control with application to a Compact Disc player mechanism*. PhD thesis, Technische Universiteit Delft, 2001.

[11] M. Dettori, V. Prodanovic, and Carsten W. Scherer. Mixed objectives mimo control design for a compact disc player. In *American Control Conference*, volume 11, pages 1284–1288, Philadelfia, Pennsylvania, 1998.

[12] M. Dettori and C.W. Scherer. Digital implementation of a Mixed Objectives Mimo Controller for a Compact Disc Player using multiprocessor system. In *American Control Conference*, pages 3630–3634, San Diego, California, 1999.

[13] M. Dettori and C.W. Scherer. LPV design for a CD player: an experimental evaluation of performance. In *40th IEEE Conference on Decision and Control*, volume 12, pages 14–22, Orlando, Florida, 2001.

[14] M. Dettori and C.W. Scherer. Mimo control design for a compact disc player with multiple norm specifications. In *IEEE Transaction on Control System Technology*, volume 10, pages 635–545, September 2002.

[15] M. Dettori and T.R. Stribos. Performance-Robustness trade-off in the Control of a CD Player using Mixed Objectives Design. In *39th IEEE Conference on Decision and Control*, Sydney, Australia, 2000.

[16] E.T. Van Donkelaar, H. Dötsch, and P.M.J. Van den Hof. Identification of model uncertainty of a Compact Disc pick-up Mechanism. *IEEE Trans. Automat. Control*, 8:47–55, 1995.

[17] H. Dotsch, H.T. Smakman, and P.M.J. Van den Hof. Adaptive Repetitive Control of a Compact Disc Mechanism. In *34th conference of Decision and Control*, pages 1720–1725, New Orleans, Louisiana, 1995.

[18] H.G.M. Dötsch. *Identification for Control Design with Application to a Compact Disc Mechanism.* PhD thesis, Technische Universiteit Delft, 1998.

[19] H.G.M. Dötsch, P.M.J. Van den Hof, O.H. Bosgra, and M. Steinbuch. Identification in view of control design of a cd player. *Selected Topics in Identification, Modelling and Control*, 9:25–30, 1996.

[20] J.C. Doyle, B.A. Francis, and A.R. Tannenbaum. *Feedback Control Theory.* Maxwell Macmillan International, New York, 1992.

[21] J.C. Doyle, K. Glover, P. Khargonekar, and B. Francis. State-space solutions to standard h_2 and h_∞ control problems. *IEEE Transaction in Automatic Control*, 34(8):831–847, 1989.

[22] G. Filardi, O. Sename, and A. Besançon-Voda. Structured robust stability and performance analysis with real perturbation of a dvd-drive $\mathcal{H}_\infty$ controller. *IEEE-CESA Conference, Lille, France*, 2003.

[23] G. Filardi, O. Sename, A. Besançon-Voda, and H.J. Schroeder. Robust $\mathcal{H}_\infty$ control of a DVD drive under parametric uncertainties. *IEEE European Control Conference, Cambridge, U.K*, 2003.

[24] K. Glover and J.C. Doyle. State-space formulae for all stabilizing controllers that satisfy an h_∞ norm bound and relations to risk sensitivity. *System and Control Letters*, 11:167–172, 1988.

[25] Keqin Gu. $\mathcal{H}_\infty$ control of systems under norm bounded uncertainties in all system matrices. *IEEE Transaction on Automatic and Control*, 39(6), 1994.

[26] B. Hniličkа, , A. Besançon-Voda, and G.Filardi. Modelling and identification of the optical part of a DVD player. *Internal report of LAG, ENSIEG, INPG*, (AP02–2), December 2002.

[27] B. Hniličkа, , A. Besançon-Voda, and G.Filardi. Control in DVD players (focus and tracking control loops. *European Control Conference (ECC), Cambridge U.K.*, September 2003.

[28] B. Hniličkа, A. Besançon-Voda, and G. Filardi. Modelling the focus error characteristic of a DVD player. *Proceedings of the 2002 IEEE International Conference on Control Applications*, pages 629–630, September 2002.

[29] B. Hniličkа, A. Besançon-Voda, and G.Filardi. Poles placement/sensitivity function shaping and controller order reduction in DVD players (focus control loop). *European Control Conference (ECC), Cambridge U.K.*, September 2003.

[30] B. Hniličkа, A. Besançon-Voda, G.Filardi, and H.J.Schroeder. Poles placement/sensitivity function shaping and controller order reduction in DVD players (radial control loop). *Computational Engineering in Systems Applications multiconference (CESA), Lille France*, July 2003.

[31] H. Hopkins. Difraction theory of laser read-out systems for optical video disc. *J. Opt. Soc. Am.*, 69(4), 1979.

[32] Schouhamer Immink. *Coding Techniques for Digital Recorders*. Prebtice Hall International, UK, 1991.

[33] M. Innocenti and G. Campa. Robust control of underwater vehicles : Sliding modes vs. lmi synthesis. In *American Control Conference*, pages 3422–3426, 1999.

[34] J. Isaloilović. *Videodisc and Optical Memory Systems*. Prentice-Hall, Inc., New Jersey, 1985.

[35] J.W.Goldman. *Introduction to Fourier Optics*. McGraw-Hill, Inc., 1968.

[36] T. Katayama, M.Ogawa, and M.Nagasawa. High-precision tracking control system for digital video disc player. *IEEE Transaction on Consumer Electronics*, 41:313–321, 1995.

[37] S. Lim and J.P. How. Application of improved l_2-gain synthesis on lpv missile autopilot design. In *American Control Conference*, pages 3733–3737, 1999.

[38] L. Ljung. Some Results on Identifying Linear Systems Using Frequency Domain Data . In *Proceedings of the 32nd Conference on Decision and Control*, pages 3534–3538, San Antonio, California, 1993.

[39] A. Oppenheim and R. Schafer. *Discrete-Time signal Processing*. Prentice Hall, Signal Processing Series, Englewood Cliffs, N.J., 1989.

[40] R. Pintelon, P. Guillame, Y. Rolain, and J. Schoukens. Parametric Identification of Transfer Functions in the Frequency Domain- A Survey. In *Trans. Automatic Control*, volume 39, pages 2245–2260, 1994.

[41] R. Pintelon, P. Guillame, Y. Rolain, and F. Verbeyst. Identification of Linear Systems Captured in a Feedback Loop. In *IEEE Trans. Instrum. Meas.*, volume IM-41, pages 747–754, 1992.

[42] R. Pintelon and J. Schoukens. Frequency Domain Sistem Identification with Missing Data. In *37th IEEE conference on Decision and Control*, volume 1, pages 701–705, Tampa,Florida, 1998.

[43] Ltd Pioneer Electric Co. *Optical DVD pick-up technical specifications*. Pioneer Electric Co., Optical Disc Division, 2000.

[44] K. C. Pohlmann. *Principles of Digital Audio*. McGraw-Hill, Inc., 3rd edition, 1995.

[45] Ltd Sanyo Electric Co. *Optical DVD pick-up technical specifications*. Sanyo Electric Co., Ltd Multimedia company Optical Device Division, 2001.

[46] C.W. Scherer, P. Gahinet, and M. Chilali. Multiobjective output-feedback control via lmi optimization. 42:896–911, 1997.

[47] C.W. Scherer, R. Nijo, and S. Bennani. Parametrically varying flight control system design with full block scalings. In *IEEE Conference on Decision and Control*, pages 1501–1505, 1997.

[48] R. Schrama. *Approximate Identification and Control Design*. PhD thesis, Delft University of Technology, Delft, Netherlands, 1992.

[49] O. Sename and L. Dugard. Robust $\mathcal{H}_\infty$ control of quarter-car semi-active suspensions. *IEEE European Control Conference, Cambridge, U.K*, 2003.

[50] R.E. Skelton. Model error concepts in control design. *Int.journal of Control*, 49:1725–1753, 1989.

[51] S. Skogestad and Postlethwaite. *Multivariable Feedback Control: analysis and design*. John Wiley and Sons, 1996. http://www.chembio.ntnu.no/ skoge/.

[52] J. J Stamnes. *Waves in Focal Regions*. Adam Hilger, Bristol and Boston, 1986.

[53] S. G. Stan. *Optimization of the CD-ROM system towards higher data throughtputs*. PhD thesis, Technische Universiteit Eindhoven, 1999.

[54] Sorin G. Stan. *The CD-ROM Drive: a brief system description*. Kluwer Academic Publisher, Boston, 1998.

[55] M. Steinbuch, P. Van Groos, G.Schootstra, and O.H. Bosgra. Multivariable Control of a Compact Disc Player using DSPs. In *American Control Conference*, pages 2434–2438, Baltimore, Maryland, 1994.

[56] M. Steinbuch, G.Schootstra, and O.H. Bosgra. *Robust Control of a Compact Disk Mechanism*. CRC Press -IEEE Press, 1996.

[57] M. Steinbuch, G. Schoostra, and O.H. Bosgra. *Robust control of a compact disk mechanism*. CRC Press-IEEE Press, 1996.

[58] Agilent Technologies. *Agilent 35670A Operator's Guide*. Agilent Technologies Inc., Everett, WA, USA, 2000.

[59] Corporation Toshiba. *DVD Specification for Read-Only Disc*, volume 1. Hitachi L.t.d and Matsushita Eletric and Mitsubishi Electric and Philips Electronics and Pioneer Electronic Corporation, 1st edition, 1996.

[60] P.M.J. Van den Hof, E.T. Van Donkelaar, H.G.M. Dötsch, and R.A. de Callafon. Control relevant uncertainty modelling directed towards performance robustnees. In *13th IFAC World Congress*, volume 1, pages 103–108, San Francisco, California, 1996.

[61] P.M.J. Van den Hof and R.P.J. Schrama. Identification and Control-closed loop issues. In *Automatica*, volume 31, pages 1751–1770, 1995.

[62] E. Vidal, K.G. Hansen, R.S. Andersen, K.B. Poulsen, J. Stoustrup, and T.S. Pedersen. Linear quadratic controller with fault detection in compact disk players. *IEEE International Conference on Control Applications, Mexico City-Mexico*, September 2001.

[63] E. Vidal and B. Andersen R.K. Karlsson. Robust h_∞ control in cd players to suppress external disturbances and defect on the disk. *IEEE European Control Conference, Barcelona-Spain*, July 2002.

[64] E. Vidal, J. Stoustrup, et al. Deterministic method for obtaining nominal and uncrertainty models of CD drivers. *Proceedings of the 2002 IEEE International Conference on Control Applications*, pages 637–642, September 2002.

[65] E. Vidal, J. Stouststrup, P. Andersen, T.S. Pedersen, and H.F. Mikkelsen. Open and closed loop parametric system identification in compact disk players. *Proceeding in the American Control Conference*, pages 25–27, 2001.

[66] E. Vidal, J. Stouststrup, P. Andersen, T.S. Pedersen, and H.F. Mikkelsen. Parametric uncertainty with perturbations restricted to be real on 12 CD mechanisms. *Submitted to Automatic Control Conference, Colorado, USA*, 2003.

[67] J.F. Whidborne and J.B. Yang. Multiobjective design of low complexity digital controllers. In *IEEE International Symposium on Computer Aided Control System Design*, volume 1, pages 27–32, Glasgow, Scotland, U.K., September 2002.

[68] Lihua Xie, Minyue Fu, and Carlos E.Souza. $\mathcal{H}_\infty$ control and quadratic stabilisation of system with parameter uncertainty via output feedback. *IEEE Transaction on Automatic and Control*, 37(8), 1992.

[69] K. Zhou. *Essentials of Robust Control*. Prentice Hall, New Jersey, 1998.

[70] Yu Zohu and Maarten Steinbuch. Estimator-based sliding mode control on an optical disc drive under shock and vibration. *IEEE International Conference On Control Applications, Glasgow Scotland*, 9:25–30, 2002.